ONLINE CONDITION MONITORING OF RAILWAY WHEELSETS

by

Arash Amini

A thesis submitted to
The University of Birmingham
For the degree of
DOCTOR OF PHILISOPHY

School of Electronic, Electrical and Systems Engineering
College of Engineering and Physical Sciences
University of Birmingham
May 2016

Synopsis

Wheelset failures can occur unexpectedly resulting in very serious derailments. The rail industry has focused on the improvement of maintenance through the effective use of online condition monitoring of rolling stock and rail infrastructure in order to reduce the occurrence of unexpected catastrophic failures and disruption that arise from them. The basic components comprising a railway wheelset are the wheels, axle and axle bearings. Defective bearings due to their position within the wheelset configuration can be very difficult to detect. Existing wayside technologies based predominantly on Hot Axle Box Detectors (HABDs) are only able to detect a faulty axle bearing only after it has practically failed. Trackside Acoustic Array Detectors (TAADs) on the other hand have not yet proven their effectiveness as an alternative technique for the early detection of faulty axle bearings. For these reasons the rail industry has shown an increased interest in the development of novel effective and low-cost techniques which can be applied for the online evaluation of rolling stock wheelsets and axle bearings in particular.

Detection of wheelset faults in a timely manner increases efficiency as it helps minimise maintenance costs and increase availability. The main aim of this project has been the development of a novel integrated online acoustic emission (AE) and vibration testing technique for the detection of wheel and axle bearing defects as early as possible and well before they result in catastrophic failure and subsequently derailment. The approach employed within this research study is based on the combined use of accelerometers and high-frequency AE sensors mounted on the rail or axle box using magnetic hold-downs. AE is readily able to detect the high frequency noise arising from wheel tread defects interacting with the surface of the rail head at the wheel-rail interface. Despite the fact that axle bearings are not interacting directly with the rail head surface, noise signals arising from defects on the roller or race of a faulty axle bearing can be transmitted through the wheel and

subsequently through the rail and hence are also detectable with AE sensors. However, since both wheel tread defects, such as flats or shelling, and axle bearing faults are detectable with the AE sensors there is a need to have a means to distinguish between the two types of defects. For this reason, accelerometers have been employed. Accelerometers have been already used in certain state-of-the-art impact load detector devices and therefore it is well known that they can detect wheel tread defects as well as quantify them. However, accelerometers are far less sensitive to axle bearing faults unless the defect has reached critical severity. Therefore, by employed accelerometers together with AE sensors it is possible to both detect wheel tread and axle bearing defects as well as distinguish between the two. Moreover, it is possible to quantify wheel tread defects.

Special consideration needs to be given in filtering out unwanted noises and vibrations in the vibration and AE signals respectively. This is achieved by comparing the signal from the defected wheel with the original signals from a normally functioning wheel of equal dimensions as well as various signal processing techniques based on moving RMS ,moving kurtosis filtering, spectral analysis etc. Furthermore, the application of advanced signal processing methods such as the high frequency resonant technique (HFRT), Time Spectral Kurtosis (TSK) and Kurtogram are considered and evaluated.

Within the framework of this project several experiments have been carried out under laboratory conditions, as well as in the field at the Long Marston test track and in Cropredy on the Chiltern Railway line to London.

From the results obtained it has been confidently concluded that the combined use of vibration and AE analysis provides infrastructure managers with a strong diagnostic tool for early diagnosis of wheel and axle bearings faults. The technique has also been proven to be very efficient in detecting faults when onboard instrumentation is employed. The analysis carried out on data obtained during the various laboratory and field trials together with the key findings of this study are discussed in detail within this thesis.

Acknowledgments

First and foremost I express my gratitude to my parents. I attribute my PhD to their encouragement and effort, without which the completion of this thesis was impossible.

I offer my sincerest regards to my supervisor, Dr Mayorkinos Papaelias, who has supported me throughout my research with his patience and knowledge.

Special thanks to Prof Clive Roberts for his supervision and problem solving, Mrs Mary Winkles for tracking me down for deadlines and reports and Prof Claire Davis for her valued scientific guidance and appreciated clarifications.

I would also like to express my gratitude to Miss Jennifer Dolan for her help.

My sincere thanks also goes to Mr Patrick Vallely, who provided the opportunity for the field experiments in Cropredy Network rail site.

Last but not the least, my warm thanks to Dr Mani Entezami, Dr Hamed Rowshandel and Mr Adnan Zentani, for their technical support over the past few years.

Publications

Journal Papers

- A. Amini, M. Entezami, M. Papaelias "*Onboard detection of railway axle bearing defects using envelope analysis of high frequency acoustic emission signals*". Journal of *Case Studies in Non-destructive Testing and Evaluation*,vol 6, p 8-16 June 2016.
- M. Papaelias, A. Amini, Z. Huang, P. Vallely, D. Cardoso Dias, S. Kerkyras "*Online condition monitoring of rolling stock and axle bearings*". Proceedings of IMechE-Part F: Journal of *Rail and Rapid Transit* vol. 230 no. 3, p 709-723 *March 2016.*

Conference papers

- A. Amini "*Advanced wayside monitoring of rolling stock wheelsets using integrated high-frequency acoustic emission and vibration analysis*". Remote Condition Monitoring (RCM) on Railway workshop, March 2016, Istanbul, Turkey.
- A. Amini, Won 3rd award poster Presentation "*Online condition monitoring of railway wheelsets*" at BLUEBEAR 2014 conference, December 2014, Birmingham, UK.
- M. Papaelias, Z. Huang, A. Amini, P. Vallely "*Advanced wayside condition monitoring of rolling stock wheelsets*". ECNDT 2014, October 2014, Prague, Czech Republic.
- Z. Huang, A. Amini, L.Wang, M. Papaelias, S. Kerkyras "*Online evaluation of railway axle bearing faults using acoustic emission and vibration analysis*". NDT 2014, BINDT, July 2014 Manchester, UK.
- Amini, M. Papaelias "*Online Condition Monitoring of Railway Wheelsets*". *Next Generation Rail* Conference, June 2013, London, UK.
- Amini, M. Entezami, M. Papaelias, S. Kerkyras "*Condition monitoring of railway wheelsets using acoustic emission*". CM 2013 Conference, June 2013, Krakow, Poland.

- P. Yılmazer, A. Amini, M. Papaelias "*The structural Health Condition Monitoring of Rail Steel Using Acoustic Emission techniques*". NDT 2012, BINDT, September 2012, Rugby, UK.

List of Abbreviations

AE	Acoustic emission
ACFM	Alternating Current Field Measurement Inspection Technique
ANC	Adoptive Noise Cancellation
Bw	Bandwidth
BPFI	Ball pass frequency inner race
BPFO	Ball pass frequency outer race
BSF	Ball spin frequency
CM	Condition monitoring
dB	Decibel
ECT	Eddy Current Inspection
EMI	Electro-magnetic interference
EMAT	Electromagnetic acoustic transducer
Fc	Centre frequency
FFT	Fundamental train frequency
FTF	Fundamental train frequency
HABDS	Hot box or hot axle bearing detectors
HFRT	High Frequency Resonant Technique
HDD	Hit Driven

MFL	Magnetic Flux Leakage
MPI	Magnetic Particle Inspection
MPH	Miles per hour
NDT	Non-Destructive testing
PAC	Physical Acoustic Corporation
PK-PK	peak-to-peak
RCM	Remote Condition Monitoring
RMS	Root Means Square
SNR	Signal to Noise Ratio
TAADS	Trackside acoustic array detectors
TSK	Time Spectral Kurtosis
TDD	Time Driven
UT	Ultrasonic inspection
WILD	Wheel impact load detector
WPD	Wheel Profile Detector

Contents

List of Figures

List of Tables

Chapter 1 : Introduction

Due to the increasing demand for safer and quicker rail transportation, rolling stock wheelsets are required to sustain higher axle loads, speed and usage. This means that more rigorous and reliable inspection and maintenance strategies need be in place in order to optimise reliability, availability, maintainability and safety (RAMS). While in service, wheelsets are constantly exposed to harsh operational conditions including rolling contact fatigue, dynamic loads, thermal variations and impact. Gradual deterioration of the structural integrity of the wheelsets can increase the risk of failure and possibility of delays due to disruption. Wheel tread defects can give rise to excessive noise and vibration whilst they can inflict damage on rail track infrastructure due to the higher impact loads generated with every wheel revolution. In addition, wheel and axle bearing faults that remain undetected will almost certainly result in a derailment. Serious derailments such as the one that took place in Eschede in 1998 (Figure 1-1) can cause significant network disruption, unnecessary costs, put lives at risk and reduce the overall popularity of rail transport among the general public [1].

Figure 1-1: Remains of the high-speed train involved in the Eschede accident (Germany) in 1998 [2].

In order to detect surface-breaking and internal flaws inspection of wheelsets is carried out during production and maintenance using various non-destructive testing (NDT) methods such as visual inspection, conventional ultrasonic testing (UT), magnetic particle inspection (MPI), liquid penetrant inspection (LPI) and eddy current testing (ECT). These inspection processes are time consuming and prone to human error [3]. Moreover, in most cases the wheelset is required to be removed from the train first before inspection can be carried out. Exceptions to this rule are the hollow axles used in passenger trains which can be ultrasonically inspected without the need of removing the wheelset from the train. Defects on the wheel tread, such as flats and shelling, result in increased noise and vibration levels and reduce passenger comfort. In the case of rail freight, sensitive goods may be damaged due to excessive vibration leading clients to opt for road freight transport over rail. In addition, wheel tread defects lead to higher contact stresses and impact loads at the wheel-rail interface which may cause damage to initiate or propagate faster. Wheel flats and shelling may also act as precursors to axle bearing fault initiation and subsequent propagation [1].

In recent years, there has been much progress in on-line predictive maintenance of rotating machinery within the oil and gas and maritime sectors. These advances have led to the implementation of a reliable condition monitoring methodology based predominantly on trending of vibration signatures. Occasionally acoustic emission (AE) has also been used to complement vibration analysis. Vibration measurements on rotating machinery can hence be carried out on a routine basis. Where AE is employed, it is not essential in many cases to trend the data from a particular machine being measured as long as a correct threshold for the damaged condition has been established [4].

Within this research study the application of these two techniques in combination is investigated for the onboard and wayside condition monitoring of rolling stock wheels and axle bearings. The key findings along with the signal processing methodology employed are discussed later in the present thesis.

According to Stratman et al [5] the average cost of a derailment is approximately $340,000, whereas the average cost of a wheelset is $830. This means by preventing only 1 derailment per year would cover the cost of 400 removed wheelsets detected by the condition monitoring systems and at the same time it would help the safety of railroad.

1.1 Project aims and objectives

The wheelset is a critical component of railway rolling stock. The vast majority of derailments attributed to rolling stock as the cause are related to wheel or axle bearing failures. The current technology employed by the rail industry for monitoring the condition of wheelsets has several limitations particularly when the evaluation of axle bearings is concerned. With the use of rail networks across the world continuously increasing it is important not just to eliminate the likelihood of derailments but also to reduce to reduce disruption caused by serious wheelset faults that necessitate the unexpected stopping of affected rolling stock. With the advent of the 24-hour railway the operational requirements will become even more stringent leading to an urgent need for effective condition monitoring of railway rolling stock and infrastructure alike.

Within this study, a new approach based on high-frequency acoustic emission and vibration analysis techniques has been proposed for efficient and cost effective online evaluation of rolling stock wheels and axle bearings using both onboard and wayside instrumentation. The limitations of existing monitoring techniques are thoroughly presented providing a clear analysis of the strong industrial need for a breakthrough in this area. The advantages and disadvantages of onboard and wayside monitoring are evaluated under laboratory conditions as well as under realistic operational conditions based on field trials. Field trials have been carried out at the Long Marston test track using rolling stock with artificially induced defects in order to evaluate the efficiency of the proposed technique. Moreover, a pilot system has been installed on the UK rail network at Cropredy (Chiltern rail line) with the help of Network Rail. The system installed at the Cropredy site is currently in 24-hour operation and data are

collected from hundreds of trains every day. The data collected are consequently evaluated using various signal processing techniques.

The proposed work is delivered through the completion of several objectives:

- Initial review of rolling stock wheelsets, faults and inspection techniques.
- A general review of condition monitoring techniques for railway wheelsets.
- Background review of vibration and AE techniques.
- Laboratory experiments based on a single wheel, motorised trolley and test rig.
- Design a customised Matlab application to log and analyse data in time and frequency domains.
- Field trials.
- Comparison of the results from vibration and AE techniques from laboratory and field experiments.

The methodology and main results obtained during this research study are discussed within the present thesis. The main conclusions of this work together with recommendations for future directions are provided in the final chapter.

1.2 Structure of the thesis

The structure of this thesis is described below;

Chapter 2 – Rolling stock wheelsets, faults and inspection techniques

A literature review was carried out in relation to rolling stock wheelset components including wheels, axles and axle bearings. In addition, different types of defects arising from these parts were considered, as well as a review of destructive and non-destructive testing's for railway wheelsets.

Chapter 3 - Remote condition monitoring techniques for railway wheelsets

A general review of the current state of work for monitoring the railway wheelsets is explained in this chapter. This includes wheel impact load detector, wheel profile detector, hot axle box bearing detector, SKF axletronic and Perpetuum. Furthermore the main problems of using these techniques were discussed.

Chapter 4 - Vibration and acoustic emission inspection techniques

This chapter describes the theory and basic principles of both vibration and acoustic emission techniques and background research on different applications which apply to these techniques. Moreover, different signal processing techniques in order to increase the signal to noise ratio in the data were defined.

Chapter 5 - Laboratory experimental setup and test procedures

Vibration and acoustic emission instrumentations are presented in this chapter. A set of laboratory-based experiments were performed on a single wheel, motorised trolley pushing the wheel and a laboratory test rig consisting of defective bearings, these results are then discussed.

Chapter 6 - Field Trials

This chapter presents the test configurations and results from onboard and wayside measurements at Long Marston test field and Croperdy site. The collected data from the field experiment is then used for further analysis.

Chapter 7 – Comparison of AE and vibration analysis

In this chapter, the results from laboratory and field experiments are reviewed. Comparisons between the vibration and acoustic emission techniques in detecting wheel flat defects, test rig experiments, effect of speed and defect size and detecting bearing with lubricant contamination were made. The strengths and limitations of each method are discussed.

Chapter 2 ：Rolling Stock Wheelsets, Faults and Inspection Techniques

2.1 Wheelsets

Railway wheelsets consist of three main components; the wheels, axle and axle bearings. The photograph in Figure 2-1 shows an example of a wheelset model on London underground depot. Wheelset failures are not uncommon and occur unexpectedly. Faults can develop on any of the aforementioned components, but the most common are related to wheel and axle bearings defects. Bearing failure can occur before the bearing reaches the end of its intended design lifetime due to abnormal operational conditions while in-service or poor lubrication. The continuous increase in train operating speeds means that failure of a wheel or axle bearing can lead to very serious derailments, causing loss of life, injuries, severe disruption in the operation of the network, damage to the tracks, unnecessary costs, and loss of confidence in rail transport by the general public [6].

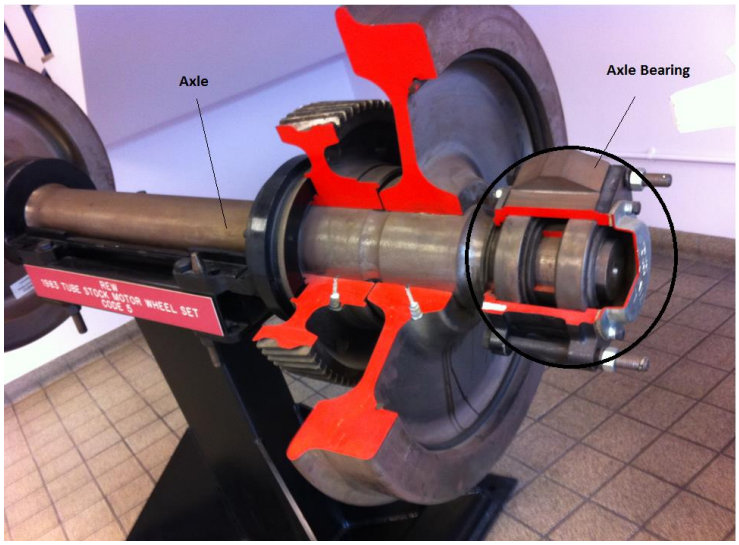

Figure 2-1: Image of a wheelset model in London underground Acton depot.

2.2 Train Wheel Metallurgy

In order to predict fatigue lifetime, wear resistance, corrosion resistance and general mechanical properties of the wheels, the chemical composition of the steel grade used in manufacturing should be considered. Table 2-1 summarises the steel grade composition used for the production of train wheels.

Table 2-1: Steel chemical composition used in manufacturing of wheels [7].

C	0.52%(max0.56)	Si	0.28%(0.20-0.40)	Mn	0.81%(0.70-0.95)
P	0.02%(max 0.035)	S	0.012%(max 0.035)	Cr	0.15%(max 0.30)
Ni	0.11%(max0.30)	Mo	0.04%	V	0.05%
Cu	0.15%(max 0.30)	Al	0.00%	Sn	0.01%
H	1.1 ppm(max2.0)				

The content of the alloying elements can profoundly influence the wear resistance, rolling contact fatigue lifetime, overall fatigue lifetime and corrosion resistance of the steel grade used in wheel manufacturing. The addition of Mn provides better toughness. Although the

formation of MnS inclusions increases ductility of steel, they also act as crack initiation points and therefore, their overall content within the microstructure needs to be kept low. The addition of Cr increases hardness due to the formation of carbide precipitates. Hence, the wear resistance of the wheel is higher. Ni and V as alloying elements contribute to the higher toughness exhibited by the steel alloy. However, S and P should be kept as low as possible to avoid their deleterious effects on the mechanical properties since particles formed by these elements can act as crack initiation points reducing fatigue and wear resistance [7] .

The schematic in Figure 2-2 shows the main geometrical features of a standard monobloc train wheel.

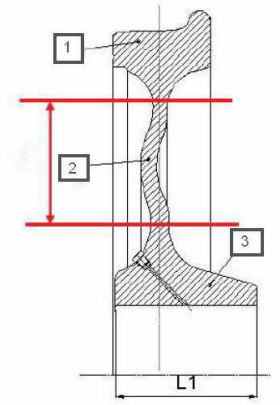

Figure 2-2: 1 Rim - 2 Web - 3 Hub - L1 Hub-width [8].

2.3 Wheel Defects

There are several types of wheel defects that may develop in-service. These include wheel flats, shells, metal build-up, ovality, rubbing flange and corrugation. Defects at the wheel tread can be detected by both accelerometers and AE sensors due to the vibrations and impact noises produced. In theory, it may also be possible to detect cracks propagating in the bulk or on the tread of the wheel due to Rolling Contact Fatigue (RCF) using AE. Although this has not been reported in any past studies, simulated trials using a Hsu-Nielson source (pencil break) have clearly shown that the transient elastic waves can be transmitted

through the wheel to the rail via the wheel-rail interface. Once the stress waves have been transmitted into the rail, they will propagate along its length. AE sensors will be able to detect such transient signals provided that they have not attenuated below an acceptable amplitude level. Due to the small contact area at the wheel-rail interface, heavy axle loads result in high pressure providing sufficiently good coupling quality for the stress waves to be transmitted from the wheel to the rail despite the fact that no couplant may be present. If the wear rate is bigger or equal to crack growth, surface cracks will be removed naturally unless their rate of propagation exceeds the wear rate of the wheel. However, in modern steel grades used in manufacturing of railway wheels this phenomenon is not likely to occur due to the high hardness they exhibit and hence increased wear resistance. As a result RCF crack initiation and subsequent propagation can occur particularly due to thermal effects arising during frequent or heavy braking. In most cases RCF cracking is avoided by frequent reprofiling of the wheels, thus removing crack initiation points or RCF cracks which are still at their very early stage of evolution. However, in the event that RCF cracks have exceeded a certain size, reprofiling is not sufficient and the wheel affected will need to be discarded. If RCF remains undetected, it will gradually grow resulting in shelling at the tread. Damaged wheels should be removed from service within 24 hours if any single cavity detected is greater than 15 mm long or any multiple cavities separated by 50 mm have a total length of 15 mm circumferentially around the wheel [9]. Similarly, axle bearing faults on the roller or race will produce transient signals due to impacts as the bearing rotates and this can be transmitted via the lubricant to the wheel and from there through the wheel-rail interface to the rail and subsequently to a nearby AE sensor. The various types of defects affecting wheels are discussed next.

2.3.1 Wheel Flats

A wheel flat is a flat area on the wheel tread caused by unintentional sliding of the wheel along the rail normally due to heavy braking. During heavy braking there is insufficient

adhesion between the wheel and rail to allow transmission of the braking, causing the wheel to lock up and slide along the rail head. Prolonged sliding of the wheel along the rail head results in high levels of friction causing the wheel tread to wear rapidly at the contact area. The worn area loses its roundness and becomes flat. The formation of wheel flats gives rise to high impact loads and vibration inflicting damage on the rail infrastructure, higher levels of vibration decreasing passenger comfort and increased noise levels [6]. Small wheel flats can gradually be removed due to uniform wear during rolling of wheel on the rail and subsequent braking events where the wheel has not been blocked. In extreme cases heat may build-up rapidly resulting in sufficiently high temperatures to melt the steel at the wheel tread area. In this case, metal build-up will form on the wheel tread necessitating the replacement of the wheel.

2.3.2 Thermal, Rolling Contact Fatigue and Fatigue Cracking

Cracking in a wheel is normally associated with Rolling Contact or thermomechanical fatigue. Several train classes including freight trains employ brake blocs that are designed to apply high levels of friction when they are in contact with the wheel tread in order to decelerate the train. However, during the braking process, temperature will naturally increase due to friction whilst high stress levels will be present. The combined effects of high stress levels and temperature can cause the initiation and subsequent propagation of cracks on the surface or near the surface of the wheel tread due to thermomechanical fatigue.

Since steel grades used for manufacturing of modern railway wheels are much harder than those employed in the past, wear levels are consequently low. As a result, there is sufficient time for RCF cracking to initiate and subsequently propagate unless the wheel is turned in time in order to remove the initiation sites or very small RCF cracks that may have already initiated between maintenance periods.

Cracking in the bulk body of Monobloc wheels is relatively rare. In most cases cracks developing in the bulk of the wheel arise due to manufacturing defects present in the

microstructure of the steel used. In older steel grades, the presence of free hydrogen atoms in the steel microstructure would cause hydrogen cracking. Hydrogen molecules present in the microstructure cause pores to form. These pores act as stress raisers causing penny-shaped cracks to initiate and propagate rapidly eventually leading to final fracture [8]. However this is a rare defect type nowadays because of the significant improvements and advances in steelmaking quality. Nonetheless, other types of inclusions such as MnS can cause crack initiation and propagation. MnS can also influence the formation of RCF cracking.

2.3.3 Hollow Worn Wheels

The change in the shape of the wheel caused by wear may result in thin wheel flanges and hollow worn wheels. Hollow wheels can destroy natural steering by reducing the rolling radius difference and giving rise to resistance in rolling. This leads to faster degradation of the wheel and increased energy consumption. Moreover, it also increases the wear of the rail head. This type of wheel defect is associated with higher risk of rail rollover derailment [10].

2.3.4 Tread Run Out

This defect occurs when the wheel tread is no longer circular or concentric with respect to the axle bearing surface. Thermal effects caused by rapid heating and cooling due to braking or sliding and RCF are the causes of this type of defect [10].

2.3.5 Wheel Metal Build-up

As mentioned earlier, in extreme cases of heavy braking, temperature can rise at sufficiently high levels to melt the steel at the wheel rail interface. This results in material debris from the wheel, the brake block, and the rail debris to be welded on the wheel tread. Metal build-up normally occurs in wintry and cold conditions [8].

2.3.6 Corrugation

In wheelsets employing brake blocks certain areas of the wheel tread can become warmer than others. These warmer regions will exhibit thermal expansion and hence be subjected to more wear than the colder area. When the wheel cools down, the material volume at these warmer spots decreases. This combined with the non-uniform wear pattern of the wheel causes the formation of a corrugated pattern. Corrugation is the main source of noise for in service rolling stock [10].

2.3.7 Other Types of Wheel Defects

Other types of defects affecting rolling stock wheels include spalling which is related to local material loss over the whole running surface, scaling due to laminar metal flow over the whole running surface and tread roll over.

Figure 2-3 shows some of the common wheel defects discussed herewith.

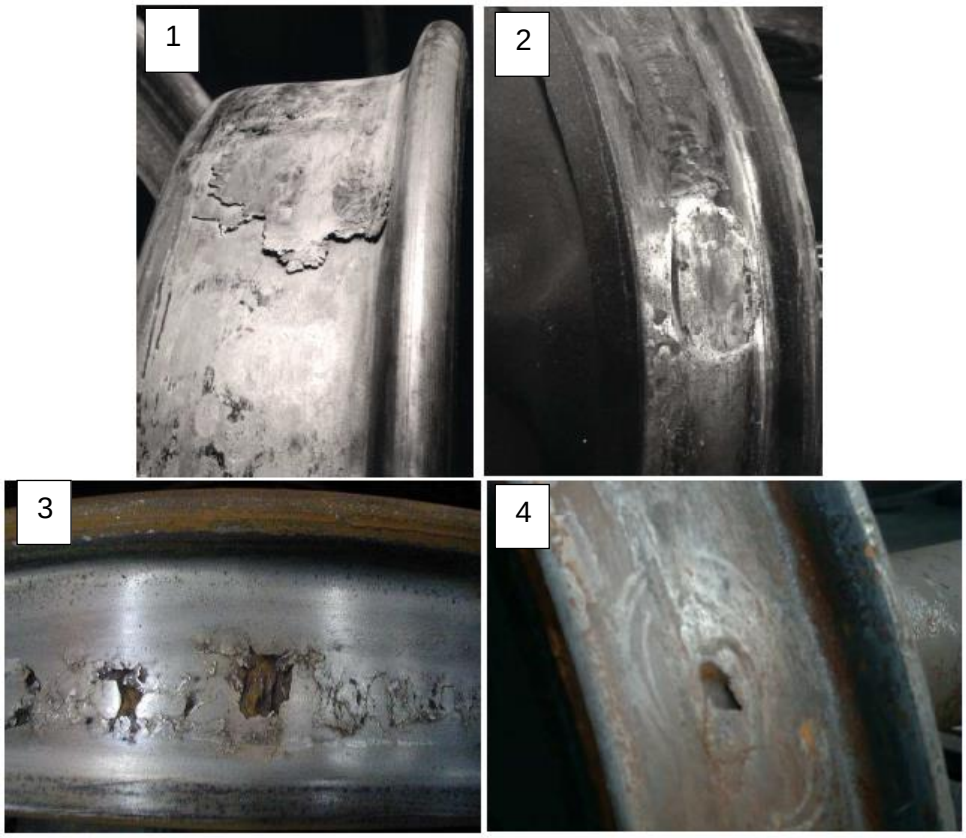

Figure 2-3: Wheel Defects: (1) Metal build-up (2) Wheel flat (3) Shelling (4) Cavities [8].

Table 2-2 indicates the maintenance actions that need to be taken for wheels affected by tread run out and flat defects according to the industrial Railway Group Standard [11]. The maintenance actions are dependent on the type of vehicle and size of the defect.

Table 2-2: Actions to be taken upon discovery of wheel flat and tread run out [10].

Vehicle type	Tread run-out and wheel flat	Vehicle to be removed from service
Any vehicle permitted to operate above 125 mile/h and up to 140 mile/h	Above 1.3 mm	Immediately
	0.7 mm to 1.3 mm	Within 24 hours of the fault being found
Passenger or personnel vehicles operating at speeds up to and including 125 mile/h	Above 3.0 mm	Immediately
	1.3 mm to 3.0 mm	Within 24 hours of the fault being found
Non-passenger vehicles, locomotives, power cars, driving van trailers and on-track machines	Above 3.0 mm	Immediately
	1.3 mm to 3.0 mm	On completion of the journey
Freight vehicles up to 17.5 tonnes axle load	Above 5.0 mm	Immediately
	3.0 mm to 5.0 mm	On completion of the journey. The speed to be restricted to 60 mile/h
Freight vehicles equal to or over 17.5 tonnes axle load	Above 4.0 mm	Immediately
	2.0 mm to 4.0 mm	On completion of the journey. The speed to be restricted to 60 mile/h
Other vehicles	Above 4.0 mm	Immediately
	2.0 mm to 4.0 mm	On completion of the journey. The speed to be restricted to 60 mile/h

2.4 Axle Bearings

Bearings are the most important components in any rotating machinery [12]. The axle bearing in railway rolling stock is responsible for transmitting the weight of the vehicle directly to the wheel. In industry, bearings are considered as critical mechanical components. Bearing defects unless detected in time will cause malfunction and may even lead to catastrophic failure of the machinery affected. Bearings will produce certain levels of vibration and noise regardless of whether a defect is present or not. However, if a defect is

indeed present, it will cause significant changes in the vibration and noise levels. It is therefore desirable to have a technology that can reliably detect bearing defects at an earliest stage of their development. This would allow the evolving damage to be repaired in time, particularly when the rail vehicle is already scheduled for maintenance, resulting in fewer operation interruptions and maximising rolling stock availability.

Bearing defects can be categorised as ‘distributed’ or ‘local’. Distributed defects such as surface roughness, waviness etc. and the variation of contact force between rolling elements can increase level of vibration or AE. Localised defects such as cracks, pits, spalls etc. can generate a pulse of vibration or AE in a very short duration. This pulse produces vibration and noise which can be monitored to detect the presence of a defect in the bearing [13, 14].

Vibration and acoustic emission analysis are two techniques which can be applied in remote condition monitoring of axle bearings. Measurements can be carried out both onboard and wayside. Of course onboard measurements are far more straightforward although the sensors need to sustain much higher vibration levels during rolling stock operation. Wayside monitoring on the other hand is more challenging but the sensors are exposed to relatively less harsh operational conditions in comparison with the onboard method.

RCF arises from repeated cyclic or stochastic stresses on the axle bearings. RCF occurs at the weakest point of the material where at micro-scale there is a large dispersion in material strength or resistance to fatigue because of the in-homogeneities in the material, e.g. due to the presence of inclusions such as MnS. Bearings are normally manufactured from Cr-based steel grades with high hardness and wear resistance. The subcomponents of the bearing such as the rollers, are case hardened to increase their resistance to rolling and impact damage.

The main factors which are important in determining dynamic capacity and fatigue life include the, 1) size of rolling elements, 2) number of rolling elements per row, 3) number of rows of rolling elements, 4) conformity between rolling elements and races, 5) contact angle

under load, 6) material properties, 7) lubrication quality, 8) operating temperature and 9) operating speed. Bearing damage may be caused due to manufacturing issues, poor handling during shipment and storage (e.g. corrosion), abnormal installation, or in-service during normal or abnormal operation. Due to the adverse operational conditions under which axle bearings operate the risk of failure is an important factor. Therefore maintenance strategies employed by rolling stock operators are very conservative and based on corrective and preventive measures. In the presence of any type of defect regardless of its severity, the modus operandi dictates the immediate replacement of the bearing concerned.

In the beginning of the 20th century, engineers directed their attention to predicting the remaining lifetime of bearings. As a result several theories were developed for the determination of the remaining bearing lifetime for a given load and operational speed (e.g. in 1924 by A. Palmgren whose theory was later popularised by Miner; W. Weibull in 1939; G. Lundberg, E. Ioannides and T. Harris in 1985; and E. Zaretsky) [15].

Most of the research associated with advances in the technology of bearings is the result of the requirements for highly reliable bearings used in aircraft turbine engines. The high operational speed and safety levels that need to be achieved necessitate the implementation of highly reliable bearings with long in-service design lifetimes. Table 2-3 summarises the most significant milestones in bearing technology in recent decades [16].

Table 2-3: Significant Milestones in bearing Material and Manufacturing technology [16].

Significant Milestones	Year of Introduction	Improvements
Vacuum degassing and vacuum melting	1958	Releases entrapped gasses & reduces quantity of harmful inclusions
Non-destructive testing (eddy current & ultrasonic methods)	1962	Better detection & elimination of material faults
Argon atmosphere protection during teeming	1963	Improved material homogeneity & cleanliness
Recognition of importance of grain flow direction	1963	Improved resistance to fatigue of parallel grain flow
Recognition of importance of hardness differential	1965	Improved fatigue life with optimum hardness differential between rolling elements & races
Vacuum induction melting followed by vacuum arc re-melting (VIMVAR)	1971	Further improvements in material homogeneity & cleanliness
M50 Nil material (carburizable M-50)	1984	Improved life & fracture toughness over through hardened M-50

2.4.1 Materials for Bearings

The choice of bearing material depends on the application considered including load type and load range, as well as environmental conditions, e.g. presence of corrosive media. Bearing subcomponents (balls or rollers) are manufactured from through-hardened or case-hardened materials. Critical applications require vacuum-processed steel grades to be employed. As an example, case-hardened Cr-Ni and Mn-Cr alloyed steels according to ISO 683-17:1999 with a carbon content of approximately 0.15% in weight are the most frequently used for SKF bearings.

2.4.2 Bearing Types

A typical axle bearing assembly consists of an outer cup which houses two tapered roller cone assemblies separated by a spacer. Each roller assembly consists of a raceway, rollers

and a cage. Inboard and outboard seals, seal wear rings, a backing ring and an end cap complete the axle bearing assembly (Figure 2-4).

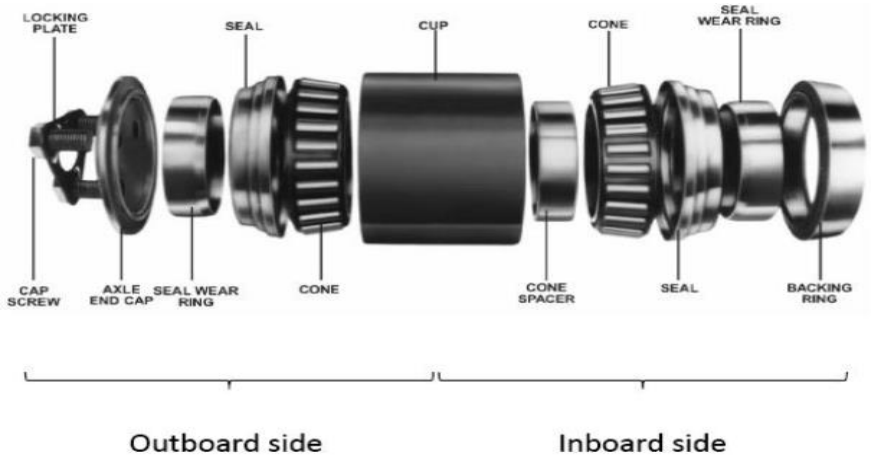

Figure 2-4: Axle bearing components [17].

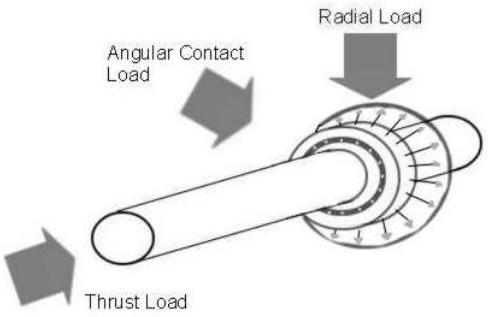

Figure 2-5 : Different types of load applied on bearings [18].

There are many different types of bearings designed to handle radial and thrust loads or a combination of them. Figure 2-5 illustrates the different types of load applicable on bearings. Hence the bearing type employed in each application needs to be carefully determined based on the specific load types and stress levels to be sustained [19].

Bearing types include:

- **Plain bearings:** Plain bearings must be made from a material that is durable, low friction, low wear to the bearing and shaft, resistant to elevated temperatures, and corrosion resistant.
- **Ball bearings:** they are extremely common as they can handle both radial and thrust loads but with only small amount of weight.
- **Roller bearings**: This type of bearing is designed to sustain high load levels. Because of the shape of the rollers, the load is distributed over a large area enabling the bearing to sustain high radial loads. However, roller bearings are not suitable in applications that involve thrust loads. Needle bearings also belong to this category and can be used for applications where space is an issue.
- **Ball thrust bearings:** Ball bearings are designed to sustain thrust loads at low speed and low load applications. Bar stools, for example, make use of ball thrust bearings to support the seat.
- **Roller thrust bearing:** This type of bearing is designed to sustain thrust loads. However the difference with ball thrust bearings is the load level the bearing can sustain. Car transmissions employ this type of bearings.
- **Tapered roller bearings:** This bearing type is designed to sustain high radial and thrust load levels. As a result of their load adaptability, they are found in car hubs due to the levels of both radial and thrust loads that car wheels are expected to sustain. Tapered roller bearings are the most common bearings employed in railway rolling stock. This is also the type of bearing considered within this project. The schematic in Figure 2-6 shows the key aspects of tapered roller bearing.
- **Spherical bearings:** Spherical bearings are widely used in the applications where rotational motion must be allowed to change the alignment of its rotation axis. Automobile suspension and engines are the common applications of these bearings. Spherical roller bearings used to be popular for railroad journal applications.

However, the popularity of this bearing type has been on a steady decline within the rail industry due to its high costs.

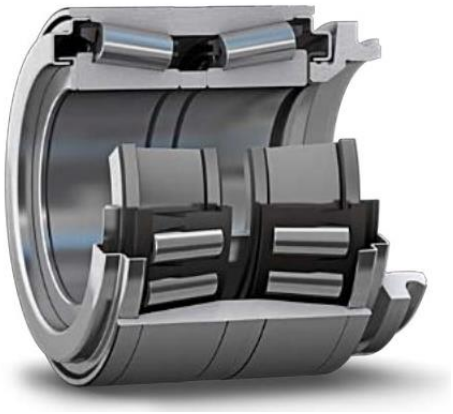

Figure 2-6 : SKF tapered roller bearing designed for railway wheelsets [20].

To avoid or reduce the metal-to-metal friction between the rolling and sliding contact surfaces, lubricants are used. The other functions of a lubricant in bearings are heat dissipation and corrosion protection. There are three types of lubricants for bearings in industrial applications including, grease, oil and dry solid lubricants (which are used for very heavy loads, slow relative movements and high working temperature). Grease lubricant is used for 90% of all rolling bearings. With the passage of time grease loses its properties and fresh grease must be resupplied at predetermined intervals [21]. Figure 2-7 shows that the most common bearing failures are related to poor lubrication.

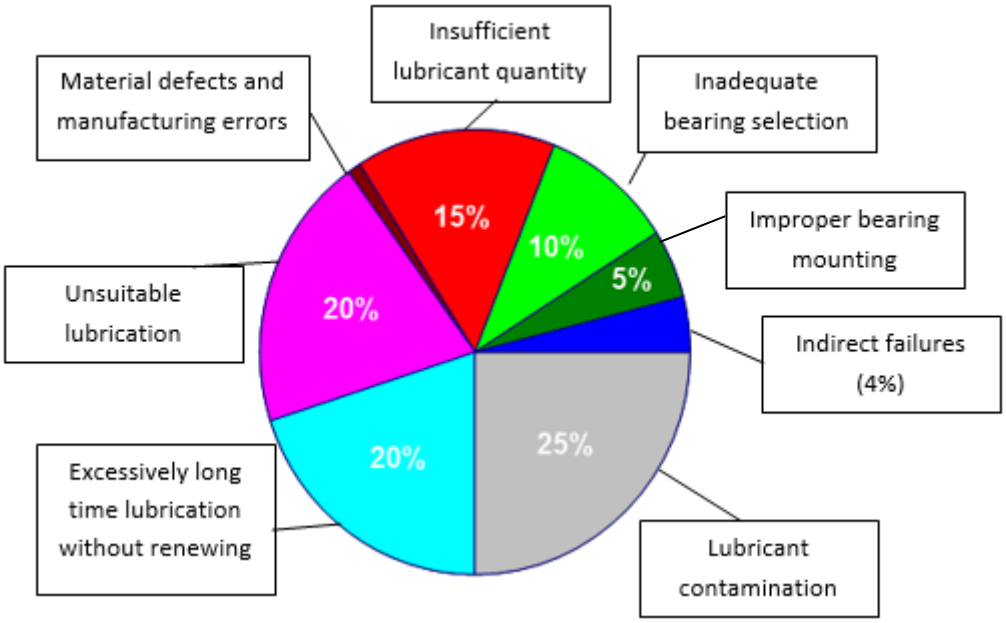

Figure 2-7: Common bearing failure causes in % [21].

2.4.3 Bearing Defects

Bearings are subjected to cyclic loadings which can often be stochastic. Moreover, they can be affected by poor lubrication or the presence of corrosive media in the operational environment. These factors combined with the loading conditions can cause gradual deterioration of the structural integrity of the different subcomponents of bearings. In-service axle bearings are required to operate under the aforementioned conditions. As a result, defects may initiate and propagate before the axle bearing reaches the end of its intended design lifetime. Nonetheless, axle bearing manufacturers normally recommend very conservative estimates for the acceptable in-service lifetime of axle bearings. Rolling stock operators based on their in-field experience gained with time quite, often keep in-service axle bearings for longer than the recommended time period suggested by the manufacturers. Keeping axle bearings in-service for longer than the time suggested by the manufacturer is not a decision taken lightly by rolling stock operators. In order to avoid

unexpected failures, a rigorous axle bearing inspection and maintenance schedule is established to ensure any defects that may have initiated or evolved are detected promptly.

Axle bearing defects may initiate and evolve for different reasons, including heavier loading, vibration and impact loads arising from wheel flats, poor lubrication, ineffective sealing, loose or tight fitting resulting in increased operational temperature and vibration, reverse loading, misalignment or manufacturing defects.

In steady-state machinery due to the high cost of catastrophic failure caused by defective bearings, it is important to detect faults early enough so maintenance can be carried out in time. However, since bearings are normally part of complex systems, e.g. a gearbox, it is very useful to identify precisely which component is defective and more specifically which bearing sub-component. This can assist the inspection engineers to diagnose the problem accurately and before it results in a break-down [22].

Bearing deterioration can be categorised into general roughness reduction and single-point defects. General roughness reduction develops gradually over a relatively long time period. However, this is not the case with single-point defects. Such defects can initiate and propagate all the way to final failure in a relatively short time. Therefore, detection needs to be prompt and this means inspection or remote condition monitoring (RCM) equipment used needs to exhibit a relatively high-level of sensitivity [23].

Figure 2-8 shows examples of various bearing defects.

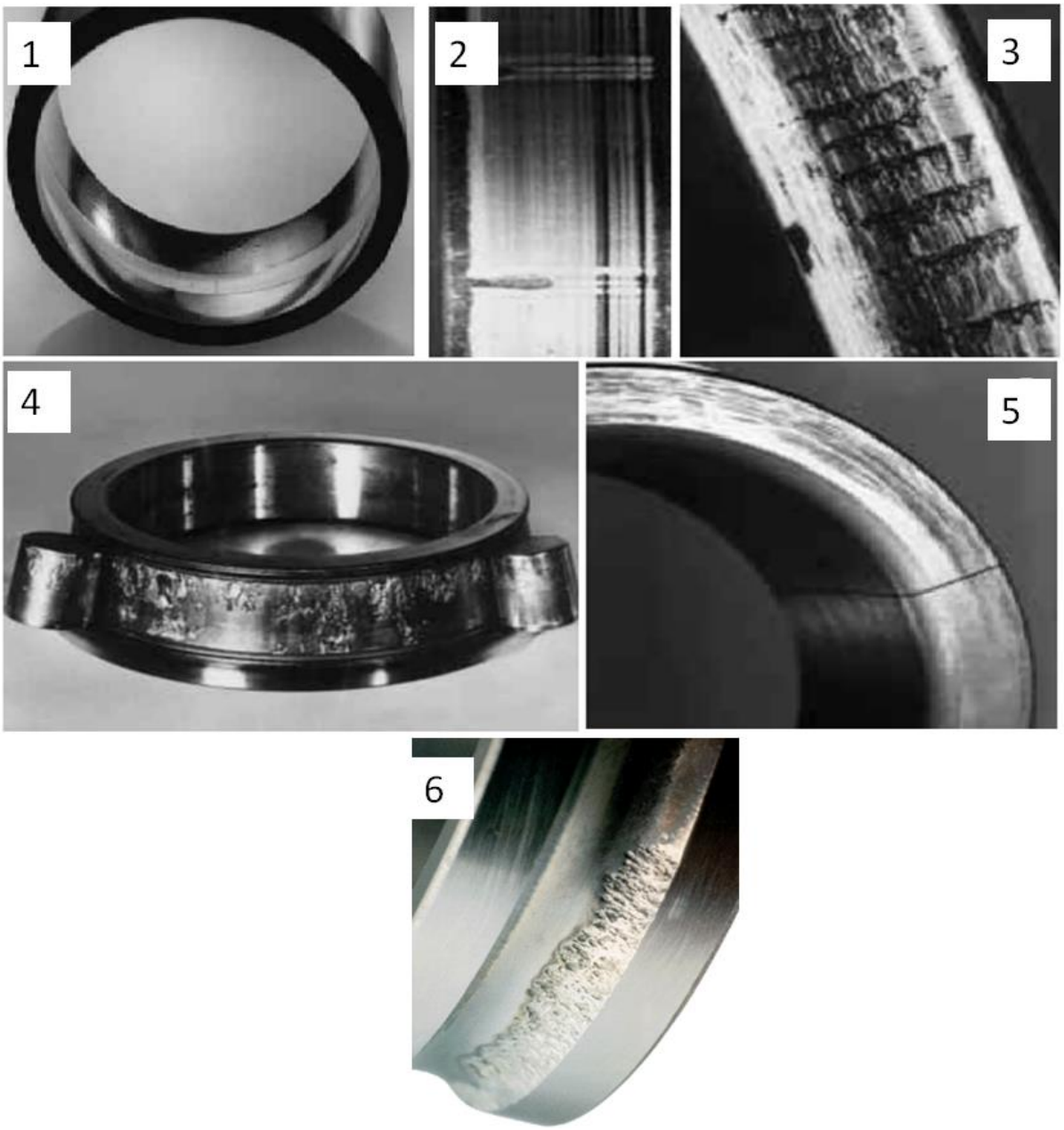

Figure 2-8: 1) Worn outer race, 2) Indentation, 3) Smeared inner race, 4) Flaking, 5) Cracking [24], 6) Brinelling caused by a static overload [25].

2.4.4 Axle Defects

Depending on rolling stock type axles may be hollow or solid. Freight trains, for example, always employ solid axles whilst high-speed passenger trains normally make use of hollow axle designs. Structural integrity issues associated with axles are normally related to general

or pitting corrosion and less often to fatigue caused by stochastic bending loads and high vibration levels.

Corrosion pitting can be described as an extremely localised form of corrosion where small pits develop on the surface of the metal. Current will be produced within the cavity, which becomes anodic, whilst the part of the metal exposed to the atmosphere will become the cathode. As a result corrosion will initiate [26]. Corrosion pits can act as stress raisers and therefore fatigue cracks may initiate and subsequently propagate from them. Unless, pitting corrosion and any associated cracking are found in time, the crack will reach critical size causing fracture of the axle and hence derailment.

Longitudinal and transverse cracks can initiate due to fatigue load during service time. Fatigue cracks will take far less time to propagate to critical severity than it took for initiation. Figure 2-9 shows some typical examples of axle defects.

Figure 2-9: Axle defects [8].

The schematic in Figure 2-10 shows the typical design of railway wheelset axles and their main features.

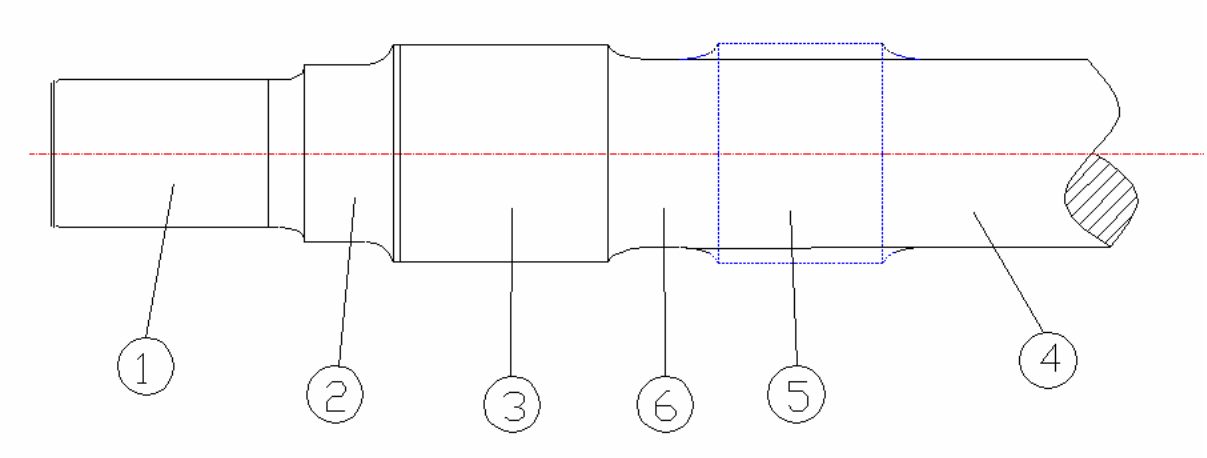

Figure 2-10: Schematic diagram of typical railway axle design and its main features: 1) Train axle , 2) Journal, 3) Collar-bearing surface, 4) Wheel seat, 5) Axle body, 6) Seat for disc, final drive or traction motor, 7) Transition zone between seats [8].

Inspection of hollow axles can be carried out using automated ultrasonic equipment without the need of disassembling the wheelset. However, this is not the case for solid axles where certain parts are not accessible. In this case, the axle will need to be disassembled from the wheels and inspection carried out. Solid axles can also be inspected using ultrasonics. Other techniques that may be employed for axle inspection, hollow or solid, include visual inspection provided any paint is removed and the surface of the metal is visible, LPI, MPI, Magnetic Flux Leakage (MFL), eddy current testing (ECT) and alternating current field measurement (ACFM) testing.

In most cases ultrasonic inspection will be employed since this NDT technique can detect and evaluate defects through the volume of the axle. Other techniques such as MFL, ECT and ACFM are more useful for near-surface and surface-breaking defects. In the case of ultrasonic testing, piezoelectric transducers are used to generate interrogating ultrasonic waves at frequencies of interest. In the case of solid axles inspection is based on scanning the axle circularly around the axle head using a straight beam probe. To achieve 100% inspection coverage in hollow axles, the ultrasonic transducer is used to scan the axle along the inner surface of the bore in a series of combined rotations and axial displacements [27].

Figure 2-11 shows the ultrasonic Inspection of a rolling stock hollow axle using transducers emitting ultrasonic waves.

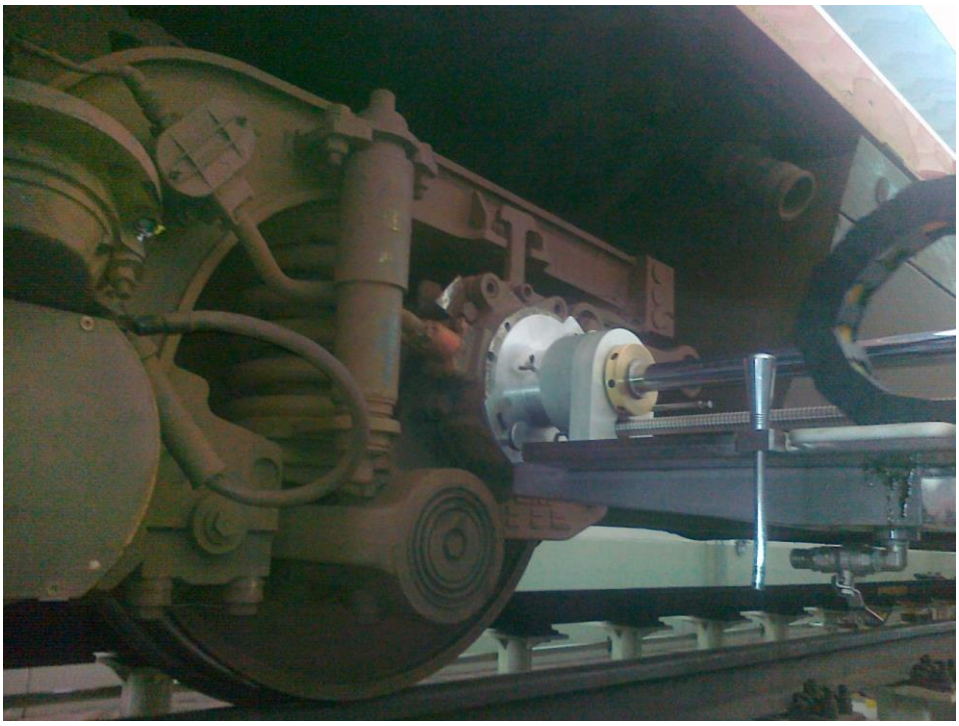

Figure 2-11: Ultrasonic inspection of a rolling stock hollow axle.

2.5 Destructive Quality Control for Railway Wheelsets

Destructive quality control is used to evaluate the steel grade composition, microstructure, cleanliness and mechanical properties during manufacturing of railway wheelsets. This is to ensure that the final product will perform consistently and within the tolerances set when it enters service. In order to carry out the necessary metallography and mechanical testing, specimens are taken from several locations and direction from a new wheelset batch. Mechanical tests carried out for every new wheelset batch include hardness, Charpy testing, fracture toughness, tensile testing, fatigue crack growth and S-N curves [7].

2.6 NDT for Railway Wheelsets

NDT includes a broad range of inspection techniques for the evaluation of different aspects of the wheelsets including surface-breaking and hidden defects, manufacturing irregularities such as large inclusions and evaluation of mechanical properties without changing in anyway the properties or structural characteristics of the component. Various types of NDT equipment based on different physical principles can be employed for quality control of newly produced and in-service wheelsets. NDT techniques employed include visual inspection, MPI, LPI, MFL, ECT and ACFM. Visual inspection can be carried out by using both naked eye and automated equipment such as lasers and cameras for the evaluation of wheel profile as well as the presence of surface-breaking flaws. To reduce the likelihood of catastrophic failure and optimise maintenance regular inspection is necessary. However, it is also necessary to optimise availability of rolling stock and therefore, inspection intervals need to be minimised to the lowest possible level. This also helps to reduce the cost of experience inspection personnel. To increase reliability and decrease the probability of catastrophic failure between inspection intervals RCM techniques are also employed by the rail industry as discussed later.

The most basic NDT method of measuring the wheel tread profile condition is to carry out a visual inspection of the flange height and thickness limit gauge. During visual testing of wheelsets, other components are also examined, including the axle boxes, axle bearings, axle, braking blocks, etc. [28]. The key NDT techniques currently used in wheelset inspection are discussed next.

2.6.1 Visual Inspection

There are existing wayside monitoring technologies that offer both manual and automated measurement tools for assessing wheel or rail dimensions to ensure they pass the minimum

requirements. Wheel profile, diameter, flange thickness, rim width, shelled tread, etc. are included in these measurements [29].

Manual measurements are performed by gauges where it should be done on offline trains and automated system such as imaging and laser measurement are used to monitor in-service trains.

2.6.2 Magnetic Particle Inspection

When a magnet is broken, two separate magnets will form, each with the same north and south orientation as the original magnet. If the magnet is just cracked but not broken completely in two, a north and south pole will form at each crack face. The magnetic flux lines will spread out when they encounter the small air gap created by the crack because the paramagnetic air cannot support as much magnetic field per unit volume as the ferromagnetic material that the magnet is made of can. Hence magnetic flux leakage will occur at the area of the crack. By applying a spray of ferromagnetic particles on the surface of the steel alloy (also ferromagnetic) that a wheel or axle is made of, surface-breaking or very near-surface flaws can be found based on the detection of any magnetic flux leaking. If there is no crack present, the flux lines produced by a powerful shoe-horse like electromagnet will remain contained within the steel alloy. However, in the presence of a surface or very near-surface crack some flux will leak. At the area where the flux leakage occurs the ferromagnetic particles applied on the surface of the steel will be attracted to close the gap generating a visual indication. In the case where the flaw is only very near to the surface but not surface-breaking the indication may be ambiguous so inspection by a suitable alternative method may also be required. Hence, MPI can be considered as a combination of two distinct NDT methods; MFL and visual inspection [30]. MPI is usually integrated with UT to provide overall inspection of the wheel and axle. MFL, ECT or ACFM can be employed instead if the inspection procedure needs to be automated rather than carried out manually [31]. Figure 2-12 shows a schematic of this method.

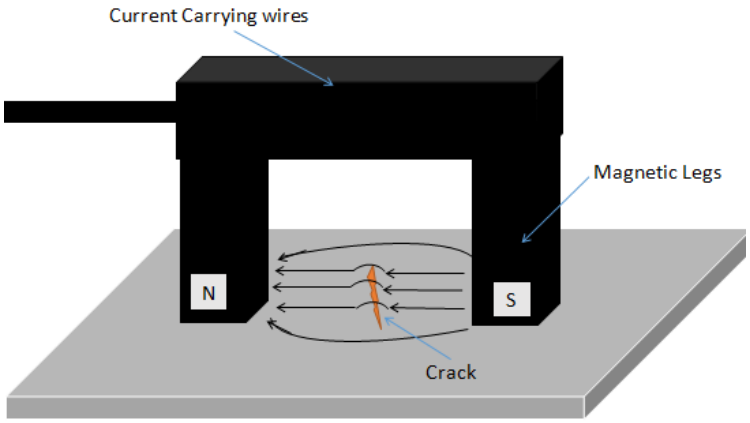

Figure 2-12: Schematic of magnetic particle inspection.

2.6.3 Magnetic Flux Leakage

In this technique, a powerful magnet is used to magnetise the sample. If there is any crack or corrosion in metal on the surface or near the surface the magnetic field will leak from the sample like in MPI. A coil sensor or Hall probe can then detect the flux leakage and its severity. The operator then needs to interpret the recorded signal in order to evaluate the severity of the defect, its nature and severity. Unlike MPI, this technique is more sensitive and can be used for detecting deeper flaws with increasing level of magnetisation [28]. However, this technique is not sensitive to very deep defects and UT needs to be used instead. MFL is particularly useful for the rapid inspection of axles for the presence of corrosion. Figure 2-13 shows the principle of MFL technique.

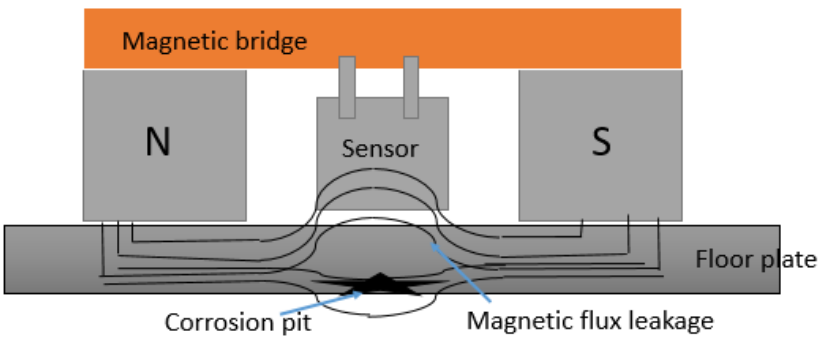

Figure 2-13: Principle of operation MFL technique [32].

2.6.4 Ultrasonic Testing

Conventional ultrasonic testing (UT) of a wheelset begins with transporting the wheelset from storage to the testing station. The UT probe is then moved down to the wheel. Normally, a suitable couplant based on water or water-based gel will be used to minimise UT losses and increase sensitivity to smaller defects during UT. Depending on the wheel geometry, different angle probes are used to make shear waves (25° to 55°) [33].

Ultrasonic Phased Arrays are a more advanced version of ultrasonic testing applicable for both wheel and axle inspection. Despite the fact that ultrasonic phased arrays are much more reliable and faster than traditionally used UT equipment, they can still miss surface-breaking defects, which means that wheelsets also need to be inspected using either Eddy current probes or, more commonly, MPI [34]. Ultrasonic phased arrays are also bulkier and more expensive but can focus or steer the interrogating ultrasonic beam to the location of interest without changing the position of the probe itself. This is particularly useful when the axle has not been removed from the rest of the wheelset.

Hackenberger [33] suggested a technique based on immersion UT for the detection of defects in wheels. It was found that shear waves are more sensitive to the presence of defects when compared with longitudinal (compressive) waves.

The electromagnetic acoustic transducer (EMAT) is an ultrasonic transducer for non-contact sound generation based on magnetostriction and Lorenz force interactions within the inspected material. Although, there is no need for application of couplant when EMATs are employed, the signal amplitude is much lower in comparison with that of a piezoelectric transducer and as a result signal to noise ratio is poor. EMAT is only preferred if inspection needs to be carried out at speed without any contact with the test piece. It can also be used at very hot environmental conditions or when couplants cannot be used due to the possibility of a chemical reaction occurring. EMATs can be used for in-service inspection of the rolling surface of the wheels in high-speed trains. The photograph in figure 13 shows an EMAT-

based system installed on-track for the online inspection of the rolling surface of wheels for the presence of RCF. The illustrated system has been reported to be capable of detecting critical defects when the train passes over the ultrasonic transducer [1].

Figure 2-14: EMAT-based system installed on-track for the online inspection of the rolling surface of the wheels [1].

Residual stresses in the rim of the wheel can develop during the manufacturing process of wheels. High residual stresses coupled with the interaction at the wheel-rail interface can cause early wear, shelling and early initiation of RCF cracks. UT based on ultrasonic wave velocity and ECT based on relative magnetic permeability changes can be used for effective evaluation of residual stresses present in the wheel material [35].

2.6.5 Eddy Current Inspection

When a coil fed with an alternating current is brought near a conductor eddy currents will be generated due to electromagnetic induction. When alternating current is applied to the coil, a magnetic field develops in and around it. The alternating magnetic field generated expands as the alternating current rises to maximum and collapses as the current drops back to zero. The interaction of eddy currents generated in the test piece with any flaws present will cause variations in the secondary electromagnetic field produced by the eddy currents giving rise to impulse changes. Hence, the eddy current effect can be used for crack detection and qualitative evaluation of their severity. ECT can also be used for, material identification,

coating thickness measurements as well as the presence of residual stresses. ECT depending on the frequency employed is able to detect surface and near-surface flaws [28].

2.6.6 Alternating Current Field Measurement Inspection Technique

ACFM is another electromagnetic technique which is very similar to ECT. An AC electric field inducer is placed on or near the surface of the sample. When no defects are present, the induced AC field flowing near the thin skin of the test piece results in generation of a uniform magnetic field above the surface. Any defect present will disturb the uniform current field lines, forcing them to flow under and around the edges of the flaw. This causes the magnetic field to become non-uniform, and sensing coils in the ACFM probe placed at X and Z orientations can detect these variations in the magnetic field. The advantages of ACFM are that inspection is less sensitive to probe handling whilst accurate evaluation of the size of the cracks can be achieved as long as they do not have complex geometry. However, ACFM can only be used for the detection of surface-breaking defects unless special setups are employed. In addition, smaller defects are more difficult to detect as larger size of inducer results in lower sensitivity [36]. Figure 2-15 presents an example of current flow around a defect.

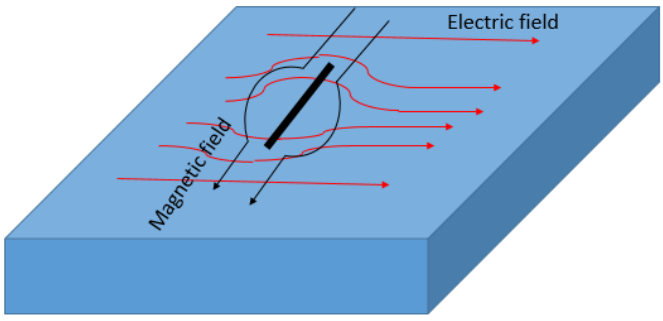

Figure 2-15: Example of current flow around a defect [37].

2.6.7 Lubricant Analysis

Lubricants play an important part in the bearing performance by reducing friction, minimizing wear and controlling the heat generated as the metal surfaces roll against each other. Effective lubrication can help maximise the design lifetime of rotating components including axle bearings [38]. Lubricants can degrade with time particularly when exposed to higher temperatures. Contamination with water and wear particles can similarly reduce the fatigue lifetime of bearings and cause the initiation and subsequent propagation of structural defects. Lubricant analysis can be effective in detecting bearing problems at their early stage by identifying the wear particle density within the lubricant or the presence of moisture. This test requires that the axle box is opened so lubricant can be collected. Then the retrieved samples are sent to the laboratory for further examination. Special care needs to be taken when collecting lubricant samples to avoid external moisture from entering into the sample giving rise to erroneous conclusions. Collection of lubricant samples is a relatively inconvenient and time consuming process [39].

2.7 Summary

In this chapter, railway wheelsets material and its components have been introduced, in addition, different types of defects and their possible causes have been reviewed. In the final section, destructive and non-destructive techniques used to examine the wheelsets in offline mode have been discussed.

The next chapter describes the current state of work to monitor the in-service train wheelsets.

Chapter 3 : Remote Condition Monitoring Techniques for Railway Wheelsets

Remote Condition Monitoring (RCM) of railway wheelsets offers distinct advantages over state of the art techniques based on conventional inspection processes. RCM, apart from providing an extra layer of defence against potential catastrophic failure of in-service wheelsets, it can help rolling stock operators increase the efficiency of their maintenance procedures. Therefore, RCM techniques provide an effective tool when applied correctly for increasing rolling stock RAMS. Moreover, RCM can also assist rolling stock operators in implementing efficient maintenance strategies based on condition or prediction, hence optimising resources and maximising the availability of rolling stock. In the following sections the most common RCM techniques currently used in railway networks across the world are discussed, including the UK.

3.1 Wheel Impact Load Detector

The shape and size of flats or shelling, wheel and rail profiles, axle load, vehicle speed and rail pad stiffness affect the impact load amplitude. Rubber rail pads are used in order to reduce vibration and noise generated by rolling stock, minimise impact damage on the rail track and prevent cracking of the concrete sleepers, where applicable [9]. An example of a typical rubber rail pad is shown in Figure 3-1.

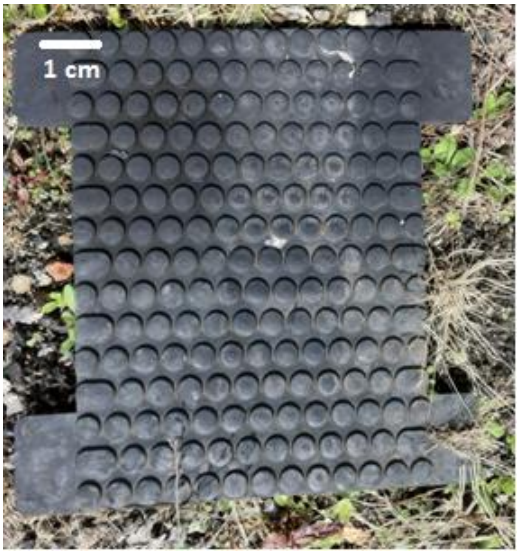

Figure 3-1: Photograph of a typical rubber rail pad.

Wheel Impact Load Detectors (WILDs) are devices which can detect the impact loads generated from the wheels of the train while it travels over them. Such systems apart from alerting the train drivers of any wheelset problems detected in time so appropriate action can be taken, they also help prevent structural damage on the rails. Wheel defects such as flats, shelling and out-of-roundness can cause the generation of high impact loads which apart from damaging rail infrastructure can also act as precursors to damage initiation in axle bearings. . Most WILD systems are based on the use of strain gauges micro-welded to the rail. The strain gauges measure the strain sustained by the rail as rolling stock goes over. Then the applied load can be calculated through a mathematical equation that relates it to the induced strain on the rail. Normally, it is also necessary to compensate for temperature variations and therefore the temperature of the rail should also be monitored. Accelerometers can be used as alternative sensors to strain gauges. In this case, vibration levels are used instead in order to relate them to actual impact loads sustained using a suitable mathematical formula such as:

$$\sum F(y) = F(t) - kx - Cv = ma$$

where k is stiffness of the structure, x is the displacement, C is the damping coefficient, m is mass, v in the velocity and a is the acceleration [40].

Each axle that goes over the instrumented site is measured and identified. If the preset threshold is exceeded an alarm is given. In extreme cases of excessive impact load amplitudes the driver may be asked to stop the train to prevent excessive damage on rail infrastructure and subsequently asked to proceed slowly to the nearest siding in order to have the affected wheel replaced [41]. High-impact wheels are most often wheels that have a flat spot on the tread surface, known as a slid flat [5].

WILDs also contribute to the noise reduction of railway operations. Flats, shelling or out-of-roundness result in excessive noise which is particularly undesirable when travelling through urban and suburban areas. Especially at night when freight rolling stock tends to operate most, such defects can increase the noise produced by moving trains resulting in operational restrictions being implemented to mitigate this problem. Also detecting wheel tread defects timely helps increase passenger comfort as well as quality of service for sensitive freight products moved over rail. The schematic in Figure 3-2 shows the basic principle of a WILD system when a train passes over an instrumented site. The system comprises of strain gauges or accelerometers, power supply, digital data acquisition card (DAQ) and signal processing unit. The signal processing unit analyses the voltage amplitudes generated by the sensors and relate them to an actual axle load. Subsequently, the axle load amplitudes measured for each wheelset are transmitted to a Supervisory Control and Data Acquisition (SCADA) centre. When an alarm is generated, appropriate signalling station is notified and the signallers subsequently inform the driver of any action that is required to be taken in order to resolve the issue and permit the train to continue towards its intended destination [42]. Although WILDs are not able to detect axle bearing faults, they are particularly useful in minimising the occurrence of impact loads that can result in crack initiation and crack propagation up to 100 times faster than normal [5]. Also, since wheel tread defects are

known to be a precursor to axle bearing faults, detection of such wheel defects may enable more careful evaluation of the axle bearings of any wheelsets affected.

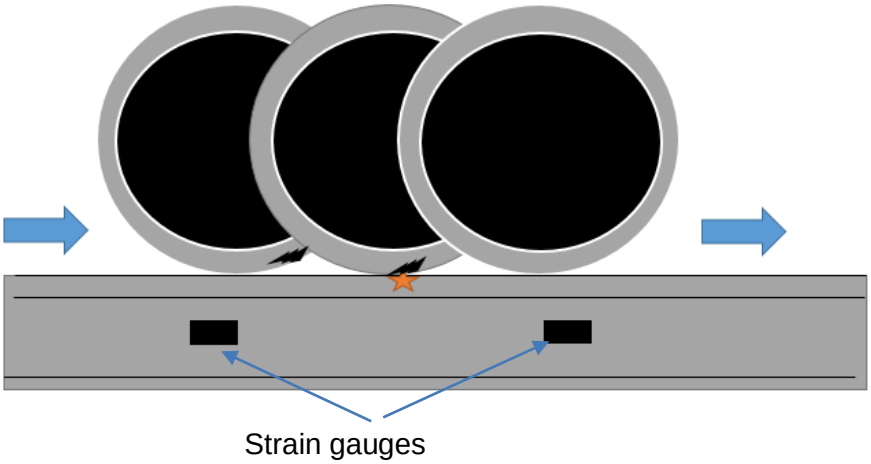

Figure 3-2: WILD System [41].

3.2 Wheel Profile Detector

Wheel Profile Detectors (WPDs) are based on the use of scanning lasers in order to determine the exact profile of the wheel tread. All the information is then compared against standard healthy profile. The use of WPDs eliminates the need for manual profile inspection [42].

WPDs are real-time measurement systems using a combination of lasers and video cameras to automatically measure the wheel profile while rolling stock is in motion. WPDs are mounted wayside in the track area. The system acquires relevant data and analyses them. Some prediction is also possible with respect to the time remaining prior to re-profiling. The data acquired from WPDs include, wheel profile and wear, wheel diameter, height and thickness of the flange, back-to-back distance and wheel inclination [43].

3.2 Hot Box or Hot Axle Bearing Detectors

Hot Axle Box Detectors (HABDs) use infrared sensors which are installed on the track in order to detect any failed axle bearings. HABDs have been in use for a few decades and are basically a last line of defence system which is able to detect failed axle bearing from their increased temperature. Once a HABD detects an axle box with a temperature above the preset threshold an alarm is given to immediately stop the train. The reporting approach is the same as for WILDs. The HABD measures the axle boxes of passing rolling stock as they move over the instrumented site. If an alarm is given the relevant signalling station is informed. The signallers then advise the driver of the affected rolling stock to stop the train and proceed at slow speed to the nearest siding for further investigation of the problem. Unfortunately, HABDs are prone to errors since they are affected by the heat signature of the environment around the axle box. Hence, a brake event slightly before passing the instrumented section may result in higher temperature being reported. Normally, the signallers will continue monitoring the affected train until the next instrumented point before allowing it to progress at normal speed when a false alarm is suspected.

Complete HABD systems apart from monitoring the axle box temperature, are also able to measure the temperature of the wheel or disk brakes of passing rolling stock [44]. HABDs which are able to monitor other components in addition to the axle box are generally more expensive but also add to the usefulness of these trackside systems.

For high speed trains with operational speed >250km/h onboard axle box temperature sensors are required to be installed by law [45]. When onboard temperature sensors are available train operators have to review the activation records of on-vehicle hot axle detectors and HABDs at regular agreed intervals in order to identify trends and incidents that could compromise safe running.

The distance between two HABDs is normally based on the available budget to buy, install and maintain such systems, the type of rolling stock travelling along a particular line (mixed, passenger or freight only), the operational speed, traffic density and distance between stops [46]. The schematic in 6 shows an example of a HABD.

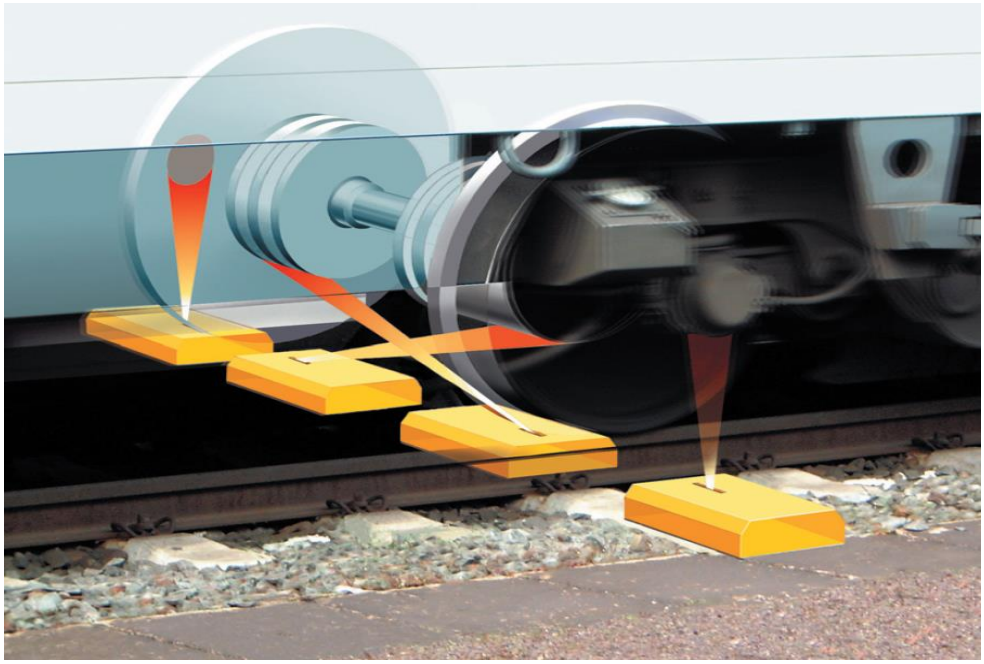

Figure 6: The infrared sensors installed at defect detector locations [47].

3.4 Trackside Acoustic Array Detectors

Trackside acoustic array detectors (TAADS) make use of arrays of high-fidelity microphones used to listen to the audible noises produced by the axle bearing of passing rolling stock. The operating frequency of the microphones is normally between 22-44 kHz. This means that they are prone to errors arising from the sounds of the surrounding environment as well as the measured train itself (e.g. wheel flats or noise from the engine).

Wayside acoustic detectors determine the noise produced by the bearing as the vehicle passes permitting its inspection without having to disassemble the bogie. There are a number of commercial products available such as (RailBAM) and Trackside Acoustic

Detection System (TADS). Such systems should be more effective than HABDs since they are supposed to be able to detect developing bearing faults at an earlier stage. Moreover, they are able to trend individual wheelsets over time every time they pass from the instrumented site. Unfortunately, there is no sufficient evidence available in the literature proving the operational capability of these systems. The author of the present study has been unable to find any signals acquired from TAADs that indicate reliably the presence of an axle bearing fault. Figure 3-3 shows an example of a TAAD.

Figure 3-3 : The trackside acoustic detector system [48].

TAADs have been extensively used in Australia, the U.S. and Canada. In the UK and in some parts of Europe their application on the rail network has been more recent and are yet to be deployed widely. Although TAADs are generally more expensive than HABDs per instrumented site, fewer systems are required to be deployed over the network This is due to the fact that TAADs are supposed to be able to detect axle bearing defects earlier thus permitting sufficient time to carry out maintenance before catastrophic failure occurs. However, since TAADs are not able to detect all axle bearing defects with the same efficiency, HABDs should still be employed.

Another drawback of TAADs is the clearance required for the microphone arrays to be installed, The housing structure that needs to be installed trackside is of substantial size and this can be particularly problematic when a third rail is present or when the clearance between two lines is too small (e.g. four-foot).

3.5 SKF Axletronic

SKF is one of the leading axle bearing manufacturers. SKF has recently developed an integrated onboard condition monitoring system for monitoring railway axle bearings in real-time. Apart from using the standard temperature sensor, the SKF Axletronic system combines vertical and/or lateral acceleration measurements. In its original concept, this system also incorporated an AE sensor but the most recent design has focused on the use of a temperature sensor and accelerometer only probably to simplify data acquisition requirements and reduce overall cost. The SKF Axletronic can be installed in axlebox bearing units or axlebox front covers and can provide continuous feedback about the bearing condition [49]. Figure 3-4 shows SKF Axletronic sensor systems installed onto the bearing seal as an integral part of the bearing unit.

Figure 3-4 SKF Axletronic [49].

Unfortunately due to the cost of the SKF Axletronic system, its use is probably only cost-effective and justifiable primarily for high-speed trains. Nonetheless, other passenger trains could also be instrumented with this system. However, in the case of freight rolling stock due to the rolling stock nature as well as the small margin of profit freight leasing companies and freight rolling stock operators have, the cost of this system is currently prohibitive.

3.6 Perpetuum

Perpetuum's self-powered, wireless sensing technology is an under developing system which makes a use of combined vibration energy harvesting and real-time wireless sensing. The purpose of the system is to provide real time information that enables the rail industry to monitor the wheel bearings and wheels. Since the railway is a 'natural' source of vibration, this vibration can be harvested to enable the sensor nodes to be self-powered. These sensors can provide many benefits in terms of longevity and ease of installation [50].

3.7 Problems of Existing Technologies

Conventional wayside monitoring techniques currently employed by the railway industry are although beneficial they are also expensive. In the case of WILDs and WPDs reliable operation has been proven in the field already. HABDs remain inefficient since they are still prone to false alarms and involve a high cost but they offer infrastructure managers and rolling stock operators a last chance to prevent a catastrophic derailment when things have gone wrong already. TAADs can improve reliability by potentially being able to detect axle bearing faults at earlier stages. However, it has been difficult for the author of the present study to find satisfactory scientific evidence that proves the operational capability of these systems.

There is a clear need of novel low-cost systems that are able to identify reliably axle bearing faults and wheel defects at an early stage. They can also identify wheelsets affected by severe faults to be removed in-time, while at the same time allow wheelsets with less severe faults to safely remain in service for slightly longer and until suitable maintenance can be carried out [5].

Furthermore, by minimising installation complexity on the network can substantially increase the market potential of these new wayside systems.

HABDs as mentioned earlier are the most common wayside monitoring systems used for the detection of faulty axle bearings in-service. However these systems cannot detect damage at its early stages, since when temperature rises to levels above the alarm threshold set the axle bearing has already practically failed and there are only a few minutes left before it seizes completely. Once the axle bearing has seized, the wheel blocks giving rise to abnormal motion and loading pattern of the affected wheelset. Eventually these abnormal loads are high enough to cause rupture of the axle and result in derailment of the train. In some cases overheating bearings may not be detected at all due to environmental conditions or other causes. In particular, current HABD systems may miss overheating roller bearings [51]. Due to their relative high cost, hot box detectors are usually spaced at relatively great distances from one another (as much as 30 km apart or even more); hence faulty axle bearings can seize at any time in between and result in a derailment [52]. Early detection of bearing defects could prevent derailments associated with axle bearings faults in the future and thus permitting efficient preventive maintenance instead of corrective and emergency maintanance actions. Hence, the development of a reliable, effective and cost-efficient condition-based strategy for monitoring and diagnosing axle bearing faults at an early stage is necessary for railway industry.

TCII has estimated that TAADs are able to detect at least 35% of hot bearing failures based on the current capabilities of such systems [53]. However, TAADs still face operational

challenges in detecting less severe defects, especially in inboard bearings. This system relies on the detection of an acoustic signal which is generated far away from the sensors. Therefore constructive and destructive interference and attenuation of the acoustic waves can affect the reliability of TAAD measurements.

Despite the important advances in trackside monitoring technology techniques, at present, there is no system that can reliably detect axle bearing faults early enough, at low cost and with minimum intervention required for installation and maintenance [54].

3.8 Summary

In this chapter various condition monitoring techniques commercially available in the market for the railway wheelsets were described. It was concluded that the current condition monitoring techniques such as HABDS and WPDs are not suitable for early bearing fault detection. In addition in TAADs system, despite having the potential of early fault detection, it has been difficult for the author of the present study to find satisfactory scientific evidence that proves the ability of this system to detect the bearing defects. Therefore, because of the possibility of failure in detecting a defective bearing in the conventional approaches, and also their high installation and instrumentation costs, there is a need to develop a new condition monitoring system in this area.

Chapter 4 : Vibration and Acoustic Emission Inspection Techniques

Vibration is a mechanical phenomenon that occurs when an object executes an oscillatory motion about a position of equilibrium. Vibration signals from rotating machinery provide information about the cause of vibration. Hence, this technique can be used to detect early precursors to machine failure, allowing damaged machinery components to be repaired or replaced before an expensive or catastrophic failure occurs [13, 55].

Free vibrations occur when the system is disturbed shortly and then allowed to move without restraint. Forced vibrations happen when the system is continuously pushed by an external stimulus. This leads to a phenomenon called resonance frequency which occurs when the driving frequencies approach natural frequency of free vibration. The result is a rapid increase in vibration amplitude.

Direct detection of bearing vibration signals and spectral analysis of vibration signals from defective bearings in rotating machinery is a well-developed technology and widely used in many industries. When a ball rolls over a defect, it produces an impact which results in a vibration and sound pulse. The amplitudes of these pulses differ depending on the rotational speed, size of the defect and bearing loading conditions [56]. Examples of vibration applications are electronic motors and industrial pumps. Detecting axle bearing faults in railway rolling stock is an application which has been under development so far.

In the research study conducted during the IDEA safety project, the objective was to investigate if the accelerometers on the rail had a sufficient signal-to-noise ratio to allow reliable diagnosis of the condition of the axle bearings. Two different series of tests including onboard with promising results and wayside were carried out during the experiments. Wayside measurements could not reveal the bearing defects as the background noise

severely masked the defect-related signals which had attenuated during transmission from the bearing to the rail [57].

Piezoelectric accelerometers

Industrial piezoelectric accelerometers are the first choice for most vibration measurements since they have a wide frequency response, good sensitivity and performance and are easy to install. The frequency range of the accelerometer used varies widely depending on type of application [58]. However, typically the operational frequency range in most cases is between 5 Hz and 10 kHz. Figure 4-1 shows a sketch of an accelerometer with internal components.

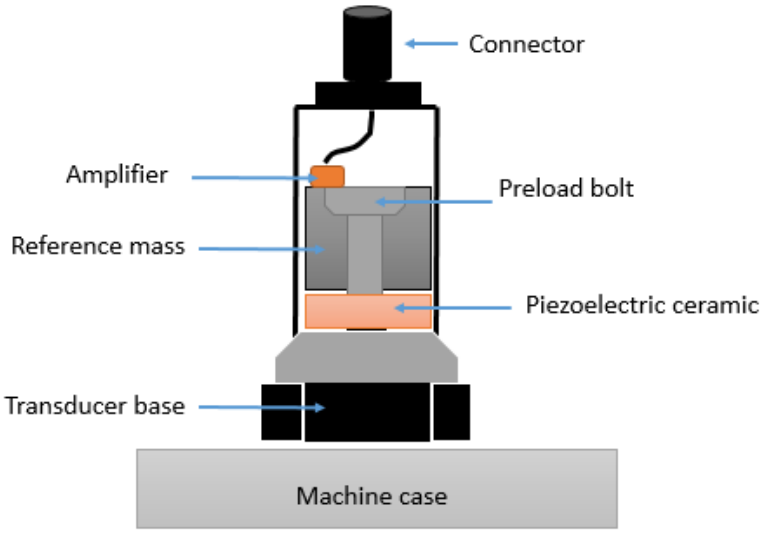

Figure 4-1: Accelerometer with internal components [59].

Acoustic emission (AE) is a structural health monitoring technique which is conventionally defined as the generation of elastic waves made by a sudden redistribution of molecules inside or on the surface of a material [60]. When an external stimulus such as temperature or load is applied on a material it will cause it to deform elastically. The released energy

produced by this deformation will be in the form of stress waves which can be recorded by piezoelectric AE sensors due to the displacement they cause on the surface of the component being monitored. Sources of AE can vary from an earthquake caused by a fault in the earth's crust to small cracks propagating in a component [61]. Other applications of AE include monitoring welding joints, bridges, railways and aerospace structures manufactured from different materials including alloys, plastics and composites [62]. Less often AE has been used for monitoring rotating and reciprocating machinery, in most cases as a supplementary technique to vibration analysis.

Although the principles of AE testing have been known since antiquity, the application of AE as a modern CM technique for detection and evolution of damage in structural, rotating and reciprocating components is fairly recent. The number of published studies on AE has increased drastically from 1960 onwards indicating strong interest in this particular CM technique [63].

AE was originally developed for non-destructive testing of static structures but over the last 35 years, its applications have been extended to monitor dynamic structures including rotating machines. Due to the high sensitivity AE sensors exhibit in comparison with traditional techniques, earlier detection becomes possible. This is particularly important for any CM technique since the ultimate objectives are to enable effective use of the data generated for optimised planning of maintenance scheduling as well as minimising the likelihood of unexpected failure. However there are some limitations which are discussed later in this chapter [64]. Catlin [65] noted that high frequency AE signatures attenuate rapidly. Thus it is important that AE sensors are positioned as closely as possible to the component of interest where a defect might develop. As an example, it is often practical to place the AE sensor on non-rotating member of the machine, such as the bearing or gear casing.

Detection of the AE signals can provide valuable information about the structural health of materials and components. Hence, AE has a broad range of industrial applications. Since the AE technique is passive, unlike most other NDT methods, it does not inject any energy of any form to the object under examination. Instead AE sensors are used to detect surface displacements caused by the stress waves emitted from the source of interest (i.e. energy released) which through the piezoelectric effect are then converted to electric signals that can be visualised after digitisation. Under certain conditions, AE data analysis can provide an immediate indication with respect to the risk of occurrence of failure of in-service components being tested with this technique [66]. Although results from AE testing can detect how much damage has been sustained by a structure or component, this technique is not able to estimate the size or shape of a defect. In order to obtain an overall picture of the actual nature of the defect detected other NDT methods should be used to supplement the information obtained from AE testing.

The use of AE for health monitoring of rotating machinery can provide a significant improvement over standard vibration analysis techniques even in inherently high-level noise environments. Low frequency vibration signals associated with bearing defects can be masked by low frequency environmental noise from the surroundings. However, stress waves emitted at much higher frequency ranges can provide a clearer indication. Moreover, continuous monitoring can safely allow the evaluation of damage evolution within a system or component while in-service. In vibration analysis, it is normally necessary that defects reach a certain level of severity that is sufficient to cause changes in the resulting vibration signature in order to be detected. Therefore, the sensitivity of vibration in comparison with AE is by default lower [67]. In addition, by the time a significant change in vibration has been observed the remaining operational or useful life of the bearing may be short so the time window available for necessary maintenance may be very small before final failure occurs.

The frequency bandwidth in typical AE measurements is typically in the range of 20 kHz to 1 MHz although in most cases it is more useful to focus in the range between 100-500 kHz

[62]. The AE signal excitation arising from bearing defects is a broadband phenomenon which produces stress waves in a wide frequency range, particularly above 100 kHz. Therefore, AE signals have often a signal-to-noise ratio which is noticeably higher than that obtained with standard low frequency vibration monitoring. This allows the presence of a bearing defect to be detected significantly earlier [68].

Raw AE data sometimes may not be sufficient to provide reliable indication regarding the actual condition of a system or component being monitored. In this case, AE signals need to be filtered prior to carrying out any further evaluation. The details about filtering and signal processing of vibration and AE signals are discussed in the following chapter.

AE has several advantages. Firstly, it is a relatively low cost technique since large structures and machines can be monitored with relatively few sensors. It is a reliable process which has been standardised and appropriate certification procedures exist like in the case of vibration analysis. AE monitoring can be used to monitor high speed applications including axle bearings in railway rolling stock which are also the main interest of this study. Installation of AE sensors is fast and easy with minimal surface preparation required. Moreover, sensors can be attached using simple magnetic hold-downs or adhesives such as araldite. More importantly the installation of the AE sensors is non-invasive. AE as a technique has higher sensitivity in comparison with conventional vibration testing enabling early detection of developing faults.

Like any other NDT technology, there are some drawbacks associated with application of AE as a diagnostic tool. As such, the AE signals are subject to attenuation as they travel over distance and through different interfaces. Hence, it is always desirable to mount AE sensors as close as possible to the area where the emission source is expected, i.e. where damage may occur. Furthermore, different sources may give rise to AE activity at the same time, making location and identification of different sources a rather challenging task which can only be addressed through the use of appropriate signal processing techniques [69]. Piezoelectric sensors can also be sensitive to electromagnetic interference (EMI) which if

present needs to be addressed as it can give rise to artefacts in the signals captured. This particular problem can be addressed by grounding the sensor but this may not always be straightforward. The temperature limitations of the AE sensors used need to be taken into account when applying this technique. Therefore, for high temperature applications above 150°C the type of piezoelectric crystal employed should be chosen according to its Curie temperature [70].

Within the framework of this study AE was employed in combination with vibration analysis for the evaluation of wheel tread and axle bearing condition of railway rolling stock. The formation of subsurface cracks due to the stress induced by the rolling action of bearing elements in contact with the inner and outer races will generate AE activity. Also surface-breaking defects impacting on the opposing surfaces of the bearing (e.g. races or rollers) will also give rise to high energy AE signals which can be detected in time. Other types of faults detectable with AE include deterioration of the lubricant quality including lubricant breakdown, foreign matter in the lubricating medium and moisture ingress. Figure 4-2 shows the main aspects of the AE technique from source to data visualisation and subsequent analysis.

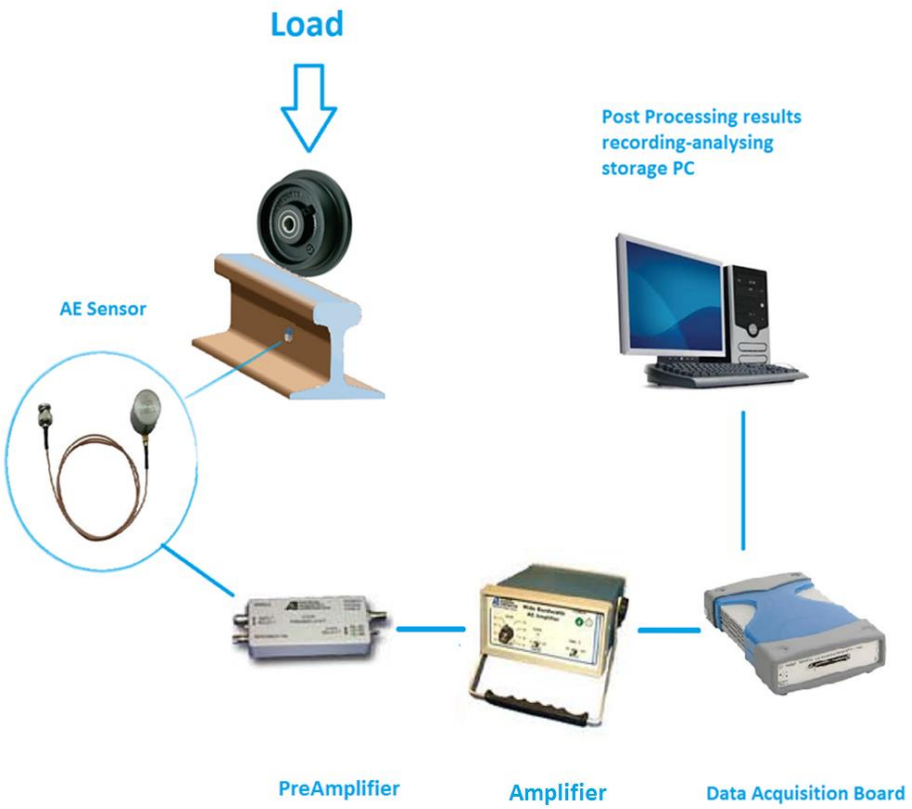

Figure 4-2: The AE Inspection process. AE waves from the wheel are detected by the piezoelectric sensor. The detected AE waves are converted to electric signals that are amplified and subsequently digitised using an appropriate data acquisition board.

4.1 Theory and Basic Principles of AE

AE can arise from sources as small as dislocation movement during elastic deformation of materials. AE waves are also detectable when plastic deformation occurs due to loading a material above its yield point. The sensitivity of an AE system depends on the amount of background noise (undesired signals received by the sensors). Attenuation will also happen because of damping of ultrasounds, scattering and reflections as the waves travel through the various interfaces present between the source and the location of the sensor. Therefore, the intensity of detected AE signals will be lower with increasing distance although the level

of attenuation will depend on the material type as well as the coupling quality of the sensor. The AE signals after amplified are digitised using a data acquisition card and subsequently are logged, displayed and analysed using suitable computer and software [71].

In order to acquire AE signals two different data capturing approaches can be employed. The first approach referred to as Hit Driven Data (HDD) technique, is threshold and time controlled. In this case, AE data are only acquired when the signal voltage exceeds the present threshold and timing parameters. The second approach, referred to as Time Driven Data (TDD), is independent of any threshold setting and the entire waveform is captured over a present time period which can range in duration from a fraction of a second to continuous. In both HDD and TDD the AE signal are recorded at a predetermined constant sampling rate which is normally dependent on the frequencies of interest during testing. Choosing correctly the sampling rate is very important as it can influence profoundly the quality of the data captured. In both approaches, basic AE parameters can be evaluated and acquired upon collecting the AE waveforms. Among the HDD parameters, some of the most commonly used are amplitude, duration, and signal strength [72].

AE sensors are typically piezoelectric sensors manufactured from ceramic materials such as lead zirconium titanate (PZT). However, in certain advanced applications non-contact Electromagnetic Acoustic Transducers (EMATs) or laser interferometers can be used instead. For high-temperature applications alternative ceramic materials can be used instead. In piezoelectric materials, the mechanical strain causes changes in the polarisation of the crystal giving rise to an electric signal. Certain AE sensors may employ an integral pre-amplifier. Sensors with integral pre-amplifiers do present certain advantages however, they also involve bulkier and heavier sensors which may not be always appropriate. In addition, such sensors only allow a single amplification level which may not be sufficient depending on the type of application considered. AE sensors can be classified according into their frequency response to resonant or wideband frequency sensors. Wideband

sensors exhibit a relatively flat response over a wide range of frequencies whilst resonant sensors exhibit higher sensitivity at resonance frequencies. The exact resonance frequencies depend on the geometrical characteristics (thickness) of the piezoelectric crystal. In noisy environments, it is always desirable to choose a resonant sensor rather than a wideband in order to reduce the effect of noise outside the frequencies of interest. . As mentioned earlier, AE sensors can operate up to a certain temperature above which the Curie point of the crystal is exceeded and polarisation is lost. Different piezoelectric materials have different Curie points but also their sensitivity and structural reliability need to be considered as well when considering them for an application.

Important parameters of AE signals include, the peak signal amplitude, signal threshold which differs depending on the application, energy, signal duration, counts (the number of AE peaks that exceed the preset threshold), and the average frequency of the entire AE signal.

A number of phenomena take place when AE waves propagate along the structure. Attenuation causes the decrease in AE amplitude due to energy lost. This energy loss can be caused from dispersion, diffraction, scattering or reflection of the signal at the various interfaces. Dispersion happens because of the different frequencies comprising the AE waves resulting in different speed of propagation. Diffraction and scattering occur due to deflection or bending of the waves passing through a discontinuity such as grain boundaries, inclusions, cracks, holes and sharp edges [73].

Sources of AE in rotating machinery include impacting, cyclic fatigue, friction, turbulence, material loss, cavitation, leakage, etc. As an example, moving of bearing rollers over a defect in the outer race will result in generation of AE waves due to impact. These waves propagate on the surface as Rayleigh waves which are detectable with AE sensors. Rayleigh waves are a combination of longitudinal and transverse waves, causing up and

down and side to side oscillations of the surface of the material in the same direction that the wave is moving [74].

There are two primary mechanisms of AE wave generation in the case of bearing applications. The first one is subsurface crack growth which might occur when rolling elements are in contact with the raceway at the defective zone. The second type is due to defect impacts such as a spall in the roller with the rest of the bearing structure [75].

4.1.1 Installation of AE sensors

The type of installation of AE sensors depends on the application. For example glue is commonly used for pipe inspection, magnetic hold-downs are usually used in metallic pressure vessels, rolling sensors used for the inspection of moving applications and welded or mechanical holders used in high temperature applications. In this study, magnetic hold-downs are used in both onboard and wayside measurements carried out during experimental work.

4.1.2 AE sensor calibration

In order to calibrate AE sensors, a known source which produces acoustic signal of known amplitude and shape should be used. An ideal calibration source generates waves with a broad range of frequencies into the test specimen and contains a smooth frequency spectrum over the entire range [76]. Mechanical sources such as pencil lead break (or Hsu-Nielsen source as so often referred to), capillary fracture and metallic ball impact are ideal because they can generate reference AE waves with all the above characteristics [77].

Calibration of AE sensors in this project has been carried out using pencil lead breaks. This calibration process involves the breaking lead tip (3mm long, either 0.3 or 0.5 mm in diameter and 2H in hardness) using a simple mechanical pencil. When the pencil lead is pressed and broken against the test piece, an impulse AE signal very similar to signals

produced by a crack is released over a very broad range of frequencies ranging from a few kHz all the way to several MHz. This simulation can be very helpful to determine the reproducibility of AE transducer response and ensure that coupling of all sensors to the test piece is consistent [27].

4.1.3 AE sensor coupling

Correct coupling of an AE sensor to the surface of the material being tested is one of the most important aspects of this technique. The couplant is used to remove the air between the sensor and material interface arising from roughness as well as reduce the effect of acoustic impedance mismatch between the test piece and the sensor interface. The acoustic impedance (ratio of acoustic pressure flow) of air is much lower than that of the sensor face or material face causing loss in transmission. Hence, to facilitate the transmission of sound waves between the transducer and the piece being tested it is necessary that a suitable coupling is used [78]. Due to the nature of the AE test which can be carried out over prolonged time periods it is very important that a suitable couplant is selected. For example, water-based gels which are applicable in standard ultrasonic testing may not be applicable in AE testing where the structure needs to be monitored over several days or weeks at varying temperatures. The piezoelectric crystals which are commonly used for AE sensors have high acoustic impedance. If a couplant cannot be used in a particular application, a very high force must be applied on the sensor to improve the transmission. However, using couplants will always ensure better transmissibility [79]. Alternatively, contactless EMAT sensors could be employed but the signal to noise ratio of these sensors is much lower than piezoelectric elements.

There are a number of couplant types to choose from, typically liquid, gel, grease or dry elastomer couplants. Other types of couplants based on compounds or adhesives can be used which provide bonding of the sensor to the surface. Choosing the right couplant depends on the type of measurement, whether the sensor is going to be permanently

bonded, possible corrosion between the couplant and the surface of the material being tested, surface condition, and the environmental conditions such as temperature and humidity [80]. Grease and Vaseline are used to couple AE sensors to the rail track or bearing case in this project. A thin layer was applied in order to achieve better results. This was done by applying a small amount of couplant to the centre of the sensor face and uniformly pushing the sensor down on the surface of the material.

Some surface preparation is also necessary. Loose paint or oxidation layers can affect the transmissibility of the AE signal from the test piece to the sensor. Flatter and smoother surface will generally result in better coupling quality. After applying the couplant, the sensor should be mounted on the surface of the structure or machine to be monitored. The sensor mounting can either be based on rigid bonding, welding or clamping with magnets to the surface of the structure.

4.2 Current State of Work on Acoustic Emission and Vibration Inspection Techniques

Randall used vibration monitoring technique to detect helicopter gearboxes including bearing and gear faults. It provided a difficult situation with respect to bearing diagnostics because of masking of the bearing fault signature by gear signals. He applied a technique called adaptive noise cancellation (ANC) to separate the bearing signals by using a non-identical gear signal as a reference [81].

Previous research carried out on wheelsets using AE has been reported by other research groups. An analytical rotating model developed for AE signals propagation from a moving source were found to be dependent on vehicle speed and load. Results were split into two categories; those arising from healthy wheels and those from defective ones at different speeds (low or 5km/h, medium or 20 km/h and high or 40 km/h). Placing more than one AE

sensor on the rail track and establishing sensor locations can provide evidence of flats present on lower railcar speeds, but for exact location of the defect further analysis of the raw AE data is required. In addition, it is not possible to predict the shape and size of the defect using AE inspection [82]. The distance of multiple sensors should be πD/2 as, if a flat happens to impact the rail close to the sensor, it will cause higher peaks than if it happens after πD distance from the sensor. In the other word, the probability of detecting a defect near to one of the sensors will have maximum value. Therefore, the positioning of the sensors is highly important in analysing data (where D is diameter of the testing wheel).

Previous research has also indicated that the background AE signals from normal rail-wheel interaction is dependent on speed. Peaks in the signals can be related to relatively small surface defects. Such defects can be located using appropriate data processing. It has also been observed that AE signals are sensitive to load levels [82].

Scuffing in bearings can occur due to lack of lubrication. This can occur without any warning. Sreedhar and Balasubramaniam [83] investigated the effect of low lubricant level on the AE signature. The energy content was found to be inversely proportional to the lubricant oil level. It was noted that the main changes in the frequency bandwidth were in the range of 20-30 kHz.

Shiroishi et al. [84] demonstrated the ability of accelerometers and low frequency acoustic sensors to detect and diagnose bearing defects. In the series of experiments reported by McLaskey and Glaser [77], the performance of the accelerometer was comparable to or better than the AE sensor in detecting different defect types. The peak ratio was the most reliable indicator of localised bearing defect compared to kurtosis, RMS and Crest Factor. McLaskey and Glaser [77] also suggested that a time domain method such as RMS is more reliable for interpreting non-localised defects (e.g. insufficient lubrication) whereas frequency-based analysis such as the High Frequency Resonance Technique (HFRT) is suitable for localised defect detection (e.g. inner race defects). The AE technique has also

been employed by Miettinen et al. [85] and Holroyd [86] to monitor the lubricant condition in rolling elements and plain bearings. Miettinen et al. used greased deliberately contaminated by different particle sizes in their experiments.

Bangoli et al. [87] investigated the increase in AE intensity for a bearing with outer race defect both in frequency and time-domain. Outer race defect was also detected in the spectrum of the demodulated AE signal. Price et al. [88] applied vibration and AE techniques on a 4-ball bearing and concluded that the AE sensors are able to find the damage earlier than vibration sensors. The rise in the amplitude showed changes in the defective bearing.

Roger [89] installed a number of bearing monitoring systems including vibration and AE on trains. For signal processing he employed spike counting and RMS above the threshold level-based analysis. He found that kurtosis is sensitive to point spiky character in vibration signatures which is suitable to be applied for bearing condition monitoring. He also stated that the AE measurement is an appropriate method to defect fatigue crack growth in the race and rolling elements of the bearings.

Bansal et al. [90] noticed a slight change in AE peak-to-peak (PK-PK) value by increasing the load, however the peak value for a reconditioned bearing was five times bigger than that for a new bearing.

Li et al. [91] stated that the critical size for a bearing defect is 6.25 mm^2 (0.01 $inch^2$), however the size of the bearing was not mentioned. Once the critical defect size is detected, it is necessary to immediately shut down the machinery affected as soon as possible and replace the bearing. This critical size established from AE and vibration experiments carried out by Li et al was employed for the development of an algorithm used to forecast defect propagation.

Badi et al. [92] successfully used AE sensors to inspect automotive gearbox bearing defects. The artificially induced faults were identified correctly. The main drawback of the approach was the bulky sensors employed.

Yoshioka [93] has shown that the AE signal enabled identification of bearing defects before they appeared in the vibration signals. In addition, location of the defect was identified during fatigue life tests on thrust loaded ball bearings. Hawman also [67] supported the advantage of AE system to defect very small outer race bearing defect compared to the vibration technique at earlier stages of evolution.

Li et al. [94] developed a bi-coherence analysis technique to diagnose outer race and roller bearing defects using very low frequency vibration. This technique enables earlier detection. The sampling frequency for these series of tests was 1000 Hz which is below the mechanical resonance of the bearing (structural resonance). In this case the time and frequency signals of healthy and defective bearings are similar therefore finding fundamental bearing frequencies is not straightforward.

Mohrin and Mba [95] noted that increasing the outer race defect size causes an increase in the value of amplitude and RMS in the AE signals acquired. However, for inner race defects this was not observed for all cases considered. This can be caused by the large attenuation of the inner race defect when the AE sensor is attached to the bearing casing. It has been suggested based on the observations made during this investigation that a suitable threshold level should be at least above 30% of the maximum background noise [95]. A pattern recognition-based signal processing method was also developed to separate healthy bearings from faulty ones [96].

Vibration analysis for monitoring the condition of bearings and gears is a technique that has been long established and thoroughly understood. There are also a few commercial systems that employ AE as an additional technique and a number of studies have also been published in relation to this technique for monitoring rotating machinery. However, only a limited number of studies have been published in relation to non-steady state rotating machines and systems such as rolling stock axle bearings. Singh et al. [97] conducted two experiments to study the capability of vibration and AE of detecting gear pitting defects.

From the results obtained they concluded that both detection techniques were able to find the simulated defect but the AE technique had a much greater signal to noise ratio.

Anastasopoulos, et al. [98] reported significant changes in AE counts after emergency braking. In the plots in Figure 4-3 the amplitudes of the AE hits generated from a passing test train with healthy wheels before any emergency brake and after 3, 6 and 7 emergency brakes are shown. A higher density of AE hits has been recorded together with their location.

Also AE amplitude versus time plots were reported from a healthy wheel as reference a wheel with a 2.5cm flat present on the tread (shown in Figure 4-4). The additional peaks in the AE signal from the deteriorated wheel supposedly indicate the presence of wheel flat.

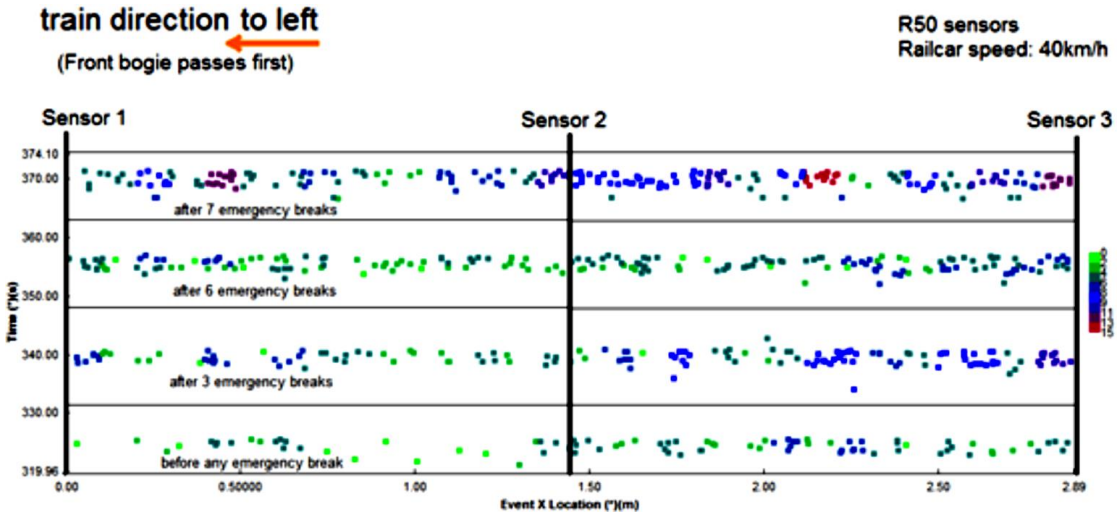

Figure 4-3: AE events location graphs of AE signals density for 32km/h railcar speed with different defects statuses [98].

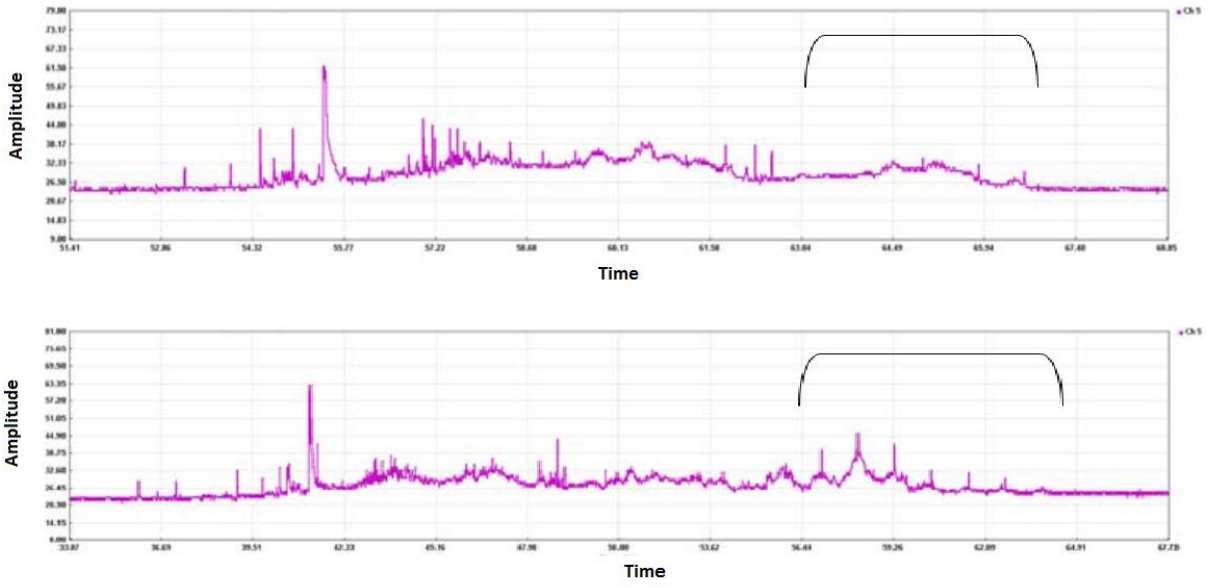

Figure 4-4: Reference train movement (top) 2.5cm flat defect surface (bottom) Extra peaks are visible in the defective wheel [98].

The AE technique can be used to locate the defect on structures using various location techniques including, linear, zonal or triangulation. These techniques are based on time of arrival of an AE event as it is detected by two or more sensors. By knowing their positions and distance between them together with the wave speed propagation in the structure being monitored it is possible to locate with a certain degree of confidence the exact location of the defect. Normally, the closest peak to the sensor is the one with the highest amplitude or energy captured. One-dimensional location is based on a linear approach and requires the use of two AE sensors. In this case the source of AE activity should be between the two sensors in order to locate it successfully. Zonal and triangulation location require at least three or more sensors. Figure 4-5 shows an example of one-dimensional location on a rod like structure.

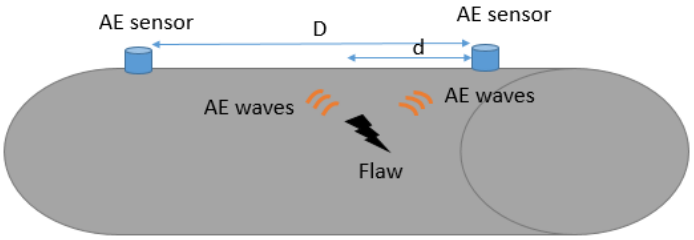

Figure 4-5: Linear AE source location [99].

The location of the AE source can be calculated using:

$$d = \frac{1}{2}(D - \Delta T.V)$$

where,

d = distance from first hit sensor, D= distance between two sensors,

V = Wave velocity

Yoshioka and Fujiwara [100] also reported they were able to locate ball bearing defects by monitoring the AE signals generated during experiments carried out in the laboratory. Salvan et al. [101] also tried to locate bearing defects in high-speed post office mail sorting machinery using AE sensors.

AE-based monitoring offers significant advantages over conventional vibration analysis when slow rotating machines are considered. Smith [102] reported that for large defects and moderate operating speeds, vibration-based monitoring techniques will generate satisfactorily results. However, at low speeds and small defects vibration-based detection becomes extremely difficult due to the small effects that these defects will have on the overall vibration signature of the structure. Kuboyama [103] also provided further details on the difficulties encountered when using vibration monitoring form monitoring machinery operating at low rotational speeds. Jamaludin et al. [104] suggested that below 16 RPM rotational speed should be considered as low. They also stated that at such low rotational

speed, the energy generated from a bearing defect might not cause changes in the overall vibration signature. In this case, the defect will remain undetectable. However, it should be noticed that better results may be obtained if low-frequency accelerometers are employed.

There is no international standard to classify rotating machines as slow or high speed machines but the limit for low-speed machine is normally considered to be below 20 RPM. Miettinen and Pataniitty carried out a case study on AE measurements using a laboratory test rig rotating at a speed between 0.5 and 5 RPM. The AE sensor was mounted on top of the bearing and the signal was filtered using a narrow band-pass filter whose centre was at 150 kHz. Their study showed that the AE measurement is a very sensitive method for the detection of bearing faults in slow rotating machinery. The pulse count method was used for monitoring rolling bearings with AE pulses counted over a specific time (for example 20 days). The rising level of pulse counts indicated the presence of an evolving defect in the bearings tested. Higher rotating speed results in higher resolution of AE signals i.e. better signal to noise ratio [14].

Crack initiation and propagation is one of the most common sources of AE. Cracks and other discontinuities in a material act as stress concentrators. While they are under an external load, they release energy in the form of stress waves that are detectable by AE sensors [105]. Fatigue crack growth tests were performed using three-point bending tests on notched and pre-cracked cast manganese steel samples at the University of Birmingham. Cast manganese steel is a manganese alloy with high capacity for work-hardening upon impact and is commonly used for manufacturing of railroad crossings as well as armoured vehicles including battle tanks [106, 107].

During tests a fatigue test machine, crack growth was monitored using Direct Current Potential Drop (DCPD) and two AE sensors. Figure 4-6 shows the experimental setup. The plot in Figure 4-7 shows high amplitude peaks corresponding to the occurrence of crack growth with each loading cycle.

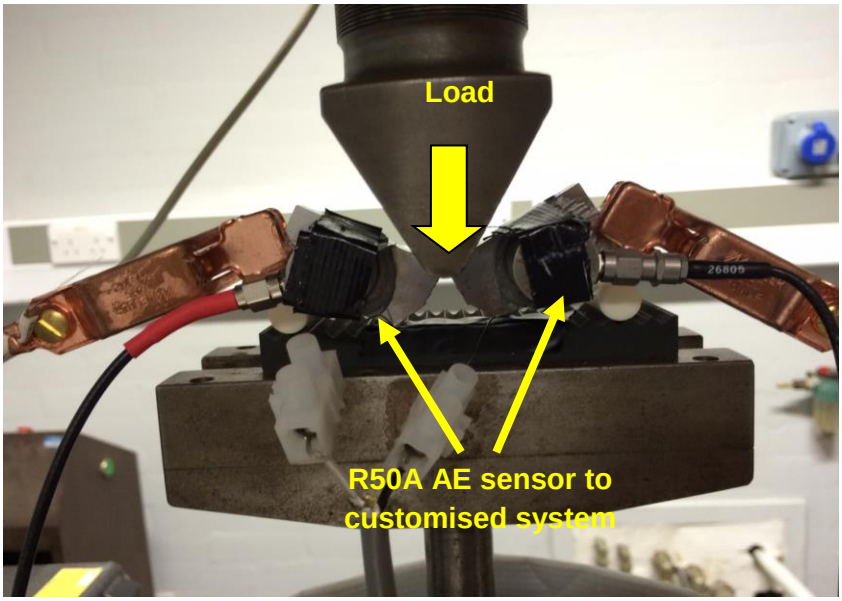

Figure 4-6: Experimental setup of fatigue test using AE

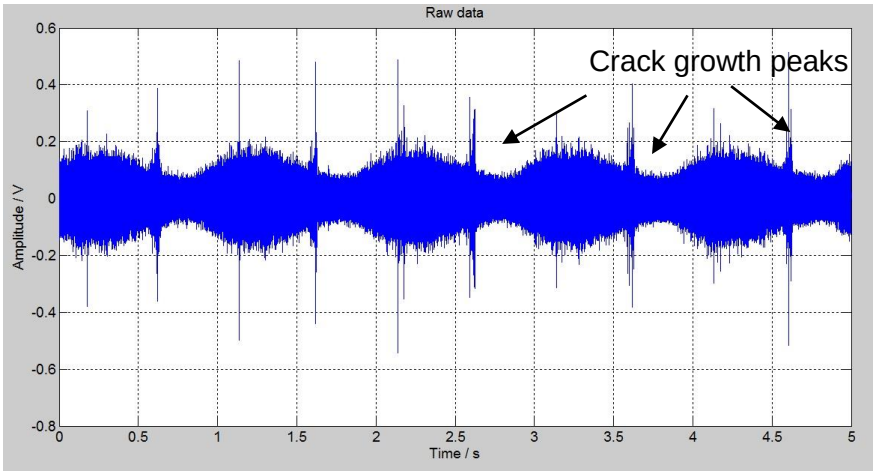

Figure 4-7: Raw acoustic emission data set showing fatigue crack growth.

Fleischmann et al. [108] investigated the behaviour of low carbon steel specimens during tensile testing using AE sensors. The specimens went through a period of intense AE activity during tests near the yield point.

Budano et al. [105] carried out a number of experiments on steel samples with different ultimate tensile strength and microstructure. It was revealed that different AE activities arose

during the fracture processes. More specifically ferrite-pearlite microstructure generated strong signals which were easier to interpret than the other steels considered.

4.3 Comparison Between Vibration and Acoustic Emission Techniques

AE is generally able to detect faults, earlier than vibration monitoring. AE is also capable of detecting faults before spalling occurs due to generation of burst-type signals [109]. This becomes possible due to the fact that AE employs high frequency sensors which are far more sensitive than accelerometers operating at a low and limited frequency range. However, the sampling rates employed in AE are also much higher in comparison with vibration since the Nyquist theorem also needs to be considered during acquisition. Thanks to the higher operational frequency AE has higher resolution and more accurate results can be acquired during early stages of fault development [14].

The other advantage of AE over vibration monitoring is that at a very low frequency of rotation, the vibration velocity amplitude becomes weak. Hence, vibration measurement may have limited success in detecting a fault in such cases. The AE technique has been revealed to be more sensitive when compared with vibration for detection of early faults especially in low speed situations [110]. Nonetheless, integration of vibration monitoring with AE at low rotational frequencies may be beneficial in order to improve the reliability of data analysis after measurements have been carried out [109]. The plots in Figure 4-8 show signals acquired from a defective bearing using both an accelerometer (with operational frequency 3 Hz – 18 kHz) and an AE sensor with operational frequency between 20-100 kHz. It should be noted here that due to the use of a magnetic hold-down with the accelerometers vibrations above 5 kHz are damped. Therefore, the actual operational range of accelerometers held in place with magnets does not exceed 5 kHz. As it is evident from the

plots presented, the AE technique gives noticeably better results in comparison with the vibration measurements for the detection of early-stage defects in low speed bearings. The qualitative plot in Figure 4-9 shows the sensitivity level exhibited by different techniques in monitoring evolution of defects in bearings.

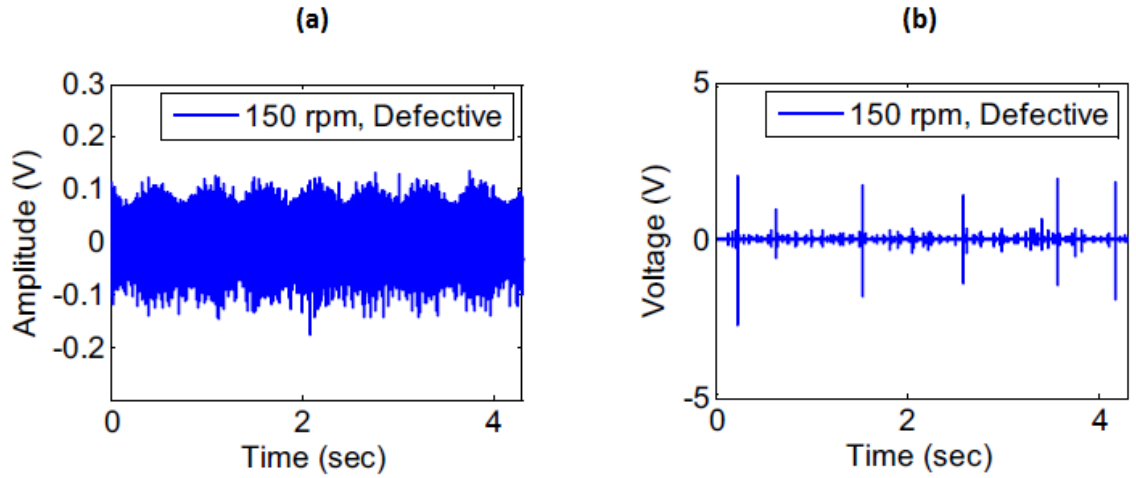

Figure 4-8: Time domain graphs from a defective bearing rotating with 150 rpm a) vibration signals b) AE signals [109].

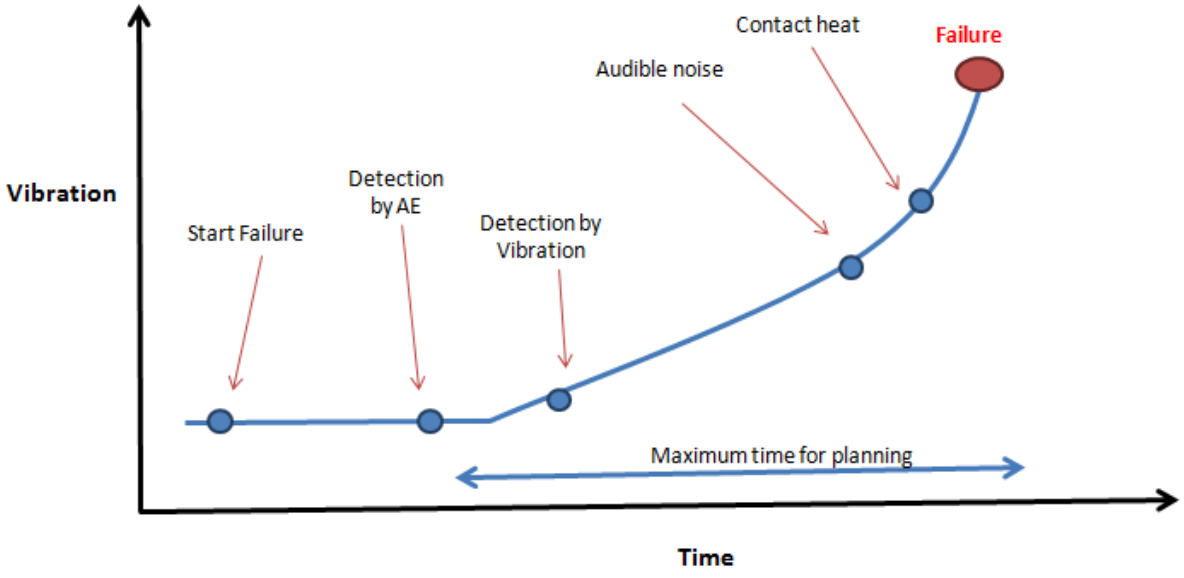

Figure 4-9: Increasing vibration in bearings due to developing defects through the time [73].

Sundt [111] studied the ability of the AE technique in detecting the presence of foreign particles such as sand in bearing lubricant of a pump unit. During this case study it was also shown that the high frequency AE signals contained information about the presence of a hairline race crack which vibration analysis had failed to detect. Such a defect is considered an early form of damage in a bearing and thus vibration monitoring would not be able to detect any changes in the vibration signature of the bearing being monitored. Finely [112] also developed a high frequency AE system which during tests was proven to be more effective than conventional low frequency sound and vibration techniques in detection of race bearing defects.

As mentioned before, a very important feature of AE signals is that they generally have a high signal to noise ratio. This means that the signals related to the actual machine condition can be clearly separated and are not buried in other unimportant signals. This feature of the AE technique makes the use of signal processing based on time-domain suitable, simplifying analysis. This allows generic time-domain signal processing algorithms to be used effectively. Due to their high signal to noise ratio AE signals are also sensitive to non-repetitive or random signals which may have both beneficial or detrimental effect in the measurement carried out [113].

AE sensors, in contrast to accelerometers can be located anywhere in the vicinity of the AE source. Accelerometers on the other hand are generally insensitive in directions other than the measurement direction. Although the AE measurement is non-directional, it must be noted that every interface the acoustic waves have to travel through causes attenuation due to scattering and reflection. The higher the frequency of the AE waves the higher the effect will be as distance between the source and the AE sensor increases. Therefore, the sensor should be mounted as close as possible to the point of interest [113].

Raw vibration and AE data were obtained by the author during laboratory experiments using a defective wheel mounted on a test trolley and pushed over a test track a few metres long.

From the measured data, it could be clearly seen that the flat on the tread of the defective wheel could easily be ascertained from the high-amplitude peaks in the time-domain signal. However, as it can be presumed, in actual operational situations, detection of such defects is as straightforward due to the presence of background noise arising from various environmental sources such as wheel traction. Therefore further analysis of captured raw data is necessary using appropriate signal processing algorithms.

4.4 Analysis of Vibration and AE Signals in Rotating Machinery

According to the research carried out by the author in collaboration with other researchers from the University of Birmingham and industrial partners, a combination of signal processing techniques is needed in order to successfully detect and identify the type and severity of wheel and axle bearing defects in rolling stock wheelset. Digital signals can be analysed in time, frequency or time-frequency domains. Traditionally the most common analysis of AE signals acquired during monitoring of rotating machines is based on the evaluation of peak-to-peak values, moving RMS, moving kurtosis, moving Crest Factor and power spectrum (Fast Fourier Transform or FFT).

4.4.1 Time-domain analysis

Time series signals can be used to diagnose fault and failure by using statistical parameters based on evaluation of moving RMS, Crest Factor, Skewness and Kurtosis of the raw signal [16].

4.4.2 Moving root-mean-square

The simplest analysis approach in time domain is to calculate the RMS (root-mean-square) values from the raw signal. The RMS value of a signal is a time analysis feature that is the

measure of energy content. The following equation is used to calculate the root mean square value of a data series [114] :

$$RMS = \sqrt{\frac{1}{N}\sum_{n=1}^{N} x_n^2} \tag{1}$$

where N is the number of data.

The moving RMS is a process of calculating RMS values in the signal divided into windows of a specified size such as the length of one wheel revolution. The plot shown in Figure 4-11 is an example of measured moving RMS of a passing railcar with a wheel flat defect. Analysis of the raw dataset using moving RMS allows the calculation of the main peaks of interest in the acquired signal.

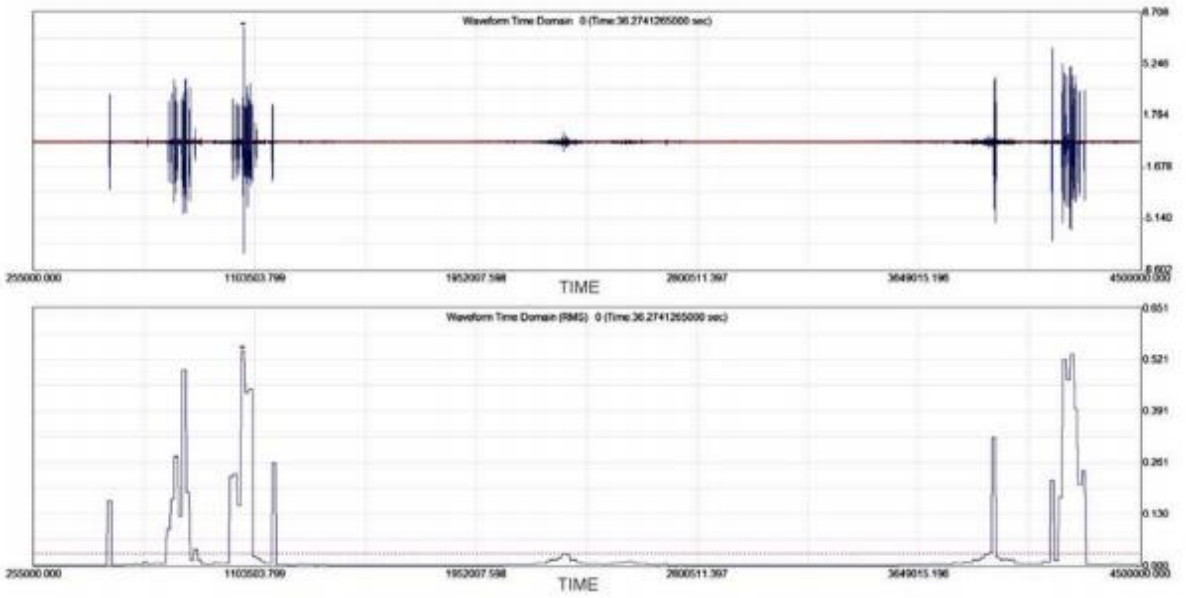

Figure 4-10: Raw AE waveform (top) and moving RMS graphs (bottom) acquired by a PAC R50 sensor during passes of a railcar with a wheel flat defect [115].

4.4.3 Moving kurtosis

Kurtosis is a word of Greek origin. It means "bulging" or "swelling" and is related to the degree of sharpness of peaks in a signal. Hence, it is used as a method for measuring the relative peakedness or flatness of a distribution as compared to a normal distribution. For a healthy rotating machine, the kurtosis value is close to 3. Any value greater than 4 indicates the presence of a defect which may lead to a failure in the monitored system [13]. Kurtosis of less than 3 indicates a low peak with a fat midrange on either side which is referred to as Platykurtic. Conversely, kurtosis greater than 3 indicates a sharp/high peak with a thin midrange and fat tails which is called leptokurtic. figure 30 shows different generic forms of kurtosis.

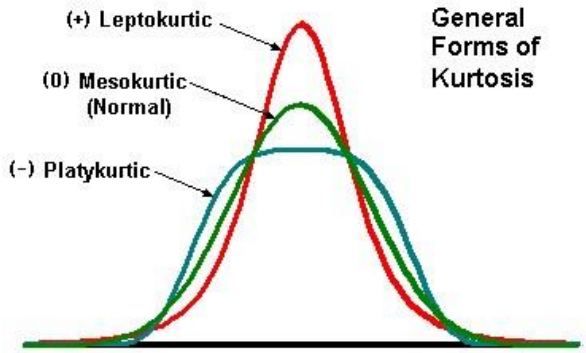

Figure 4-11: General forms of kurtosis [116].

Table 4-1 shows kurtosis values of deterministic and random signals.

Table 4-1 : Summary of statistical analysis of deterministic and random signals [117].

Type of Signal	Kurtosis
Triangle wave	1.5
Square wave	1
Normal distribution	3
Flat distribution	1.8
Sine + normal	1.8
Sine + flat	1.8

To calculate kurtosis, the difference between each value and the average of all values is calculated (Xi - $\bar{X}$). The fourth moment about the mean is given as:

$$\mu_4 = \frac{\sum_{i=1}^{n}(X_i - \bar{X})^4}{n} \tag{2}$$

The calculation formula for kurtosis is K = μ_4 / σ_4 where μ_4 is the fourth moment about the mean and σ_4 is the fourth moment about standard deviation of the signal.

$$K = n\frac{\sum_{i=1}^{n}(X_i - \bar{X})^4}{(\sum_{i=1}^{n}((X_i - \bar{X})^2)^2} \tag{3}$$

In order to detect the presence of a defect, a threshold can be applied, for example greater than 4. Any value above this threshold suggests the presence of a fault in the system measured [118].

Figure 4-12 shows the evolution of kurtosis with increasing operational cycles for a gear tooth with a rotation speed of 1000 rpm. The increasing value of kurtosis suggests a gradual development of spalling as the experiment progressed. A broadband AE sensor was used in this experiment. From the plot a clear increase in kurtosis amplitude is observed after 3000 cycles. This proves the suitability of AE for early detection of defects before occurrence of

apparition of spalls, by detecting the generated bursts. Thus, kurtosis of AE signals could be considered as an efficient tool to predict faults in rotating machinery.

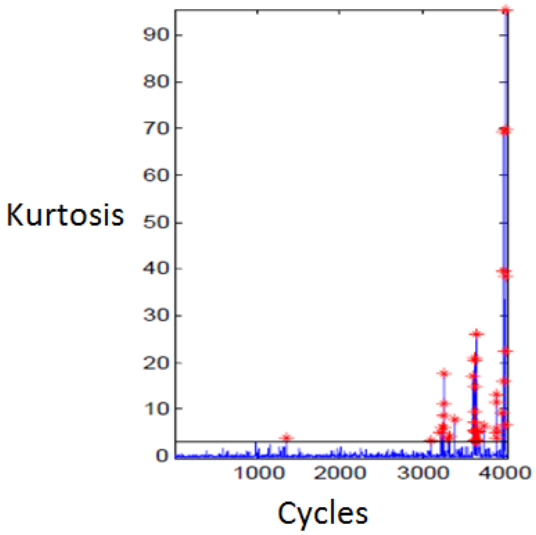

Figure 4-12 : Evolution of the kurtosis for a Gear tooth in different cycles- any peak more than the threshold is counted as a fault [119].

Moving kurtosis is a process of calculating the kurtosis value of the raw signals by dividing them into windows of a specified size. This method can be used to find defects causing an increase in the kurtosis values calculated for the chosen window. However, in noisy environments including non-Gaussian waves, this method might not be effective.

4.4.4 Multiple sensor analysis

In order to increase the signal to noise ratio, multiple sensor analysis can be used.. By using more than two sensors, the detection of defects manifesting themselves simultaneously may become possible through the evaluation of similarities with background noise. Since these signals will be non-random there is a better chance of distinguishing the defect related signals from background noise.

4.4.5 Moving Crest Factor

The Peak to Average ratio is the peak amplitude divided by the RMS value of a waveform as:

$$Crest\ Factor = \frac{Peak}{RMS} \tag{4}$$

The purpose of calculating the Crest Factor is to obtain an idea of impact-related events captured in a waveform. These impacts in the present study can be associated with wheel flats and metal build-up-related defects.

In a perfect sine wave, with amplitude of 1, the RMS value is equal to 0.707, and the Crest Factor is then equal to 1.41. This wave contains no impact, therefore Crest Factors with a value higher than 1.41 imply the presence of an impact and hence defect. The FFT defines any signal by the sum of set of sine waves. But this does not work well when a signal consists of non-periodic events, impacts or random noise. In FFT, both impact and random noises give rise to the same spectrum as shown in Figure 4-13. Therefore the Crest Factor can be a useful tool for obtaining further information of what is actually happening in the waveform [114].

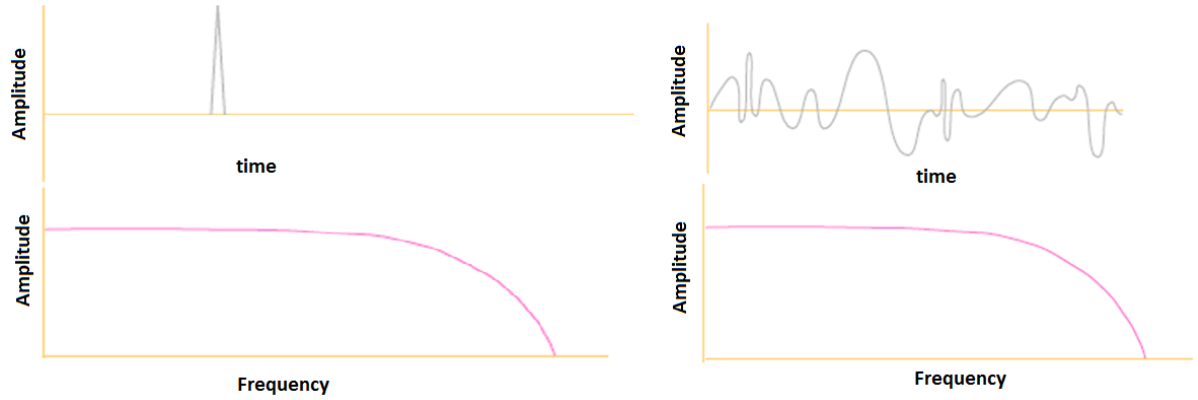

Figure 4-13: An Impact signal (left) random noises (right) – both have the same spectrum in Frequency domain [114].

The Crest Factor is very sensitive to sharp peaks which do not last very long and have low energy [120]. A typical vibration signal from a machine with a large imbalance and no other problems will have a Crest Factor of approximately 3. However, as the bearings begin to wear, impacts will begin to occur. At this instance the Crest Factor will begin to increase greatly. The reason behind the sensitivity of the Crest Factor to the presence of sharp peaks in the waveform is that the peaks do not last very long in time, and therefore do not contain much energy. Sometimes the RMS of a defective system may remain low and Crest Factor values will increase. This shows that a simple vibration measurement instrument that only calculates the RMS level will not be able to detect a defective bearing, at least in this case [118].

4.4.6 Signal enveloping

Sometimes spectral comparison of a waveform is not suitable for detecting damage in a machine. This is because the energy produced by defects is mixed by more dominant signals such as background noise. For this reason, envelope detection is commonly used in signal processing. This technique involves a band-pass filter to eliminate very high or low frequencies in the waveform [108]. Figure 4-14 shows an example of envelope detection using Hilbert transform.

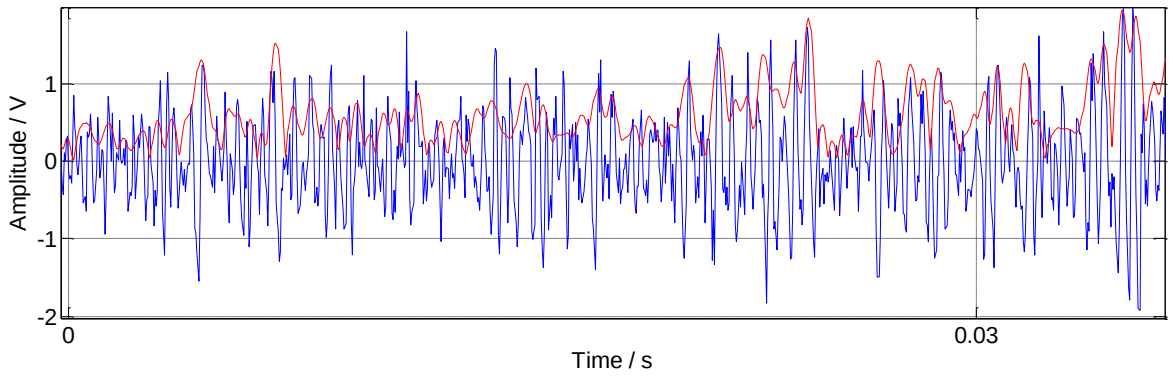

Figure 4-14: Envelope detection [121].

The Hilbert transformation allows the calculation of the envelope of the signal [122].

4.4.7 Frequency domain methods

The frequency-domain analysis is related to signal processing approaches as a function of frequency based on the information gathered from the time-domain signal measured. Whilst certain information is more easily interpreted in the time domain, more detailed analysis of vibration and AE data captured from measured rotating and reciprocating machinery is often carried out in the frequency domain. Frequency domain or spectral analysis of vibration and AE signals is the most widely used technique for defect identification in rotating machinery.

4.4.8 Resonance frequency

Resonance frequency is the frequency at which a broadband signal will have its maximum amplitude. Normally, the signal amplitude at the resonance frequency will be much higher than the amplitude at other frequencies. Normally resonant sensors resonate at several frequencies but at some particular frequencies resonance will be stronger. Resonance frequencies are independent of the speed of rotating machineries. They depend on the mass configuration and material type. In the case of AE and vibration measurements, there are two types of resonance frequencies which should be considered.

The first type is the resonance frequencies of sensors. These are the result of natural resonance of the mechanical structure of the accelerometer or AE sensor itself. Typical piezoelectric accelerometers exhibit a resonance frequency between 20-30 KHz whilst most resonant AE sensors have resonance above 100 kHz. The R50a used in this project exhibits multiple resonances with one of interest being at 170 kHz. Wideband sensors in comparison with resonant sensors have a much flatter response in a wide range of frequencies whilst resonant sensors will exhibit higher sensitivity at the frequencies that they resonate.

The second type is related to the measurement of the component's natural frequencies initiated by shock excitation associated with structural irregularities. Every structure has one or more resonance frequencies. An impact test, also called excitation measurement, can be used to determine these frequencies which should be performed on a non-running machine or structure. The resonance frequency of a train axle bearing is shown in Figure 4-15. Excitation has been achieved by impacting the stationary wheelset using a hammer. It is very important not to confuse between these two types of frequencies and their bandwidth [64]. Bearing natural frequencies are independent of rotational speeds [123].

There has long been a debate about the best method of choosing the frequency band for demodulation in spectral envelope analysis. One of the most commonly used method for measuring a system's natural frequency is to excite it with an impacting mass and measure its vibrational response. Impact testing using an instrumented hammer is another method for identifying the resonance frequencies. This method is basically the same as a regular impact test, except that an instrumented hammer is used to excite the system and measure its response. The instrumented hammer, consists of an accelerometer at one end, which is used to measure the vibration. The advantage of using an instrumented impact hammer is the fact that it allows creation of a visual model of the vibrating body [124].

.

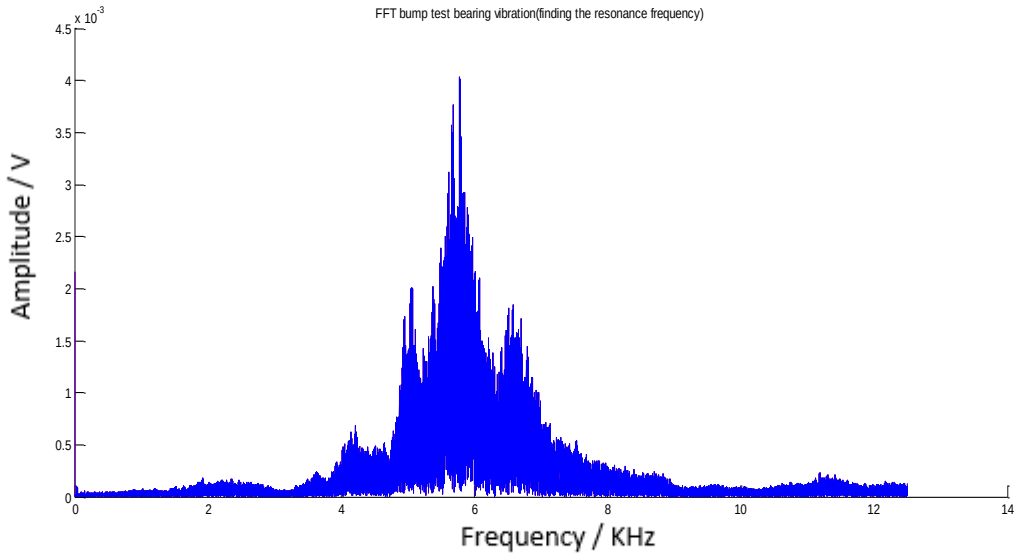

Figure 4-15: Power spectral plot showing the arising frequencies and their amplitude in order to find the resonance frequency of a railway wheelset.

4.4.9 High frequency resonance technique

To enable the accurate defect detection and classification, a major challenge that needs to be addressed is the identification of the characteristic frequencies of roller bearings. Figure 4-16 shows the cross-section of a typical roller bearing and the different types of rollers employed.

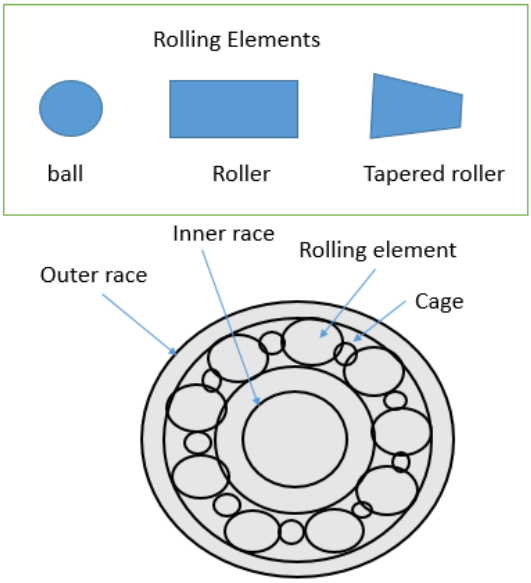

Figure 4-16: Rolling element bearing components [125].

Certain bearing defects, such as roller and race defects, give rise to a fundamental frequency. Knowing the fundamental frequency of the defects is paramount in diagnosing the exact nature of the problem rather than only distinguishing a faulty axle bearing from a healthy one. When an axle bearing rotates, any irregularity in the race surfaces or in the roundness of rolling elements will excite periodic frequencies or otherwise fundamental defect frequencies. The amplitude of these frequencies or tones is an indication of the severity of the defect detected. Ball bearings illustrate four distinct tones or frequencies.

These frequencies depend on the bearing geometry and rotational speed. Once the type of the bearing and the shaft speed are identified, the defect frequencies can be calculated. The information regarding characteristic frequencies of an axle bearing are generally provided by the manufacturer of the bearing. The formulae for calculating these specific frequencies are the following [126, 127]

:

$$BPFI = \frac{N}{2} \times F \times (1 + \frac{B}{P} \times Cos\theta)$$

$$BPFO = \frac{N}{2} \times F \times (1 - \frac{B}{P} \times Cos\theta)$$

$$FTF = \frac{F}{2} \times (1 - \frac{B}{P} \times Cos\theta)$$

$$BSF = \frac{P}{2B} \times F \times [1 - (\frac{B}{P} \times Cos\theta)^2]$$

where

BPFI=Ball pass frequency inner race (Hz)

BPFO=Ball pass frequency outer race (Hz)

FTF=Fundamental train frequency –Frequency of the cage (Hz)

BSF=Ball spin frequency circular frequency of each rolling element as it spins (Hz)

N=Number of balls

F=Shaft frequency (Hz)

B=Ball diameter (mm)

P=Pitch diameter (mm)

θ =Contact angle.

It should be noted that these formulae are theoretical, and the difference between calculated and measured bearing frequencies can be as high as several Hz.

Each time a defect impacts on the mating element, a pulse of short duration is generated that excites the resonances periodically at the characteristic frequency [128]. By

demodulating one of these resonances, a signal suggestive of the machine condition can be obtained. In fact, the signal is band-pass-filtered around one of the resonance frequencies, hence eliminating most of the unwanted vibration signals from other sources. This band-pass-filtered signal is then demodulated by an envelope detector in which the signal is rectified and smoothed by low-pass filtering to eliminate the carrier or band-pass-filtered resonance frequency. The spectrum of the envelope signal in the low-frequency range is then obtained to get the characteristic defect frequency of the machine measured [13].

For a bearing in healthy condition, the frequency of rotation and its harmonics are detectable. The earliest indications of bearing problems are in the ultrasonic frequency range. These frequencies require AE measuring equipment. Later, when damage evolves, the frequency drops to about 20 to 60 kHz (stage I). In stage II condition, small defects within the bearing structure begin to cause impacts. These impacts excite the natural frequency of the bearing components. Bearing defects are detectable in this stage by analysing the vibration data using high frequency resonance technique (HFRT). Stage III condition has the fundamental bearing defect frequencies present. As wear increases, more harmonic frequencies occur that are detectable in the vibration spectrum. Stage IV is the last condition prior to the occurrence of final failure. At this stage final failure of the bearing can occur at any moment. During this time, the bearing fundamental frequencies begin to disappear from the spectrum and be replaced by random broadband high-frequencies. The different stages of bearing failure are shown in Figure 4-17.

The dominant peak at 1 RPM (also called 1X) is due to imbalance of the rotor. The presence of the 2 RPM (or 2X) component in the spectrum is mainly due to shaft misalignment, asymmetry or bent shaft. There can be other defects that give rise to peaks at 1X, 2X etc., such as electrical problems [129].

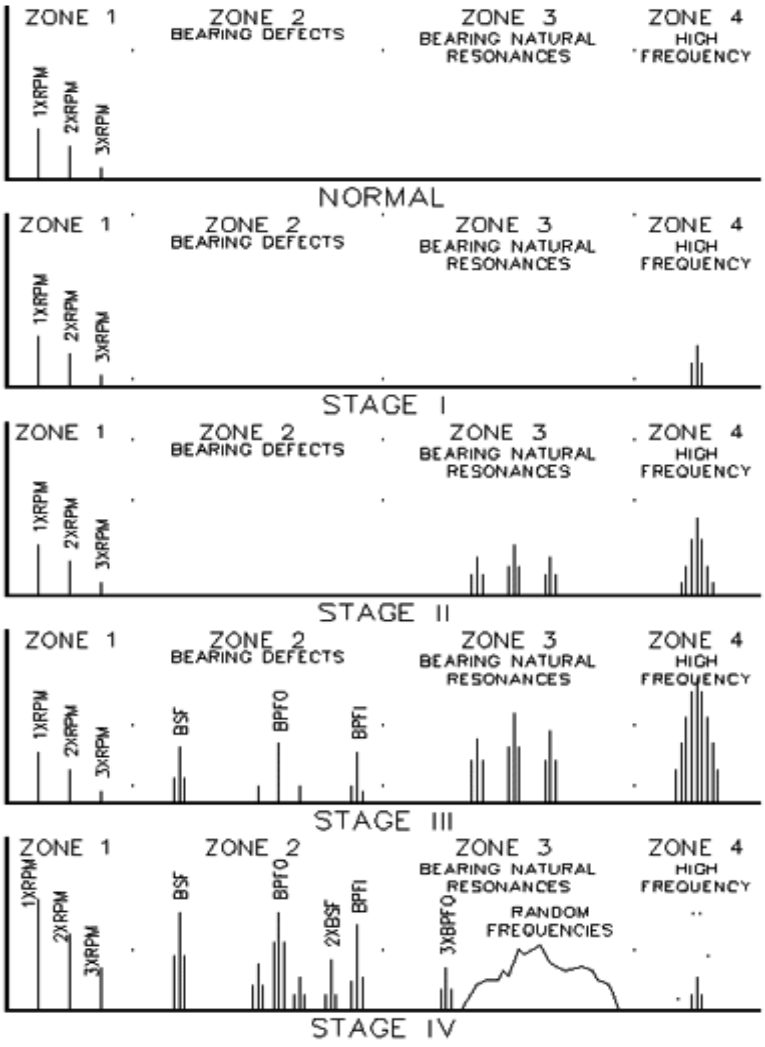

Figure 4-17: Frequencies of growing bearing defects [130].

The main idea of the high-frequency resonance technique is to eliminate the disturbance influence by using band-pass filtering around the resonance frequency highlighting the fault feature within the envelope spectrum. More than one resonance may be excited, as it is likely that in practical systems several natural frequencies will fall within the frequency range. In practical applications the resonance frequency band may vary due to different types of bearings used. At early stages of evolution of an axle bearing defect, the chance of detecting it reliably using conventional power spectral analysis is low. HFRT analysis provides an effective extraction method from low signal to noise ratio when vibration or AE signals are considered [58, 131].

The band-width of the filter should be at least twice and preferably more than four times the maximum expected characteristic defect frequency, in order that the filter can pass the carrier frequency and at least one pair of modulation sidebands [58]. After finding an optimum frequency band, this method allows identification of bearing defects by extracting characteristic defect frequencies from the vibration or AE signals. However, vibration or AE in an operating machine might be excited not only from bearings but also from others components such as gears, shafts, couplings, whether in good condition or faulty condition [23]. Figure 4-18 shows the steps of demodulating a vibration or AE signal.

The Hilbert transform is a transformation of a signal from time-domain to time-domain. Positive frequency and negative frequency components are shifted by +90 and -90 degrees. The Hilbert transform of g(t) is the convolution of g(t) with the signal $\frac{1}{\pi t}$. This results in the following equation [132]:

$$[g(t)] = g(t) * \frac{1}{\pi t} = \frac{1}{\pi} \int_{-\infty}^{\infty} \frac{g(\tau)}{t-\tau} d\tau = \frac{1}{\pi} \int_{-\infty}^{\infty} \frac{g(t-\tau)}{\tau} d\tau$$

The Hilbert transform represents the analytical signal and it is the magnitude of the envelope of the original signal. Envelope detection or amplitude demodulation is the technique in extracting the modulating signal from an amplitude-modulated signal.

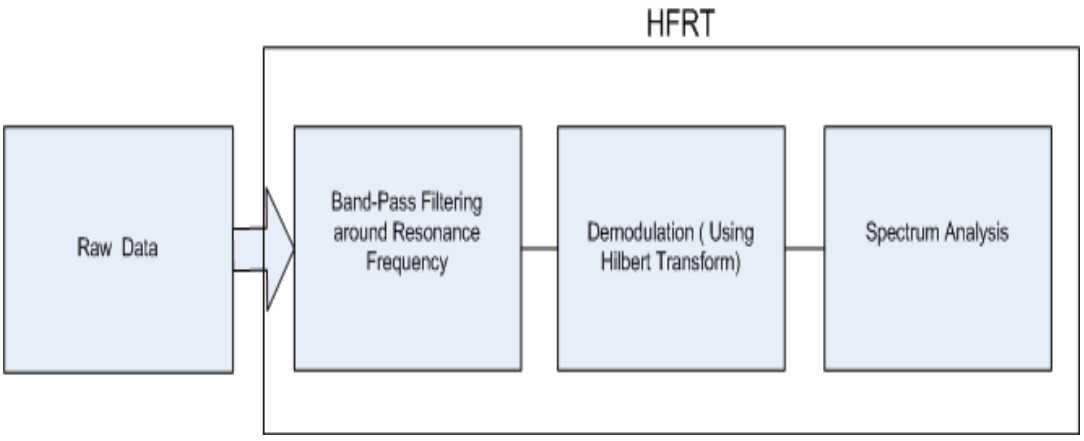

Figure 4-18: Schematic of high frequency resonance technique.

It should be noted that the raw spectrum of a bearing fault signal with low signal to noise ratio usually contains little diagnostic information, being dominated by the resonance frequencies that are excited. Whereas the envelope signal obtained by amplitude demodulation contains the required information about the repetition frequency of impacts and any modulation caused by passage of the fault through the load zone.

Generally, the rolling elements do not carry equal loads around the circumference of the bearing. The schematic shown in Figure 4-19 is a radial loaded bearing with rolling elements where the shaded parts show the proportion of the load which is supporting. The maximum load is in the vertical position with the darkest shading (roller A). This behaviour makes the roller bearing defects to be amplitude modulated through each revolution. That means amplitude of the impact from the defect is different in each roller revolution, because defects on the inner race and rolling elements periodically move into and out of the loaded zone. However a defect on the outer race generally remains in the same position relative to the loaded zone.

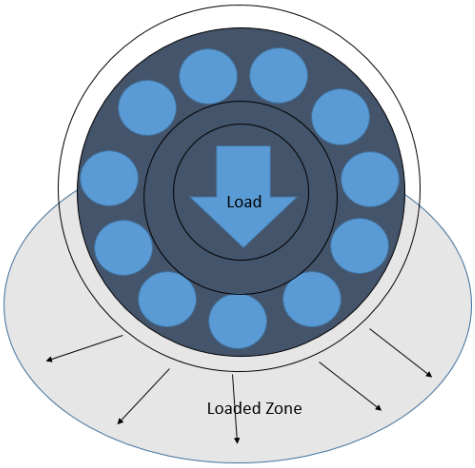

Figure 4-19: Load zone of the bearing [18].

As a result, for roller defect the peak in HFRT has sidebands of the fundamental train frequency (FTF) whereas for outer race defect, the peak is clear without any sideband. Also

in the raw data at the time domain, the impacts from roller defect are modulated by amplitude.

Spectral envelope analysis is a similar approach to HFRT, however the bandpass filter should be around different frequency bandwidth rather than the resonance frequency. This bandwidth can be evaluated by different analyses such as Kurtogram.

4.4.10 Time spectral kurtosis (TSK)

Spectral kurtosis (SK) is an analysis technique based on measuring kurtosis values in specific frequency bandwidths. Time spectral kurtosis (TSK) is capable of demonstrating the signal in 3 axes; x: time, y: frequency and z: kurtosis amplitude. The TSK technique can indicate not only the transients in the frequency domain, but also their locations in the time domain [51]. Defects in rolling element bearings, which are usually similar to short impulses caused by the impact from the defect, can be determined using the TSK technique. The kurtosis value of a normal distribution signal is around 3. A value greater than 3 indicates peaks which are related to AE activities caused by defects in the signal [133]. However, false detections can occur when processing signals collected from wheel-bearings from in-service trains. These errors can be caused by impulses arising from random sources reducing the overall ability of TSK to detect bearing faults. TSK is rarely used despite being appropriate for fault detection. This could be because it has not been clearly defined or the methods were not completely understood [134]. To determine the SK the signal is passed through a set of band-pass filters. Then the kurtosis values of the filtered signals are calculated [133].

The Kurtogram is kurtosis (fourth-order spectral analysis) in different window frequency bandwidth which has been recently introduced for detecting and characterising non-stationeries in a signal. The purpose of the Kurtogram is to find the optimum window size (resolution) where kurtosis is at its maximum [135]. A short window will yield high SK values and consequently may be favoured. However, too short window will also produce an SK with low kurtosis value so that some details will be lost [136]. Figure 4-20 shows an example of

SK computed with different frequency windows. The optimum window number in this example is between 32 to 64 which has higher value of kurtosis than 128 and 256 windows number. Choosing such a window number will result in a spectral resolution of about 750-1500 Hz per line. The schematic in Figure 4-21 illustrates the binary tree Kurtogram estimator.

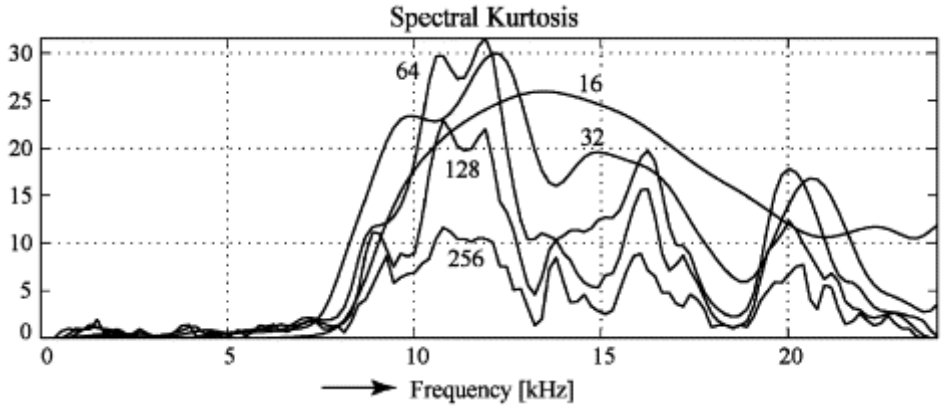

Figure 4-20: SK computed for different frequency windows N_w=16, 32, 64, 128, 256 of a signal from rolling element bearing with outer race defect [134].

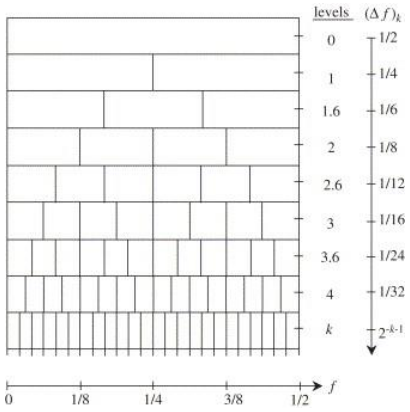

Figure 4-21: Binary tree Kurtogram estimator [136].

The ability of the Kurtogram in diagnostics of wind turbines has been shown by Barszcz and Randall [137]. It was used to find an optimal band-pass filter. It was stated that the optimal central frequency and bandwidth of the band pass filter as found as those values which jointly maximise the Kurtogram. However, the main drawback for the Kurtogram is similar to

SK. The inability of the Fast Kurtogram to detect the fault in a jet engine signal is caused by a relatively high repetition rate of impacts, and high non-Gaussian noise level including strong random impacts.

This problem has been shown by Chen [51] when a signal was simulated combining Pink noise, cyclic impulse and a single impulse. Cyclic impulse was based on the simulation of bearing defect noise impacting repeatedly with time. The SK value of an interference impulse (single impulse) was larger than the defect-related impulse (cyclic impulse). Therefore by selecting a centre frequency according to the maximum value of SK, the defect frequency cannot be discovered.

Antoni [136] suggested the use of the Kurtogram for designing a band-pass filter which can be applied in order to increase the signal-to-noise ratio, thereby preserving the impulse-like nature of the signal.

4.4.11 Moving Cepstrum

Cepstrum was first introduced in 1987 as a suitable method for analysing vibration signals [138]. It can be considered as an aid for the interpretation of the spectrum by finding the harmonics arising from the presence of defects [139]. Cepstral analysis is a tool for detecting periodic signals in a frequency spectrum. It can be obtained by the Inverse Fourier Transformation (IFT) of the power spectrum (FFT). Instead of frequency in X axis, it has Quefrency which is measured in seconds and is the reciprocal of the frequency *spacing* in Hz in the original frequency spectrum. The Cepstrum technique appears to be an appropriate analysis method for detecting changes in the spectrum which may not be immediately obvious [140, 141].

Cepstrum is the squared magnitude of the IFT of the logarithm of the squared magnitude of the FFT of a signal as shown in the following equation [142]. Table 4-2 shows the terms used in Cepstral analysis.

$$\text{Cepstrum} = \{ \text{FFT}^{-1}(\log \{ \text{FFT} [x(t)] \})^2 \}^2 \quad (5)$$

Table 4-2: Terms in Cepstral analysis.

Derived Terms	Original Terms
Cepstrum	Spectrum
Quefrency	Frequency
Rahmonics	Harmonics
Gamnitude	Magnitude
Saphe	Phase
Lifter	Filter
Short-pass Lifter	Low-Pass Filter
Long-Pass Lifter	High-Pass Filter

Because the AE or vibration spectrum of a rotating machine can be complex and contains several sets of harmonics and their sidebands, such as bearing frequencies, Cepstral analysis can be used to find these harmonics [143]. Figure 4-22 shows an example of converting spectral to Cepstral analysis. The raw data is a simulated signal from a measured rotating machine. The peak at 7.46 quefrency and its harmonic indicate the fault at 134 ($\frac{1}{7.46}$) Hz.

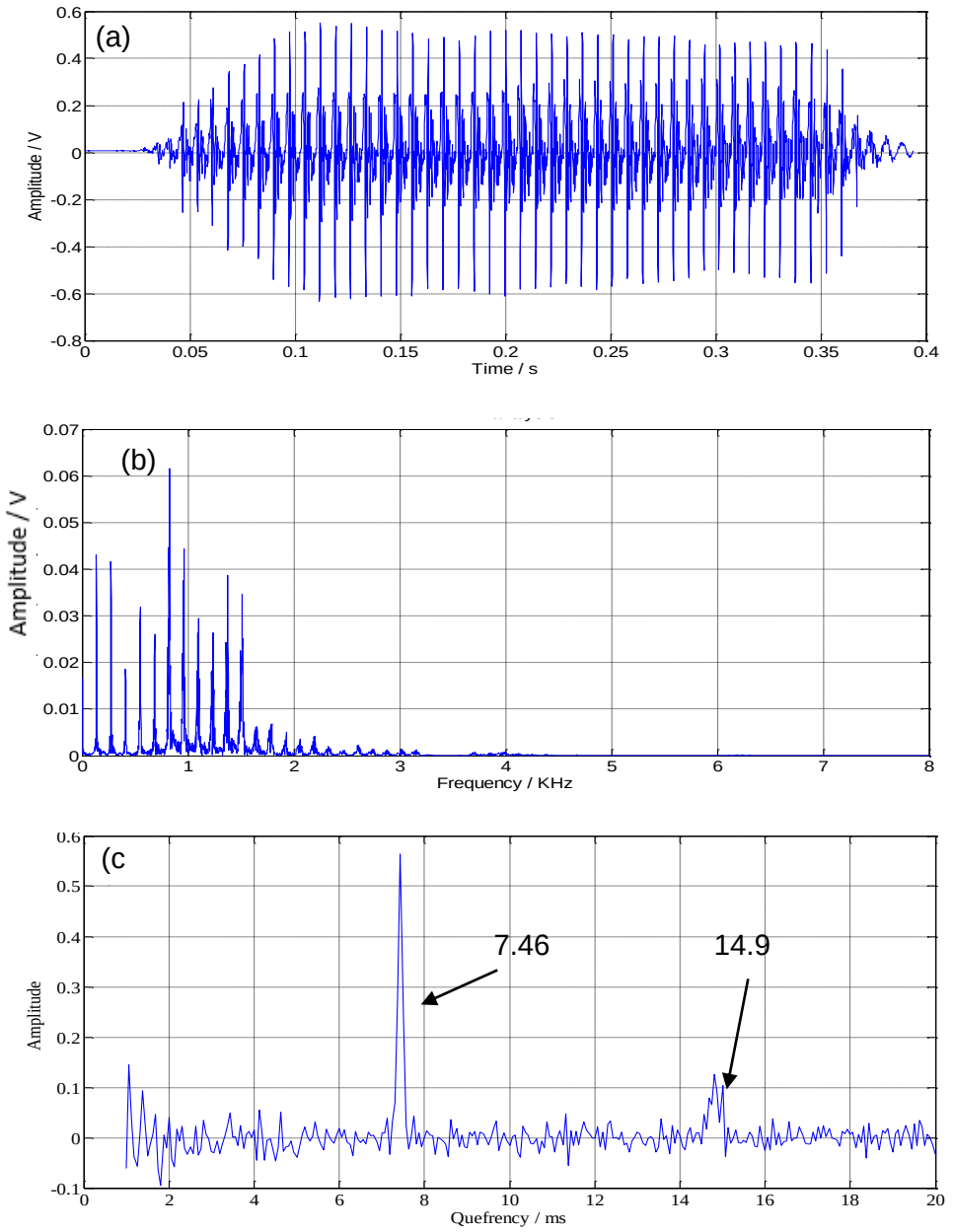

Figure 4-22: a) Raw data, b) Power spectrum, c) Power Cepstrum result.

4.4.12 Wavelet transform

In recent years, the wavelet transform method has been suggested by some researchers to extract very weak signals for which FFT becomes ineffective. It can provide different time-frequency distribution from a repetitive signal and some research claimed this method can be used in applications such as speech recognition and fingerprint verification. However no

research has been done for analysing vibration and AE data measured from wheelsets [144].

4.5 Summary

A background review of AE and vibration techniques along with the history, calibration methods and current state of work have been described in this chapter. AE is defined as the generation of elastic waves made by a sudden redistribution of molecules inside or on the surface of a material. Vibration is a mechanical phenomenon which occurs when an object shows an oscillatory motion about a position of equilibrium.

In addition, comparison between AE and vibration analysis findings in previous studies has been discussed. AE is generally able to detect faults earlier than vibration technique, this is due to its high frequency range and higher sensitivity. It is also capable of monitoring machines rotating at a low frequency (below 20 RPM).

Furthermore, various signal processing analysis on both AE and vibration data from rotating machineries were reviewed. These include moving RMS, moving kurtosis, multiple sensor analysis, moving Crest Factor, HFRT, TSK, Moving Cepstrum and wavelet transform.

Chapter 5 : Laboratory Experimental Setup and Test Procedures

5.1 Instrumentation

5.1.1 AE instrumentation

Figure 5-1 shows the equipment used for AE measurements during the experimental work carried out as part of this study. The customised system consists of the following components: a) AE resonant and wideband sensors procured from Physical Acoustics Corporation (Ltd) (PAC UK – now MISTRAS), b) Agilent U2531A aata *a*cquisition board and decoupling box, c) standard desktop computer with customised data logging and signal processing AE system software written in MATLAB by the author, d) pre-amplifier procured from PAC UK, e) AE Amplifier also procured from PAC UK, and f) BNC cables.

.

Figure 5-1: Instruments used in experimental work

Three different types of sensors have been considered during the experimental work of this project (Figure 5-2). In research applications, wideband AE sensors are useful where frequency analysis of the AE signal is required and in helping to determine the main frequency band of AE sources for noise discrimination and selection of a suitable resonant AE sensor. The PAC WD AE sensor has a diameter of 17.8 mm and its main resonance lies at 450 kHz. Its operating frequency range is from 100 kHz to 900 kHz.

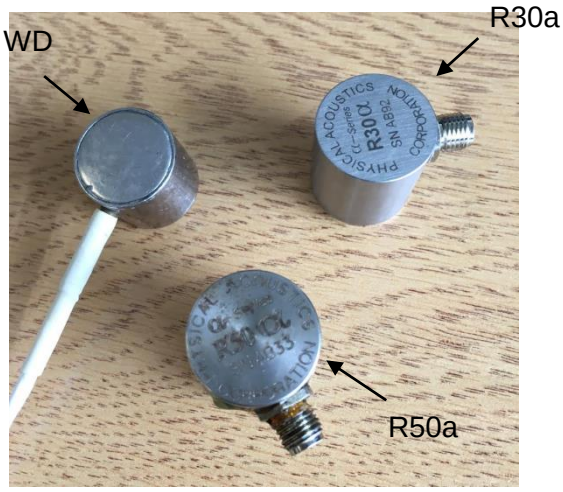

Figure 5-2: AE Sensors used in the experiments.

General purpose sensors are designed to be low cost, high sensitivity, resonant type sensors, medium size, medium temperature range, and are used in most AE applications. Due to the difference in cost between general purpose sensors and all other sensor families, one would move away from general purpose sensors only if there is a need for a different size or shape sensor due to space limitations, need for a different frequency range (such as wideband), different application temperature (such as high or low temperature) or environmental (such as waterproof) requirement. As a rule, one should always look towards selection of a general purpose AE sensor first, since they have the best price and performance of all the rest of the sensor families [145]. Two types of general purpose sensors have been used in the experiments (R50α and R30α).

The R50α Sensor has an operating frequency range of 100 - 700 kHz and resonant

frequency of 170 and 350 kHz. Figure 5-3 shows the calibration curve for the R50α sensor. As it is shown there are two main resonance frequencies for this sensor type.

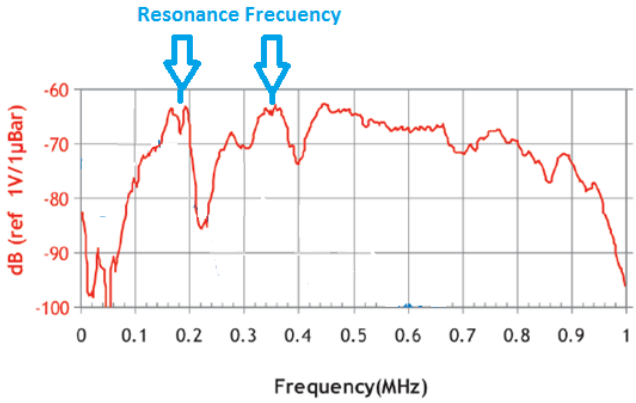

Figure 5-3: R50α sensor Calibration curve- Calibration based on ASTM E976 [145].

The R30α sensor has an operating frequency range between 150 kHz and 400 kHz. Its main resonance frequency is at 330 kHz. Figure 5-4 shows the calibration curve for the R30α sensor.

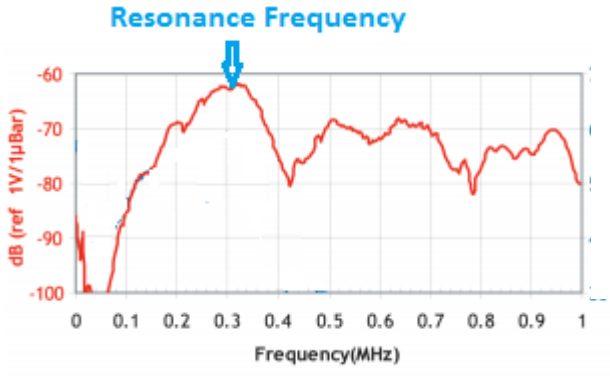

Figure 5-4: R30α sensor Calibration curve -Calibration based on ASTM E976 [145].

The type of AE sensor installation is usually defined by the type of application which is going to be tested:

- Glue (superglue type) which is commonly used for piping inspections.
- Magnetic hold-downs usually used to hold sensors on ferrous pressure vessels with grease or oil coupling.

- Bands used for mechanical attachment of sensors in long term applications.
- Waveguides (welded or mechanically attached) used in high temperature applications.
- Rolling sensors used for inspecting rotating structures [146].

Magnetic hold-downs were used to attach the AE sensors during the series of experiments in this study.

Pre-amplifiers are placed close to the sensors in order to amplify the tiny electric signals generated by the sensor. Further amplification is achieved by the use of a main amplifier. Both amplifiers are used to increase the signal strength before digitised by the data acquisition card. Preamplifiers can be built as integral parts of the sensor or connected as independent components to the AE sensor. The preamplifiers used in this project are directly connected to the AE sensors in one end and to an amplifier in the other. To power them, DC power is needed which is supplied by the amplifier.

The pre-amplifiers used in this study have three selectable gain settings of 20, 40 and 60 dB. The desired setting can be selected by adjusting the switch to the required position. They are compatible with both single-ended and differential sensors. The gain is a measure of the ability of an amplifier to increase the power or amplitude of an input signal to the output. Therefore, it is the ratio of the amplitude of the output to the input. It is often expressed in logarithmic decibel (dB). The amount of gain should be adjusted for every experiment if the load, speed or size of the experiment differs. It is clear if the amount of gain is lower or higher than the optimum, signals will be either too small or saturated in amplitude and will not be possible to be analysed.

In addition to amplifying the signals, the pre-amplifiers also provide band-pass filtering. There are two types of PAC pre-amplifiers which filter the signals in the range of 20-1000 kHz and 100-1000 KHz respectively. The second type is more preferable as it filters out low-frequency signals which are predominantly associated with unwanted environmental mechanical noise.

The output voltage of an AE sensor is usually very small therefore both a pre-amplifier and amplifier areneeded to strengthen the signal before it is fed to the digitiser. The PAC AE2A second generation series of AE Amplifiers system used in this project covers AE bandwidths from 3 kHz up to 2 MHz. It is capable of amplifying the AE signal from 0 up to 61dB in 3 dB steps.

The Agilent U2531A data acquisition board digitises the AE and vibration signals acquired during testing and acts as interface between the logging computer and the sensors. It is connected to the computer with a Universal Serial Bus (USB) cable. It is decoupled using a decoupler and is able to acquire data up to 2 MS/s with 12-bit resolution if used in single channel mode. This board also supports multiple channels if lower sampling rates are used [147].

5.1.2 Vibration instrumentation

Wilcoxon piezoelectric accelerometers, model 712F shown in Figure 5-5, with operating frequency of 9 Hz to 15 kHz was used during the series of experiments (appendix C). This accelerometer has a resonance frequency greater than 45 KHz which is above the measurement frequency range. Its required power is provided by a 12 channel Mistras accelerometer power supply model LP241-12 shown in Figure 5-6.

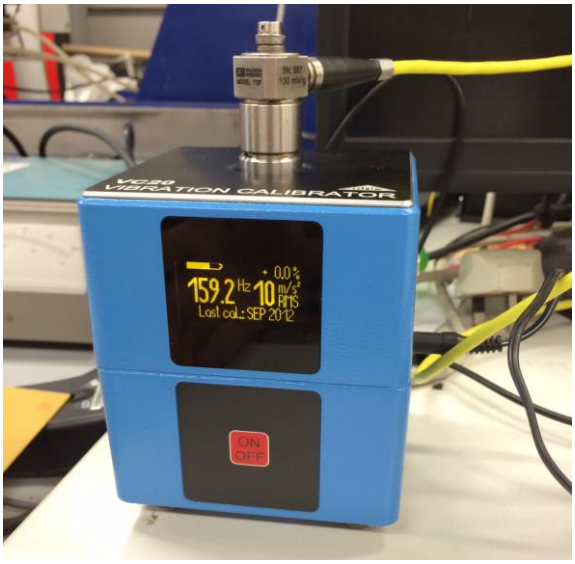

Figure 5-5: 712F Wilcoxon accelerometer and VC20 vibration calibrator.

Figure 5-6: Mistras accelerometer power supply model LP241-12.

The accelerometers used during tests were calibrated using a vibration calibrator vibrating with 159.2 Hz frequency (Figure 5-5). This calibration method is called 'back to back' comparison which is the easiest and least expensive calibration technique [148]. The sensor was mounted on the calibrator using the built-in magnets. A sinus wave with a single frequency of 159.2 Hz was generated by the calibrator which could be observed in the FFT results of the data.

An executable customised software (UOB analyser) was developed by the author using MATLAB in order to log the data for up to 12 channels as well as for analysis in both time and frequency domains. This software is a dedicated Windows™- based software for data logging, analyses and display of both AE and vibration signals. It is capable of running all the essential analysis for both AE and vibration data. Digital filtering and evaluation of

converting raw signals to moving RMS, kurtosis, Crest Factor, HFRT and time spectral kurtosis (TSK) are features included in the software. The program was tested during laboratory experiments including bearing monitoring and also structural examination of cast manganese steel material during fatigue testing of notched sampled. It was also employed during the Long Marston field trials. Moreover, the software is capable of carrying out multiple measurements at duration and time intervals specified by the system's operator. The screenshot in Figure 5-7 shows the main screen and some of the key functionalities of the software created.

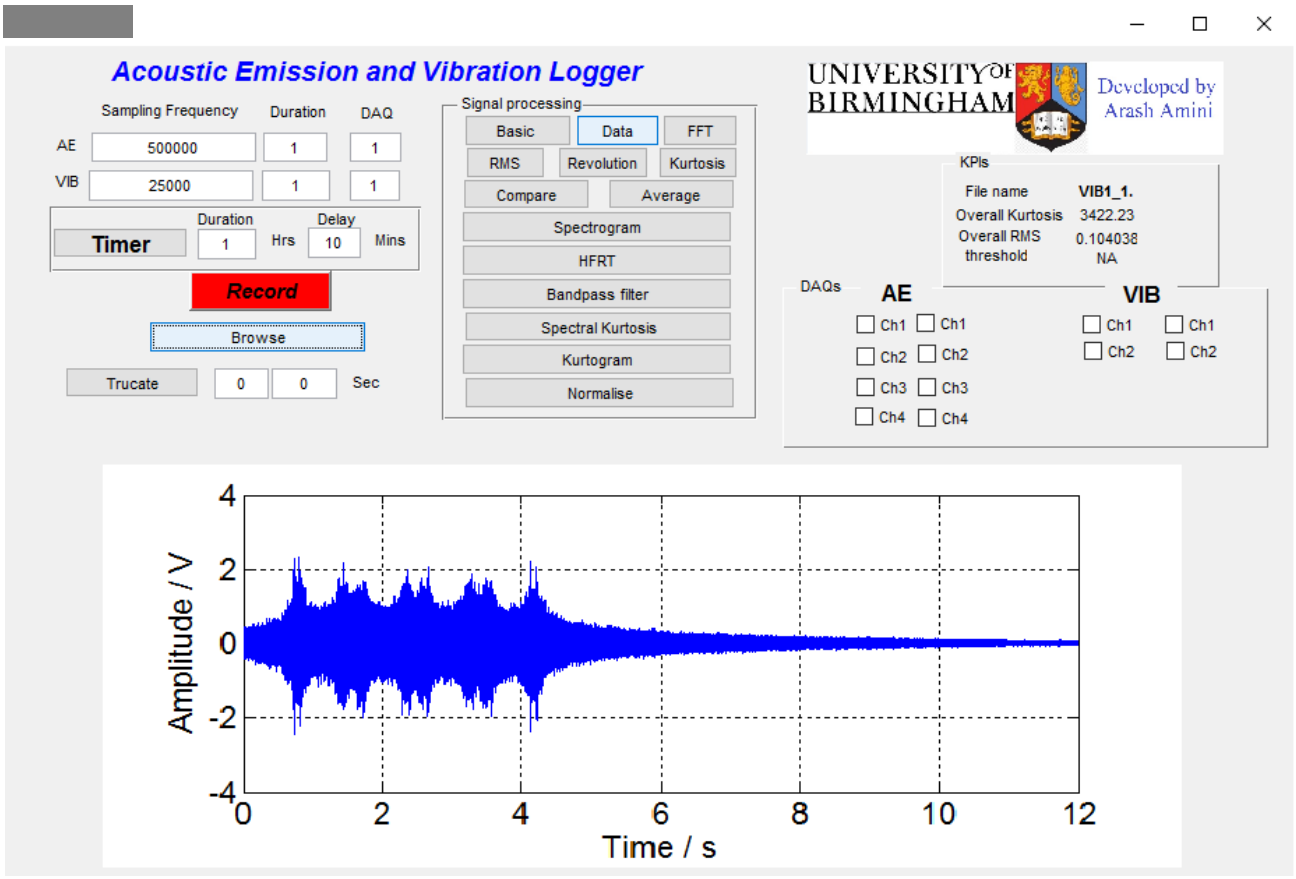

Figure 5-7: Executable customised logging and analysis software developed by the author using Matlab.

Figure 5-8 shows a flowchart explaining the customised logging and analysing software. In order to acquire the data, test configuration such as duration time, sampling rate and number

of data acquisition boards (DAQ) need to be entered. In addition, there are two options of recording and timer, for automatic acquiring, available. Data can be analysed and interpreted using the signal processing techniques described in chapter 4 of this thesis.

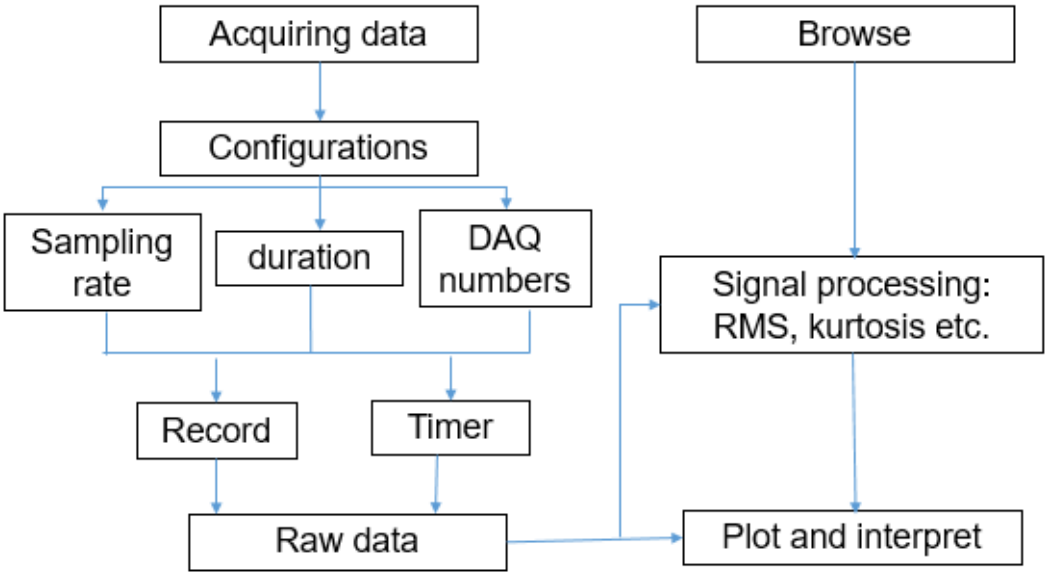

Figure 5-8: Flowchart explaining the customised logging and analysis software.

5.2 Laboratory-Based Testing

The following laboratory-based experimental work was carried out:

1- Testing of all devices including a preamplifier, amplifier, 4 channel Hub and data acquisition board to evaluate whether the frequency filtering with the preamplifier (below 100 kHz) is correct. Alternating currents were transmitted at different frequencies using a waveform generator, model Agilent 33500B, through the test devices. The output signals were checked using an oscilloscope, model Tekronix TDS2012B, to examine the frequencies passed or filtered through the devices.

2- Hsu-Nielsen calibration tests using mechanical pencil lead tip breaks were used to calibrate the AE sensors.

3- Accelerometers were calibrated using a vibration calibrator.
4- Metal impact tests simulating metal with metal impact caused by a defect such as a wheel flat.
5- Wayside vibration and AE tests using a railway wheel at scale that was installed on a test trolley and moved along a short test track. During these tests healthy and defective (wheel flat and metal build-up) conditions were simulated.
6- Roller bearing tests using a custom-built test rig to simulate the onboard AE and vibration measurements.

Field experiments were also carried out under realistic conditions at the Long Marston test track with the help of VTG Rail and Motorail Logistics. Various wheel tread and axle bearing defects were simulated during these field trials carried out at speeds between 20 MPH and 30 MPH (32-48 km/h). The rolling stock used for the tests were tanker wagons made available by VTG Rail. Finally, an integrated AE-vibration system was used to instrument permanently a site at Cropredy on the Chiltern rail line connecting London Marylebone with Birmingham Moor Street Stations. The instrumented line is used by both passenger and freight trains with trains passing as often as every five minutes. A Hot Axle Box Detector (HABD) is installed adjacent to the customised AE-vibration system. The installation has been carried out in collaboration with engineers from Network Rail and Krestos Limited. Details of the work carried out at Long Marston and Cropredy are reported in later chapters of this thesis.

Prior to undertaking any simulation tests the AE sensors were checked to ensure they remained calibrated and coupled correctly at all times in order to generate consistent signals. Calibration was carried out, as mentioned earlier, using a Hsu-Nielsen source test. The Hsu-Nielsen source test involves pressing a lead tip (0.3 or 0.5 mm in diameter, 2H hardness) at an oblique angle against the surface of the test piece at which the sensors have been mounted, until it breaks. The fracture of the tip generates a broadband signal which can be used to check the amplitude of the AE response captured at different

amplification gains as well as the frequency response of the sensor. The release of strain energy within the lead tip breaking is caused by the sudden recoil of the compressed atoms upon the surface of the metal when fracture occurs and does not originate from within the lead itself [27]. Figure 5-9 shows a burst type AE signal generated by a lead tip break prior to a bearing rig test.

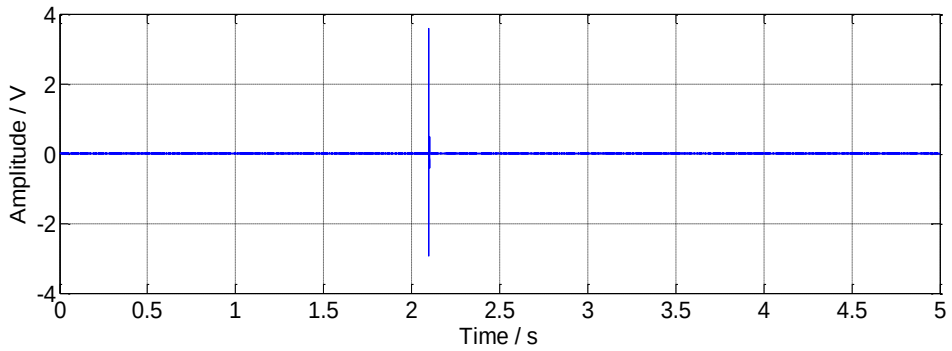

Figure 5-9: A burst AE signal following the fracture of a lead tip.

In addition, impacting a piece of metal on the rail surface simulates impacts similar to defects such as wheel flat. To do so a small piece of metal was used to impact on the rail track. This is a useful test for evaluating the response of the AE transducers and accelerometers for the entire system prior to each measurement. Impact test can be also be used to obtain the resonance frequency of the structure in order to apply further analysis such as HFRT as shown in Figure 5-10.

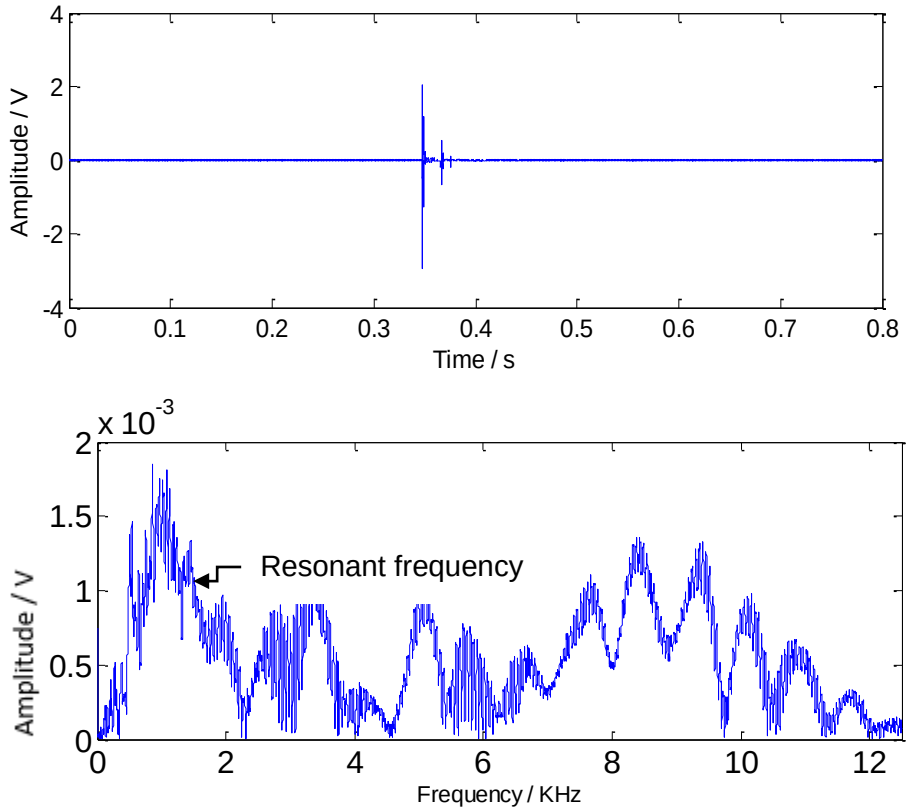

Figure 5-10: Impact test on the bearing during laboratory experiments in order to evaluate the resonance frequency of the bearing.

Figure 5-11 presents the raw AE signal from a test carried out using the test trolley without any wheel defects. While the trolley is moved along the test track for 5 s period a lead tip is broken at 2.6 s of the test giving rise to a strong burst signal which is clearly visible. The moving RMS plot of the raw signal is also shown with the lead tip break event showing as a clear high energy peak at 2.6 s. As it was mentioned earlier, lead tip breaks emit waves in a broad range of frequencies including those that are of interest in crack growth detection. Therefore, this experiment proves that wheels on healthy condition generate very little background noise and a crack growth event in the vicinity of the AE sensors would be detectable. In real life test conditions, other possible background noises can occur due to friction between the wheel flange and rail (also a defect), bogie hunting and the engine.

Another important source of undesired background noise is the friction of the wheel against rail due to roughness.

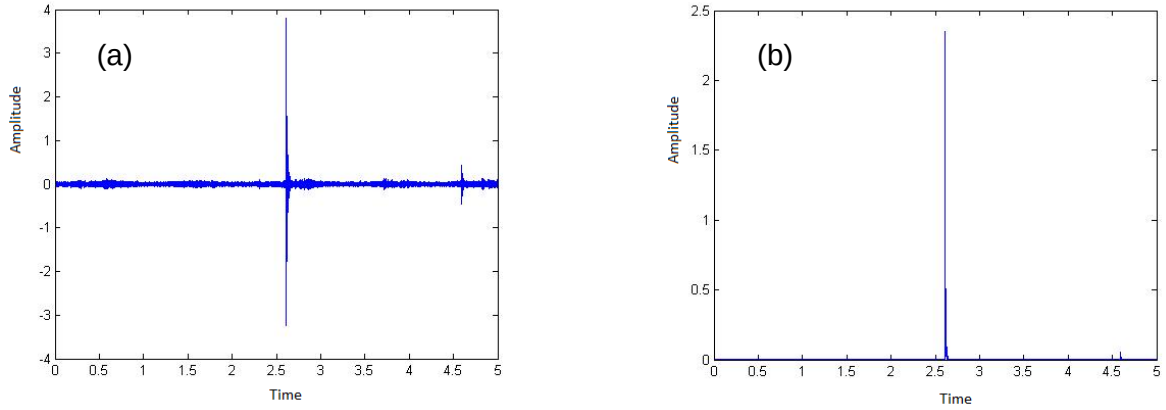

Figure 5-11 : Simulated AE event during movement of the test trolley using a lead tip break. a) Raw data and b) moving RMS plot.

As previously mentioned, WD AE sensors are used in order to find the frequency bandwidth arising from different defects. Figure 5-12 shows the power spectrum following FFT analysis of a bearing with roller defect rotating at 400 RPM mostly excited in100-150 KHz. This frequency range is close to the resonance bandwidth of R50α sensor.

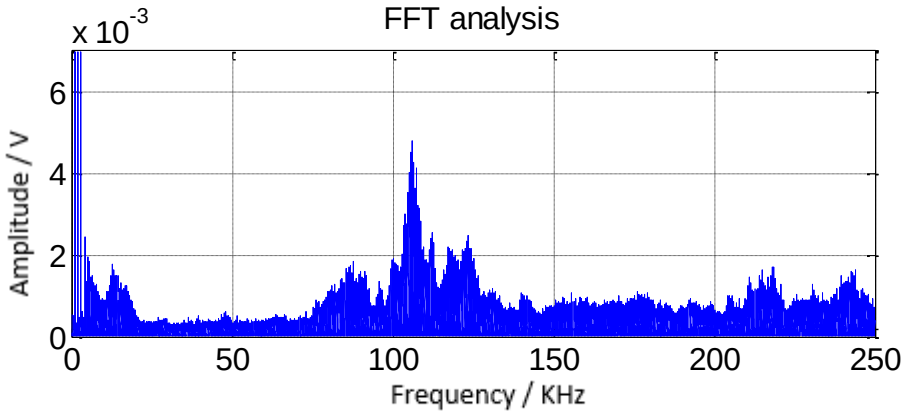

Figure 5-12: Bearing with roller defect tested with a WD AE sensor.

Experiments were carried out changing some of the parameters to attain the best result, in terms of minimum analysis time and working on higher frequencies. Sampling rates of 0.5, 1, and 2 MS/s were considered. Choosing a sampling rate of 2 MS/s can provide results in the

frequency domain up to 1 MHz (Nyquist rule). However, no peak appears for frequencies at a range higher than 0.25 MHz therefore lower sampling rates can be effectively used. Higher sampling rates also need higher processing times because of the larger volume of data generated. Data acquisition for a field unit is a very important consideration since the volume of data that needs to be logged, processed and stored is considerable when several hundreds of trains are monitored every day. Keeping the sampling rate and data logging time as low as possible helps minimise the volume of data that needs to be handled and simplifies computational capacity required to be deployed. Therefore using a sampling rate higher than 0.5 MS/s is unnecessary. The results from lead tip break tests in conjunction with R50a sensor were analysed and compared in the frequency domain as shown in the plots in Figure 5-13 for three different sampling rates (0.5, 1 and 2 MS/s).

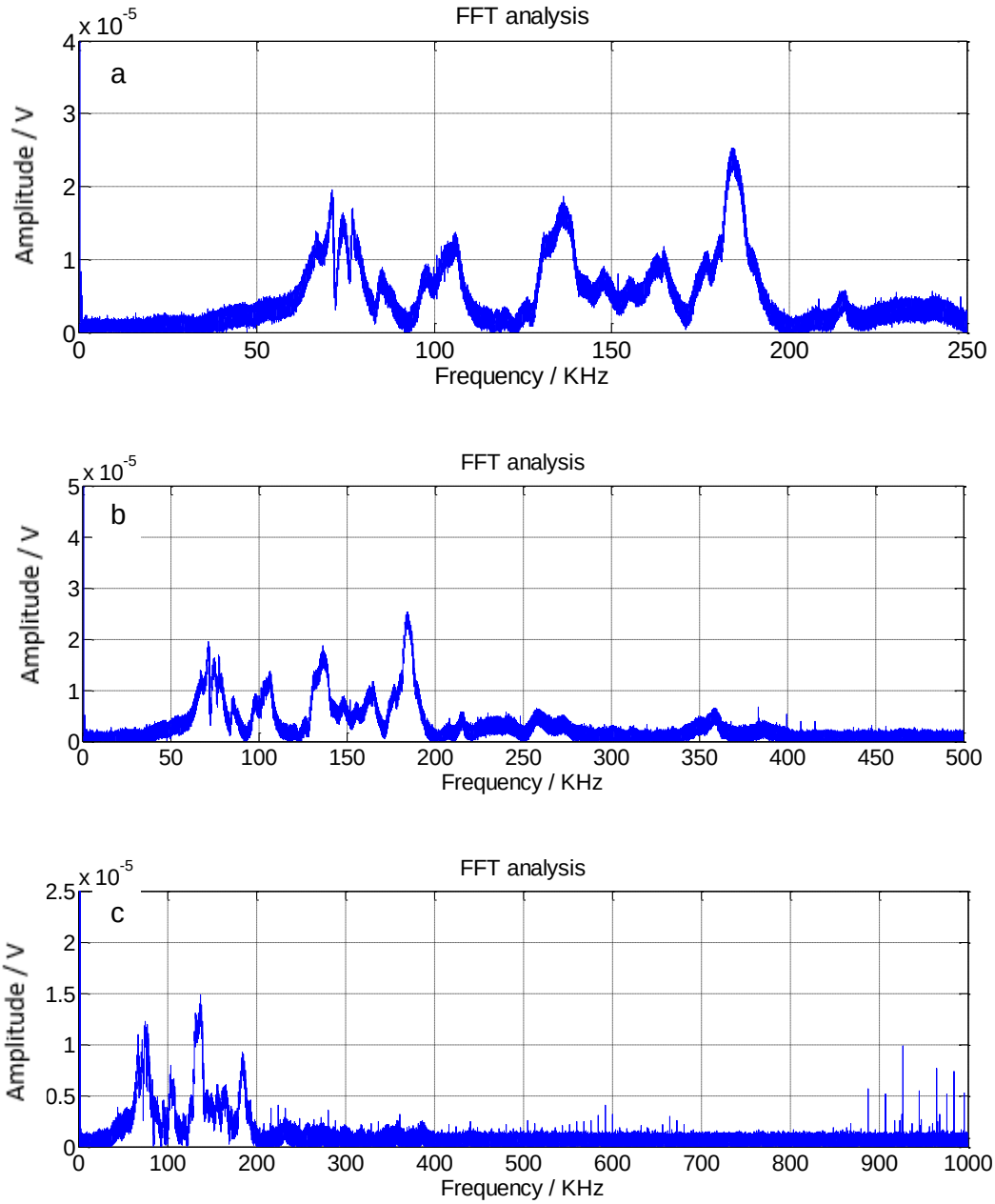

Figure 5-13: Power spectrum plots for a R50α sensor at sampling frequency a) 500 kS/s, b) 1 MS/s and c) 2 MS/s.

Higher sampling rates such as 1 and 2 MS/s with acquisition times lasting for a few seconds generate a huge amount of data resulting in longer processing times and requiring more powerful computer processor to carry out the analysis. As it is evident from the tests carried out there is no visible peak at the frequency range above 0.25 MHz. Therefore the optimum sampling rate is 0.5 MHz. The R50α sensor has resonance frequencies at 170 kHz. These

resonance frequencies are excited after detecting a signal from a defect such as a metal to metal impact. From the results of the tests at different sampling rates with different sensors, it was decided that the use of the R50α sensor for future experiments is appropriate thanks to its resonance at 170 kHz.

Another important aspect of the experiments is the signal amplitude measured in V. The signal amplitude is directly related to the energy of the source as well as the amplification used. It is very important that the raw signals are not saturated to enable correct analysis later on using the various algorithms considered in this study. For this experimental setup the amplitude range is $\pm$10 V. The signal amplitude is also dependent on distance of the AE source from the sensor. An AE source closer to the sensor will generate higher amplitude signals due to less damping and scattering of the waves. Severe defects such as a large wheel flat will generate high amplitude AE events which will repeat themselves at regular time intervals with every wheel revolution. It is therefore very important to choose an appropriate gain level at the amplification stages to avoid saturated signals but also to ensure interesting AE events related to the presence of defects are captured. Low gain levels will lead to very low signal strength making analysis very difficult. Hence, in order to get the optimum signal level, different gains should be considered for different experimental setups. Figure 5-14 shows the raw signal captured with very low amplification.

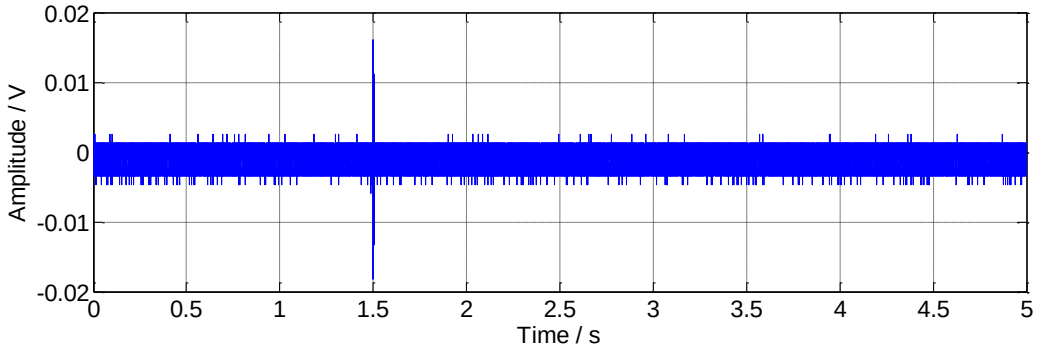

Figure 5-14: Example of AE signal metal bump test, low amplitude due to using very low amplification.

Figure 5-15 shows the resulting spectrum after FFT analysis has been carried out on a signal containing multiple lead tip breaks. The response of the R50α sensor is very similar in terms of the frequency response to that of a single pencil break as the same peaks in the power spectrum are visible. Thus, using spectral analysis only, it is not possible to evaluate the number of defects similar in nature but simply assess whether a defect is present. FFT used as the only analysis technique is insufficient to predict all wheel defects. It is necessary to use additional signal processing techniques for wheel tread and axle bearing monitoring.

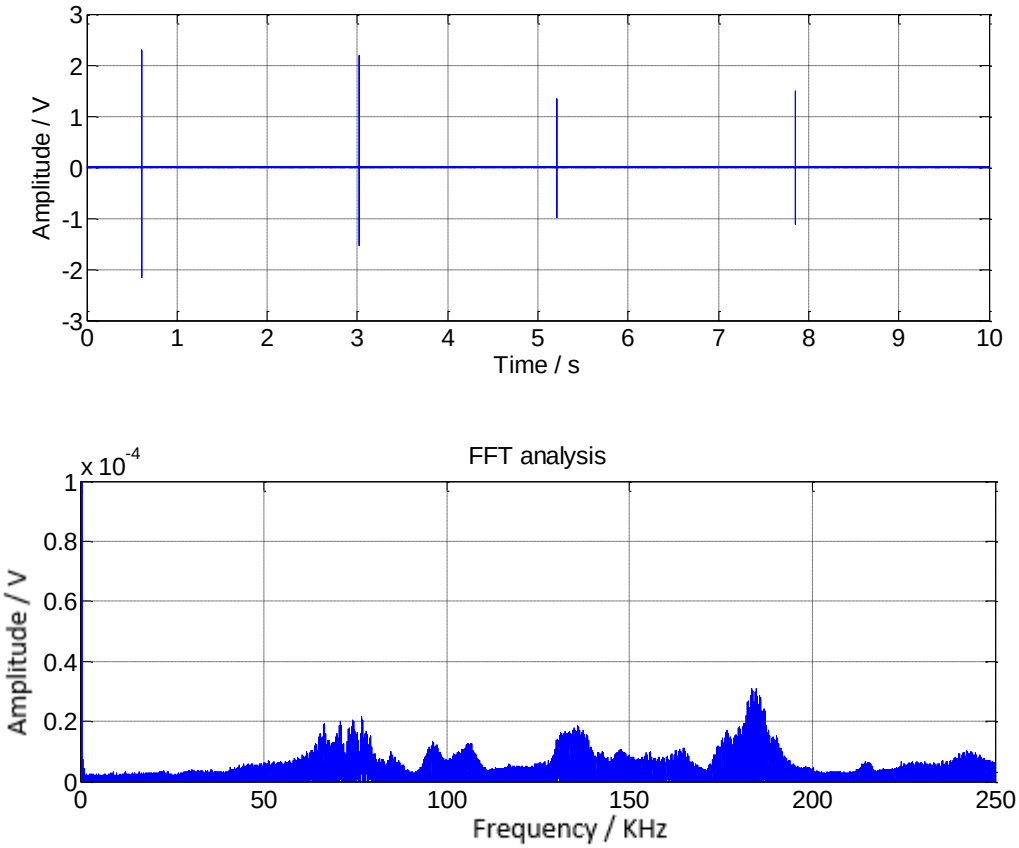

Figure 5-15: Multiple lead tip breaks a) raw data b) the resulting power spectrum.

RMS analysis generates only a single value for a dataset, however, by using the moving RMS, data are divided in overlapping windows, and the RMS is then calculated for each window generating very useful results. Figure 5-16 show the moving RMS plot of the raw signal containing multiple lead tip breaks.

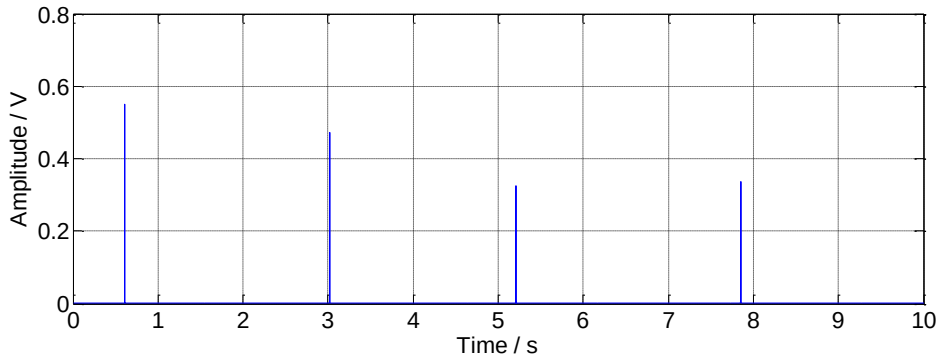

Figure 5-16: Plot showing the moving RMS of the raw signal containing multiple lead tip breaks.

As discussed earlier in this report, kurtosis values of less than 3 for a measured machine consist of normal distribution noises, hence, no fault is present. However, any value above 3 may potentially be related to the presence of a fault.

Figure 5-17 shows the moving kurtosis result for the same raw signal containing multiple events arising from consecutive lead tip breaks. The background signal has kurtosis values around 3. It should be noted that kurtosis has high computing time in comparison with other signal processing algorithms such as moving RMS due to the more complex mathematical calculations involved.

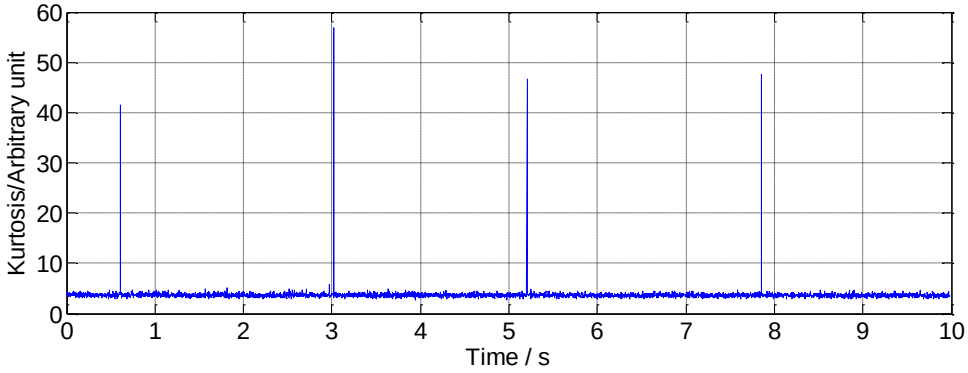

Figure 5-17: Plot of moving kurtosis results for raw signal containing multiple events arising from consecutive lead tip breaks within a 10-second acquisition period at 500 kS/s

5.2.1 Single wheel laboratory test

Experiments were carried out using laboratory scale-sized railway wheel with 0.16 m diameter. During tests the wheel was rotated against a small rail section with an average speed of 1 m/s. The conditions tested were for a healthy wheel and for a wheel with either a flat or metal build-up present in the tread. These faults were induced artificially. In the case of the wheel flat, a flat area was ground on the tread of the wheel, as shown Figure 5-18 using a power tool. The metal build-up defect was simulated by placing a piece of metal and blue tac to glue it on the tread in order to simulate impacts caused by metal build-up type defects. The impacts were clearly visible with every wheel revolution, as distinct peaks even in the raw signal.

Figure 5-18: Artificially-induced wheel flat.

The AE sensor was coupled on the rail using Vaseline and kept in place under constant load using a magnetic hold-down. The AE signals detected by the sensors were amplified using a pre-amplifier and then an amplifier. The amplified signal was then fed through a 4-channel decoupling box to a 12-bit Agilent 2531A data acquisition board before finally being logged by the PC using the UOB analyser customised software written in Matlab. Figure 5-19 shows the experimental setup for this set of tests.

Figure 5-19: Scaled-down railway wheel used for initial laboratory experiments.

Figure 5-20 shows some of the results from this experiment. Wheels with metal build-up, flat defect and healthy condition were manually rotated at speed of 1 m/s on the rail in 5 s recording time. Signal from the healthy wheel shows low amplitude AE activities due to the wheel/rail interface. The wheel with the metal build-up defect created clear impacts on the rail which results in producing high amplitude peaks in the AE signal. The wheel containing flat defect was rolled slower (0.2 m/s) compared to the others and created 2 transient AE bursts, first when the rail reached the flat and second time when passed it.

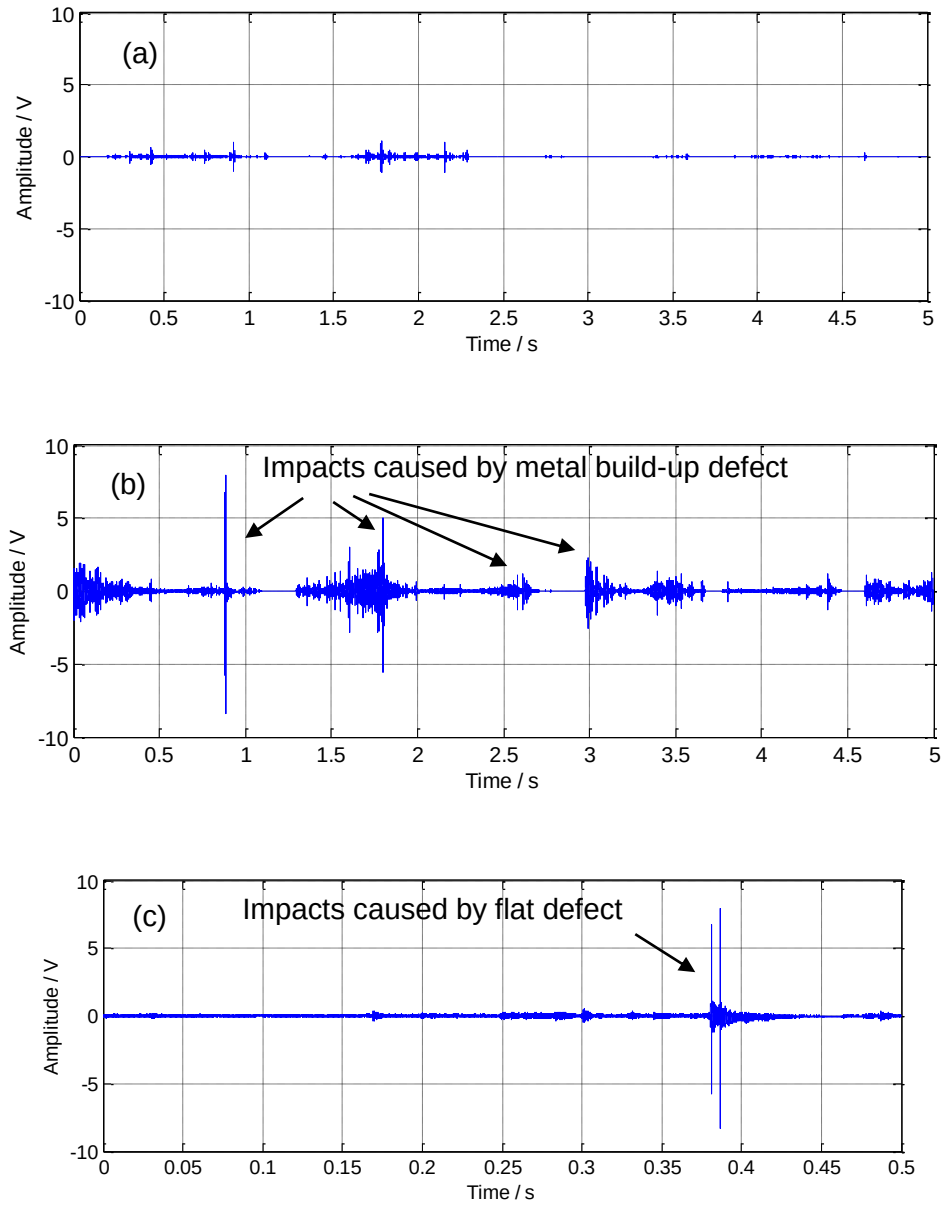

Figure 5-20: Results from the single wheel laboratory tests, a) Healthy wheel, b) Wheel with metal build-up defect, c) wheel with flat defect

5.2.2 Motorised trolley tests

Additional experimental work was carried out using a motorised test trolley with the help of Dr Hamed Rowshandel. These tests were designed in a way that simulated as close as possible the actual operational conditions under a laboratory environment. Figure 5-21 shows the motorised trolley on which the test wheel was mounted together with the rest of

the experimental setup. The motorised trolley was moved along a 7m-long test track and during testing the speed was set to be constant at approximately 2.5 m/s using a motor controller.

Figure 5-21: Experimental work with motorised trolley.

Figure 5-22 shows the raw AE signal acquired during these tests. The peaks seen in the raw data are related to the metal build-up defect impacting on the surface of the rail head every time the wheel completes a revolution. The peak seen at 2.9 s has higher amplitude because this is the point at which the wheel passed directly over the sensor's position. An AE source closer to the sensor has lower attenuation and therefore higher energy although this is also dependent on the impact loads associated with each impact event.

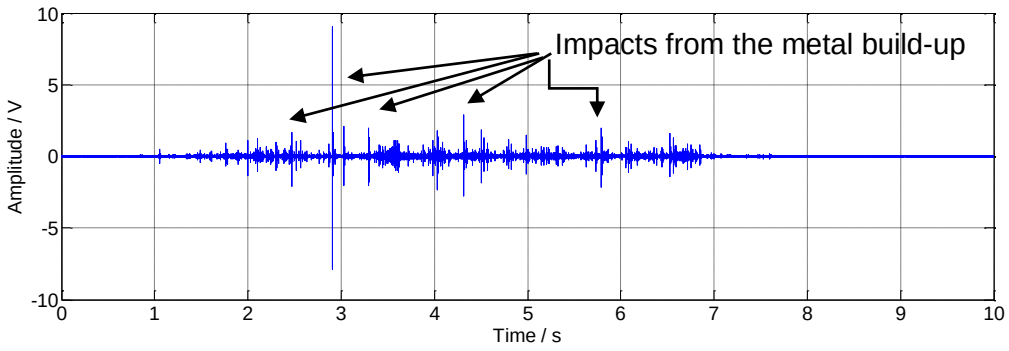

Figure 5-22: Wheel with metal build-up defect moving with automatic trolley.

Figure 5-23 shows the raw AE signal without the presence of the metal build-up defect. The signal is distinctly quieter and no peaks are evident.

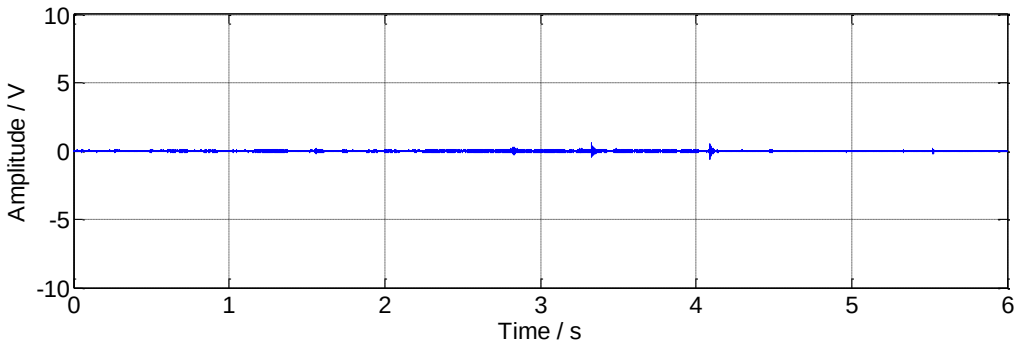

Figure 5-23: AE wayside monitoring of healthy wheel moving automatic trolley.

TSK analysis carried out on the raw signal obtained for the defective condition is able to successfully confirm the wheel defect. The resulting plot in Figure 5-24 following the processing of the raw signal with the TSK algorithm clearly shows a great rise in kurtosis values in the frequency range of about 100 kHz at 2.9 s. This result supports the fact that TSK analysis is capable of identifying a wheel tread defect.

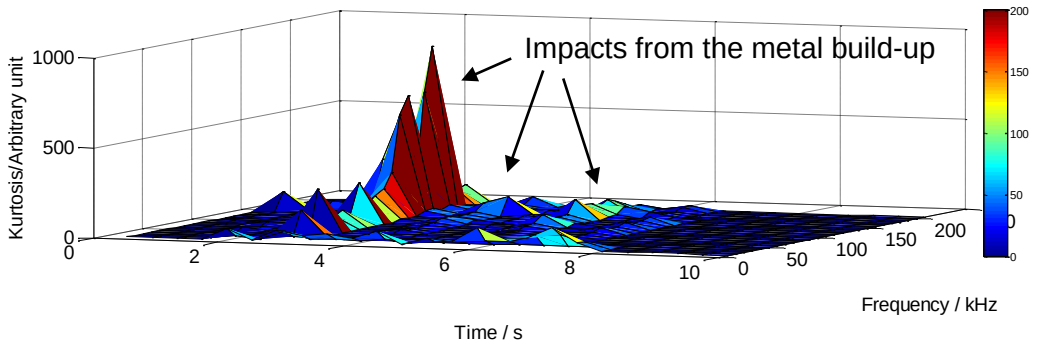

Figure 5-24: TSK analysis of the AE wayside measurement testing the wheel with metal build-up defect, moving with automatic trolley.

5.2.3 Laboratory test rig experiments

Further laboratory experiments were carried out with a bearing test rig. Bearings free of defects and bearings with various induced defects were used during these experiments. The bearings were rotated in the customised test rig at speeds between 100-1000 RPM. An AE

sensor and accelerometer were mounted separately on the bearing housing in order to detect the stress waves and vibrations generated by the various bearing defects. The bearing samples used in the laboratory rig tests were PFI Inc. model PW29530037CSHD automotive wheel bearing with dimensions of 28 x 53 x 37 mm. Due to small size of the test bearings, in this instance, the AE sensor had to be kept in place with duct tape since the attachment of magnetic hold-down was not possible and once again the AE sensor was coupled using Vaseline. Figure 5-25 shows the test rig used for this set of experiments.

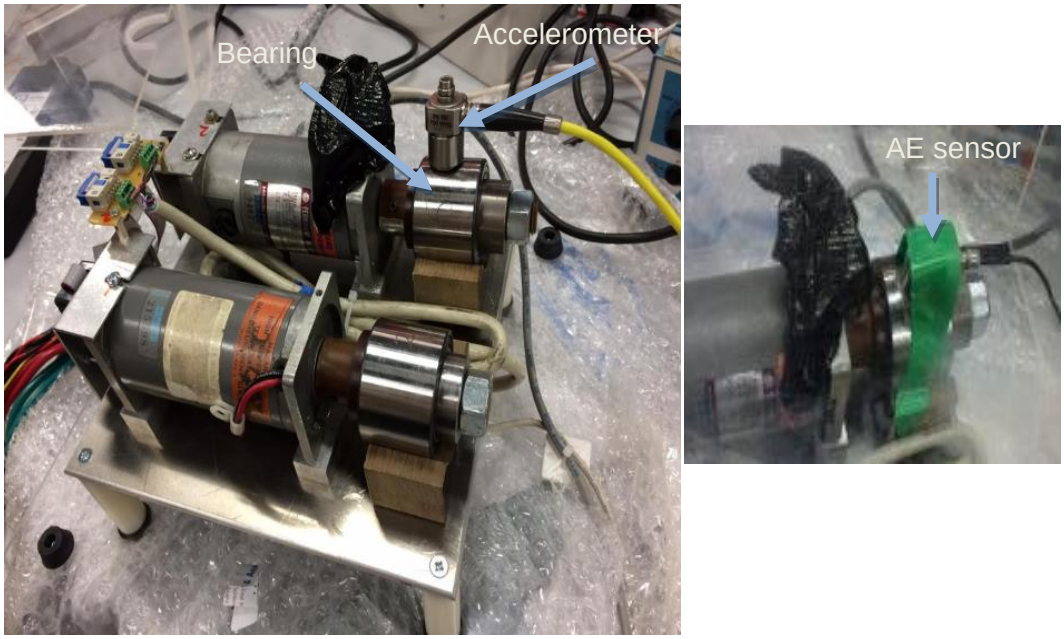

Figure 5-25: Customised laboratory bearing test rig at the University of Birmingham.

Bearings used in this set of tests included healthy, lubricant contamination, outer race and roller defects and different defect severities were simulated. The test bearings were disassembled in order to artificially induce the defects and then put back together and mounted on the test rig prior to testing at different RPM and loading conditions. Figure 5-26 shows one of the test bearings after disassembling in order to induce lubricant contamination. Figure 5-27 shows different types of induced defects in the bearings used for

laboratory experiments. The various defects, corresponding code and description of defects are summarised in Table 5-1.

Figure 5-26: Example of a rig double-raw tapered roller bearing.

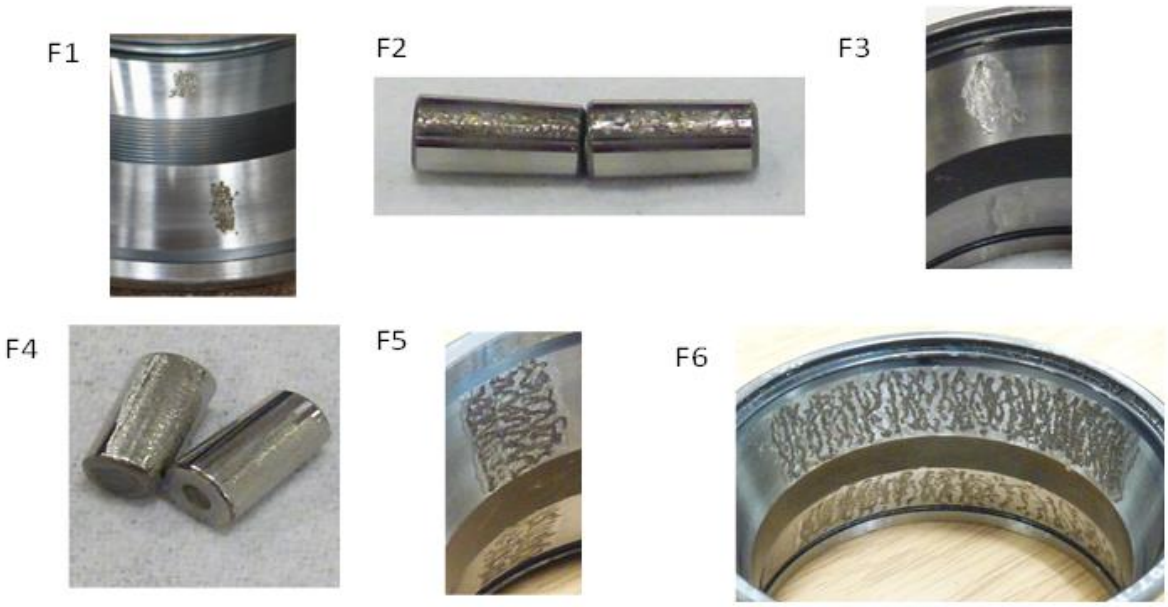

Figure 5-27: Different induced bearing defects used for laboratory experiments with the customised test rig.

Table 5-1: Sample codes and description of bearing defects employed during test rig experiments.

Lab Test ID	Description
F0 (H)	Good condition, no introduced defects.
F1	Minor damage to one small area on each outer race, consisting of surface roughening by means of an electrical discharge engraver. Fault length 1.7% of circumference.
F2	Minor damage to one small area of one roller in each cage, again consisting of surface roughening by electrical discharge engraver. Fault length 10% of circumference.
F3	Similar to F1 above, but damage is a little larger and deeper, inflicted by means of a small rotary grinder. Fault length 2.9% of circumference.
F4	Similar to F2 above Single faulty roller in each cage. Small rotary grinder. Fault length 50% of circumference.
F5	Roughened fault, same position on each outer race. Damage inflicted by small cutting wheel and engraver. Fault length 6.6% of circumference.
Lubricant contamination	Bearings with 0.5 % and 1% weight ratio of sand contamination in the lubricant-

The results for measurements carried out at 500 RPM were considered for both healthy and defective (outer race defect) bearings and a load of 5 bar was applied on the sample bearings during testing. Table 5-2 illustrates the characteristic frequencies of the bearings used during the rig tests. There might be an offset between the frequency achieved by HFRT and the table which has been caused by variations in the rotational speed during the test.

Table 5-2: Fundamental frequencies of bearings in the rig test. Highlighted frequencies and their harmonics expected to observe at 500 RPM for the bearings with outer race and roller defects.

	Speed(RPM)						
Defect types	150	250	300	400	500	600	1000
FTF	1.1	1.8	2.2	2.9	3.6	4.4	7.3
BPFO	23.1	38.4	46.1	61.5	76.9	92.3	153.8
BPFI	29.4	49.05	58.8	78.5	98.1	117.7	196.2
BSF	19.7	32.9	39.5	52.7	65.85	79	131.7

Bearings with 0.03 grams of sand contamination (0.5 % weight ratio) and 0.06 grams sand contamination (1% weigh ratio) in the lubricant were also considered during test rig experiments. The amount of grease in the test bearings is approximately 6 grams. Furthermore a series of experiments were completed on the bearings rotating at different speed. Experiments were carried out for both AE and vibration measurements. The results are compared in chapter 7.4 in order to observe the effect of defect size and type at different rotating speeds.

5.2.4 Results

Figure 5-28 and 68 show the AE and vibration signal differences for a healthy bearing and one with a roller defect (F2). The peaks in the AE signal for the bearing containing a roller defect can be clearly seen in both AE and vibration raw data. These peaks are generated by the impacts between the roller defect and the races of the bearing. Spectral analysis of the AE signal based on FFT also confirms the presence of a defect due to the rising amplitude of the overall power spectrum of the captured signal. Therefore, the presence of the defect is manifested over a broad frequency range. Similar results are observed in the vibration signal. Nonetheless, spectral envelope analysis is needed in order to find the characteristic frequencies of the defect. In addition, the plot of the moving RMS for the defective bearing

shows the peaks from the bearing defect. Analysis based on the moving kurtosis algorithm does not provide a consistent result when analysing the raw signal although there is a clear increase in the peak values for the bearing with the roller defect. The high amplitude moving kurtosis peak observed at 3 s for the healthy bearing might be the cause of external noise sources, such as the motor of the test rig, or surrounding non-Gaussian noises (Figure 5-28). This peak nonetheless can be discarded using trending. In the case of vibration, analysis is more consistent for all algorithms for this particular defect type and severity as seen in Figure 5-29.

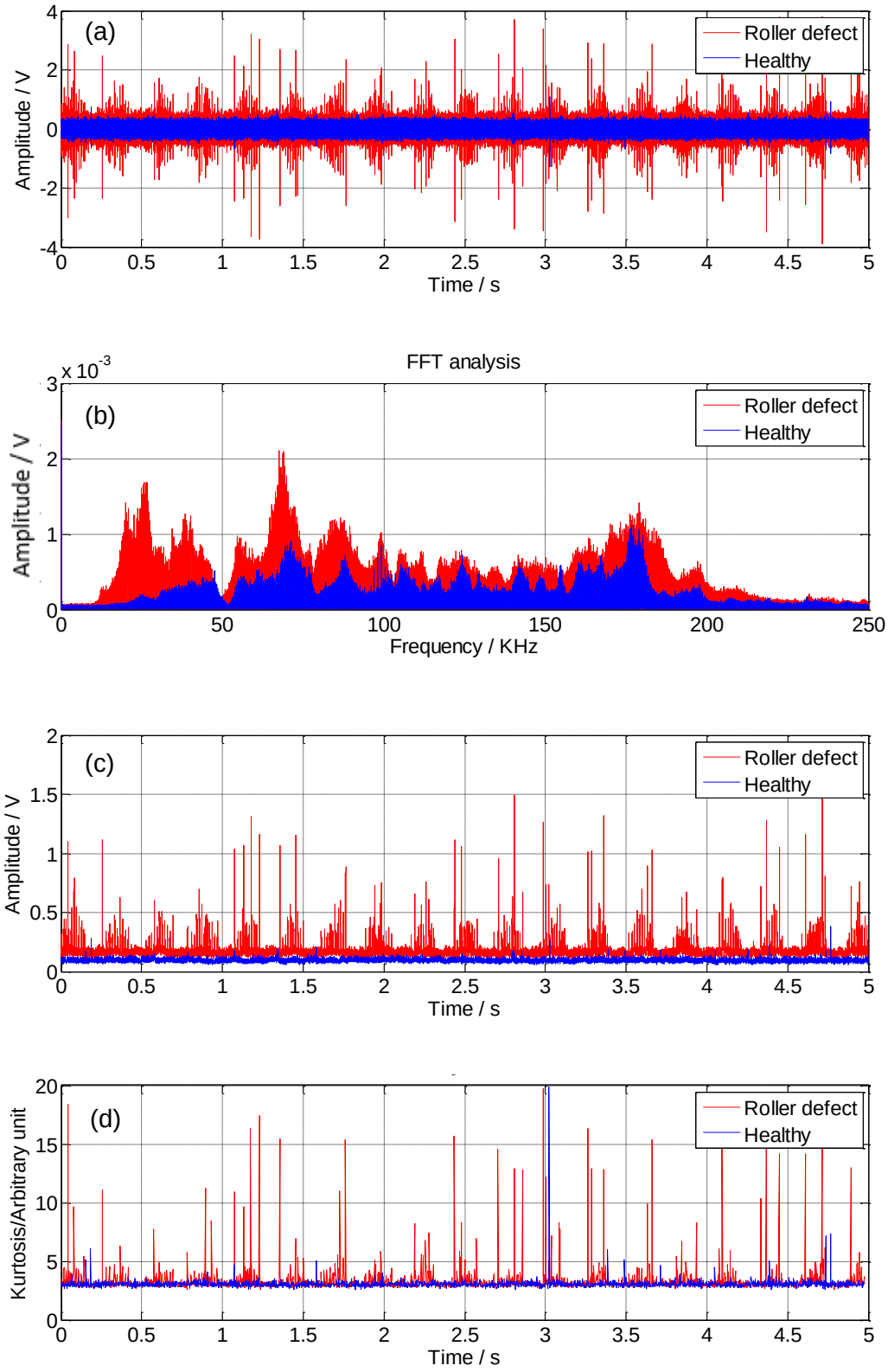

Figure 5-28: Comparison between AE data from healthy and bearing with roller defect (F2) at 500 RPM for a) Raw data plot, b) Power spectrum, c) Moving RMS plot and d) Moving kurtosis.

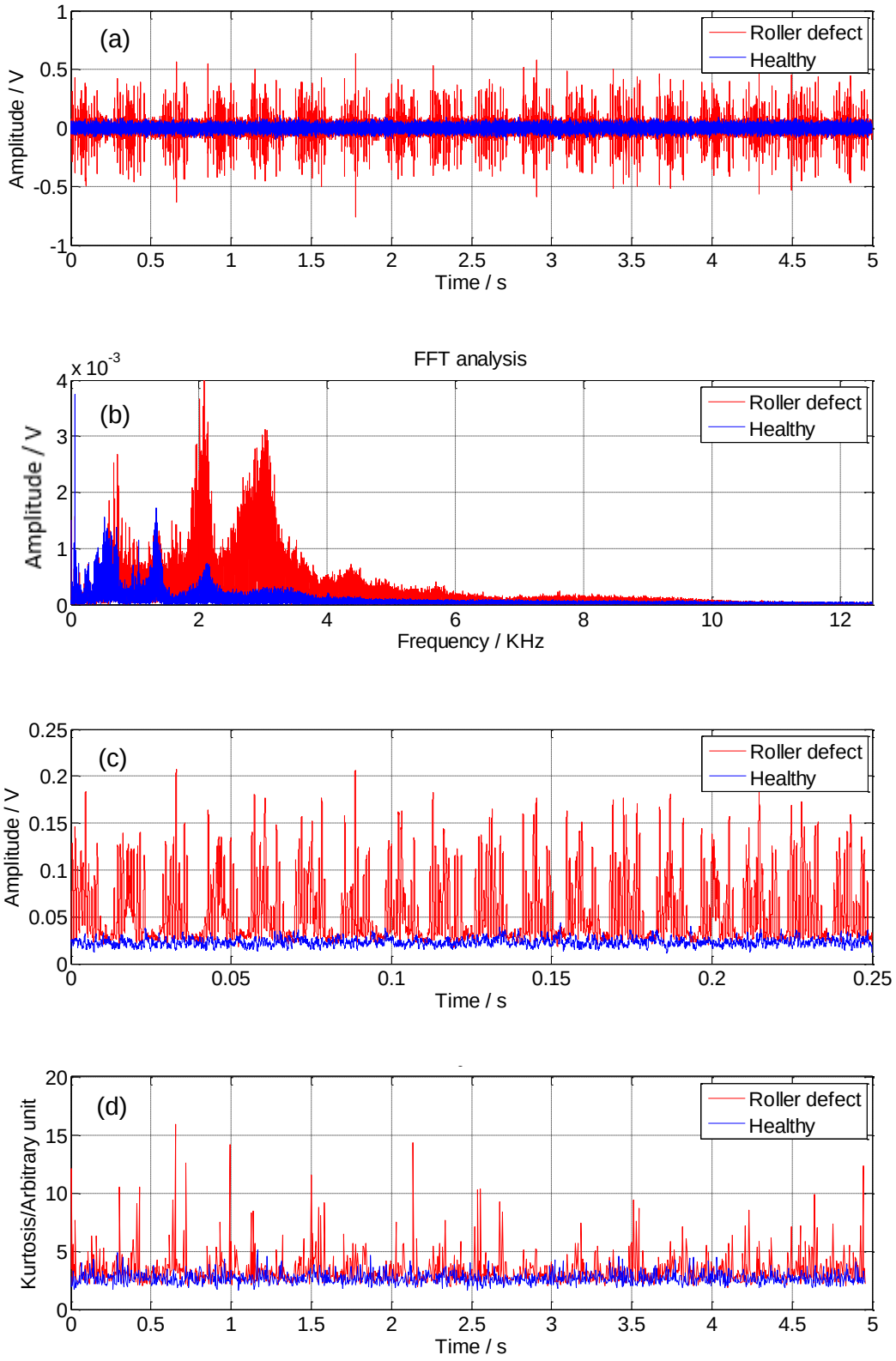

Figure 5-29: Comparison between vibration data from healthy and bearing with roller defect (F2) at 500 RPM for a) Raw data plot, b) Power spectrum, c) Moving RMS plot and d) Moving kurtosis.

The overall values have been calculated and are summarised in Table 5-3, showing that all values for both AE and vibration tests are higher in the case of the defective bearing.

Table 5-3: Comparison between Overall values from healthy and bearing with roller defect (F2) at 500 RPM.

	AE		Vibration	
	Healthy	**Roller defect**	**Healthy**	**Roller defect**
PK-PK / V	2.35	7.68	0.21	1.39
RMS / V	0.09	0.19	0.02	0.06
Crest factor	11.3	19.29	4.34	9.54
Kurtosis	3.2	10.57	3.05	11.48

Figure 5-30 shows the spectral envelope analysis of AE and vibration signal on a healthy bearing used in test rig experiments. It is evident that no indication appears in the analysis approach confirming that there is no defect present.

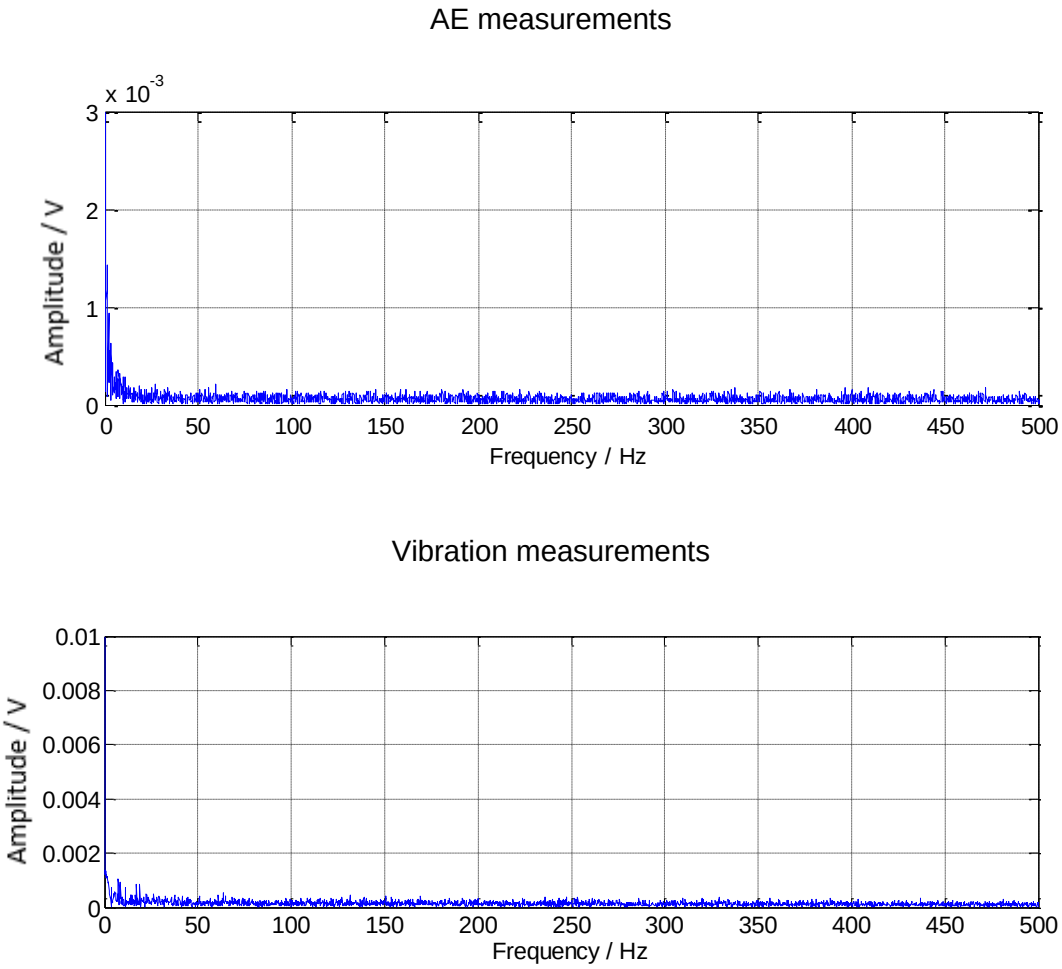

Figure 5-30: Spectral envelope analysis for the AE and vibration signals from a healthy bearing tested using the customised test rig at a rotational speed of at 500 RPM.

In the case of the defective bearing, the fundamental frequency and its harmonics arising from the impulses caused by the impact of the bearing defect as it rotates have been excited. The AE and vibration spectral envelope analysis results for a sample bearing with an artificially induced roller defect (F2) are shown in Figure 5-31. From the analysis carried out a peaks at the characteristic frequency of 62.5 Hz in AE and 63.5 Hz in vibration and its harmonics are evident. The peak seen at the aforementioned characteristic frequency confirms the presence of the roller fault as it is in agreement with the fundamental frequency of the bearing at the rotating speed used during testing. There is a slight offset between the characteristic frequency given by the analysis and the table which is caused by a slight variation in the rotational speed during testing. It should be noted that if the severity of the

defect is high (i.e. the bearing condition is at stage 3 in terms of severity so close to failure), the fundamental frequency of the defect appears at lower frequency which can be simply detected using FFT analysis. However if the severity level is low, the fundamental frequency of the defect is only detectable in the resonance frequency (demodulated signal) which can be revealed by spectral envelope analysis.

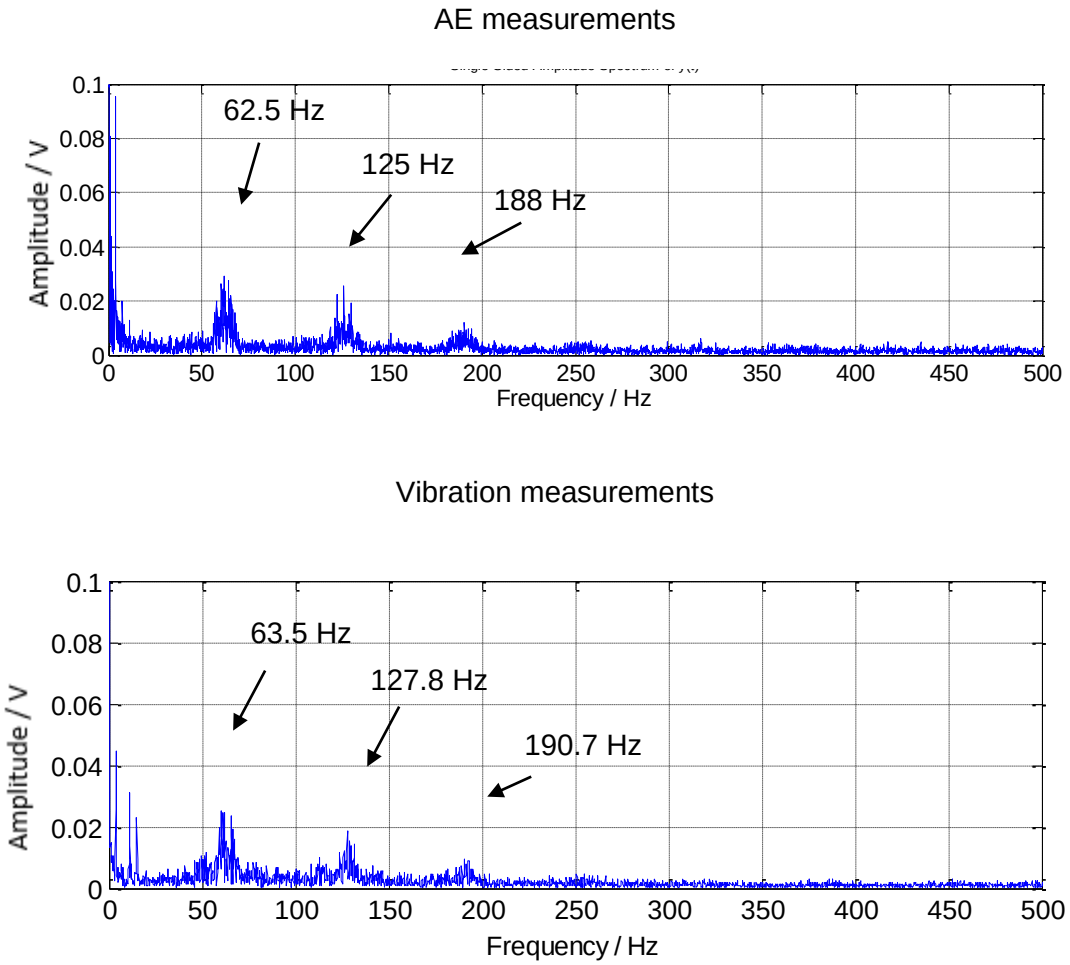

Figure 5-31: AE and vibration spectral envelope analyses for a defective roller bearing (F2) at 500 RPM.

Similar analysis from the bearing with outer race defect (F1) is demonstrated in Figure 5-32. The Peak at 77 Hz and its harmonics indicate the characteristic frequency of the outer race defect.

AE measurements

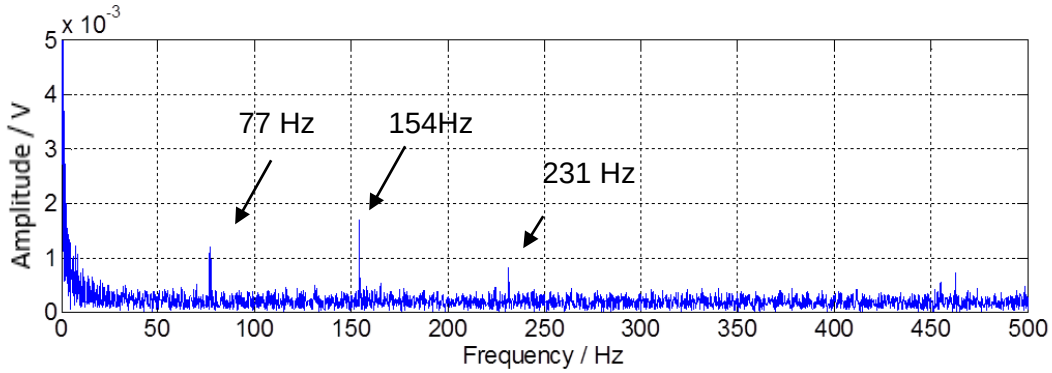

Vibration measurements

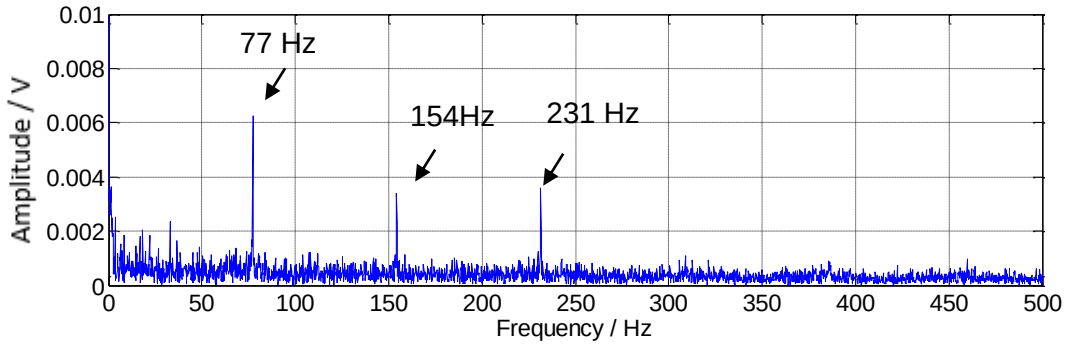

Figure 5-32: AE and vibration spectral envelope analyses for a defective roller bearing (F1) at 500 RPM.

It was suggested by Antoni [136] that Kurtogram-based analysis can be applied on data in order to find an optimum band-pass filter which increases the signal to noise ratio. This optimum frequency band-pass can be used for spectral envelope analysis increasing the possibility of finding the bearing fundamental frequencies which are buried in the noise. In this study, the frequency and band-pass window at which the Kurtogram is at maximum were chosen and applied on AE and vibration data. The fast Kurtogram algorithm used has been proposed by Antoni [136].

A sample Kurtogram of vibration analysis of the bearing with 6.6% outer race defect (F5) at a rotating speed of 500 RPM is presented in Figure 5-33. In addition, the signal was band-pass filtered at the determined centre frequency of 104416 (fc) Hz with bandwidth (Bw) of

4166 Hz based on the maximum kurtosis in Kurtogram. The results are presented Figure 5-34. To assess the improvement in the signal-to-noise ratio, the values of Crest Factor and kurtosis were calculated before and after filtering.

As it was mentioned earlier, the Crest Factor is defined as the ratio of the peak value by the RMS. It is a traditional method of measuring smoothness of a signal and therefore if the number of spikes (generated by the impact from defects) increase, it results in rising the value of Crest Factor. Furthermore, increasing values of kurtosis is also another approach to identify the presence of possible bearing defects. From the result it is evident that the filtered signal using band-pass filter proposed by Kurtogram generates higher Crest Factor and kurtosis values. Therefore, this shows the capability of the Kurtogram method in de-noising the vibration signals.

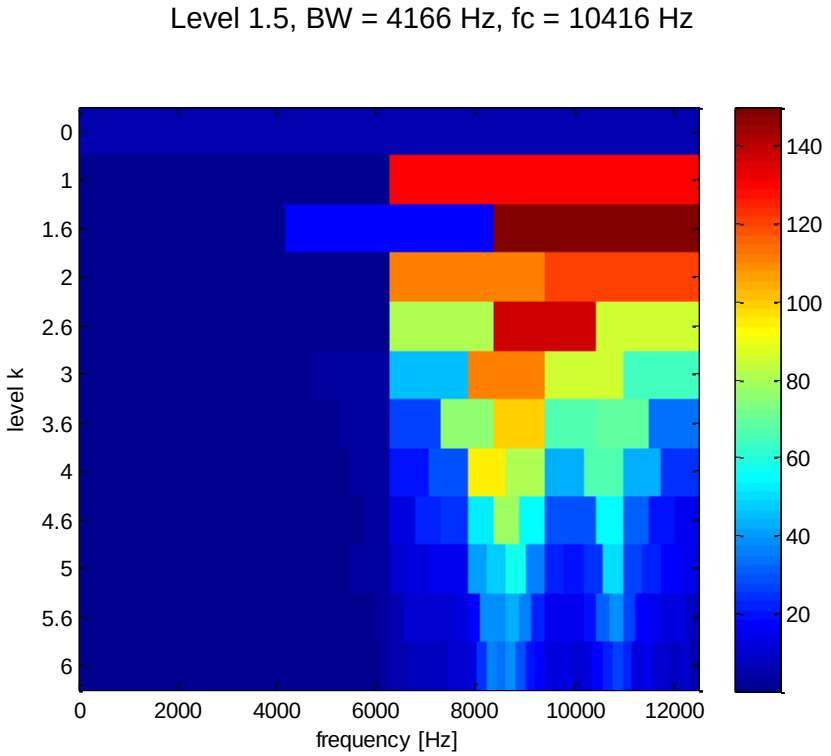

Figure 5-33: Kurtogram from vibration analysis of the bearing with 6.6% outer race defect (F5) tested at 500 RPM.

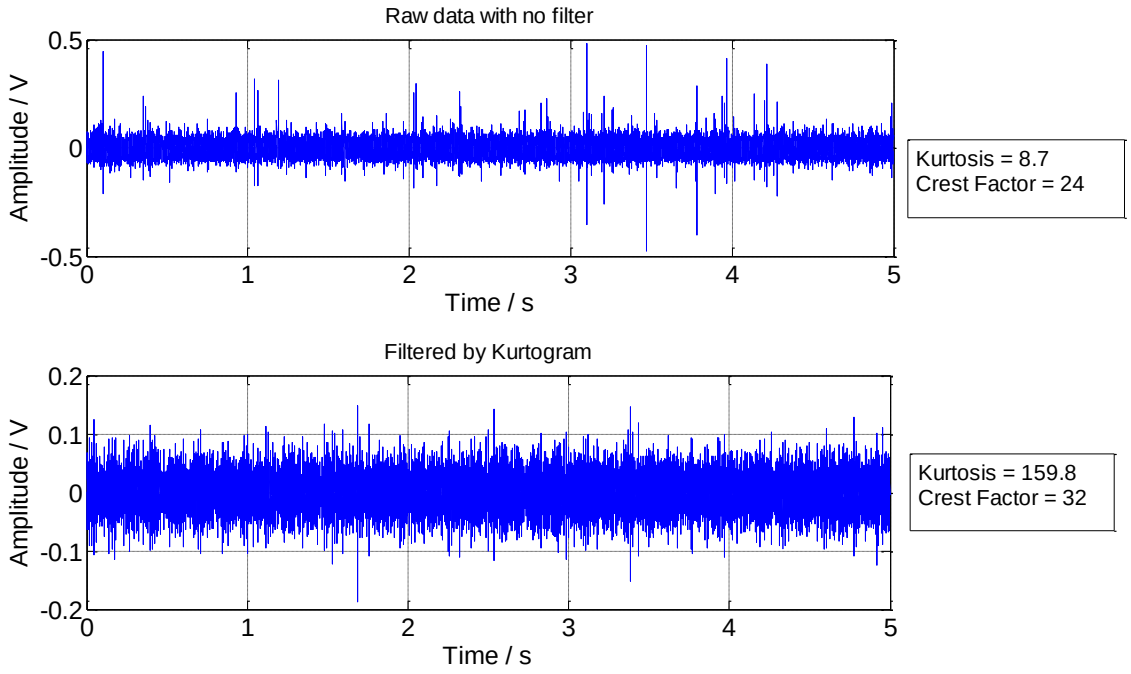

Figure 5-34: Comparison between unfiltered and filtered vibration analysis signal of the bearing with 6.6% outer race damage (F5) tested at 500 RPM.

Analysis was carried out by applying the Kurtogram method to the bearing with minor outer race damage (F1). A band-pass filter with centre frequency of 9375 Hz with 6250 Hz bandwidth was identified by Kurtogram analysis (Figure 5-35). The significant increase in the value of kurtosis and Crest Factor of the filtered signal confirms the successful de-noising process. Figure 5-36 shows the comparison between unfiltered and filtered vibration analysis signals of the bearing with minor outer race damage at 300 RPM rotational speed. In addition, the spectral envelope analysis was applied on both filtered and unfiltered signals. The spectral envelope analysis of the signal without filtering shows only one peak at 46 Hz indicating the outer race defect according to the manufacturer data sheet. On the other hand the spectral envelope analysis of the filtered signal includes the fundamental frequency of the outer race defect in 46 Hz along with five of its harmonics in 92, 138, 184, 230 and 276 Hz. Therefore the spectral envelope analysis of the filtered signals clearly discriminates the defect frequency better than the unfiltered signal (Figure 5-37).

Level 1, Bw=6250 Hz, fc=9375 Hz

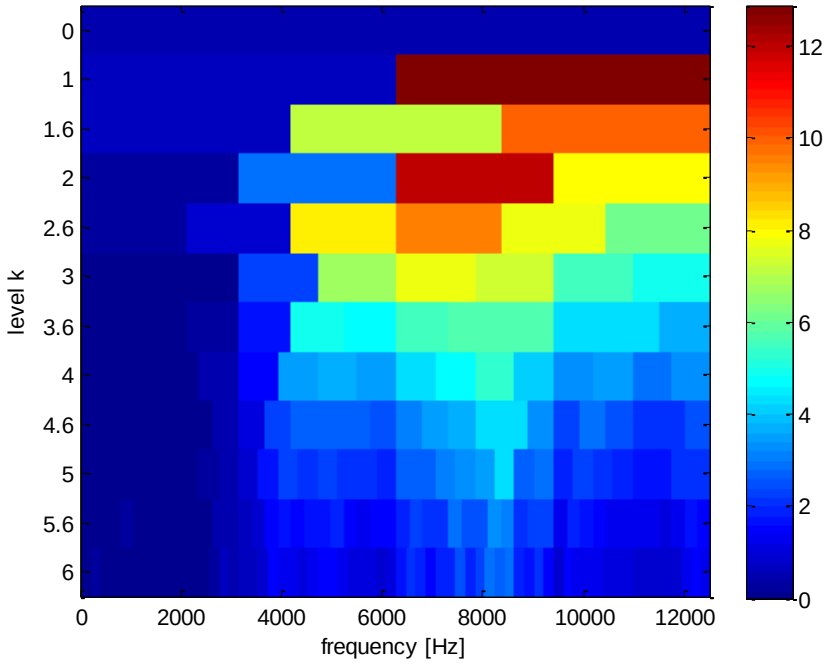

Figure 5-35: Kurtogram from vibration analysis of the bearing with minor outer race defect (F1) - 300 RPM.

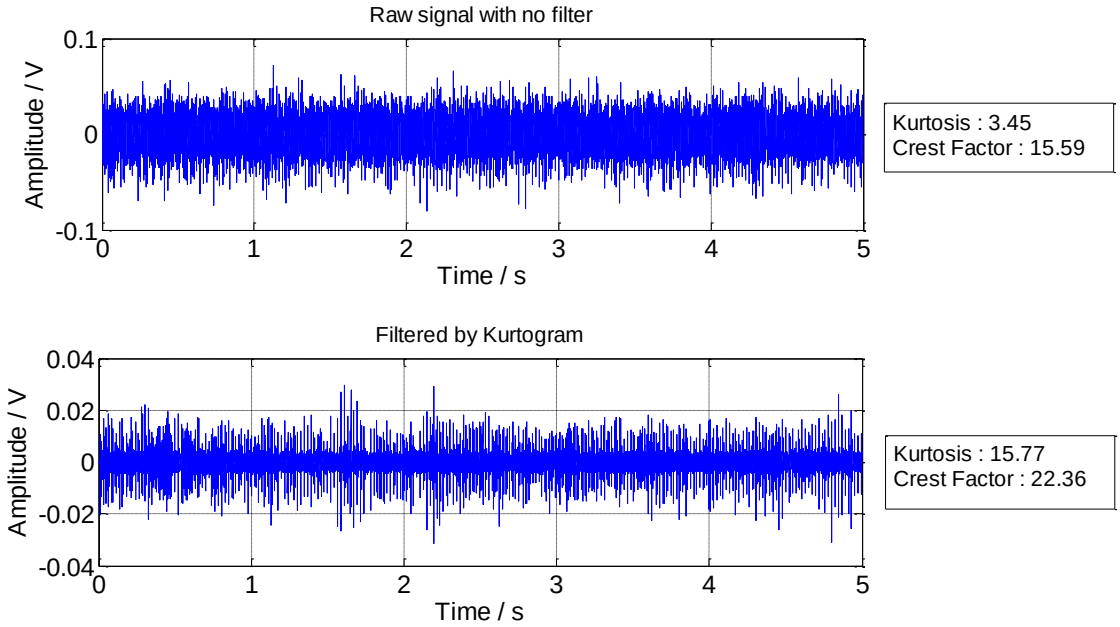

Figure 5-36: Comparison between unfiltered and filtered vibration analysis signal of the bearing with minor outer race damage (F1) – 300 RPM.

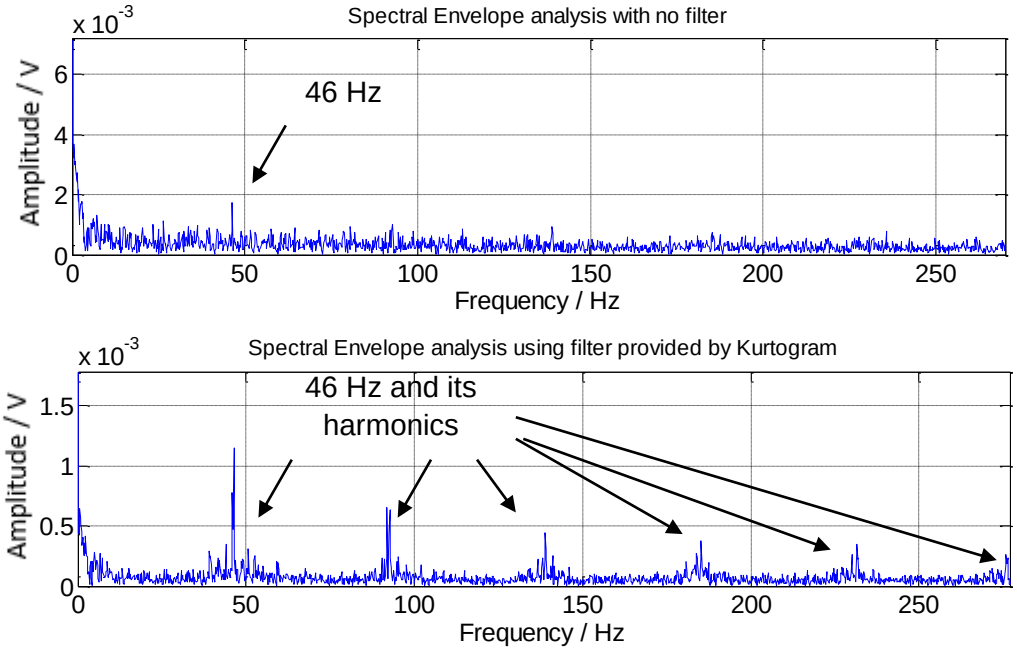

Figure 5-37: Comparison of the spectral envelope analysis between unfiltered and filtered vibration analysis signal of the bearing with minor outer race damage (F1) – 300 RPM.

The same steps were carried out on the bearing with minor outer race defect (F1) but this time at 100 RPM rotating frequency. Spectral envelope analysis failed to find the peaks related to fundamental frequency of outer race defect in the signal due to the low energy impacts occurring from such as small defect at low rotating speed. Nevertheless after applying band-pass filter identified using the Kurtogram, peaks at 15 and 30 Hz appeared. However, these peaks are mixed with those from background noise. Figure 5-38 and Figure 5-39 show a comparison of the results from vibration test of the bearing with minor defect at 100 RPM rotational speed.

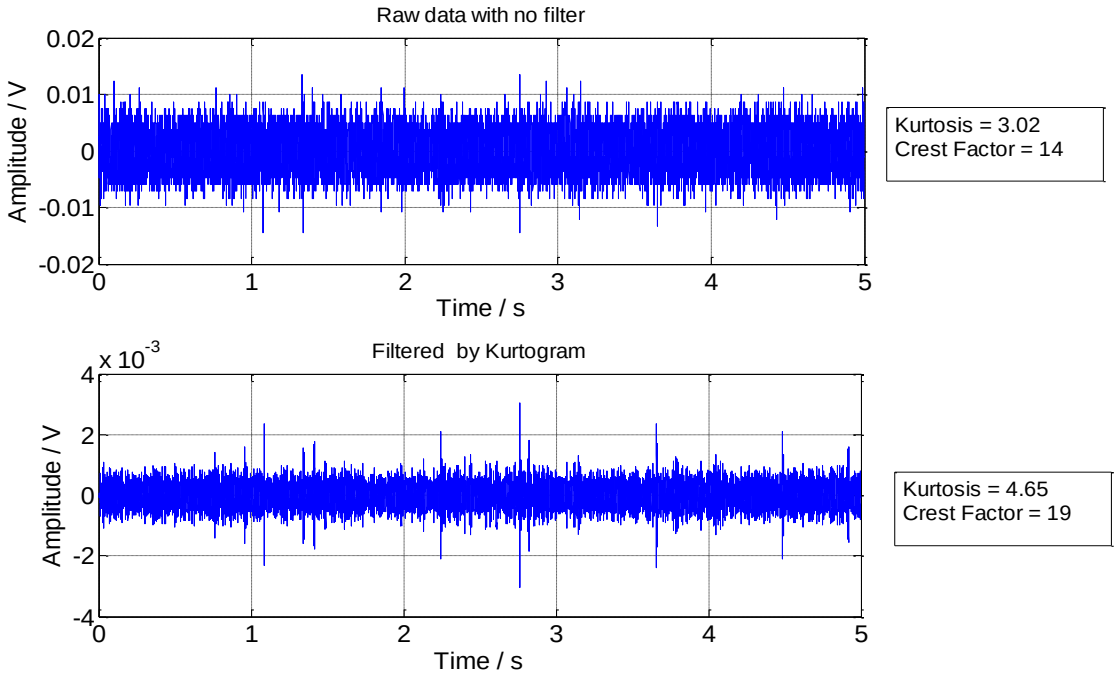

Figure 5-38: Comparison between unfiltered and filtered vibration analysis signal of the bearing with minor outer race damage (F1) at 100 RPM.

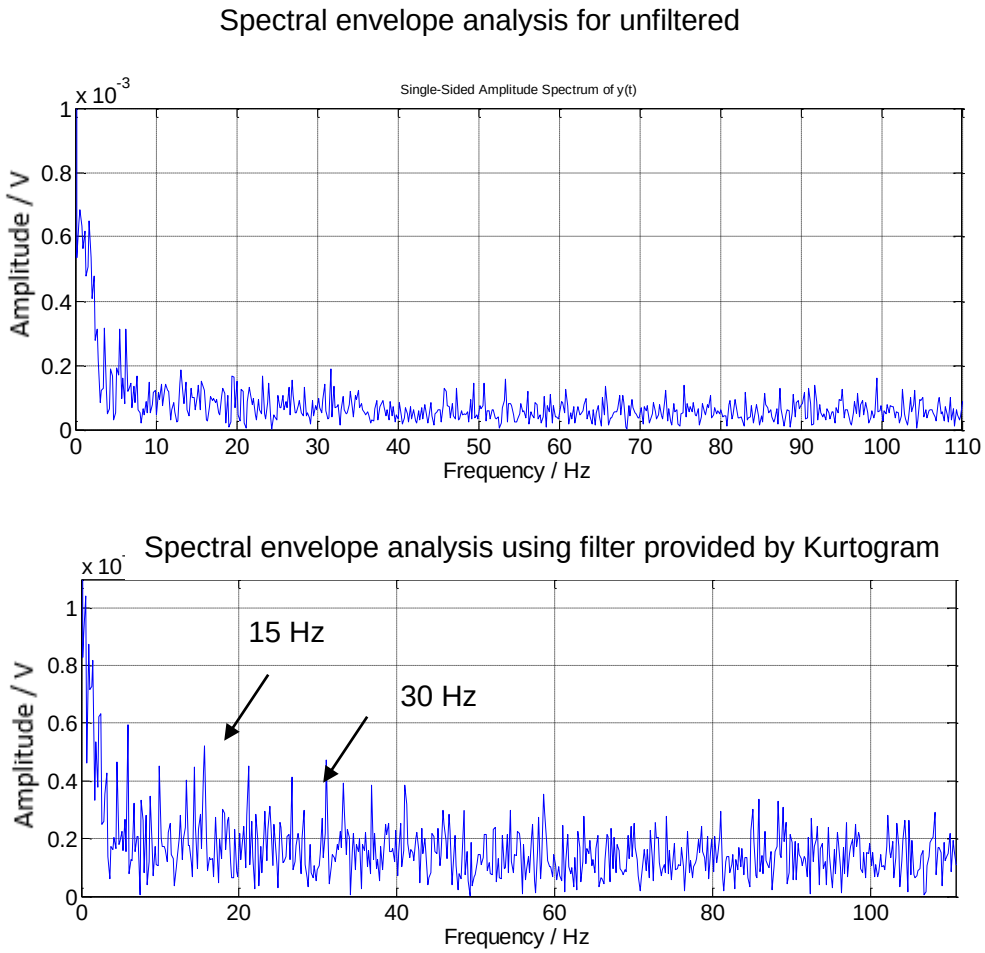

Figure 5-39: Comparison of the spectral envelope analysis between unfiltered and filtered vibration analysis signal of the bearing with minor outer race damage (F1) at 100 RPM.

Finally, the AE signal obtained from measuring the bearing with minor damage at rotational speed of 300 RPM was assessed. Yet again using a Kurtogram enabled an increase in the signal to noise ratio of the AE signal to be achieved. Overall kurtosis and Crest Factor values of the filtered signal increased significantly. Spectral envelope analysis shows the outer race defect frequency at 46 Hz with its harmonics along with a rotating frequency of 5 Hz, which were not detectable in the unfiltered signal (Figure 5-40 and Figure 5-41).

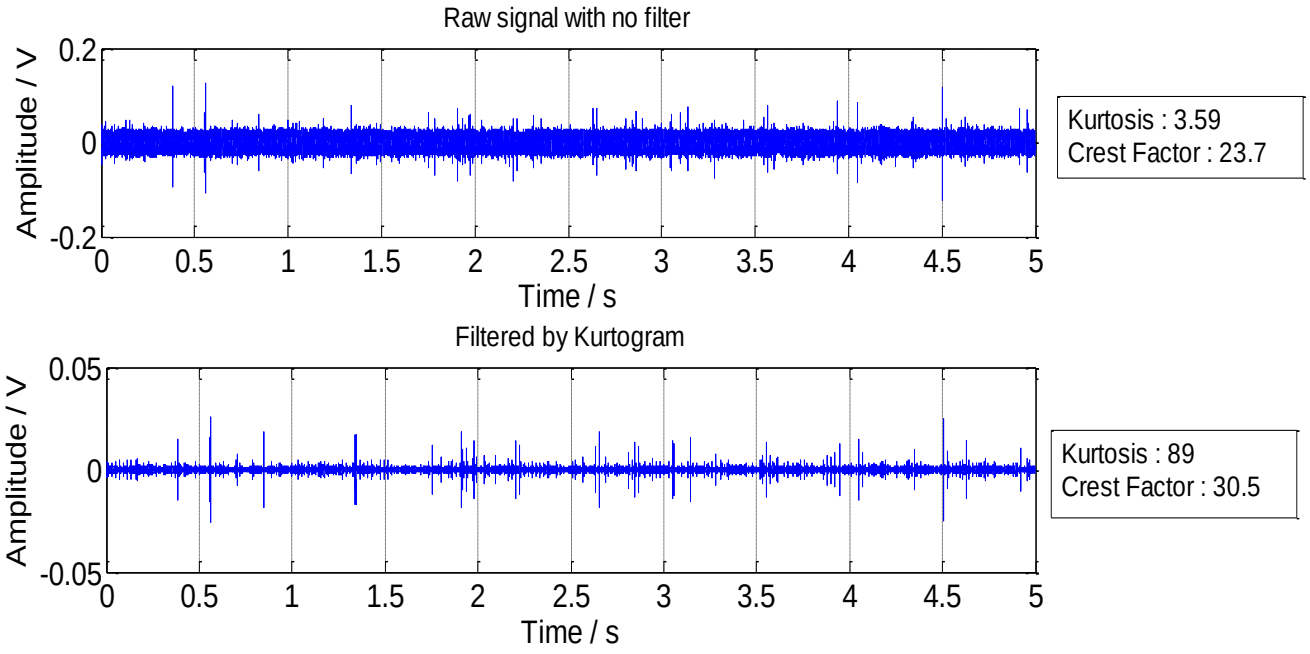

Figure 5-40: Comparison between unfiltered and filtered AE analysis signal of the bearing with minor outer race damage (F1) at 300 RPM.

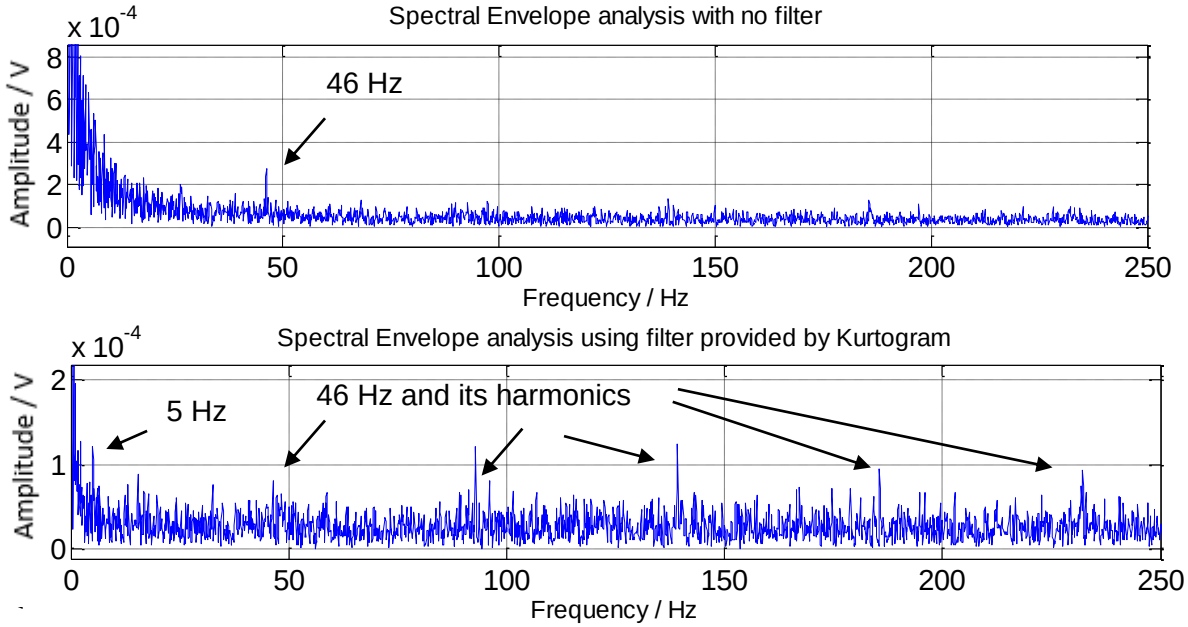

Figure 5-41: Comparison of the spectral envelope analysis between unfiltered and filtered AE analysis signal of the bearing with minor outer race damage (F1) at 300 RPM.

Cepstral analysis was applied on the vibration data taken from the laboratory bearing rig test at a rotating speed of 500 RPM. A healthy bearing and bearings with two different defect

sizes were considered. The result obtained for the healthy bearing does not show any indication of a fault being present. Cepstral analysis of the measurement for the bearing containing small outer race defect (F1) reveals a small peak at 0.013 s quefrency which indicates the outer race defect at 76.9 Hz ($\frac{1}{(0.013)}$) and also a peak at rotating frequency of 8.3 Hz ($\frac{1}{(0.116)}$). These peaks show an increase in amplitude when the defect size increases. Figure 5-42 shows the comparison of the cepstrum analysis of the vibration signal for the bearings with different defect sizes. For the measurement of healthy bearing no relevant peak appears in the plot of the power cepstrum. The power cepstrum of the defective bearings (F1, F5) show the presence of peaks corresponding to an outer race defect along with Rahmonic at 0.026 s. The amplitude of the cepstrum of the bearing with F1 defect is 0.03V whereas for the bearing with F5 defect is 0.06. From the results obtained, it can be concluded that cepstral analysis is capable of revealing the harmonics of the bearing defect, however the result from the bearing with significant outer race defect is more representative.

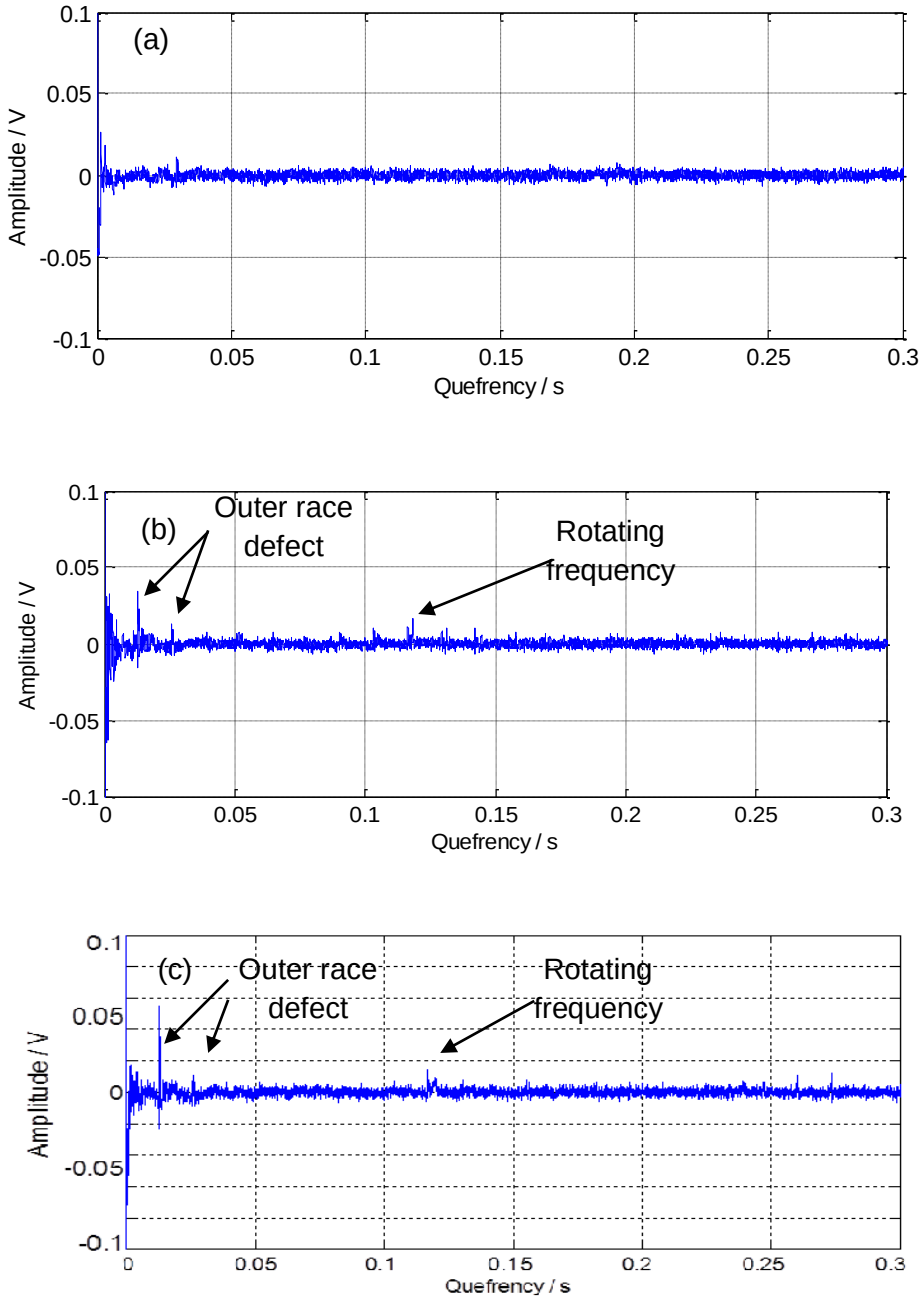

Figure 5-42: Cepstral analysis of the laboratory bearing rig vibration test at a rotating speed of 500 RPM – a) Healthy, b) F1 defect and c) F5 defect.

Cepstral analysis does not reveal the bearing defects in the AE data. The reason can be the concealing of the harmonics in the high frequency noises, which make the bearing frequencies disappear in invert FFT of the ceprstum algorithm. Figure 5-43 shows the cepstrum analysis of the laboratory bearing rig, AE test of the bearing with the F5 defect.

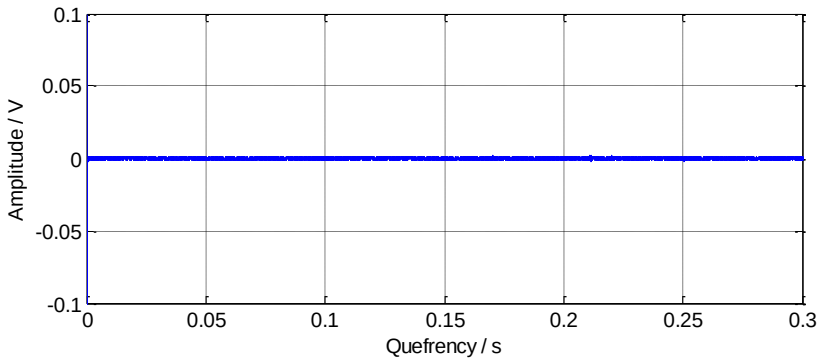

Figure 5-43: Cepstral analysis of the laboratory bearing rig AE test at 500 RPM rotating, bearing with F5 defect.

In order to evaluate the capability of vibration and AE techniques to monitor lubricant contamination in the test bearings, a relevant set of experiments was carried out. During these experiments the sensitivity of each technique was investigated and compared to each other.

Figure 5-44 presents a comparison of the vibration and AE measurements of the bearing with 1 % weight ratio lubricant contamination and healthy bearing running at 60 RPM. In general, an increase in all overall values is observed which means sand contamination can cause metal to metal interactions that have a signature which is evident at both lower and higher frequencies. The results from this set of measurements are summarised in Table 9.

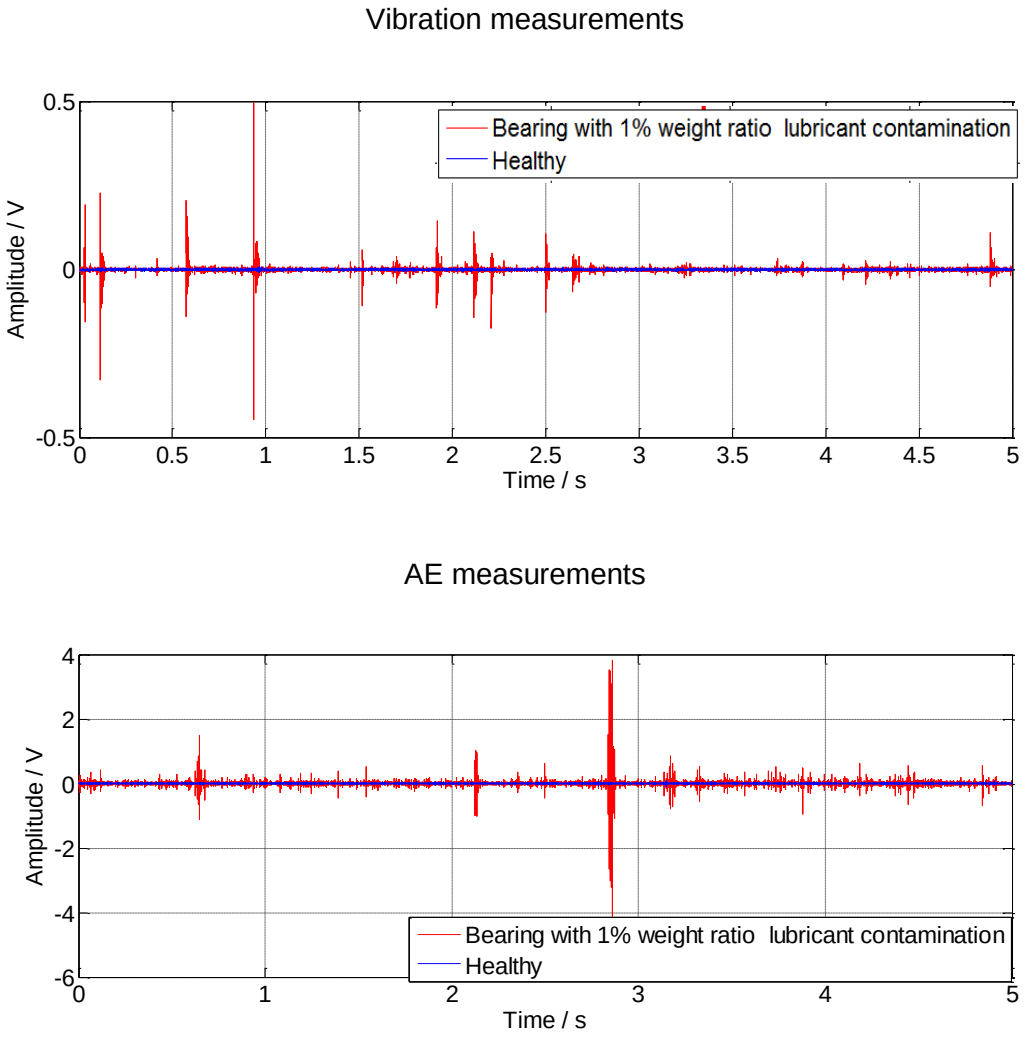

Figure 5-44: Comparison of the vibration measurement of the bearing with 1 % weight ratio lubricant contamination defect and healthy bearing at 60 RPM.

Table 5-4: Overall values of vibration measurement of the bearing with 1 % weight ratio lubricant contamination defect and healthy bearing at 60 RPM.

Vibration	Healthy	Bearing with lubricant contamination
PK-PK	0.01	0.94
RMS	0.001	0.005
Kurtosis	4	1942
Crest Factor	13	39

AE	Healthy	Bearing with lubricant contamination
PK-PK	0.2	7.94
RMS	0.002	0.03
Kurtosis	20.1	2320.6
Crest Factor	46.7	126.3

The laboratory experiments demonstrated the ability of the AE and vibration techniques with the signal analysis approach employed to characterise the defective bearings considered under constant rotating speed and static loading conditions. However, the ultimate aim of this study has been to evaluate the condition of railway wheelsets. In this case the evaluation of the axle bearings involved is much more complicated, as in the field loads are dynamic, wheel tread impacts can occur stochastically and the rotating speed can vary during measurements adding considerably to the overall complexity of the problem at hand.

5.3 summary

In this chapter instrumentations of AE and vibration tests and various laboratory experiments were described. Three different types of piezoelectric AE sensors were tested and R50α sensor, from Physical Acoustics Corporation (Ltd) (PAC UK – now MISTRAS), with resonance frequency of 170 and 350 KHz was chosen for the field trial experiments. Wilcoxon piezoelectric accelerometers, model 712F was used for the vibration measurements. AE sensor calibration was done using pencil lead break (or Hsu-Nielsen

source) and coupled by a layer of Vaseline on the surface of the testing material. The accelerometers used during tests were calibrated using a vibration calibrator vibrating with 159.2 Hz frequency.

Executable customised logging and analysis software developed by the author and a flowchart explaining the software was also demonstrated.

Laboratory-based experiments were carried out on a single laboratory scale-sized wheel, with an artificially induced defect, rotating manually against a small rail section. Also a motorised trolley included on the test wheel was moved along a 7 metre long test track. Furthermore, laboratory experiments were carried out with a bearing test rig. Bearings free of defects and bearings with various induced defects were used during these experiments. Results of healthy and defective wheels and bearings were compared and discussed at the end of this chapter.

Chapter 6 : Field Trials

Experiments were carried out in Long Marston test track involving both onboard and wayside measurements. Figure 6-1 shows the Long Marston test track section where tests were carried out. A number of artificially induced faults were considered including wheel flats, lubricant contamination, race and roller defects. The defects on the roller and race were three different sizes (2,4 and 8 mm). Tests were carried out at a speed of 30 MPH (48 km/h) in the direction forward (engine in front) and 20 MPH (32 km/h) in the direction backwards (engine in the back). The freight cars used in the experiments were pulled over a straight section of jointed (continuously welded after re-railing of the test section was completed) track a few hundred metres long. The sampling rate for AE signals was set at 500 kS/s and vibration at 25 kS/s. The duration of the acquisition was 10 s for the onboard tests and 12-24 s for the wayside tests depending on the number of freight wagons used during testing. Between one and four wagons were used during the various set of trials. Ultrasonic coupling of the AE sensor was achieved using vaseline. The Wilcoxon accelerometers employed have a built-in magnet to keep them in place. The AE sensors where held in place using magnetic hold-downs. The axle bearing of the test freight wagons were manufactured by Timken (Timken bearing model 99591-99100). Appendix B shows the characteristic frequencies of the train bearing provided by the manufacturer. Figure 6-2 shows the artificially induced 4 mm roller bearing defect.

Figure 6-1: The Long Marston test track section where the majority of tests were carried out prior to re-railing.

Figure 6-2: Example of a defective bearing with 4mm roller defect

6.1 Long Marston Onboard Measurement

Recent studies have shown that CM systems installed onboard are more likely to detect an axle bearing fault, especially at the early stage of its evolution [149]. This is due to the fact that the sensors are closer to the axle bearing and hence to the source of the arising signal. Onboard systems are able to measure continuously or more often the condition of the bearings acquiring data over a larger number of revolutions of the same axle bearing. On the other hand, wayside systems can only measure the axle bearings of a passing train when they pass along the instrumented location. In addition, the wayside system is exposed to noise from the entire train being measured which is not the case when the onboard system is considered. The onboard system can record several revolutions depending on the acquisition time employed. This normally needs to be set at a sufficient length in order to capture at least a few revolutions to minimise unwanted impulse effects on the signals acquired [150].

The other advantage of the onboard system over the wayside, is its ability to monitor continuously rather than intermittently. It is also capable of providing an alarm of a fault immediately when the signal processed indicates the presence of a defect [54]. On the other hand, onboard devices would have to be rugged enough to continuously operate in the high vibration impact environment commonly found in the rail industry. Also since each axle bearing would require its own detector, an onboard system will be costly to install and maintain [54]. Moreover, the problem of powering the system would need to be resolved. The situation is simpler for passenger trains where power is more readily available and cost justification is more evident. If an onboard CM system can be installed and maintained at acceptable costs, they may offer considerable advantages over wayside systems.

Figure 6-3 shows an example of the onboard sensor setup on the bearing case. Vibration and AE data were collected using an accelerometer and AE sensor, which were attached to the axle box housing using magnetic hold-downs. The sensors should be located as close to

the bearing as possible, with a good mechanical pathway between the bearing and the sensors to assist in the transmission of vibration and acoustic waves. In general, the best results were obtained when the sensors were located close to the loaded zone of the bearing. The sensors should be fixed securely to the casing to ensure good transmission of the high-frequency vibration and AE signal. In this set of experiments bearings that were tested included, healthy and faulty conditions with different sizes of 2, 4 and 8 mm roller and race defects and a bearing with water and sand lubricant contamination.

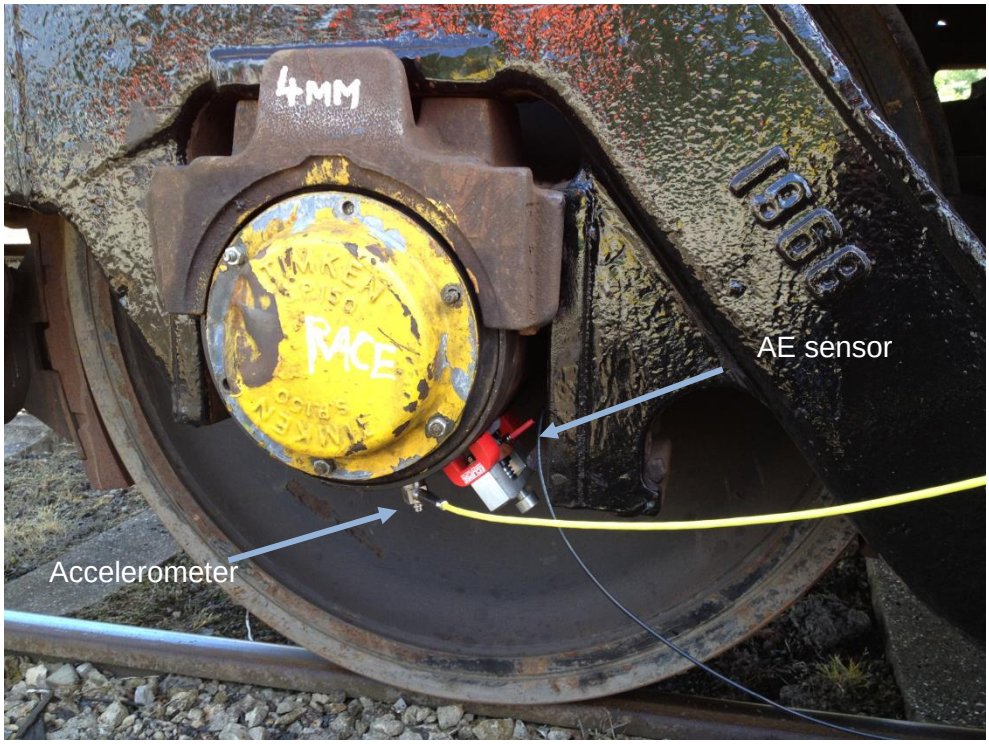

Figure 6-3: The accelerometer and AE sensor mounted using a magnetic pad and magnetic hold-down respectively on the axle box of an axle bearing with a 4 mm artificially induced race defect during onboard testing.

6.1.1 Onboard detection of localized defects in axle bearings

Figure 6-4 shows the results from onboard vibration and AE measurements. Unfortunately, due to the accelerometer cable length, vibration measurements could not be carried out on the bearings with over 8 mm race and roller defect size. The increase in signal amplitude of

the impacts with increasing defect size can be observed in results of the AE measurement. In the case of vibration analysis, it has not been possible to distinguish between the healthy bearing and the ones with different defect sizes.

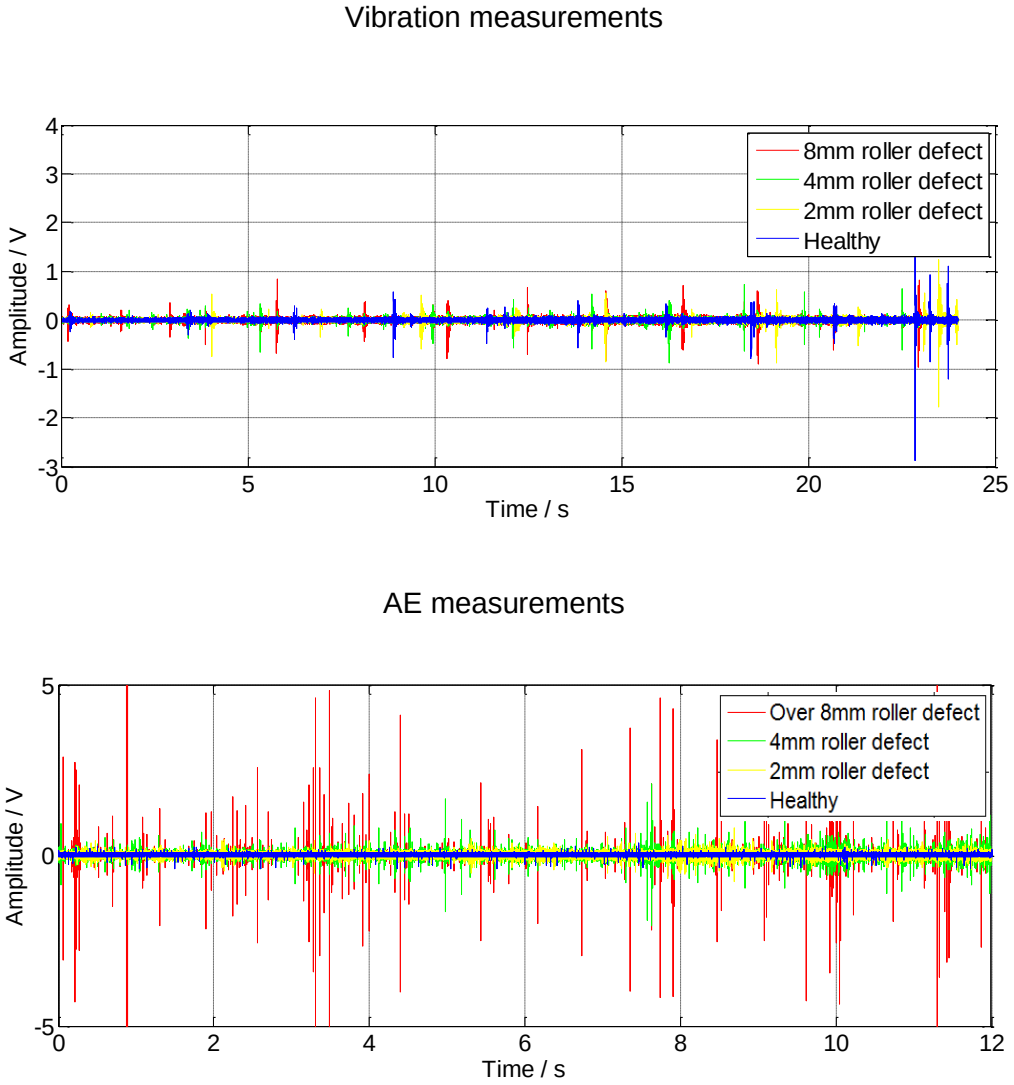

Figure 6-4: Raw data comparison from a) the onboard vibration and b) AE measurements during tests of bearings with different conditions in Long Marston.

According to the manufacturer's datasheet for the bearing type considered during the Long Marston tests, for a test train speed of 30 MPH (48 km/h), which corresponds to a wheel rotational frequency of 4.2 Hz (256 RPM), the fundamental frequency expected to arise from a roller defect is around 17.6 Hz:

4.198 Hz = Frequency of the roller defect with bearing rotating frequency of 1 Hz

4.198 × 4.2(train speed) =17.6 Hz

Figure 6-5 shows the AE data from the onboard measurement carried out on a severely damaged axle bearing (8mm roller defect). Large peaks in raw data indicate the presence of a defect but not the type of defect. In order to find the type of the defect, data should be analysed in the frequency domain using spectral envelope analysis. The charactristic frequencies do not appear in conventional FFT, however spectral envelope analysis clearly allow the detection of fundamental frequency and its subsequent harmonics. The fundamental defect frequency obtained from the spectral envelope analysis is 16.99 Hz followed by its harmonics. The fundamental frequency and the harmonics seen correspond well to the kinematics of the bearing provided by the manufacturer in the relevant technical datasheet.

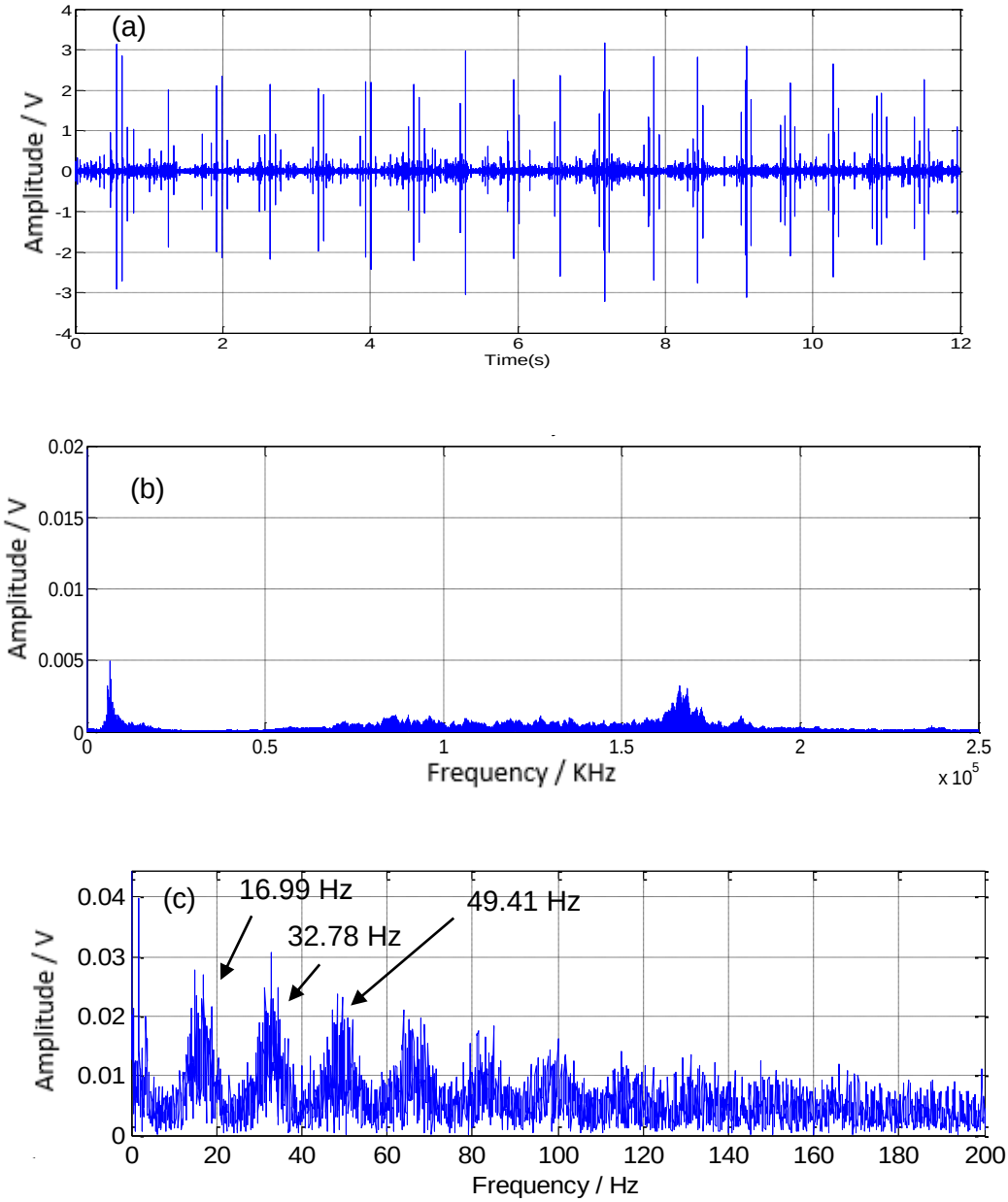

Figure 6-5: Onboard AE measurement on bearing with severe roller defect (8mm size): a) Raw data, b) FFT analysis, and c) Spectral envelope analysis.

It should be noted that the resonance frequency was identified using the impact test which was explained in the previous chapter. Figure 6-6 shows the same analysis on a bearing with 4 mm roller defect present. The lower amplitude in raw data compared to the severely damaged bearing should be taken into account. It is evident that despite using spectral envelope analysis, neither the fundamental frequency nor its harmonics were evident in the

signal. This is due to the fact that the signal was contaminated by other sources of noise which made evaluation of the type of defect more difficult. Nonetheless, it is still possible to establish that the axle bearing being measured was damaged. This is due to the fact that the defective bearings contain generate AE signals of higher amplitude.

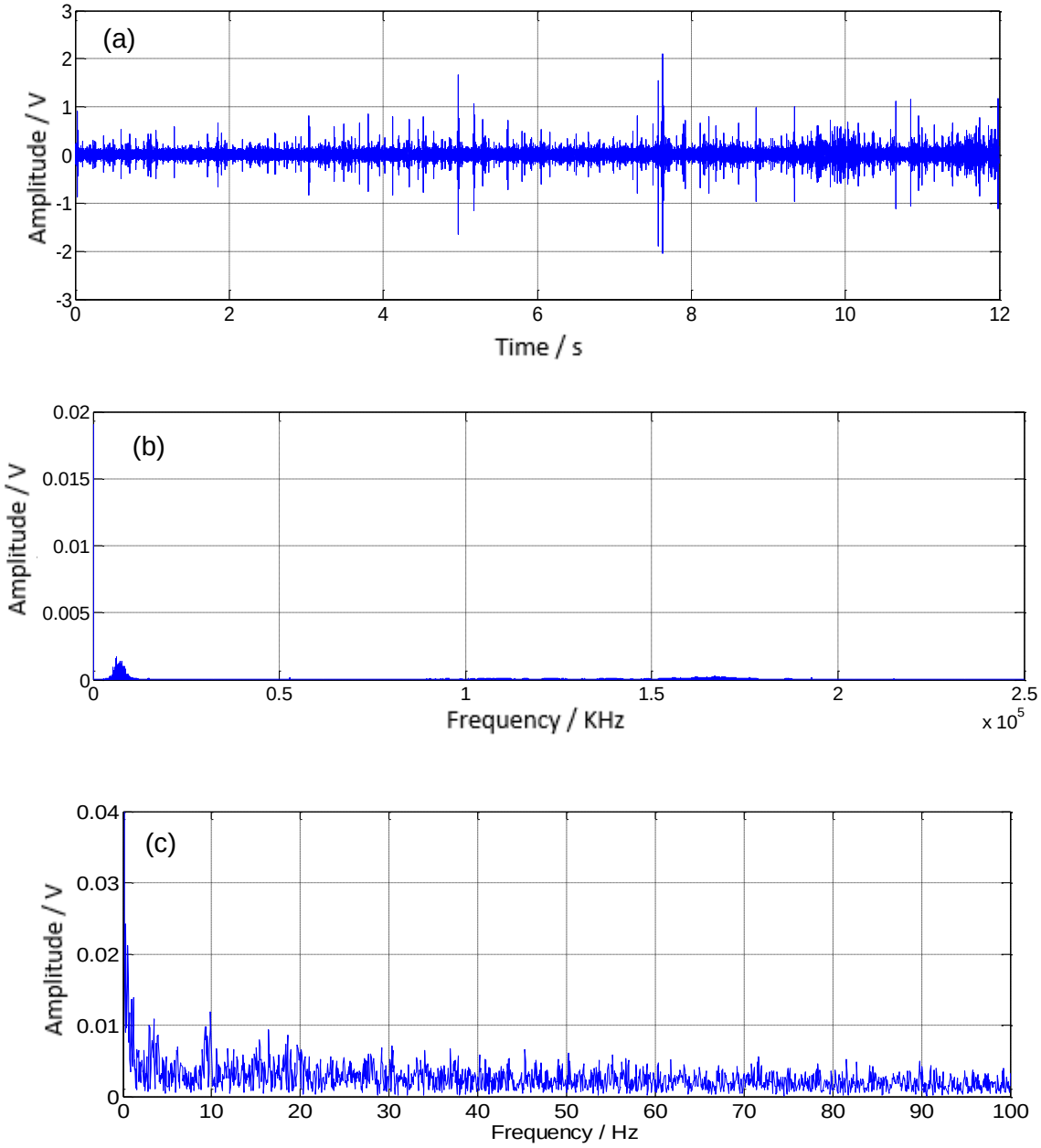

Figure 6-6: Onboard AE measurement on bearing with a 4 mm defect: a) Raw data, b) FFT analysis and c) Spectral envelope analysis.

As it was mentioned before, vibration analysis failed to distinguish between the healthy and defective bearings. However, the resonance frequency of the bearing was excited due to the

impacts from the defect. This can be observed in the power spectrum shown in Figure 6-7. This frequency was used to find the optimum frequency that should be applied for HFRT analysis. Vibration measurement was not able to detect the characteristic frequencies of the defective bearings during field testing.

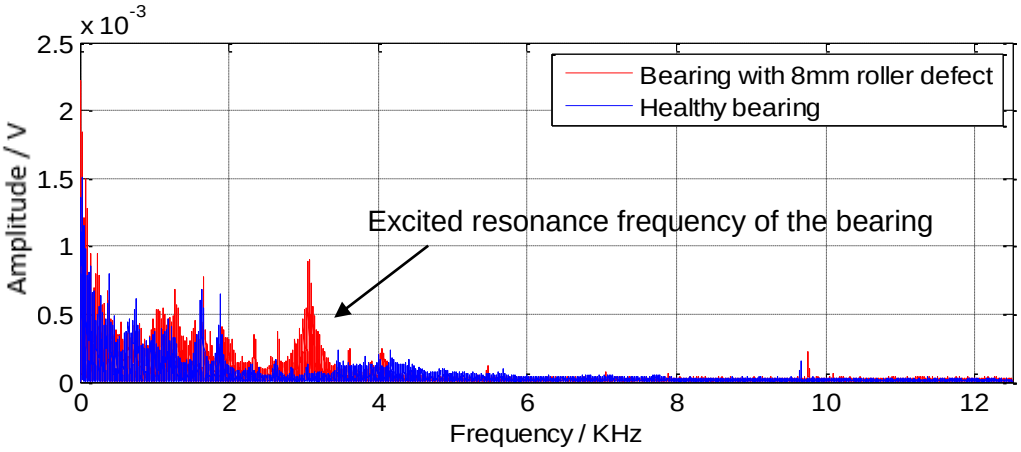

Figure 6-7: comparison between FFT of healthy and bearing with 8 mm roller defect, onboard vibration analysis.

Furthermore, the application of a Kurtogram was investigated to find the optimum band-pass frequency to be used for HFRT analysis. This method had been successful in the laboratory experiment, however, it failed in the actual operational conditions due to the high non-Gaussian noises in both vibration and AE measurements carried out.

6.1.2 Onboard detection of lubricant contamination in axle bearings

The lubricant of axle bearings was contaminated with water and sand. Subsequently both AE and vibration measurements were carried out to evaluate whether this axle bearing fault can be detected using onboard measurements. The shape of the signals measured in the case of axle bearing lubricant contamination testing is different from those obtained for roller or race defects. Metal-to-metal interactions occurring due to poor lubrication cause generation of random peaks in the AE and vibration signals. In the case of defective roller or race, peaks occur at certain times per bearing revolution.

Figure 6-8 shows a comparison between a healthy and a faulty bearing for both AE and vibration measurements. From the raw data, it is evident that AE is more suitable to distinguish between the two bearing conditions. From the vibration signal only a small difference is evident. The overall values in the AE measurement change significantly in comparison with the overall values from the vibration measurement. The results are summarised in Table 6-1.

AE measurements

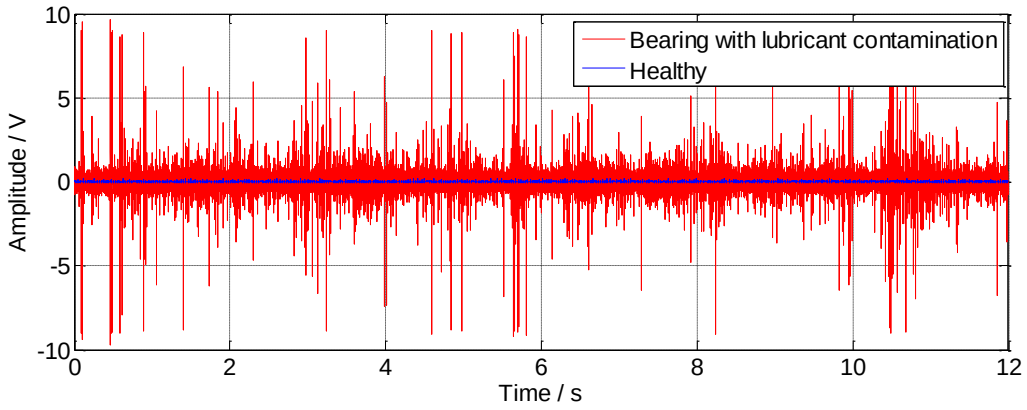

Vibration measurements

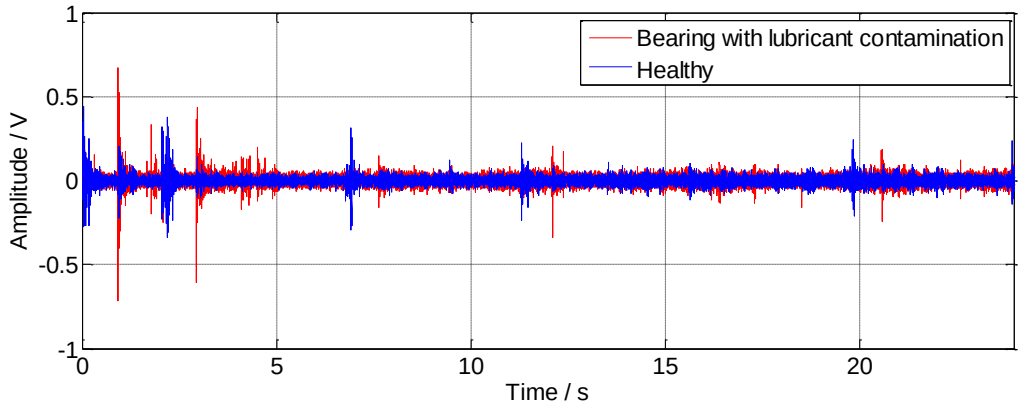

Figure 6-8: Comparison of the bearings with lubricant contamination and healthy condition measured during, Long Marston field trials.

Table 6-1: Overall values of vibration and AE measurement of the bearing lubricant contamination defect and healthy bearing, Long Marston.

AE measurement	Healthy	Sand contamination
Kurtosis	24	224
Crest Factor	20	33
PK-PK	0.25	19.37
RMS	0.01	0.21
Vibration measurement	Healthy	Sand contamination
Kurtosis	27	43
Crest Factor	26	29
PK-PK	0.78	1.38
RMS	0.02	0.02

6.2 Long Marston Wayside Measurement

The wayside monitoring systems are based on a set of particular sensors installed on the track and more specifically mounted on the rail web. The sensors were connected to an acquisition module and a data processor module installed in a shelter by the railway track as shown Figure 6-9. The wheel and rail form a direct mechanical path for the AE signals produced from the bearing to be transmitted to the AE sensors mounted on the rail i.e. the detection zone. Detecting bearing defect signals from this direct mechanical path provides more accurate results in comparison with airborne acoustic detection, because it eliminates adverse effects of surrounding noises and other environmental parameters, such as engine and other noises from the surroundings [151]. Moreover, the signals acquired contain high frequency information which makes detection of faults more likely.

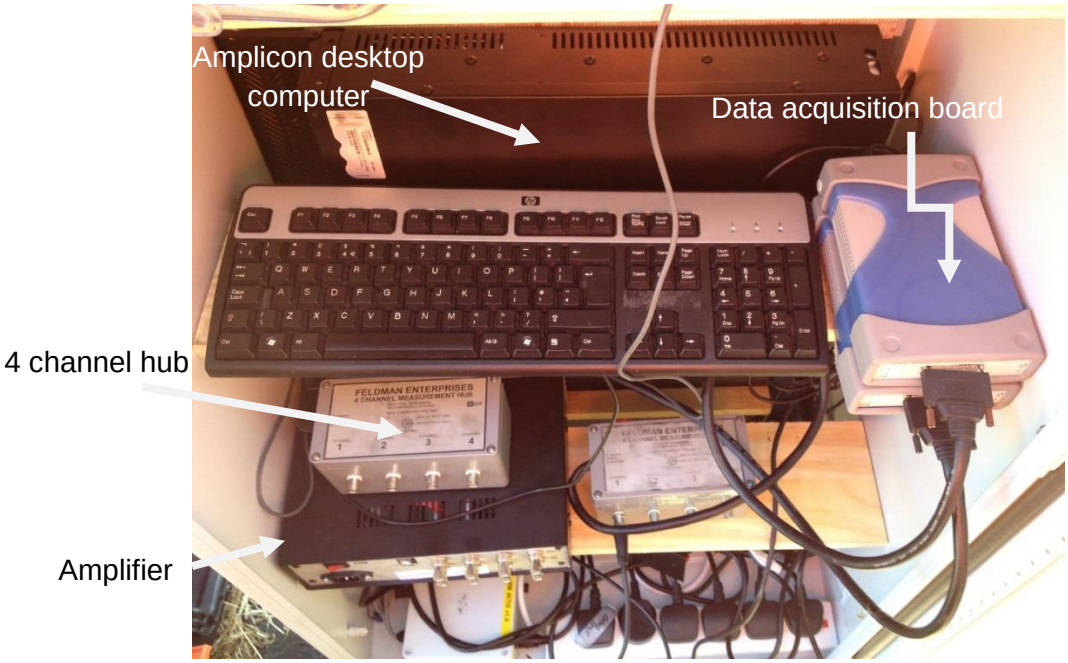

Figure 6-9: The wayside acquisition and amplification equipment placed in the test cabinet during tests in Long Marston.

Multiple AE sensors and a pair of accelerometers were used during wayside tests. Using multiple sensors offers some advantages since the signals obtained can be correlated to each other and even combined in order to improve the signal content obtained by individual sensors.Therefore, using several sensors provides increased reliability during AE measurements and permits a larger number of wheel and axle bearing revolutions to be recorded over the instrumented section of the track. Moreover, the use of multiple sensors offers redundancy, if one fails the others are still able to provide adequate monitoring.

The schematic in Figure 6-10 shows the sensor installation during wayside tests carried out in Long Marston. Figure 6-11 shows the tank freight wagon containing three bearings with faulty rollers pulled by the engine.

Figure 6-10: Installation of accelerometers and AE sensors on the track

Figure 6-11: Test car in Long Marston test field. The yellow locomotive in front pulls or pushes the test wagon depending on the direction of movement.

An optical unit capable of measuring the speed of the train and counting the number of axles was employed in order to correlate AE signals with the position of the wheels. In addition, the optical system was used to automatically trigger data acquisition during tests. This system consists of two pairs of infrared sensors. When the infrared beam is interrupted, data acquisition is triggered, the position of each wheelset is identified and the speed of the train

is calculated by knowing the distance between the two pairs of infrared sensors. Since the optical system enables the identification of exact position of each wheelset, during analysis of the signals obtained, it is possible to isolate the part of interest by truncating the signal at the time period during which the test wagon passed over the instrumented section. In this way it is possible to reduce the amount of data logged considerably and also reduce the computational cost. Figure 6-12 shows the optical trigerring system main control box, infrared transmitter and system setup in Long Marston during the field trials.

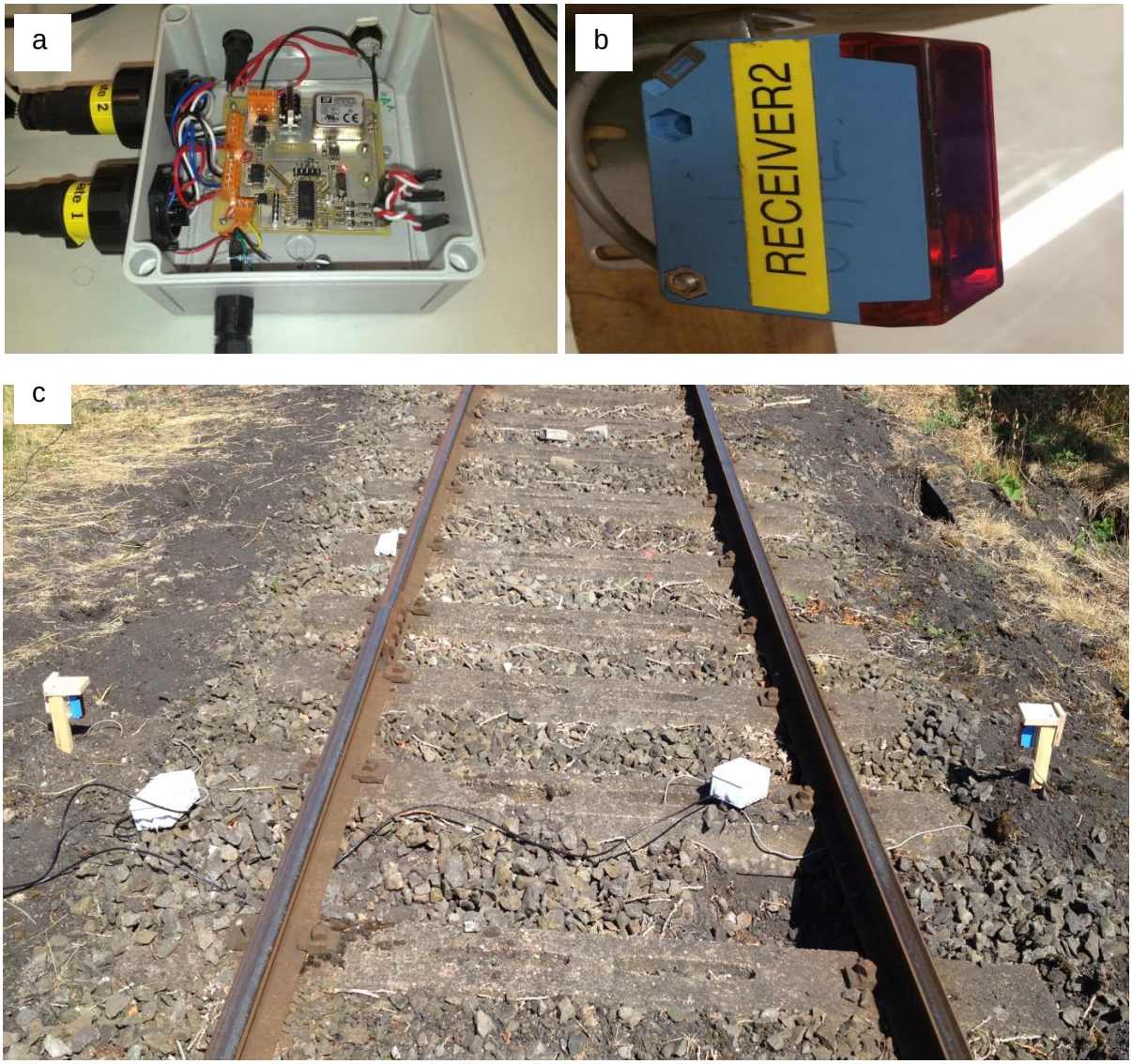

Figure 6-12 : The optical triggering system a) main control box, b) infrared transmitter and c) system setup.

The schematic in Figure 6-13 shows the installation outline of the 2nd round of trial runs carried out in March 2014 in Long Marston. During this set of experiments , all faulty bearings were located on the same side of the second, third and fourth wheelsets of the freight wagon with 2, 4 and 8 mm roller defects, respectively. The 8 mm roller defect size was manually increased using a drilling machine in round 3 trail run. Tests were carried out at up to a maximum speed of 48 km/h over a straight section of welded track approximately 1000 metres in length. The sampling rate for AE signals was 500 kHz and the duration of the acquisition was set at 12 seconds.

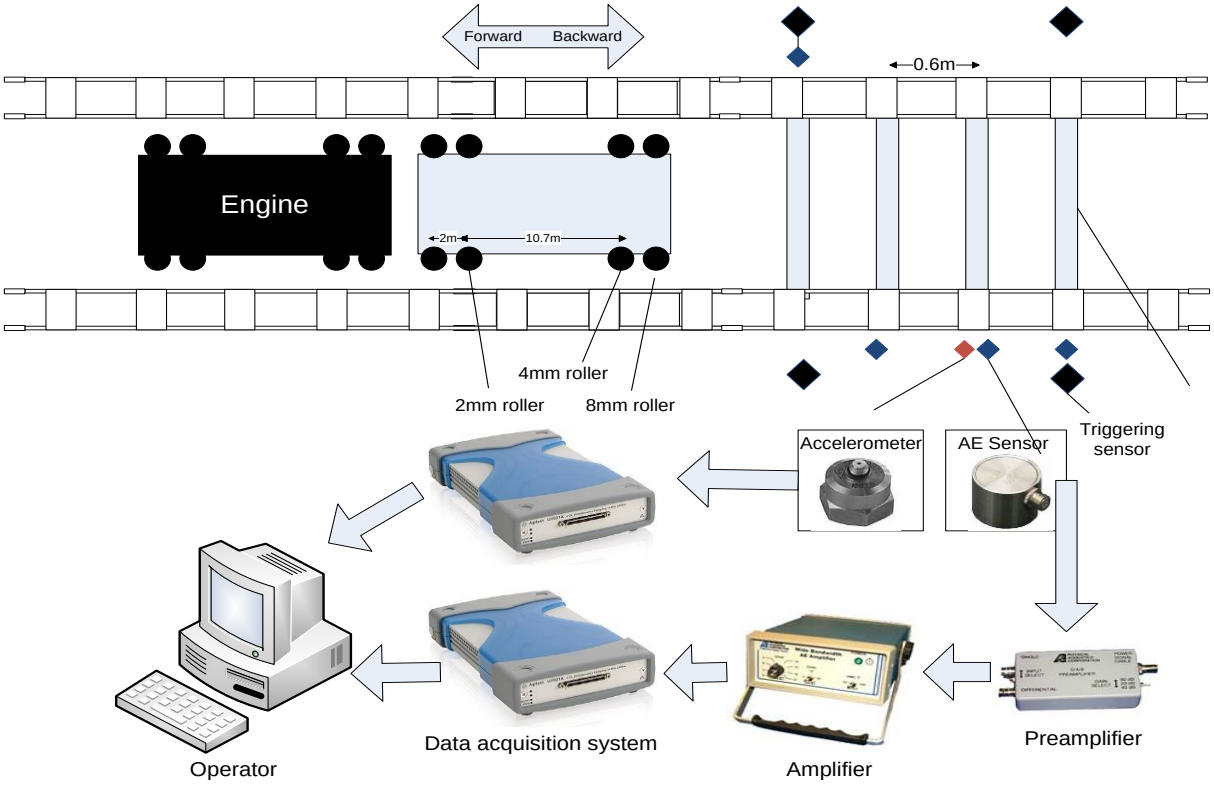

Figure 6-13: Schematic of wayside installation.

6.2.1 Results

The result of the vibration measurement from the faulty side is shown Figure 6-14. The engine noise has the highest amplitude and hence the dominant low frequency signal in the

data is distinguishable. There is no indication of the defective bearings passing by the accelerometer. Moving RMS and TSK analysis (Figure 6-15) also do not show any evidence from the faulty bearings. The engine noise still remains dominant in all below data analysis. More specifically, it is evident that vibration measurements are unable to detect the fault in the bearings since the signal does not contain sufficient information.

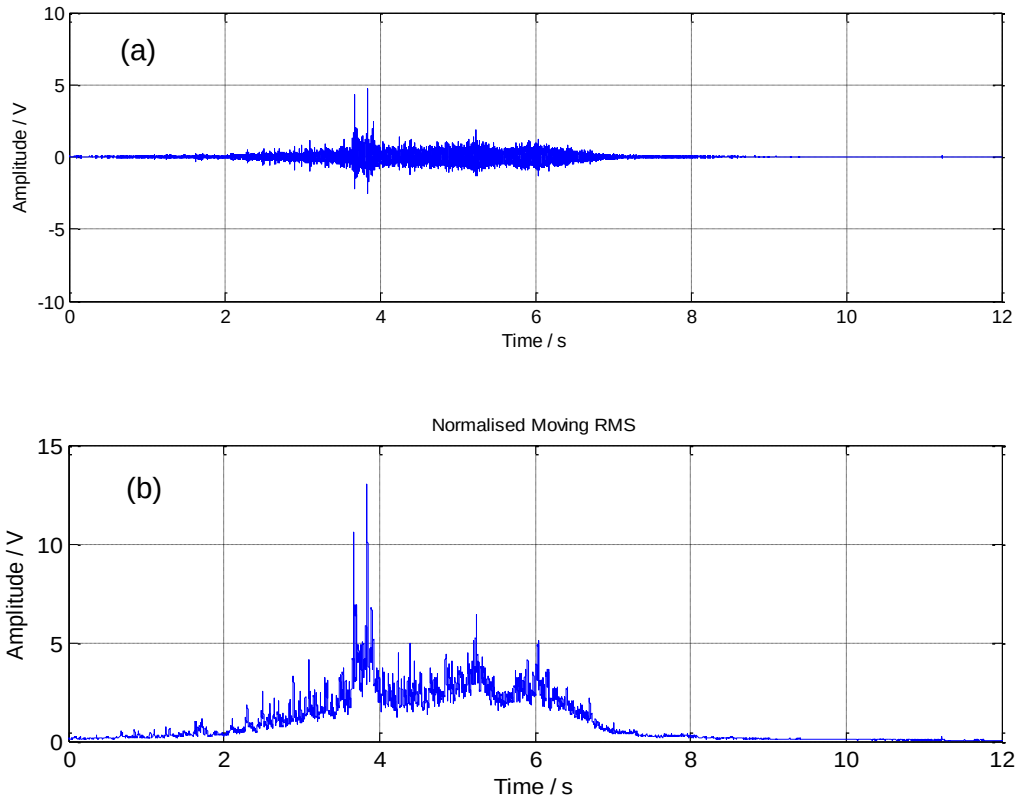

Figure 6-14: Vibration data from defective side in wayside field test, a) Raw data, b) Moving RMS analysis

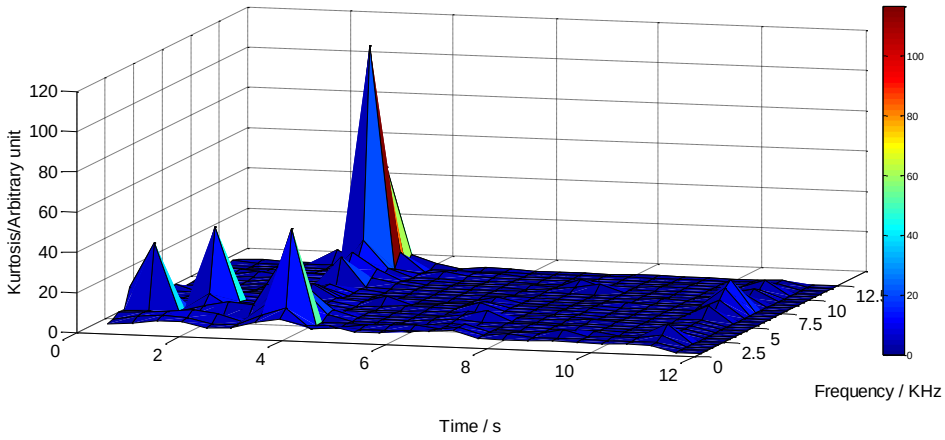

Figure 6-15: TSK diagram of vibration data from wayside field test.

Therefore, it can be concluded that vibration analysis is not a suitable method for wayside detection of bearings unless very severe defects are considered.

Figure 6-16 shows the raw AE data from one of the wayside measurements obtained during the Long Marston field trials. The red lines indicate the moment that the wheelset passed above each AE sensor. When the roller defect impacts on the bearing load zone, a peak with higher amplitude is evident. Therefore, the recorded amplitude of a particular defect might vary during each rotation. As a result the peak from an impact may not necessarily be at the exact time when the wheel is passing over the instrumented section. The signal amplitude recorded by the AE sensors is also related to the distance between source and sensor. The higher the distance the more the AE signal will be attenuated. From Figure 6-16 it can be seen that bearing defects produce high amplitude acoustic waves while passing above the sensors at 5.45 s and 6.38 s. The engine noise is another source of high amplitude AE in the raw data. In addition, there is a clear intense peak with a long duration at 7.44 s which has risen during train braking. This peak was observed after the train had already passed the detection zone.

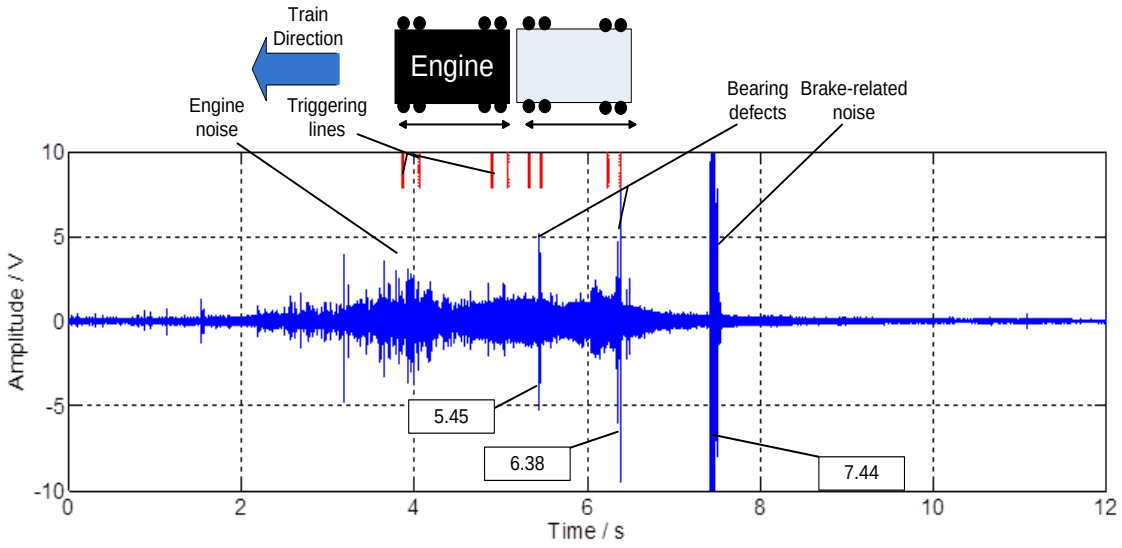

Figure 6-16: Raw AE data from defective side in wayside field test

The signal obtained from the healthy side is plotted together with the faulty side in Figure 6-17. As it can be observed, there is no sign of high amplitude peaks related to the defective bearings.

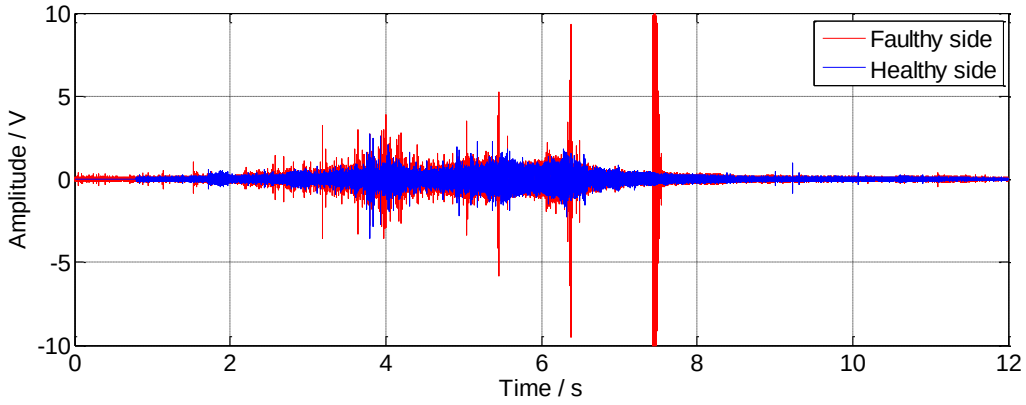

Figure 6-17: Results from AE measurements of healthy and faulty sides. It should be noted that the two measurements have been taken at separate times.

The results of the moving RMS and moving kurtosis analysis are shown in Figure 6-18. In the moving RMS plot, bearing defects are clearly evident with higher amplitude peaks seen compared with the engine noise although the amplitude of the peak related to the brake event is still high. The amplitude of the brake noise is reduced in the moving kurtosis

analysis. However, in this case the amplitude of the engine noise is increased. The bearing defects are detectable in both of these analysis methods. Therefore, by combining the moving RMS and kurtosis can improve the reliability of the analysis. The window size for moving RMS and kurtosis are based on one RPM. The train speed was 48 km/h, therefore a window size of 11750 samples was chosen in this experiment as described by the following calculation.

$$\text{Wheel circumference} = 2\pi r = 2 \times 3.14 \times 0.5 = 3.14 \text{ m}$$

$$\frac{\text{Train speed}}{\text{Wheel cirsuit}} = \frac{13.4 \frac{\text{m}}{\text{s}}}{3.14 \text{ m}} = 4.26 \text{ Hz or Number of revolutions per sec}$$

$$4.26 \times 12 \text{ s} = 51 \text{ Number of revolutions in 12 sec data acquisition}$$

$$\frac{\text{Number of data samles}}{\text{Number of revolutions in 12 sec}} = \frac{6000000}{51} = 11750 \text{ kurtosis window size}$$

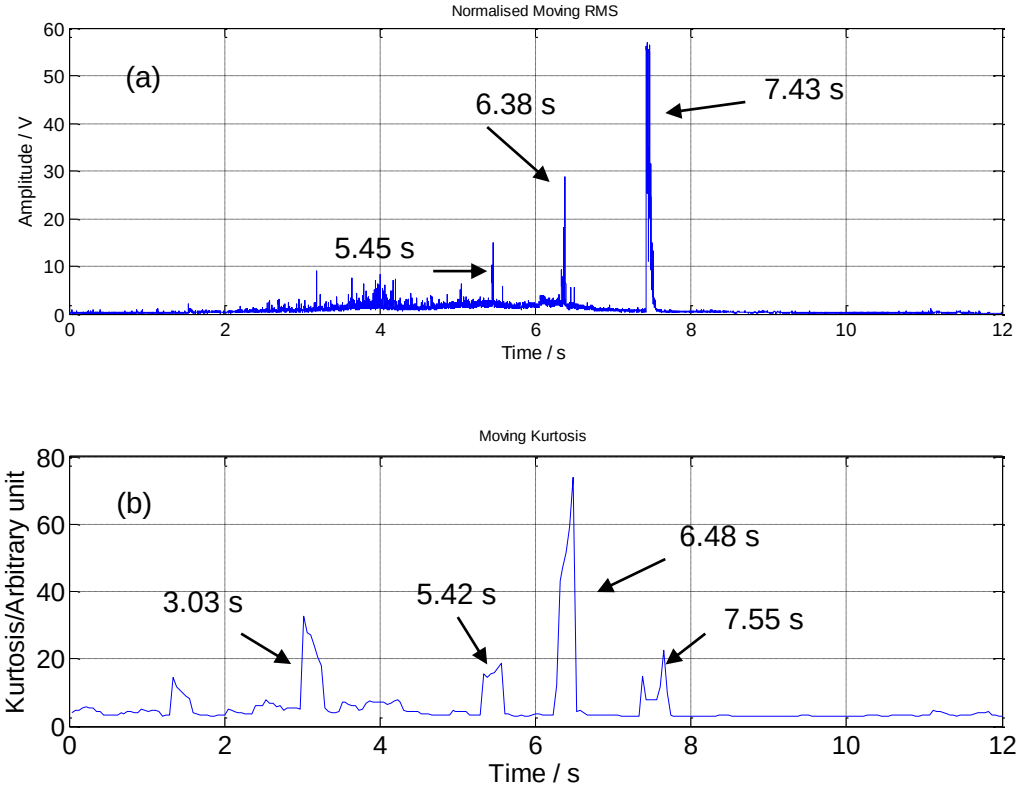

Figure 6-18: Moving RMS (a) and Moving kurtosis (b) diagrams of wayside AE measurement.

By truncating the signal around the wagon passing time, the only remaining peaks are the ones indicating the bearing defects, although this can be affected by surrouding noises. Figure 6-19 shows the truncated signal between 5-7 s in the time axis. The time difference between the peaks (0.93 s) confirms the distance between the 2 mm and 8 mm roller defects:

Train speed = 30 MPH = 13.4 m/s & Distance between bogies = 12.7 m

Time difference between 2mm and 4 mm roller defect bearings = $\frac{12.7}{13.4} \cong 0.94$ s

Time difference between the peaks in the raw data = 6.383 – 5.453 $\cong$ 0.93 s

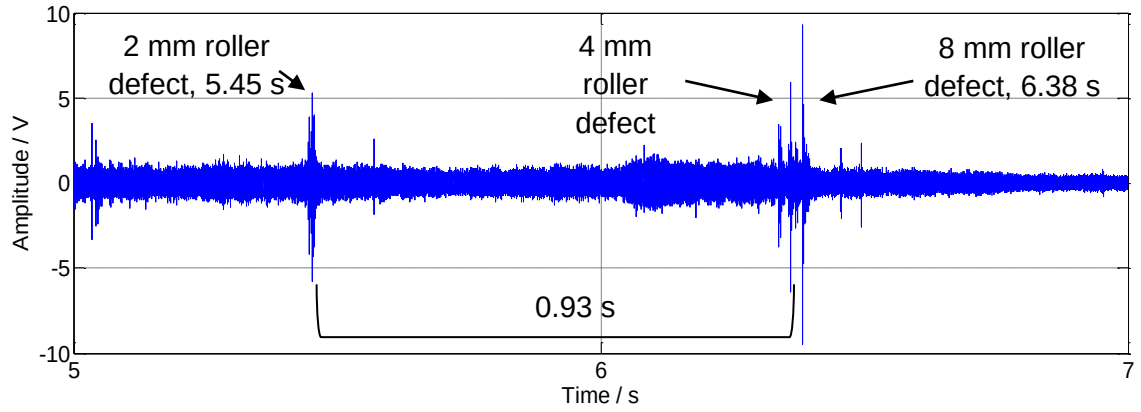

Figure 6-19: Selected 2 s period of raw data.

The presence of high amplitude AE waves in the raw data can reduce the capability of fault detection. Frequency domain analysis can be used to overcome this problem.

Figure 6-20 is a spectrogram (time-frequency diagram) of the measurement and shows that the brake-related noise remains dominant.

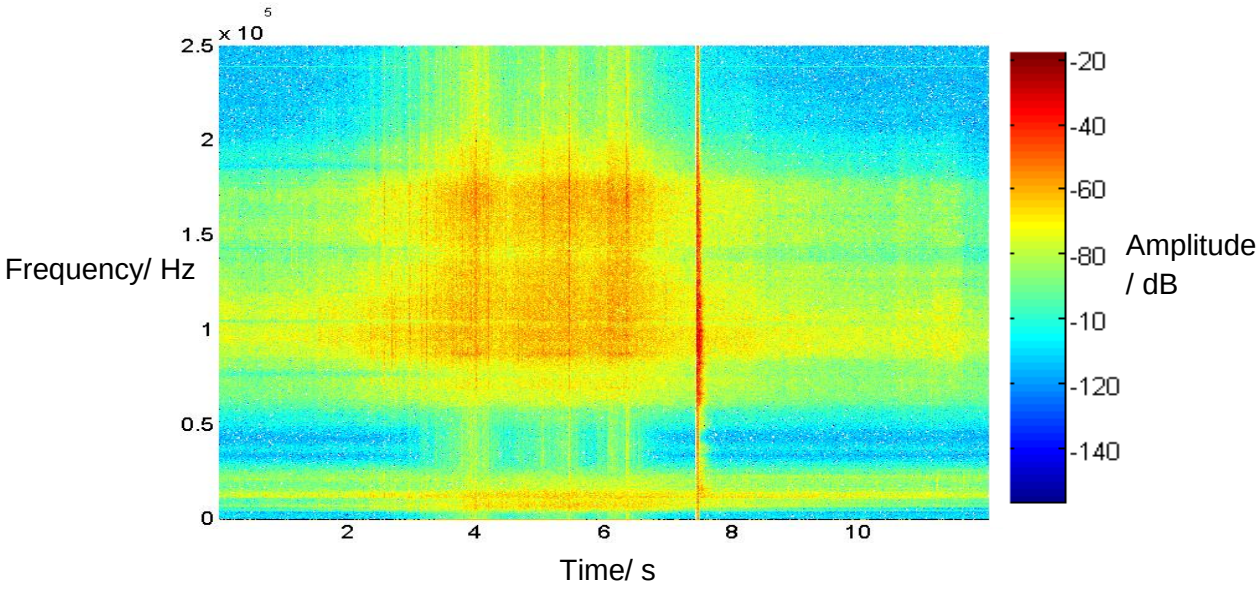

Figure 6-20: Spectrogram of AE data from wayside field test.

Figure 6-21 shows the result from TSK analysis. High amplitude peaks from the bearing defect do not indicate a normal distribution behaviour hence the value of kurtosis rises up to 260 in certain frequency bands. However, the brake-related noise contains a lower value of kurtosis in all frequency bands. TSK of bearing defects has much higher value in high frequency components compared to the brake-related noise. Therefore the TSK is capable of distiguishing between these two peaks. Engine noises contain lower amplitude in high frequency ranges. Therefore using a high-pass filter (> 150 kHz) before the TSK analysis can remove the engine noise from the data. The high amplitude peaks in raw data which have higher TSK value in frequencies between 150-250 kHz are related to the bearing defects. In addition, the engine noise usually has lower amplitude compared to the bearing defect peaks in raw data. Using a threshold-based method can also be used to eliminate the engine noise.

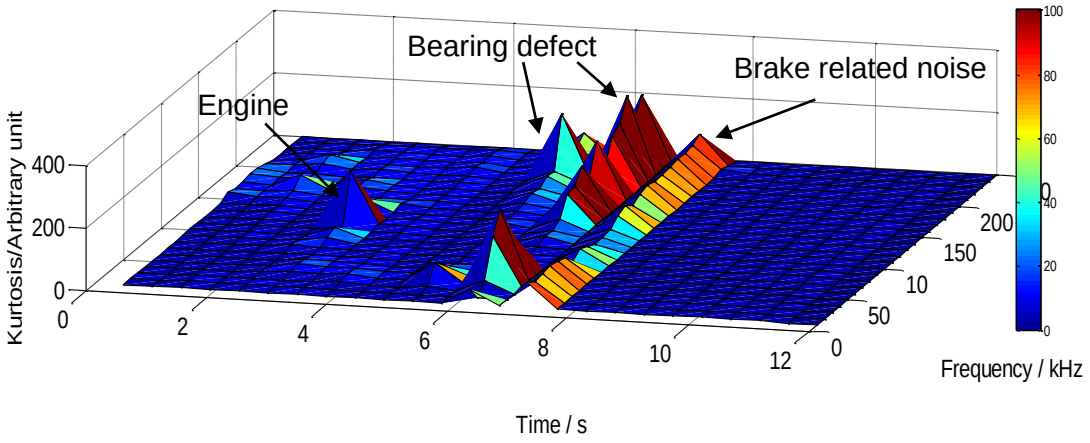

Figure 6-21: Time spectral kurtosis diagram of AE data from wayside field test.

Figure 6-22 illustrates the TSK analysis of the truncated raw data between 5-7 s. It should be noted that because of the large calculating window size, both peaks from 4 mm and 8 mm happen in one square window, and cannot be distinguished. A smaller window size provides better resolution but needs a vast amount of processing time.

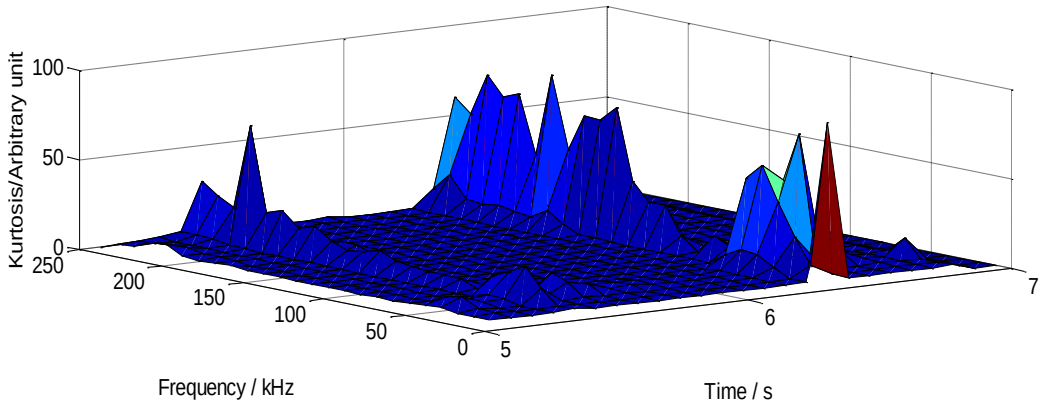

Figure 6-22: TSK of truncated raw data between 5-7 s.

6.3 Cropredy Wayside Measurement

A series of wayside measurements on Network Rail passenger and freight trains were completed in October 2015 at Cropredy. There were a total of 6 channels (4 AE and 2 vibration) installed on the track and the equipment was left there in order to record data automatically using a mechanical treadle for all trains passing over the instrumented section (direction London to Birmingham), at speeds up to 100 MPH (160 km/h). The photographs in Figure 6-23 shows the equipment used to instrument the site at Cropredy.

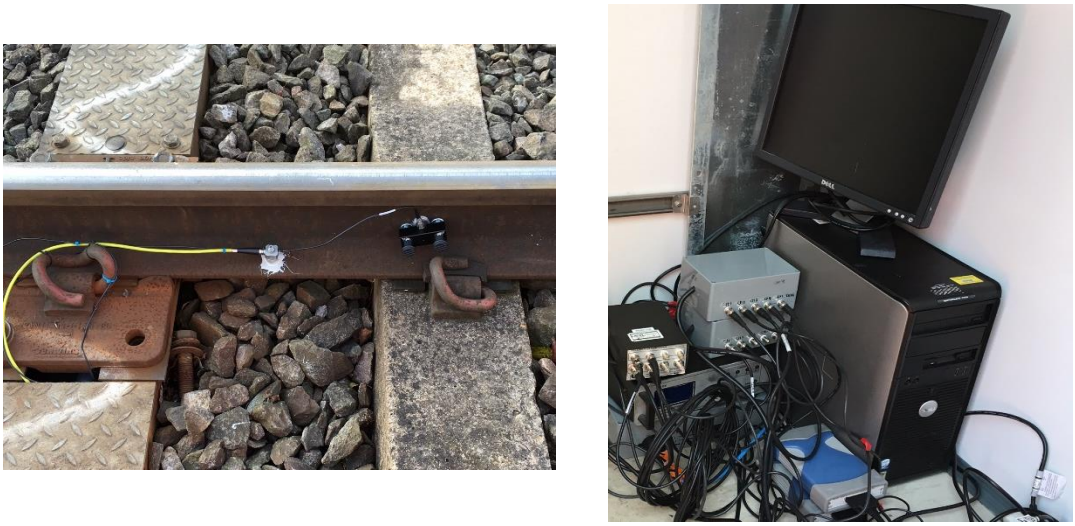

Figure 6-23: Cropredy installation in October 2015.

After analysing the collected data, no sign of defects appeared in the data. Figure 6-24 shows an example of results from the passenger trains. The total length of the train including engine and 3 wagons passed in the first 5 s of the data. Peaks from wheelset appeared in moving RMS data with low amplitude. The low amplitude peaks of the AE data collected from each axle wheel at the passing point show the amount of energy received by the sensor, hence the condition of the wheelset (they are low amplitude in this case therefore there is no defect).

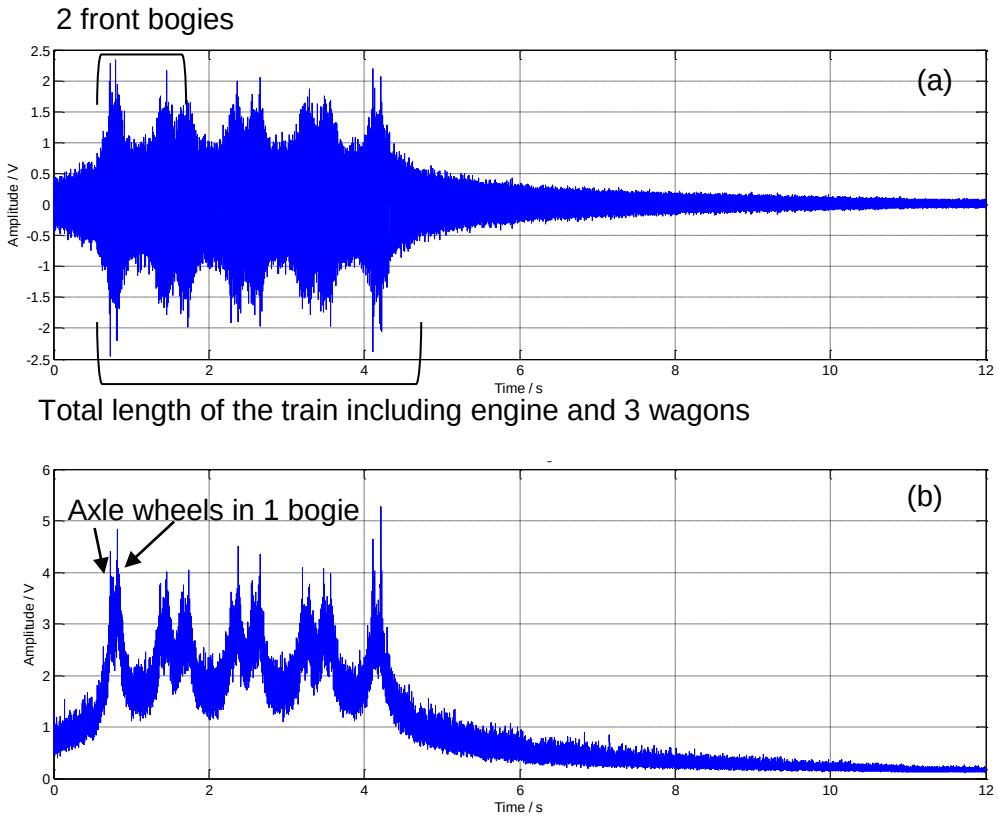

Figure 6-24: AE measurement results from a passenger train in Cropredy, a) Raw signal, b) Moving RMS analysis

The same results were collected for the freight trains, however the length of the trains was longer in comparison with the passenger trains. It can be seen from the data in Figure 6-25 that 12 s of recording was insufficient in order to cover total length of the train. Moreover maximum amplitude in the data is smaller in comparison with the passenger train. This is due to the different weights and traction systems of these trains. Passenger trains in this lane are powered by a diesel multiple unit (DMU) by which engines incorporated into each wagon. On the other hand, freight trains are powered with a single diesel engine located at the front.

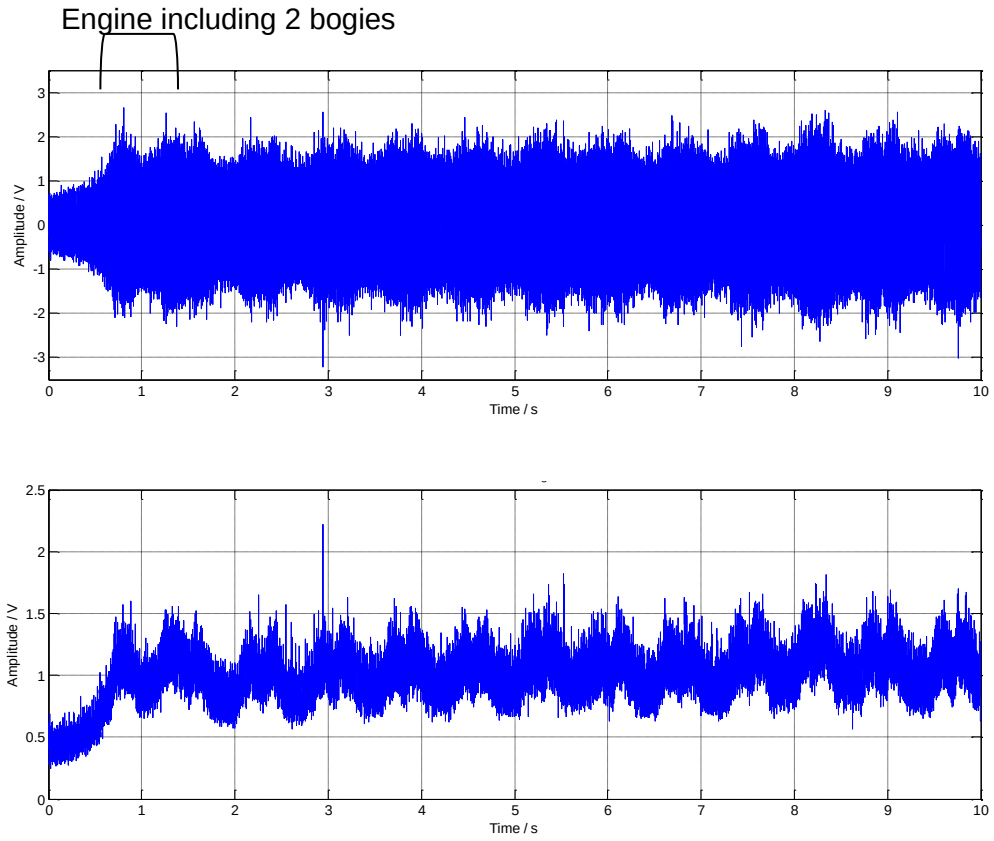

Figure 6-25: AE measurement results from a freight train in Cropredy, a) Raw signal, b) Moving RMS analysis

Figure 6-26 shows the vibration result from a passenger train. It should be noted that vibration measurements were recorded at a different time from the AE ones. This passenger train also consisted of an engine in front with 3 wagons. The moving RMS analysis provides a better observation of the train and each axle bearings that passed the accelerometer.

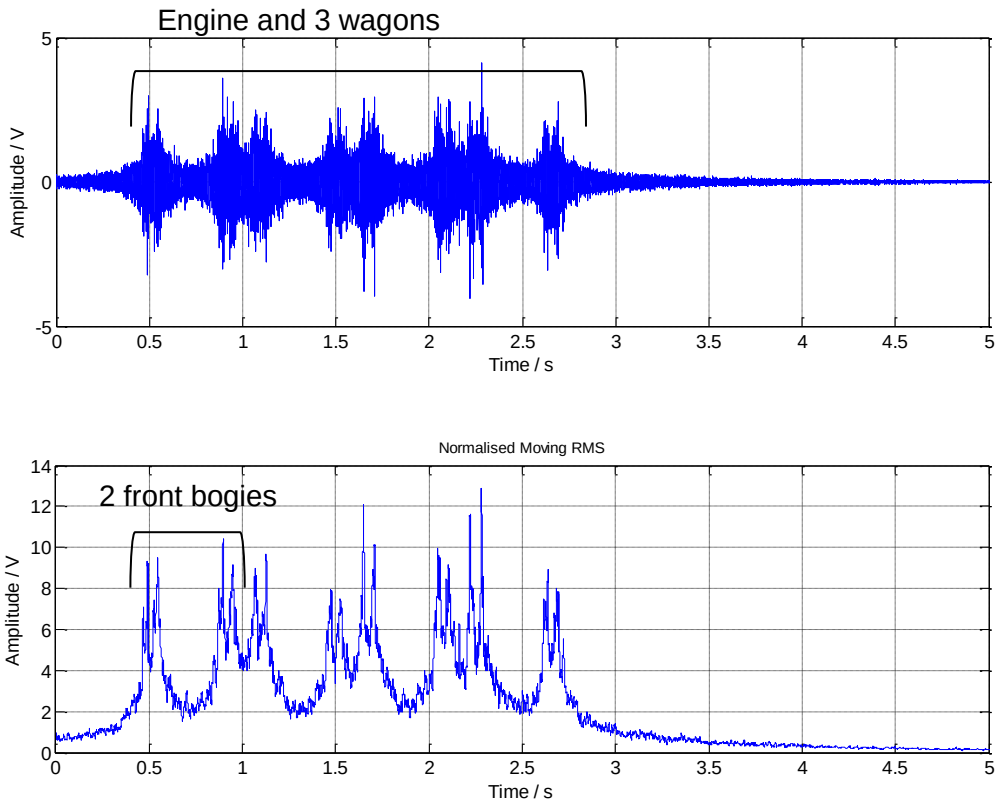

Figure 6-26: Vibration measurement results from a passenger train in Cropredy, a) Raw signal, b) Moving RMS analysis

Figure 6-27 shows the vibration signal from a freight train. From the results it can be concluded that the first 2 bogies produce a higher vibration level due to their higher weight and the engine which provides power to the train. There is no indication of a wheelset defect such as a wheel flat or bearing defect.

In order to design an appropriate threshold for AE and vibration data, there should be sufficient information about the train such as weight of each wagon and the type and speed of the train.

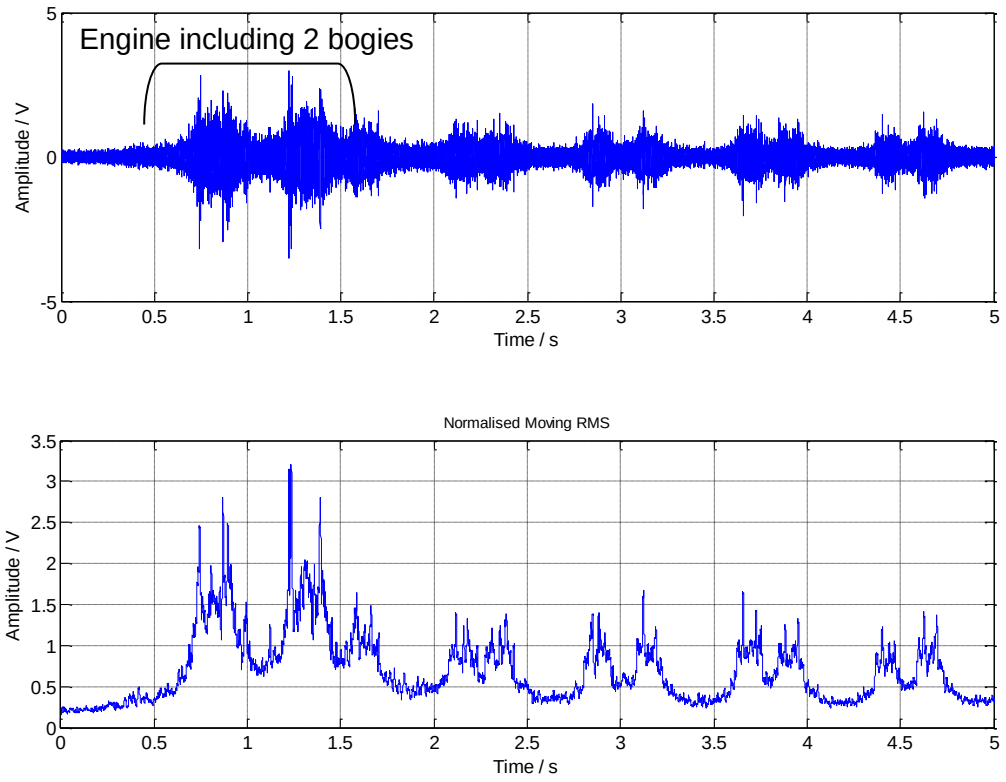

Figure 6-27: Vibration measurement results from a freight train in Cropredy, a) Raw signal, b) Moving RMS analysis

6.4 Summary

In this chapter, configurations of the field trials in both onboard and wayside measurements along with their results were presented. Tests were carried out on the railway wheelsets with a number of artificially induced faults such as wheel flats, bearing with lubricant contamination, race and roller defects. The defects on the roller and race were three different sizes (2,4 and 8 mm). Tests were carried out at a speed of 30 MPH (48 km/h) in the direction forward (engine in front) and 20 MPH (32 km/h) in the direction backwards (engine in the back).

Results from onboard measurement showed the capability of AE system to detect the roller defect with size of over 8mm. This was concluded after the bearing fundamental frequency

and its harmonics appeared at 16.99 Hz. On the other hand vibration failed to identify the bearing defects, however it was able to find the presence of the defect in frequency domain.

Furthermore, AE was able to detect the presence of the bearings with 2, 4 and 8mm roller defect in wayside measurements. TSK analysis was used in order to improve the signal to noise ratio and remove the brake-related noises in the signal. Yet again vibration failed to detect these defective bearings.

Finally a series of wayside measurements on Networkrail passenger and freight trains were presented and results were discussed. After analysing the collected data, no defect was detected in the train wheelsets.

Chapter 7 : Comparison of AE and Vibration Analysis

7.1 Comparison between AE and Vibration in Detecting Wheel Flat Defects

This section analyses results from the trolley tests using a laboratory-sized wheel with a metal build- up defect. The rails of the test track did not have consistent distance from each other, causing flange rubbing at the narrower sections during these experiments. An accelerometer and AE sensor were mounted on the trackside in order to record vibration and AE data at the same time.

The impacts from the metal build-up defect are evident in the vibration measurement while they were mixed with the high frequency noises from rubbing flange in AE, as shown Figure 7-1. This is because metal build-up causes high amplitude vibration on the track within every impact without however, additional low frequency noise. Hence, clear peaks associated with the defect with high signal to noise ratio can be observed. The peaks originating from the defect impacts are also present in the AE signal. However, they cannot be distinguished from the high frequency noise associated with the rubbing flange. It should be noted that in the vibration measurement, higher amplitude peaks occurred due to the impacts that took place closer to the accelerometer resulting in lower vibration damping.

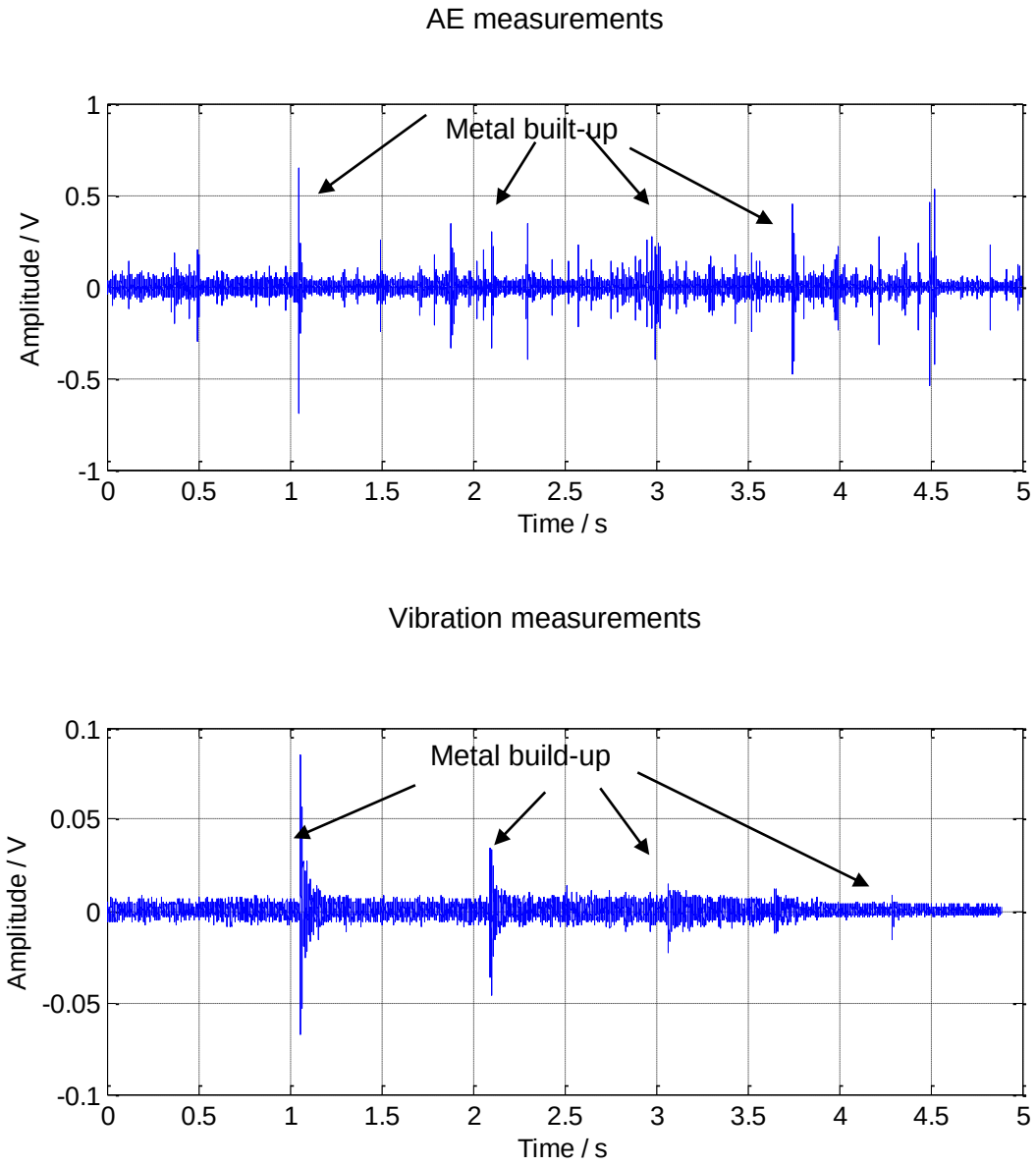

Figure 7-1: Comparison between vibration and AE signals in laboratory test using trolley with defective wheel tread.

This approach also effectively describes the idea of integrated vibration and AE signals in the wayside measurements. This means when both sensors start acquiring at the same time, vibration is only able to detect detective wheel treads without being influenced by high frequency acoustic noises as in the case of AE. AE is however capable of identifying the defective bearings, it is also able to detect wheel related defects. Therefore, vibration results can provide significant feedback when an alarm is generated with respect to whether or not a signal has arisen from a wheel defect or indeed a faulty axle bearing. Hence, peaks arising

from defective bearings and wheel flats can be reliably distinguished. Figure 7-2 demonstrates the overall operational concept of the integrated system.

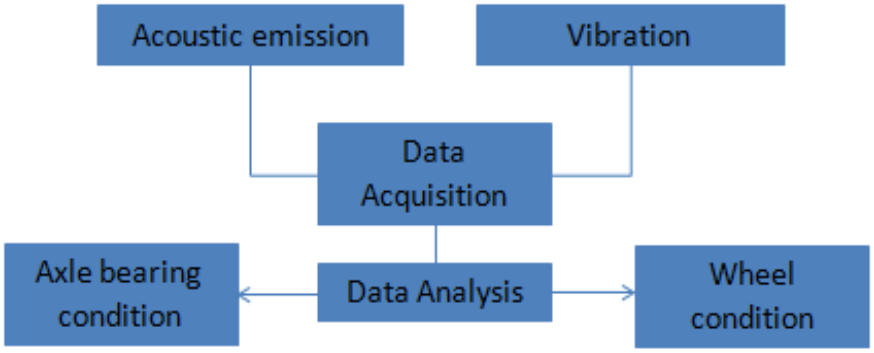

Figure 7-2: Simplified schematic showing the integrated vibration and AE system for wayside monitoring of rolling stock wheelsets.

Experiments on the defective wheel, with a flat being present, were also carried out in the field. These series of experiments included the train with an engine in front along with 2 wagons. In the first wagon the first and fourth wheels, had bearing defects (lubricant contamination) and the third wheel had a 5 cm flat induced with a power tool as shown in Figure 7-3. The schematic in Figure 7-4 shows the overall experimental setup.

Figure 7-3: Artificially induced wheel flat in the field experiments.

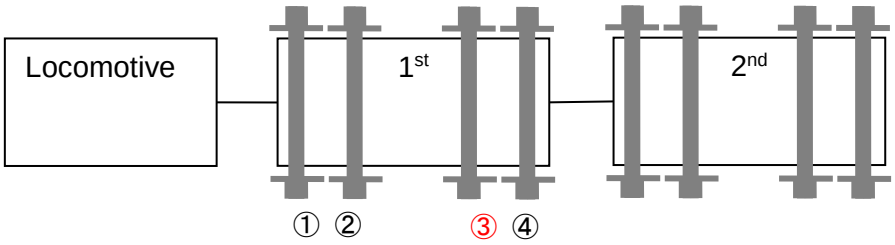

Figure 7-4: Schematic of the experiment, ①defective bearing, ②healthy bearing, ③ wheel flat, ④defective bearing.

As Figure 7-5 shows the wheel flat signature appears in vibration signal. The repetitive peaks should ideally occur once in each revolution (4.2 Hz according to the calculations in section 6.1.1). However due to background noise, possible wheel hunting, rail discontinuities, different track stiffness and signal attenuation, the impacts from the wheel flat do not have consistent amplitude. Therefore the peaks cannot be seen in every revolution. High amplitude peaks in moving RMS can also confirm the presence of the wheel flat defect.

It should be noted that vibration was not able to detect the lubricant contaminated bearing previously in onboard measurement. As the accelerometer was located closer to the defect therefore a more accurate detection is expected in the onboard measurement compared to the wayside. Hence there would be no indication from bearing defect present in the wayside measurement.

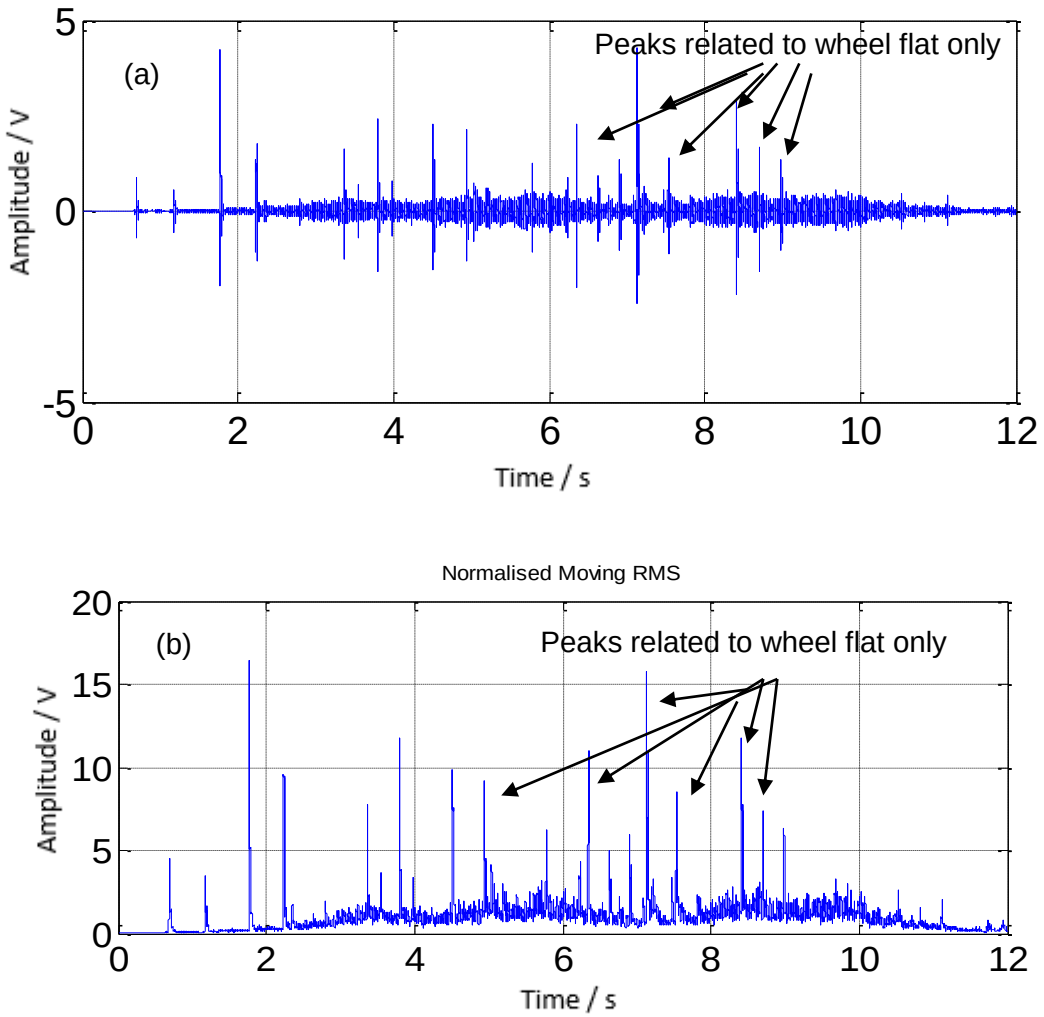

Figure 7-5: Vibration data from field experiment of the train containing wheel flat and bearing defects, a) Raw signal, b) Moving RMS analysis

On the other hand, it is expected that peaks related to bearing defects, as well as the wheel flat, are present in the AE signal. These peaks are shown in Figure 7-6, however they cannot be distinguished as the vibration and AE measurements were not acquired at the same time in this series of experiments. It should be noted that there is a possibility of high

frequency noises, such as brake, in AE data which can be cancelled by further signal processing.

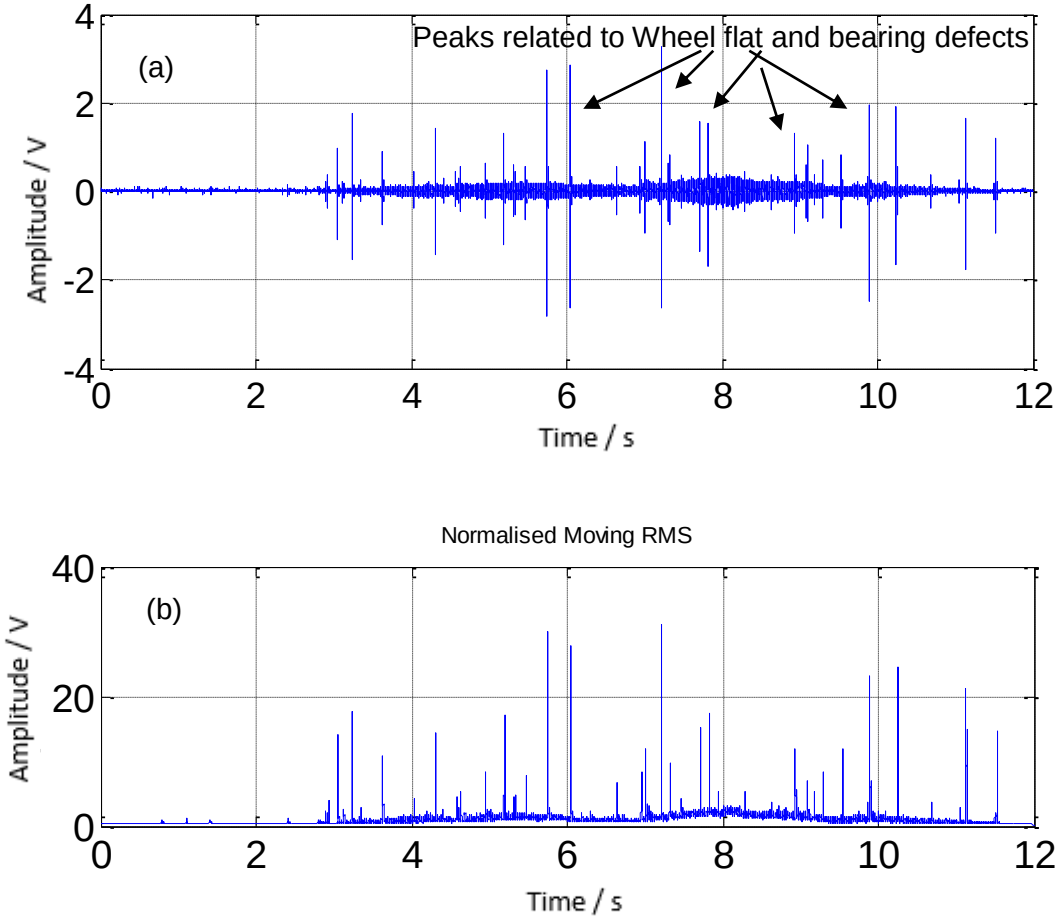

Figure 7-6: AE data from field experiment of the train containing wheel flat and bearing defects, a) Raw signal, b) Moving RMS analysis

7.2 Comparison between AE and Vibration Techniques for Test Rig Experiments

This part of the report discusses in more detail the results from the test rig experiments on bearings with various speed and defects. The bearing with the smallest size outer race defect (F1) at a rotating speed of 100 RPM was monitored and the results obtained were compared, as shown from the plots in Figure 7-7. No significant change can be observed between healthy and defective bearings in the vibration signal. The summarised results presented in Table 7-1 also show that the overall values acquired for the defective bearing do not increase. On the other hand AE is capable of detecting the outer race defect as the amplitude level increases. Despite the presence of a few high amplitude peaks in the signal from the healthy bearing, it can be observed in the raw data that its peak-to-peak value is smaller than the defective one. In addition to this, the RMS value was also double for the defective bearing. It should be noted that the shaft in the healthy bearing experiment was bent which could cause the appearance of high amplitude peaks. This issue was caught in HFRT analysis during measurements at higher rotating speed where the impacts were stronger.

Vibration measurements

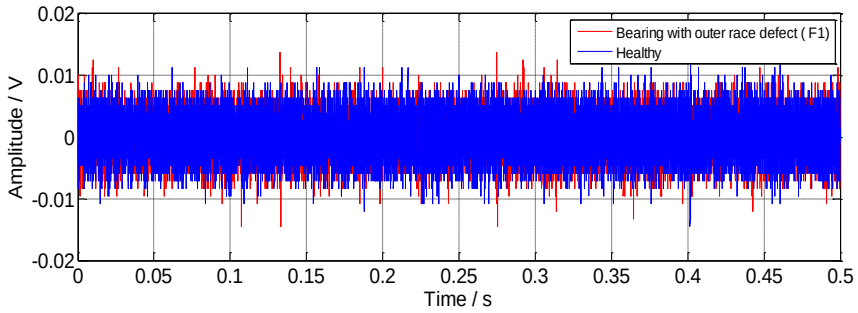

AE measurements

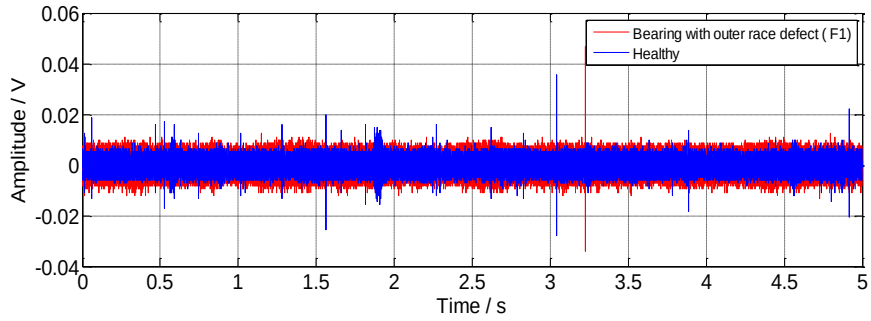

Figure 7-7: Comparison between healthy and bearing with outer race defect (F1) at a rotating speed of 100 RPM.

Table 7-1: Overall values from vibration and AE measurements of healthy bearing and bearing with outer race defect (F1) at a rotating speed of 100 RPM.

Vibration analysis	Healthy	Bearing with outer race defect (F1)
PK-PK	0.02	0.02
RMS	0.002	0.002
Kurtosis	2.96	3.02
Crest Factor	14.2	14.5
AE analysis	Healthy	Bearing with outer race defect (F1)
PK-PK	0.06	0.08
RMS	0.001	0.002
Kurtosis	3.02	3.09
Crest Factor	24	25.3

In the previous experiment, vibration analysis failed to detect the defective bearing. This is due to the low energy impacts caused by the small defect at low rotating speed. The next experiment was carried out on the bearing with larger and deeper outer race defect (F3) at an even lower rotating speed equivalent to 48 RPM. The results are compared Figure 7-8 and summarised in Table 7-2. Yet again vibration analysis failed to distinguish between the healthy and defective bearings and no significant change in the overall values can be observed. However, AE analysis was again able to detect the defective bearing as there are a number of high amplitude peaks in the raw data, as well as a significant increase in the peak-to-peak, RMS and kurtosis values.

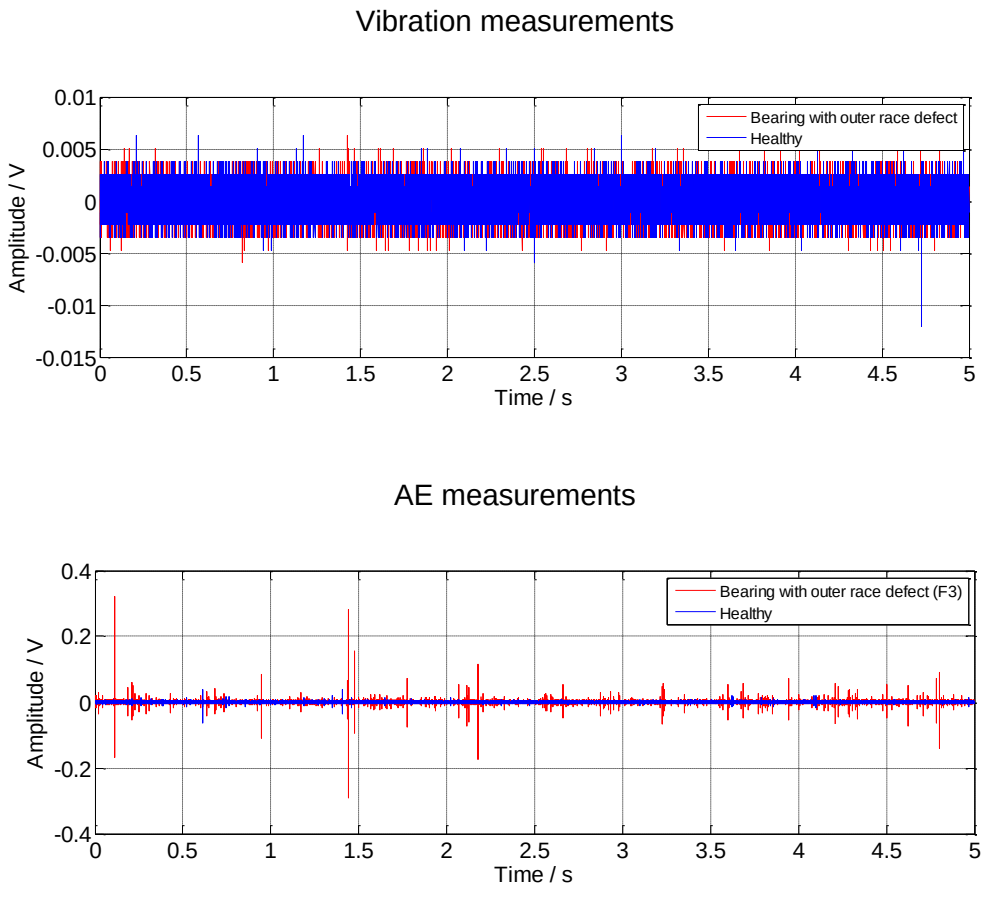

Figure 7-8: Comparison between healthy and bearing with outer race defect (F3) at a rotating speed of 48 RPM speed.

Table 7-2: Overall values from vibration and AE measurements of healthy bearing and bearing with outer race defect (F1) at a rotating speed of 48 RPM.

Vibration analysis	Healthy	Bearing with outer race defect (F3)
Kurtosis	2.6	2.7
Crest Factor	13.6	13.3
PK-PK	0.018	0.012
RMS	0.013	0.013

AE analysis	Healthy	Bearing with outer race defect (F3)
Kurtosis	7.8	1449
Crest Factor	47	49
PK-PK	0.1	0.61
RMS	0.001	0.002

In addition, a set of experiments for comparison between the healthy bearing rotating at 100 RPM and the defective bearing with the F3 outer race defect rotating at 100 RPM and at 200 RPM were completed. The amplitude of both vibration and AE signals were expected to rise by increasing the rotational speed. In vibration analysis, despite having higher amplitude peaks at the rotating speed of 100 RPM, the increase in amplitude is more significant for the rotating speed at 200 RPM as seen Figure 7-9. The results of the AE analysis show a constant rise in amplitude with increasing rotational speed.

Therefore, AE is more sensitive at lower rotational speeds, in comparison with the vibration technique and it can be concluded that vibration failed to detect the defective bearings at lower speeds. This is because the amount of vibration energy generated from the impacts caused by the defects is insufficient to be detected by the accelerometer.

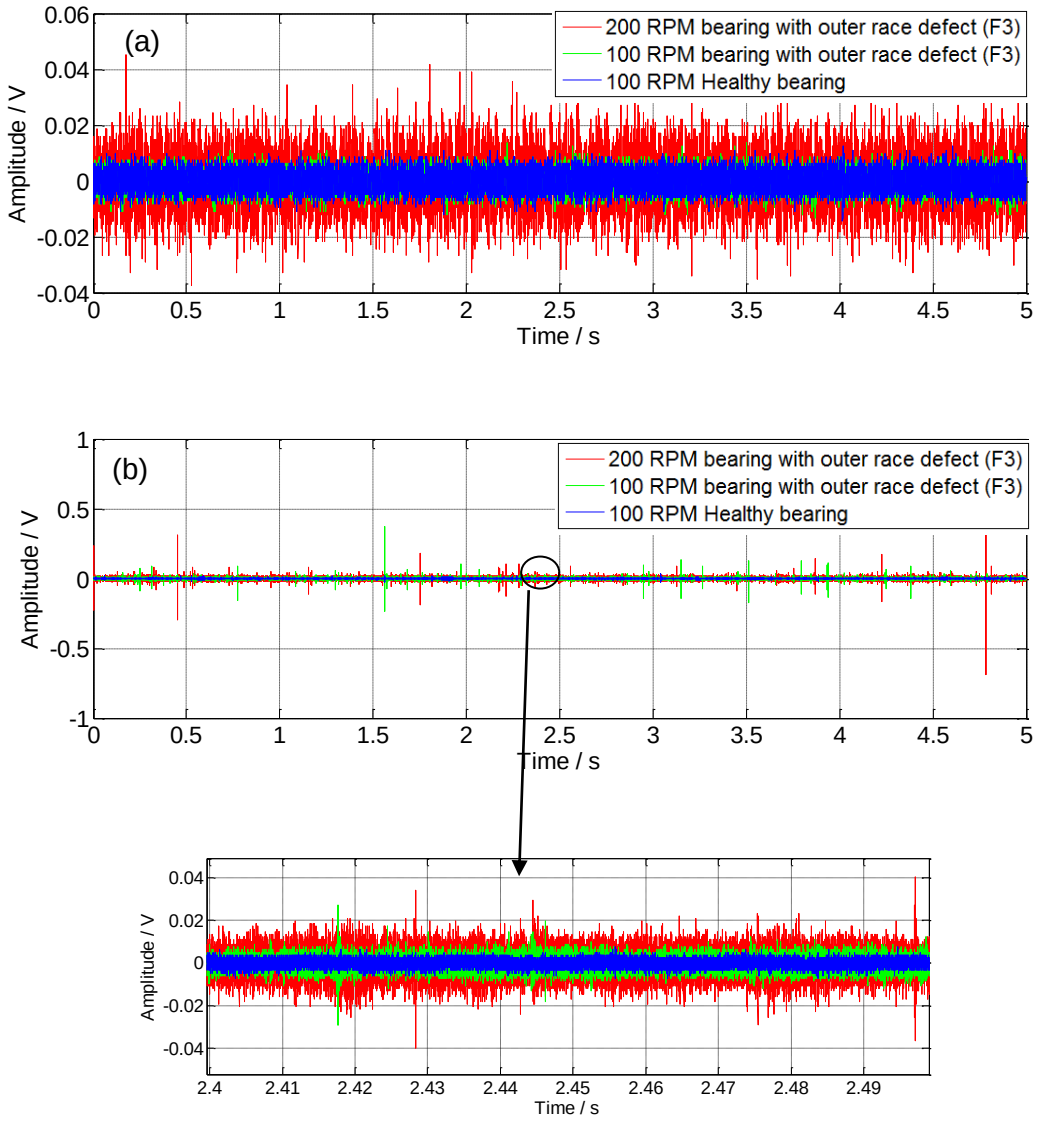

Figure 7-9: Comparison between vibration (a) and AE (b) measurements of healthy bearing rotating in 100 RPM and bearing with outer race defect (F3) at rotational speeds of 100 and 200 RPM.

7.3 Evaluation of the Effect of Speed and Defect Size on AE and Vibration

The peak-to-peak data from both vibration and AE test rig measurements at different rotational speeds are plotted in Figure 7-10. The amplitude of the vibration and AE signals increase with increasing rotational speed of the bearings. This is due to the fact that the impact produced by the defect has more energy as rotational speed increases.

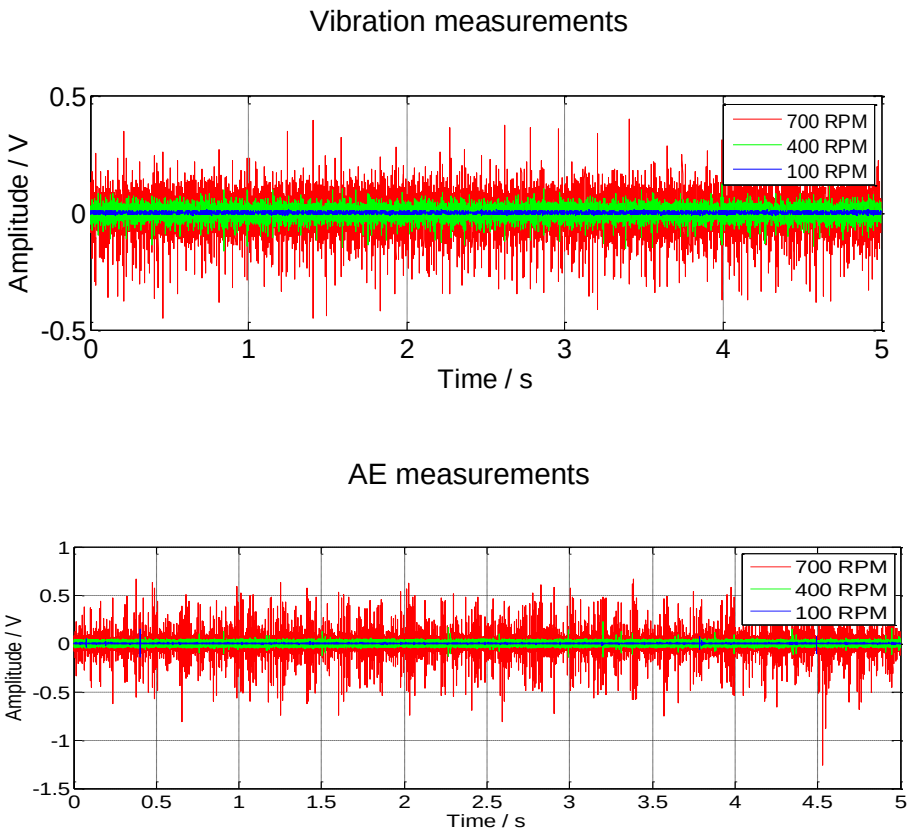

Figure 7-10: Peak-to-peak data comparison of the bearing with outer race defect in rig test by changing rotating speed.

Figure 7-11 shows the overall value variations with increasing rotational speed with Peak-to-peak and RMS values being proportional to the rotating speed. In vibration analysis, the overall kurtosis value shows a constant increase with increasing speed until it reaches 600 RPM and then it begins to decrease. As previously mentioned, the main drawback of the

kurtosis is that it begins to revert back to the undamaged value as the speed increases. In AE, because of high frequency non-Gaussian noises, the overall kurtosis value becomes minimal with increasing speed. Crest Factor based analysis provides slightly better results than kurtosis in both vibration and AE data with increasing rotating speed. It should be stressed that the analysis is based on calculation of the overall RMS, kurtosis and Crest Factor values from each of the measurements considered. The analysis based on the use of a suitable moving window (i.e. moving RMS, moving kurtosis and moving Crest Factor) would give better results, but this would require significantly more computational time.

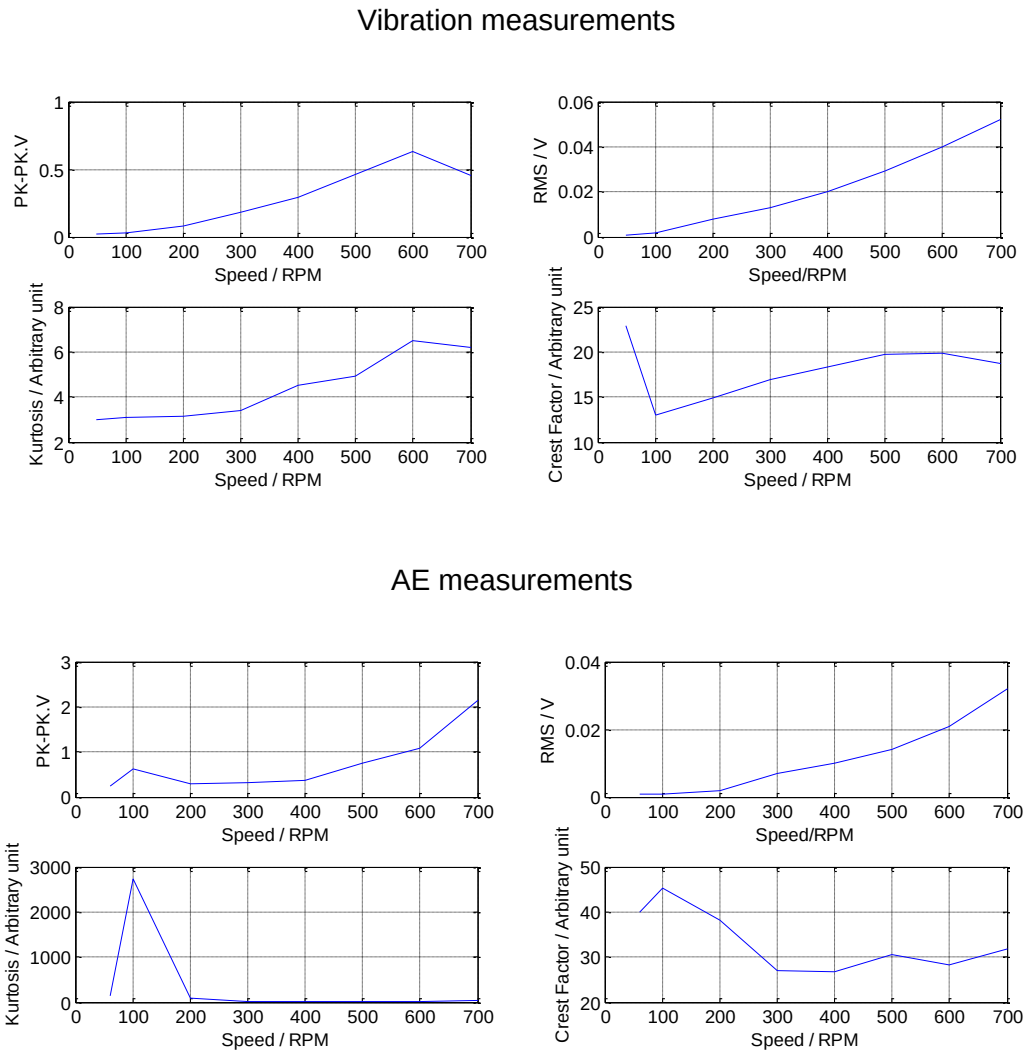

Figure 7-11: Overall value changes of the bearing with outer race defect by changing the speed.

In section 6.1.1 the effect of defect size in vibration and AE data in the Long Marston field test was demonstrated. Figure 7-12 demonstrates the overall value variations that occur with increasing defect size. There is no significant change in the amplitude and overall values of the vibration data by increasing the size of the defects. This is due to the fact that relatively smaller defects (defects in the early stages) do not produce sufficient vibration variations in order to be detectable with an accelerometer. However, from the raw data AE results it is evident that the larger defect size results in an AE signature with greater amplitude. The peak-to-peak and RMS values in the bearing with 8 mm roller defect are significantly higher than the ones containing smaller defect sizes. Kurtosis and Crest Factor without the use of a suitable moving window are not able to clearly separate the bearings with different defect sizes.

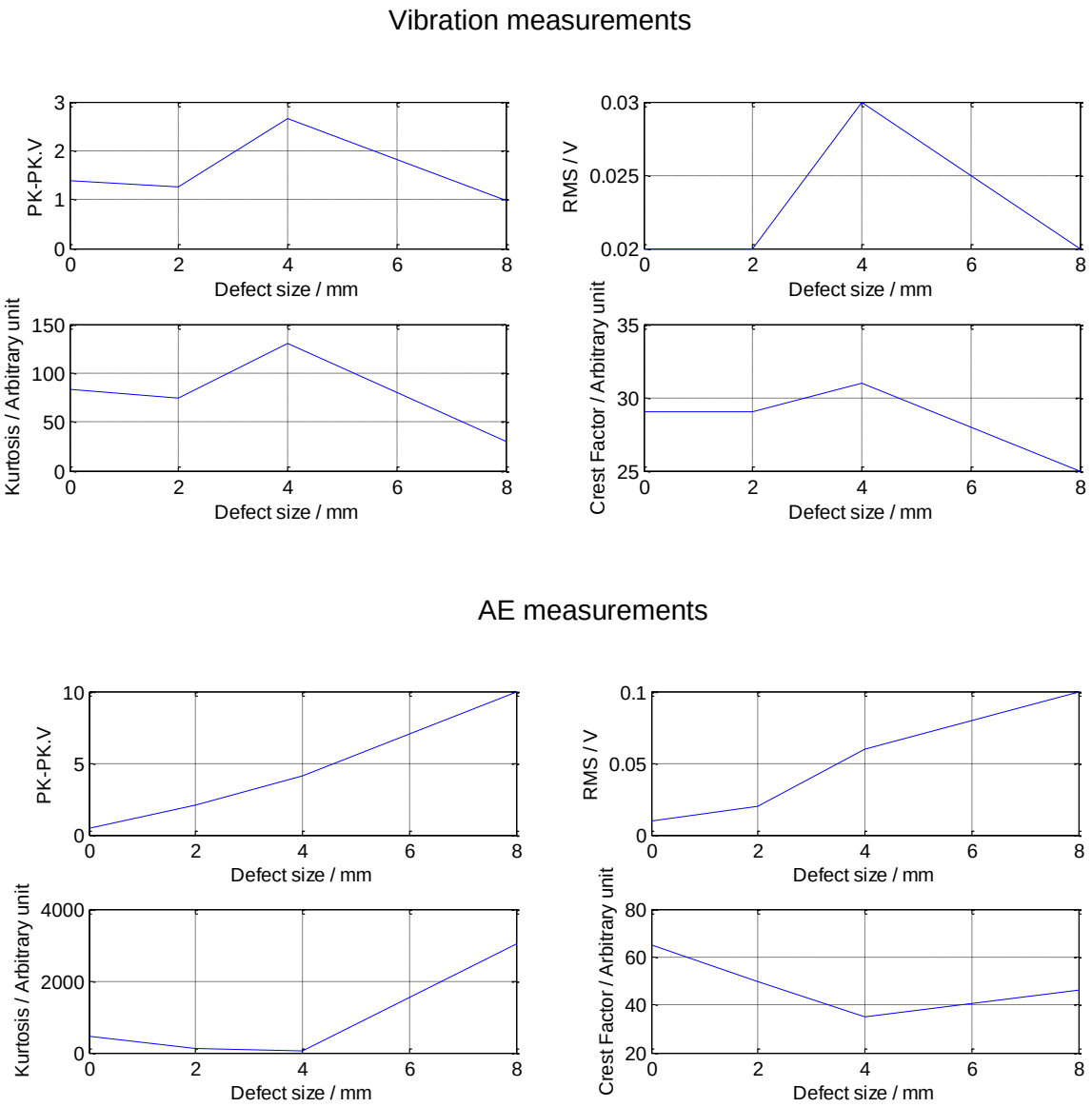

Figure 7-12: Overall value changes of the bearing with roller defect by changing the defect size - Onboard Long Marston.

The amplitude difference in the AE and vibration signature for the Long Marston tests at 32 km/h (20 MPH) and 48 km/h (30 MPH) are shown in Figure 7-13. The amplitude of the vibration signal does not show any appreciable change with increasing speed. This is attributed to the smaller effect on the vibration signature in comparison to the effect on the noise signal. The AE signature shows a slight increase with increasing speed.

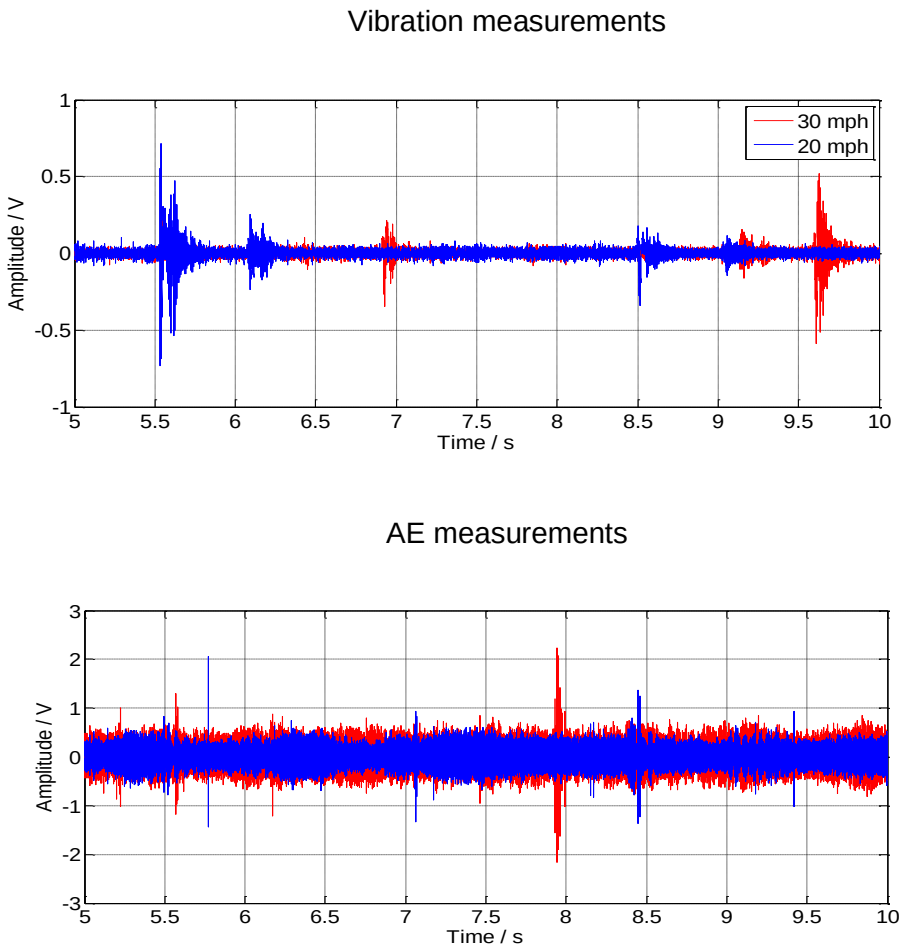

Figure 7-13: Data comparison from the onboard bearing with 2 mm roller defect, Long Marston test at two different train's speeds (20 MPH and 30 MPH).

Table 7-3 summarises the vibration and AE results for the 2 mm roller defect obtained during the field tests in Long Marston at two different speeds. The overall values for AE confirm the previous results from the laboratory test. Yet again the peak-to-peak and RMS values increase with increasing train speed. The calculated overall values for kurtosis and Crest Factor show evidence that the defect is present but does not increase with increasing speed. Finally, there was small difference in the overall values of vibration measurement. Therefore concluding that vibration shows lower sensitivity to speed changes compared to AE technique.

Table 7-3: AE and vibration Long Marston measurements overall values of 2 mm roller defect comparison in different train speed.

	AE		Vibration	
	Backward (20 MPH)	**Forward (30 MPH)**	**Backward (20 MPH)**	**Forward (30 MPH)**
PK-PK / V	3.4	4.4	1.44	1.1
RMS / V	0.11	0.15	0.03	0.02
Crest Factor	25	23	27	26
Kurtosis	4.2	3.9	59	53

7.4 Comparison between AE and Vibration Techniques in Detecting Bearing with Lubricant Contamination

For the purpose of comparing vibration and AE method in detecting early stage bearing defects, experimental work on bearings with lubricant contamination was carried out in the laboratory.

Early stage defects are not severe enough to produce high energy impacts. Therefore a bearing with 0.03 grams of sand contamination (0.5 % weight ratio), which was expected to produce low energy impact, was tested. Later a bearing containing 0.06 grams sand contamination (1% weigh ratio) was tested and the results compared. In addition to this, a series of experiments were completed with the bearings rotating at different speeds and these results are discussed below.

Figure 7-14 shows a comparison between vibration and AE results of a bearing with minor sand contamination defect (with 0.5 % weight ratio) and a healthy bearing, both running at 500 RPM. By comparing the faulty and healthy bearings in both vibration and AE analysis, it is evident that AE was more sensitive in detecting incipient damage than the vibration method. The peak-to-peak value of the faulty AE signal was 1.9 V using AE, whereas it was only 0.75 V using vibration. The number of bursts confirms that the number of impacts

measured by the AE sensor is much greater, as only one high amplitude burst appeared in 5 s of vibration measurement. In both tests the values of kurtosis and Crest Factor increased, however this amount was more significant in the AE testing. Additionally the RMS value for the vibration result remained relatively constant, conversely it increased in the AE result from the faulty bearing. The overall values are summarised in Table 7-4.

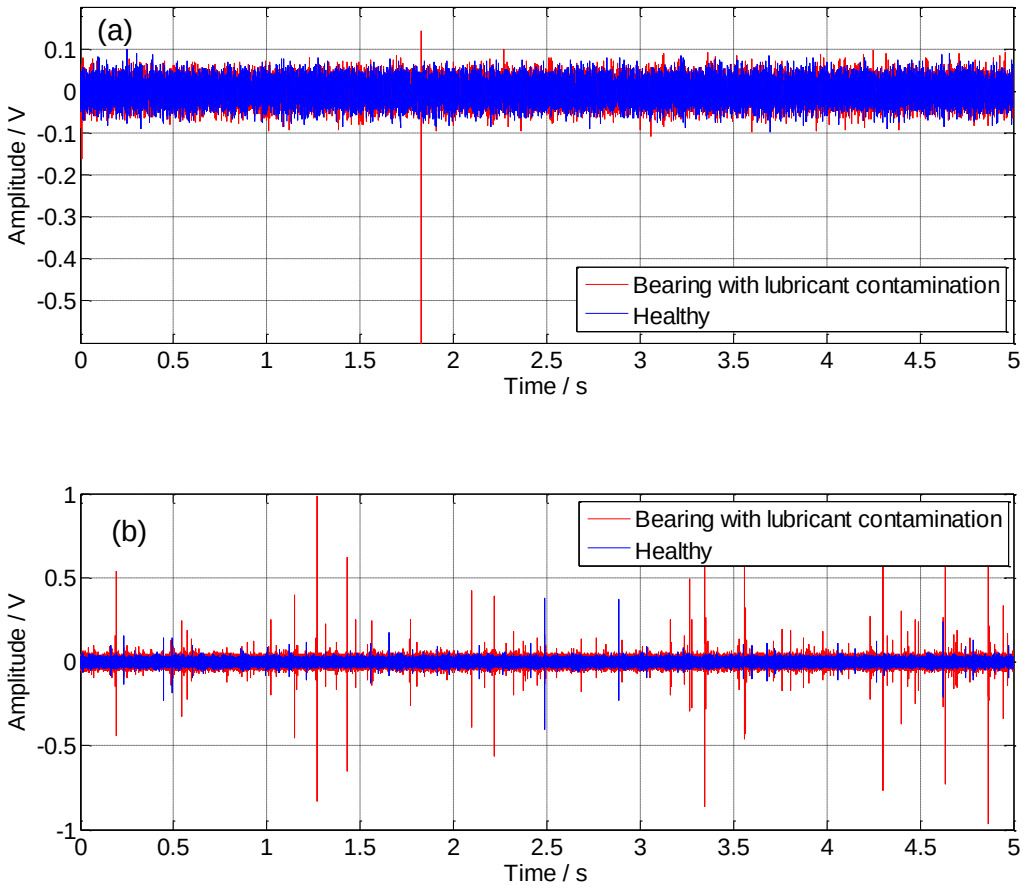

Figure 7-14: Comparison between a) vibration and b) AE measurement of the bearing with 0.5 % weight ratio lubricant contamination defect and healthy bearing at 500 RPM.

Table 7-4: Overall values of vibration and AE measurement of the bearing with 0.5 % weight ratio lubricant contamination defect and healthy bearing at 500 RPM.

Vibration	Healthy	Bearing with lubricant contamination
Kurtosis	3	7.73
Crest Factor	13	28
PK-PK	0.19	0.75
RMS	0.02	0.02

AE	Healthy	Bearing with lubricant contamination
Kurtosis	14	173
Crest Factor	31	35
PK-PK	0.77	1.9
RMS	0.01	0.015

Both techniques were evaluated at a lower rotational speed in the next stage. The bearing with the minor sand contamination was rotating at 50 RPM, which is considered a relatively low rotating speed.

There were only a few peaks observed indicating the actual vibration arise from the defect in vibration signal. Peak-to-peak, kurtosis and Crest Factor show a slight rise in their values, however the RMS value remained constant, when comparing the healthy and defective bearing (Table 7-5).

Once more AE data shows the presence of several bursts from the defective bearing which indicates high frequency impacts caused by the sand contamination. Overall values of the defect bearing show a significant increase in comparison with the healthy bearing. Figure 7-15 shows a comparison between vibration and AE signals of a bearing with 0.5 % weight ratio lubricant contamination defect and a healthy bearing, both at 50 RPM.

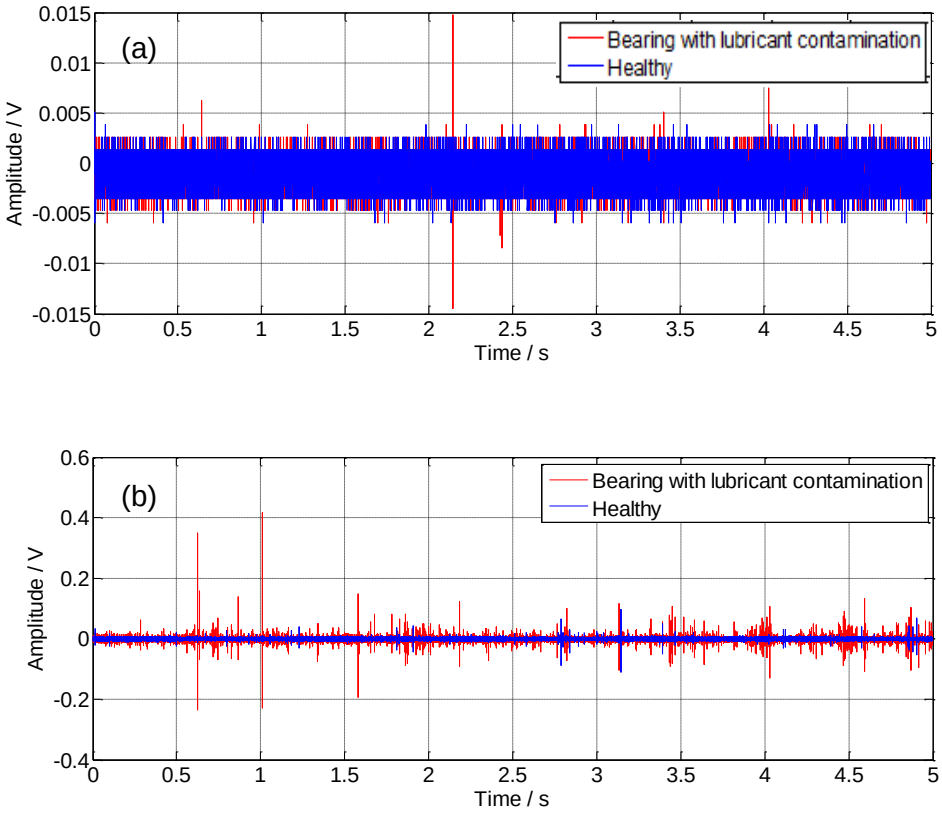

Figure 7-15: Comparison between vibration (a) and AE (b) measurement of the bearing with 0.5 % weight ratio lubricant contamination defect and healthy bearing at 50 RPM.

Table 7-5: Overall values of vibration and AE measurement of the bearing with 0.5 % weight ratio lubricant contamination defect and healthy bearing at 50 RPM.

Vibration	Healthy	Bearing with lubricant contamination
Kurtosis	4	6
Crest Factor	11	19
PK-PK	0.011	0.029
RMS	0.001	0.001

AE	Healthy	Bearing with lubricant contamination
Kurtosis	20	407
Crest Factor	34	41
PK-PK	0.2	0.65
RMS	0.002	0.003

It should be noted that by increasing the amount of sand to 1% of weight ratio, vibration is also capable of finding the defect at low rotating speed. The results of the comparisons between the vibration measurement of the bearing with 1% weight ratio lubricant contamination defect and healthy bearing were presented previously in Figure 5-44.

The contaminated lubricant test was extended to the Long Marston field test. Figure 7-16 shows a comparison between a healthy and a faulty bearing for both AE and vibration measurements. From the raw data, it is evident that AE is more suitable to distinguish between the two bearings, as vibration only shows a small difference. The overall values in AE measurement change significantly in comparison with the overall values from the vibration measurement (Table 7-6).

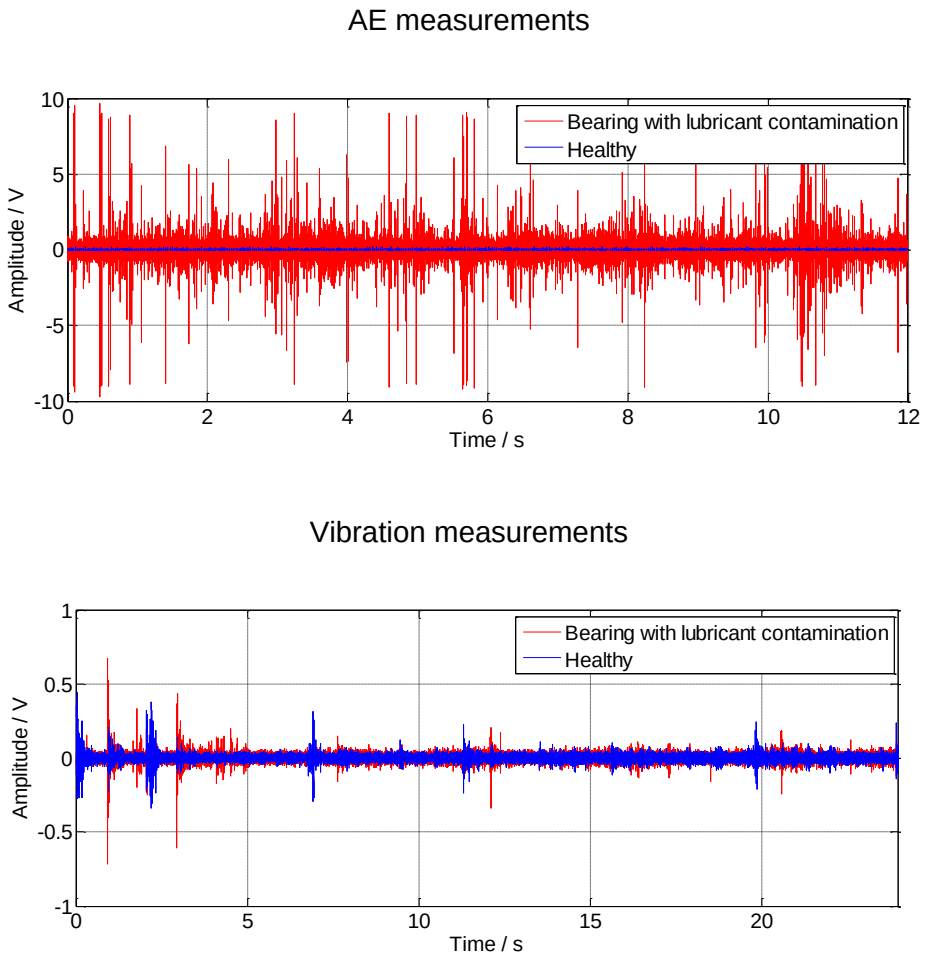

Figure 7-16: Comparison of the bearing with lubricant contamination defect and healthy bearing, Long Marston field test.

Table 7-6: Overall values of vibration and AE measurement of the bearing lubricant contamination defect and healthy bearing, Long Marston.

AE measurement	Healthy	Sand contamination
Kurtosis	24	224
Crest Factor	20	33
PK-PK	0.25	19.37
RMS	0.01	0.21

Vibration measurement	Healthy	Sand contamination
Kurtosis	27	43
Crest Factor	26	29
PK-PK	0.78	1.38
RMS	0.02	0.02

7.5 Summary

In this chapter AE and vibration data were compared in detecting wheel flat defects. Vibration data showed clear peaks associated with the defect with high signal to noise ratio, whereas AE data consisted of the high frequency noises arising from the rubbing flange in the laboratory experiments. Experiments on the defective wheel with a flat were also carried out in the field and results were presented.

AE and vibration data were compared in test rig experiments. Data from healthy and defective bearings with different defect sizes and speed were compared together. AE showed a higher sensitivity to detect the bearings with smaller size defect or lower rotating frequency in comparison with vibration technique.

Moreover, the effect of speed and defect size on AE and vibration were evaluated. It was concluded that vibration showed lower sensitivity to speed and defect size changes compared to AE technique.

Lastly, AE and vibration technique were compared in detecting bearings with lubricant contamination. It was concluded that AE was more sensitive in detecting the contamination defect in lower rotating speed compared to vibration technique.

Chapter 8 : Conclusions and Recommendations

8.1 Conclusions

This research has explored the application of AE and vibration techniques in evaluating the condition of rolling stock wheelsets, as well as investigating the use of signal processing techniques to analyse both AE and vibration signals. The author developed a customised software application, written in Matlab, for the control of the AE and vibration boards and processing the data. A number of laboratory and field tests, at the Long Marston test track, have been carried out to establish a robust and effective approach in evaluating faulty axle bearings, using a customised onboard and wayside condition monitoring system.

Defective axle bearings increase the amplitude of the peaks in both AE and vibration measurements which indicates the presence of a defect. However, It was also noted that raw data is not always adequate for interpreting the signals, so further analysis using filtering methodologies based on FFT, HFRT, kurtosis etc. are required to provide useful results.

The set of laboratory tests prove that AE and vibration techniques are successful at distinguishing between the healthy and defective bearings and finding the characteristic frequencies and their harmonics. The same has been proven under field operational conditions, as shown in the results obtained from the tests carried out at the Long Marston test track. However, in the case of small size bearing defects in Long Marston experiments, because of the low signal to noise ratio, AE is only able to detect the presence of the defect and not its type. In addition vibration failed to detect the bearing defects in the time domain signal.

The AE technique proves its ability to find the defects in low rotating speed bearings and the tests confirm that AE was more effective in the early diagnosis of the bearing defects when compared to vibration, and the same results were proposed by previous research such as [109].

Results show that band–pass filtering of both AE and vibration signal, based on bandwidth and centre frequency derived from Kurtogram analysis, can be an effective tool to cancel the background noise level. This is particularly important to detect the fundamental frequencies in bearings with a low rotating speed.

Conventional analysis methods, such as moving RMS and moving kurtosis, although capable of identifying axle bearing defects, are not ideal when signal to noise ratio is low. Extraneous noises, such as the braking system, increase the value of the RMS and a slight rise in kurtosis can lead to false identification of defects. It has been demonstrated that TSK, using the time and frequency domain, including the kurtosis values for each frequency band, enhances the ability to identify the bearing defects in such cases. The key point to analyse wayside data, is to use a triggering system in order to find the location of wheels and apply TSK to reduce the effect of surrounding noises. This is because signals from the bearing defects appear in both time domain and TSK analysis.

Further laboratory and field tests were carried out to examine the effect of defect size and speed on AE and vibration measurements of railway bearings. Rotating speed was changing from 100 to 700 RPM in the laboratory test and from 20 to 30 MPH in the field test and the defect sizes in the field test varied from 0mm to 8mm. In the bearing vibration analysis, RMS and peak-to-peak values tended to be proportional to the running speed and size of the bearing defect if the recording gain remains the same. In the laboratory vibration tests with less background noise and more stable speed, kurtosis is capable to indicate the fault. However, the value of kurtosis and Crest Factor were affected by the surrounding noises in the field experiments.

Finally, the applicability of both AE and vibration methods were studied in relation to the detection of bearings with lubricant contamination. AE proved to have higher sensitivity and ability to detect bearing with lubricant contamination compared to the vibration technique.

Overall it can be concluded that AE and vibration techniques cannot be replaced with each other in diagnosing of railway wheelsets. This is clear in the case of wayside monitoring of the wheel flats, although the signature of the defect appears in the AE signal, its signal to noise ratio might be lower in comparison with the vibration analysis. On the other hand vibration is unable to do the job of AE, because of its operational performance in lower frequencies. Cases such as crack propagation or slow rotating machinery, because of producing high frequency signature, are only detectable with AE. Therefore, both methods can complement each other to ensure early and more reliable diagnosis of the bearing failures.

8.2 Recommendations for Further Work

Some aspects have been identified as requiring further work and improvement. Using multiple AE and vibration sensors would improve accuracy and therefore reduce the possibility of overlooking irrelevant peaks in signals.

Other types of signal processing methods such as time synchronous averaging (TSA), wavelet and Empirical Mode Decomposition **(**EMD**)** may also be considered in order to improve the signal to noise ratio.

Another important parameter which can greatly affect the AE and vibration signals is load, however due to difficulty of changing loads in the train, this parameter was not considered in the field experiments of this project. Signal attenuation is another aspect that can be examined in order to find the optimum distance from the triggering system to place the sensors in wayside measurements.

The author also sees the necessity of performing further tests focusing on the train's shaft and gearbox diagnosis, which have not been considered in these tests. In addition AE technique can be applied to determine the condition of the railway tracks and detect possible crack growth in sensitive areas. Integration between AE and vibration and other wayside or onboard techniques such as hot axle box and wheel profile may also be considered.

References

[1] W. Kappes, M. Kröning, B. Rockstroh, H. Salzburger, and F. Walte, "Non-destructive testing of wheelsets as a contribution safety of rail traffic," Fraunhofer Institute Non-destructive Testing (IzfP), Saarbrücken.

[2] National Aeronautics and space adminstration, System failure case studies, available :https://nsc.nasa.gov/SFCS/SystemFailureCaseStudyFile/Download/409 [Accessed March 2015]
2007.

[3] "Development of Novel Inspection Systems for Railway Wheel sets," SAFERAIL consortium , description of work , Reference number : SCP7-GA-2008-218674,2008.

[4] M. Papaelias, A. Amini, Z. Huang, P. Vallely, D. C. Dias, and S. Kerkyras, "Online condition monitoring of rolling stock wheels and axle bearings," *Proceedings of the Institution of Mechanical Engineers, Part F: Journal of Rail and Rapid Transit,* p. 0954409714559758, 2014.

[5] B. Stratman, Y. Liu, and S. Mahadevan, "Structural health monitoring of railroad wheels using wheel impact load detectors," *Journal of Failure Analysis and Prevention,* vol. 7, pp. 218-225, 2007.

[6] M. Papaelias, "Effect of defective wheels on rail, Saferail report, Reference number :SCP7-GA-2008-218674,," 2009.

[7] A. Ekberg and P. Sotkovszki, "Anisotropy and rolling contact fatigue of railway wheels," *International Journal of Fatigue,* 2009.

[8] EN. 15313, "Railway applications — In-service wheelset operation requirements and inservice and off-vehicle wheelset maintanance " 2007.

[9] R. Dukkipati and R. DONG, "Impact Loads due to Wheel Flats and Shells," *Vehicle System Dynamics,,* vol. 31, pp. 1-22, 1999.

[10] "Guidance on railway wheelset tread, gauging and damage," Rail Safety and Standards Board, London2007.

[11] R. G. Standard, "Railway Wheelsets," ed: Rail Safety and Standards Board Limited, Available :'http://www.timken.com/fr-fr/solutions/rail/Documents/8073.pdf', [Accessed July 2015], 2010.

[12] M. A. Elmaleeh and N. Saad, "Acoustic emission techniques for early detection of bearing faults using LabVIEW," in *Mechatronics and Its Applications, 2008. ISMA 2008. 5th International Symposium on*, 2008, pp. 1-5.

[13] N. Tandon and A. Choudhury, "A review of vibration and acoustic measurement methods for the detection of defects in rolling element bearings," *Tribology International,* vol. 32, pp. 469-480, 1999.

[14] J. Miettinen and P. Pataniitty, "Acoustic emission in monitoring extremely slowly rotating rolling bearing," in *Proceedings of 12th International Congress on Condition Monitoring and Diagnostic Engineering Management, COMADEM*, 1999, pp. 289-297.

[15] E. V. Zaretsky, "Rolling bearing life prediction, theory, and application," *Recent Developments in Wear Prevention, Friction and Lubrication,* vol. 37, p. 2, 2010.

[16] I. Howard, "A Review of Rolling Element Bearing Vibration'Detection, Diagnosis and Prognosis'," DTIC Document1994.

[17] TIMKEN, "AP™ Bearings,Size and Dimensional Data, Available http://www.timken.com/fr-fr/solutions/rail/Documents/8073.pdf, [Accessed July 2015]."

[18] *Bearing Loads*. Available: http://training.bsc.com.au/Training/A9000/A9006/A9006-P04.htm, [Accessed May 2014]

[19] S. McInerny and Y. Dai, "Basic vibration signal processing for bearing fault detection," *Education, IEEE Transactions on,* vol. 46, pp. 149-156, 2003.

[20] *Bearing designs*. Available: http://www.skf.com/binary/12-62740/RTB-1-04b-Bearing-designs--TBU.pdf , [Accessed March 2014]

[21] C. Radu, "The Most Common Causes of Bearing Failure and the Importance of Bearing Lubrication."

[22] O. A. Bauchau, "Acoustic emission bearing fault diagnostics system," School of Aerospace Engineering ; Project no. E-16-N771999.

[23] M. Segla, S. Wang, and F. Wang, "Bearing fault diagnosis with an improved high frequency resonance technique," in *Industrial Informatics (INDIN), 2012 10th IEEE International Conference on*, 2012, pp. 580-585.
[24] (1994). *Bearing failures and their causes*. Available: https://ec.kamandirect.com/content/resources/2010/downloads/skf_bearing_failureandcauses.pdf
[25] *Vibration: The cornerstone of condition monitoring*. Available: http://www.wilcoxon.com/knowdesk/Bearing%20defects.pdf, [Accessed July 2015]
[26] C. PENG, L. WANG, X. GAO, Z. WANG, Q. ZHAO, Y. ZHANG, J. PENG, and K. YANG, "High-Power Locomotive Solid Axle Defect on-line Detection Technique," presented at the 18th World Conference on Nondestructive Testing, Durban, South Africa, 2012.
[27] R. Dukes and E. A. Culpan, "Acoustic emission: its techniques and applications," *Physical Science, Measurement and Instrumentation, Management and Education - Reviews, IEE Proceedings A,* vol. 131, pp. 241-251, 1984.
[28] R. Pohl, A. Erhard, H. Montag, H. Thomas, and H. Wustenberg, "NDT techniques for railroad wheel and gauge corner inspection," *NDT&E International,* vol. 37, pp. 89-94, 2004.
[29] *Wayside vehicale health monitoring systems*. Available: http://www.railway-research.org/IMG/pdf/aar_ttci_research_machine_vision_inspection_jan_2014.pdf, [Accessed March 2016]
[30] R. Pohl, A. Erhard, H.-J. Montag, H.-M. Thomas, and H. Wüstenberg, "NDT techniques for railroad wheel and gauge corner inspection," *NDT & E International,* vol. 37, pp. 89-94, 2004.
[31] G. Lutenco, V. UCHANIN, V. MISHCHENKO, and A. OPANASENKO, "Eddy Currents versus Magnetic Particles," presented at the 18th World Conference on Nondestructive Testing, Durban, South Africa, 2012.
[32] M. Afzal and S. Udpa, "Advanced signal processing of magnetic flux leakage data obtained from seamless gas pipeline," *NDT & E International,* vol. 35, pp. 449-457, 2002.
[33] D. Hackenberger and C. Lonsdale, "An initial feasibility study to develop a wayside cracked railroad wheel detector," in *Railroad Conference, 1998. Proceedings of the 1998 ASME/IEEE Joint*, 1998, pp. 65-77.
[34] J. Rudlin, A. Muhammed, and C. Schneider, "Inspection reliability and periodicity for rail axle inspection," *Insight,* vol. 48, 2006.
[35] O. Orringer, W. Paxton, D. Gray, and P. Raj, "Residual stress and its consequences on both sides of the wheel-rail interface," *Wear,* vol. 191, pp. 25-34, 1996.
[36] W. Li, G.-m. Chen, F. Liu, and Z. Li, "Study on ACFM Crack Angle Detection with 1-D Array Probe," in *Measuring Technology and Mechatronics Automation (ICMTMA), 2011 Third International Conference on*, 2011, pp. 417-419.
[37] G. Nicholson and C. Davis, "Modelling of the response of an ACFM sensor to rail and rail wheel RCF cracks," *NDT & E International,* vol. 46, pp. 107-114, 2012.
[38] C. Vale, "Advanced Approaches for Axle Bearing Condition Monitoring, ," *Faculty of Engineering, University of Porto, Portugal,* 2014.
[39] B. Herguth, "Grease Analysis - Monitoring Grease Serviceability and Bearing Condition, http://www.machinerylubrication.com/Read/296/grease-analysis , [Accessed June 2016]."
[40] Z.-F. Fu and J. He, *Modal analysis*: Butterworth-Heinemann, 2001.
[41] C. Yang, S. L, and tourneau, "Learning to predict train wheel failures," presented at the Proceedings of the eleventh ACM SIGKDD international conference on Knowledge discovery in data mining, Chicago, Illinois, USA, 2005.
[42] D. Barke and W. Chiu, "Structural health monitoring in the railway industry: a review," *Structural Health Monitoring,* vol. 4, pp. 81-93, 2005.
[43] U. Danneskiold-Samsoe, J. Gramtorp, A.-H. T. Madsen, and T.-M. A. Haure, "Plant for track-based detection of the wheel profile of train wheels," ed: Google Patents, 1993.
[44] A. Schöbel, M. Pisek, and J. Karner, "Hot box detection systems as a part of automated train observation in Austria," in *Proceedings of 14th International Symposium EURNEX-ZEL "Towards the competitive rails systems in Europe*, 2006, pp. 157-161.
[45] "Directive 96/48/EC - Interoperability of the transEuropean high speed rail system," ed: Technical Specification for Interoperability, Available: https://www.transportstyrelsen.se/globalassets/global/jarnvag/english/tsi/tsi-highspeed-operation-techntext-2008-02-01.pdf, [Accessed on March 2016]
[46] A. Blakeney, "Hot axle bearing detection,," Reference number :GE/RT8014,Railway Safety, London2001.

[47] *www.voestalpine*. Available: http://www.voestalpine.com/vaeuk/en/site/downloads.ContentPar.74129.File.tmp/VAE_HAZ_en.pdf [Accessed July 2012]
[48] G. W. E. T.W. Moynihan. (2007). *Railway Safety Technologies*. Available: https://www.tc.gc.ca/media/documents/railsafety/technologies.pdf, [Accessed June 2015]
[49] (2010). *SKF Axletronic sensors for the railway industry*. Available: http://www.skf.com/binary/21-57366/11007-EN.pdf, [Accessed February 2015]
[50] M. Jones and J. Southcombe. *Track condition monitoring using serive trains*. Available: Perpetuum Ltd, Available: http://www.perpetuum.com/news/AusRail%20Perpetuumv5%2021%20August%202015.pdf, [Accessed March 2016]

[51] B. Chen, Z. Yan, and W. Chen, "Defect Detection for Wheel-Bearings with Time-Spectral Kurtosis and Entropy," *Entropy,* vol. 16, pp. 607-626, 2014.
[52] A. C. Lamari, "Rolling stock bearing condition monitoring systems," University of Southern Queensland, 2008.
[53] *Transportation Technology Center Inc*. Available: http://www.aar.com/ , [Accessed on March 2016]
[54] W. H. Sneed and R. L. Smith, "On-board real-time railroad bearing defect detection and monitoring," in *Railroad Conference, 1998. Proceedings of the 1998 ASME/IEEE Joint*, 1998, pp. 149-153.
[55] J. Taylor, *The Vibration Analysis Handbook*: Vibration Consultants, Inc, 1994.
[56] T. Harris, "Rolling Bearing Analysis," *John Wiley and Sons, Inc.(United States), 1991,* p. 1013, 1991.
[57] Y.-J. Zhang, "Rail Vehicle Bearing Defects Detection," Final Report for Safety IDEA Project 16 ,2011.
[58] P. McFadden and J. Smith, "Vibration monitoring of rolling element bearings by the high-frequency resonance technique—a review," *Tribology International,* vol. 17, pp. 3-10, 1984.
[59] A. Bilosova and J. Bilos. (2012). *Vibration diagnostics*. Available: http://www.337.vsb.cz/materialy/vibracni_diagnostika/VIBDI_skriptaEN.pdf, [Accessed November 2014]
[60] Y. H. Pao, R. R. Gajewski, and A. N. Ceranoglu, "Acoustic emission and transient waves in an elastic plate," *The Journal of the Acoustical Society of America,* vol. 65, pp. 96-105, 1979.
[61] *ndt-ed.org*
Available: http://www.ndt-ed.org/EducationResources/CommunityCollege/Other%20Methods/AE/AE_Index.htm [Accessed July 2012]
[62] C. Grosse and m. ohtsu, *Acoustic Emission Testing*. Leipzig, Germany: Ie-Tex Publishing, 2008.
[63] H. Bar, M. Bhat, and C. Murthy, "Parametric analysis of acoustic emission signals for evaluating damage in composites using a PVDF film sensor," *Journal of Nondestructive Evaluation,* vol. 24, pp. 121-134, 2005.
[64] D. Mba and R. B. Rao, "Development of Acoustic Emission Technology for Condition Monitoring and Diagnosis of Rotating Machines; Bearings, Pumps, Gearboxes, Engines and Rotating Structures," 2006.
[65] J. Catlin, "The Use of ultrasonic diagnostic technique to detect rolling element bearing defects," in *Proceedings of the machinery and vibration monitoring and analysis meeting*, 1983, pp. 123-130.
[66] H. Vallen, "AE testing fundamentals, equipment, applications," *Journal of Nondestructive Testing(Germany),* vol. 7, pp. 1-30, 2002.
[67] M. Hawman and W. Galinaitis, "Acoustic emission monitoring of rolling element bearings," in *Ultrasonics Symposium, 1988. Proceedings., IEEE 1988*, 1988, pp. 885-889.
[68] A. Sturm and D.-I. S. Uhlemann, "Diagnosis of plain bearings by acoustic emission analysis," *Measurement,* vol. 3, pp. 185-191, 1985.
[69] R. K. Miller and P. McIntire, "Nondestructive Testing Handbook. Vol. 5: Acoustic Emission Testing," *American Society for Nondestructive Testing, 4153 Arlingate Plaza, Caller# 28518, Columbus, Ohio 43228, USA, 1987. 603,* 1987.
[70] E. MENDOZA, J. PROHASKA, C. KEMPEN, Y. ESTERKIN, S. S. and, and S. KRISHNASWAMY. *Distributed fiber optic acoustic emission sensor (FAESenseTM) system*

for condition based maintenance of advanced structures , . Available: http://www.ndt.net/article/ewshm2012/papers/th3c4.pdf, [Accessed on April 2015]
[71] "EN 13554 : Non destructive testing ,Acoustic emission , General principles," ed. Vienna: Austrian Standards Institute, 2009.
[72] "Non-destructive testing handbook," *American Society of Non-destructive testing - ISBN 0-931403-02-2,* vol. 5 , Acoustic Emissions.
[73] B. Muravin. *Acoustic Emission Wave Propagation and Source Location,* . Available: www.muravin.com , [Accessed on May 2015]
[74] I. A. Viktorov, "Rayleigh and lamb waves: physical theory and applications (ultrasonic technology)," 2014.
[75] J. C. Chuang and R. A. Sosseh, "A Survey Report of Acoustic Emission Used in Roller Bearing Fault Detection , Accessed on June 2015," 1998.
[76] F. R. Breckenridge, C. E. Tschiegg, and M. Greenspan, "Acoustic emission: some applications of Lamb's problem," *The Journal of the Acoustical Society of America,* vol. 57, pp. 626-631, 1975.
[77] G. C. McLaskey and S. D. Glaser, "Acoustic emission sensor calibration for absolute source measurements," *Journal of Nondestructive Evaluation,* vol. 31, pp. 157-168, 2012.
[78] "ASTM E650-97,Standard Guide for Mounting Piezoelectric Acoustic Emission Sensors," ed, 2007.
[79] S. Colombo, A. Giannopoulos, M. Forde, R. Hasson, and J. Mulholland, "Frequency response of different couplant materials for mounting transducers," *NDT & E International,* vol. 38, pp. 187-193, 2005.
[80] P. Theobald, B. Zeqiri, and J. Avison, "Couplants and their influence on AE sensor sensitivity," *Journal of Acoustic Emission,* vol. 26, pp. 91-97, 2008.
[81] R. Randall, "Detection and diagnosis of incipient bearing failure in helicopter gearboxes," *Engineering Failure Analysis,* vol. 11, pp. 177-190, 2004.
[82] N. A. Thakkar, J. A. Steel, and R. L. Reuben, "Rail–wheel interaction monitoring using Acoustic Emission: A laboratory study of normal rolling signals with natural rail defects," *Mechanical Systems and Signal Processing,* vol. 24, pp. 256-266, 2010.
[83] P. Sreedhar and K. Balasubramaniam. *Optimization of frequency band for the detection of lubricant oil starvation in engines using acoustic emission*. Available: http://www.ndt.net/article/nde-india2011/pdf/1-11B-5.pdf, [Accessed January 2015]
[84] J. Shiroishi, Y. Li, S. Liang, T. Kurfess, and S. Danyluk, "Bearing condition diagnostics via vibration and acoustic emission measurements," *Mechanical Systems and Signal Processing,* vol. 11, pp. 693-705, 1997.
[85] J. Miettinen and P. Salmenpera, "Acoustic emission monitoring of grease lubricated rolling bearings," in *COMADEM 2000: 13 th International Congress on Condition Monitoring and Diagnostic Engineering Management*, 2000, pp. 21-30.
[86] T. Holroyd, "Acoustic Emission as a basis for the condition monitoring of industrial machinery," in *Proceedings of the 18 th Machinery vibration seminar, Canadian Machinery vibration association*, 2000, pp. 27-29.
[87] S. Bagnoli, R. Capitani, and P. Citti, "Comparison of accelerometer and acoustic emission signals as diagnostic tools in assessing bearing," in *Proceedings of 2nd International Conference on Condition Monitoring*, 1988, pp. 117-125.
[88] E. Price, A. Lees, and M. I. Friswell, "Application of high frequency monitoring for classification of rolling element bearing failures," in *Key Engineering Materials*, 2001, pp. 173-184.
[89] L. Roger, "The application of vibration analysis and acoustic emission source location to on-line condition monitoring of anti-friction bearings," *Tribology International,* vol. 12, pp. 51-58, 1979.
[90] V Bansal, Gupta, APrakash, and Eshwar, "Quality inspection of rolling element bearing using acoustic emission technique," *Journal of Acoustic emission,,* vol. 9, pp. 142-146.
[91] Y. Li, S. Billington, C. Zhang, T. Kurfess, S. Danyluk, and S. Liang, "Dynamic prognostic prediction of defect propagation on rolling element bearings," *Tribology transactions,* vol. 42, pp. 385-392, 1999.
[92] M. Badi, D. Johnson, and G. Trmal, "The use of stress wave sensors for the diagnosis of bearing faults," in *Condition Monitoring and Diagnostic Engineering Management: Proceeding of COMADEM 90: The Second International Congress on Condition Monitoring and Diagnostic Engineering Management Brunel University 16–18 July 1990*, 2012, p. 20.

[93] T. Yoshioka and T. Fujiwara, "Application of acoustic emission technique to detection of rolling bearing failure," *American society of mechanical engineers,* vol. 14, pp. 55-76, 1984.
[94] C. J. Li, J. Ma, and B. Hwang, "Bearing condition monitoring by pattern recognition based on bicoherence analysis of vibrations," *Proceedings of the Institution of Mechanical Engineers, Part C: Journal of Mechanical Engineering Science,* vol. 210, pp. 277-285, 1996.
[95] A. Morhain and D. Mba, "Bearing defect diagnosis and acoustic emission," *Proceedings of the Institution of Mechanical Engineers, Part J: Journal of Engineering Tribology,* vol. 217, pp. 257-272, 2003.
[96] C. J. Li and S. Wu, "On-line detection of localized defects in bearings by pattern recognition analysis," *Journal of Manufacturing Science and Engineering,* vol. 111, pp. 331-336, 1989.
[97] A. Singh, D. Houser, and S. Vijayakar, "Early detection of gear pitting," in *Power Transmission and Gearing Conference, ASME*, 1996, pp. 673-678.
[98] A. Anastasopoulos, B. K, D. Papasalouros, and D. Kourousis, "Acoustic emission on-line inspection of rail wheelset," European Working Group on Acoustic Emission Vienna2010.
[99] *Introduction to Acoustic Emission*. Available: http://www.idinspections.com/?page_id=126 , [Accessed on May 2015]
[100] T. Yoshioka and T. Fujiwara, "A new acoustic emission source locating system for the study of rolling contact fatigue," *Wear,* vol. 81, pp. 183-186, 1982.
[101] S. Salvan, R. Parkin, J. Coy, and W. Li, "Intelligent Condition Monitoring of Bearings in Mail Processing Machines using Acoustic Emission," in *Proceedings of COMADEM*, 2001, pp. 67-74.
[102] J. Smith, "Vibration monitoring of bearings at low speeds," *Tribology International,* vol. 15, pp. 139-144, 1982.
[103] K. Kuboyama, "Development of low speed bearing diagnosis technique," *Detection, Diagnosis and Prognosis of Rotating Machinery to Improve Reliability, Maintainability, and Readiness Through the Application of New and Innovative Techniques,* pp. 178-185, 1986.
[104] N. Jamaludin, D. Mba, and R. Bannister, "Condition monitoring of slow-speed rolling element bearings using stress waves," *Proceedings of the Institution of Mechanical Engineers, Part E: Journal of Process Mechanical Engineering,* vol. 215, pp. 245-271, 2001.
[105] S. Budano, G. Giunta, and A. Lucci, "Acoustic Emission data analysis to evaluate damage mechanisms in pipeline carbon steels," *NDT. net,* vol. 24, 2011.
[106] R. Smith, A. DeMonte, and W. Mackay, "Development of high-manganese steels for heavy duty cast-to-shape applications," *Journal of Materials Processing Technology,* vol. 153, pp. 589-595, 2004.
[107] Mayorkinos Papaelias, Carl Slater, A. Amini, and S. Shi, "Structural health monitoring of cast manganese crossing using acoustic emission techniques," Industrial Report, May 2015.
[108] P. Fleischmann, D. Rouby, F. Lakestani, and J. Baboux, "A spectrum analysis of acoustic emission," *Non-Destructive Testing,* vol. 8, pp. 241-244, 1975.
[109] Y.-H. Kim, A. Tan, J. Mathew, and B.-S. Yang, "Condition Monitoring of Low Speed Bearings: A Comparative Study of the Ultrasound Technique Versus Vibration Measurements," in *Engineering Asset Management*, J. Mathew*, et al.*, Eds., ed: Springer London, 2006, pp. 182-191.
[110] E. Y. Kim, A. C. Tan, J. Mathew, and B.-s. Yang, "Development of an online condition monitoring system for slow speed machinery," in *Engineering Asset Lifecycle Management*, ed: Springer, 2010, pp. 743-749.
[111] P. Sundt, "Monitoring acoustic emission to detect mechanical defects," *Instrum. Technol.,* vol. 26, pp. 43-44, 1979.
[112] R. W. Finley, "Computerisation preventive maintenance systems using modified Acoustic Emission techniques," *Materials Evaluation,* vol. 38, pp. 15-20, 1980.
[113] T. Holroyd. (2008). *Condition Monitoring based on Acoustic Emission Accessed June 2013]*. Available: http://www.maintenanceonline.org/maintenanceonline/content_images/p14,16%20TPM.pdf
[114] M. Lebold, K. McClintic, R. Campbell, C. Byington, and K. Maynard, "Review of vibration analysis methods for gearbox diagnostics and prognostics," in *Proceedings of the 54th meeting of the society for machinery failure prevention technology, Virginia Beach, VA*, 2000, pp. 623-634.
[115] K. Bollas, D. Papasalouros, D. Kourousis, and A. Anastasopoulos, "Acoustic emission inspection of rail wheels," *J. Acoust. Emission,* vol. 28, pp. 215-228, 2010.

[116] (2008). *Skewness/Kurtosis* Available: http://mvpprograms.com/help/mvpstats/distributions/SkewnessKurtosis [Accessed September 2012]
[117] R. B. W. Heng and M. J. M. Nor, "Statistical Analysis of Sound and Vibration Signals for Monitoring Rolling Element Bearing Condition," *Applied Acoustics,* vol. 53, pp. 211-226, 1998.
[118] M. Norton and D. Karczub, *Fundamentals of Noise and Vibration Analysis for Engineers*. Cambridge Cambridge University Press, 2003.
[119] A. Raad, F. Zhang, and M. Sidahmed, "Acoustic Emission for gear fault detection : A promising tool," in *Surveillance 5 Cetim Senlis*, 2004.
[120] M. Lebold, K. McClintic, R. Campbell, C. Byington, and K. Maynard, "Renew of vibration analyisis methoids for gearbox diagnostics and prognostics," in *Society for Machinery Failure Prevention Technology,*, Virginia Beach, 2000.
[121] *Envelope detection*. Available: http://www.mathworks.co.uk/help/dsp/examples/envelope-detection.html, [Accessed January 2013]
[122] F. Kschischang, "The Hilbert Transform. Department of Electrical and Computer Engineering, University of Toronto," ed. PhD Thesis, Toronto, 2006.
[123] C. Tan, "Application of acoustic emission to the detection of bearing failures," presented at the International Tribology Conference 1990, Brisbane 2-5 December 1990: Putting Tribology to Work; Reliability and Maintainability through Lubrication and Wear Technology; Preprints of Papers. Institution of Engineers, Australia, 1990.
[124] C. W. De Silva, *Vibration: fundamentals and practice*: CRC press, 2006.
[125] D. Felten. (2003). *Understanding Bearing Vibration Frequencies*. Available: http://electromotores.com/PDF/InfoT%C3%A9cnica/EASA/Understanding%20Bearing%20Vibration%20Frequencies.pdf, [Accessed June 2013]
[126] N. Bosso, N. Zampieri, and A. Gugliotta, "A modular monitoring system for onboard vehicle diagnostic," *Material Evaluation,* pp. 78-85, 2012.
[127] D. E. Bently, P. Goldman, and J. Yu, "Rolling element bearing defect detection and diagnostics using REBAM® Probes," *Orbit,* vol. 22, pp. 12-25, 2001.
[128] M. L. Adams, *Rotating machinery vibration: from analysis to troubleshooting*: CRC Press, 2000.
[129] A. Muszyńska, "Misalignment and shaft crack–related phase relationships for 1X and 2X vibration components of rotor responses," *Orbit,* vol. 10, pp. 4-8, 1989.
[130] *Rolling Element Bearings*. Available: http://www.stiweb.com/appnotes/Rolling-Element-Bearings.html, [Accessed on Feb 2015]
[131] M. Xu, "Spike Energy™ Measurement and Case Histories," *ENTEK IRD International Corporation Technical Report, Online: http://domino. automation. rockwell. com/applications/gs/region/EntekWe bST. nsf/files/Xu99. pdf/$ file/Xu99. pdf,* 1999.
[132] F. R. Kschischang, "The hilbert transform," *University of Toronto,* 2006.
[133] B. Eftekharnejad, M. Carrasco, B. Charnley, and D. Mba, "The application of spectral kurtosis on Acoustic Emission and vibrations from a defective bearing," *Mechanical Systems and Signal Processing,* vol. 25, pp. 266-284, 2011.
[134] J. Antoni and R. Randall, "The spectral kurtosis: application to the vibratory surveillance and diagnostics of rotating machines," *Mechanical Systems and Signal Processing,* vol. 20, pp. 308-331, 2006.
[135] J. G. de la Rosa, A. Moreno, A. Gallego, R. Piotrkowski, E. Castro, and J. Vico, "A virtual measurement for acoustic termite detection based in the Spectral Kurtosis."
[136] J. Antoni, "Fast computation of the kurtogram for the detection of transient faults," *Mechanical Systems and Signal Processing,* vol. 21, pp. 108-124, 2007.
[137] T. Barszcz and A. Jabłoński, "Analysis of Fast Kurtogram performance in case of high level non-Gaussian noise," in *The 16th International Congress on Sound and Vibration, Krakow, Poland*, 2009, pp. 5-9.
[138] G. Busse, D. Van Hemelrijck, I. Solodov, and A. Anastasopoulos, *Emerging Technologies in NDT*: CRC Press, 2008.
[139] R. Randall, "Cepstrum analysis and gearbox fault-diagnosis," *Maintenance Management International,* vol. 3, pp. 183-208, 1982.
[140] M. Satyam, V. Sudhakara Rao, and C. Devy, "Cepstrum Analysis - An Advanced Technique in Vibration Analysis of defects in rotating machinery," *Defence Science,* vol. 44, pp. 53-60, 1994.
[141] R. B. Randall, "Cepstrum Analysis and Gearbox Fault Diagnosis," Bruel & Kjaer Precision Instruments Inc1980.

[142] *Estimating the power cepstrum of a time series*. Available: http://zone.ni.com/reference/en-XX/help/371419D-01/lvasptconcepts/tsa_power_cepstrum/ , [Accessed March 2013]
[143] S. Cornelius and G. B. Paresh, "Practical Machinery Vibration Analysis and Predictive Maintenance," 2004.
[144] G. Singh and S. A. K. Sa'ad Ahmed, "Vibration signal analysis using wavelet transform for isolation and identification of electrical faults in induction machine," *Electric Power Systems Research,* vol. 68, pp. 119-136, 2003.
[145] *pacndt.com*. Available: http://www.pacndt.com/index.aspx?go=products&focus=Amplifiers.htm, [Accessed July 2012]
[146] (2012). *Acoustic Emission Sensors Specification,Vallen Systeme*. Available: http://www.vallen.de/sites/default/files/sov1212_0.pdf , [Accessed on July 2015]
[147] B. Judd, "Everything you ever wanted to know about data acquisition," *United Electronic Industries,* vol. 20, p. 3, 2008.
[148] G. P. Ripper, R. S. Dias, and G. A. Garcia, "Primary accelerometer calibration problems due to vibration exciters," *Measurement,* vol. 42, pp. 1363-1369, 2009.
[149] M. Papaelias, " Interoperable monitoring, diagnosis and maintenance strategies for axle bearings, Maxbe report," 2012.
[150] Z. Huang, A. AMini, L. Wang, S. Keykyras, and M. Papaeilas, "online evaluation of railway axle bearing faults using acoustic emission and vibration analysis," in *BINDT*, Manchester, 2014.
[151] M. Entezami, E. Stewart, J. Tutcher, W. Driscoll, R. Ellis, G. Yeo, Z. Zhang, C. Roberts, T. Kono, and S. Bayram, "Acoustic analysis techniques for condition monitoring of roller bearings," presented at the 6th IET Conference on. IET, 2014.

Appendix B: Bearing Periodic Frequencies

99591-99100 freq results

Rotating Inner Race or Rotating Outer Race Operating at 60 RPM

Bearing: Inner ring 99591

Bearing Geometry Constants

Number of Rollers (Z):	21
1/2 Incl. Roller CL Angle for TRB (contact angle for non-TRB):	13.6 deg
Pitch Diameter:	200.7 mm
Mean Roller Diameter:	23.6 mm

Frequency Coefficients - multiply by RPM / 60 to calculate frequency

BPFI - Roller/Ball Pass Frequency Inner Race: 11.7 Hz / (Rev/Sec)

BPFO - Roller/Ball Pass Frequency Outer Race: 9.3 Hz / (Rev/Sec)

BSF - Roller/Ball Spin Frequency: 4.198 Hz / (Rev/Sec)

FTFI - Fundamental Train Frequency Inner Race Rotation: 0.443 Hz / (Rev/Sec)

FTFO - Fundamental Train Frequency Outer Race Rotation: 0.557 Hz / (Rev/Sec)

Bearing Relative Component Speeds (Revs/Sec)

Inner/Outer Race or Outer/Inner Race:	1
Cage/Outer Race:	0.443
Cage/Inner Race:	0.557
Roller/Cage:	4.198

Frequencies Resulting From Component Irregularities		
1 Hertz (Revolutions Per Second) – Inner Race or Outer Race		
Possible Source of Vibration	**Frequency (Hz)**	**Other Common Terminology**
Eccentricity Of Rotating Member	f_0 = 1	
Out-Of-Round Of Rotating Member	f_1 = 1	
Roller Irregularity (e.g., nick or spall)	f_2 = 8.396	
	4.198	BSF- Roller/Ball Spin Freq
Inner Race Irregularity (e.g., nick or spall)	f_3 = 11.7	BPFI - Roller/Ball Pass Freq Inner Race
Outer Race Irregularity (e.g., nick or spall)	f_4 = 9.3	BPFO - Roller/Ball Pass Freq Outer Race
Roller Size Variations (Rotating Inner Race)	f_5 = 0.443	FTFI - Fundamental Train Freq Inner Race
Roller Size Variations (Rotating Outer Race)	f_6 = 0.557	FTFO – Fundamental Train Freq Outer Race